UQAC
Université du Québec
à Chicoutimi

Influence de la géométrie des joints et de la rugosité de surface sur les pressions hydrauliques et la stabilité des blocs dans les évacuateurs de crues à l'échelle de laboratoire

(*Impact of Joint Geometry and Surface Roughness on hydraulic pressure fluctuations and block stability in Dam Spillways at Laboratory scale*)

Par

Vineeth Reddy Karnati

Sous la direction de Dr. Ali Saeidi, Dr. Alain Rouleau et Dr. Marco Quirion

Thèse présentée à l'Université du Québec à Chicoutimi (UQAC) en vue de l'obtention du grade de Philosophiae Doctor (Ph.D.) en ingénierie (génie civil)

Jury :

Julien Walter, Professeur, Ph.D., UQAC, Président du Jury

Éric Villeneauve, Professeur, Ph.D., Université du Québec à Rimouski, Membre externe

Adoubi Vincent De Paul Adombi, Professeur, Ph.D., UQAC, Membre interne

Ali Saeidi, Professeur, Ph.D., UQAC, Directeur

Alain Rouleau, Professeur émérite, Ph.D., UQAC, Co-directeur

Marco Quirion, Ph.D., Hydro-Québec (Montréal), Co-directeur

Québec, Canada

RÉSUMÉ

Bien que le massif rocheux offre en général une plus grande résistance à l'érosion que les dépôts alluviaux, des cas graves d'érosion de la roche ont néanmoins été signalés dans plusieurs évacuateurs de crues de barrages à travers le monde, même dans des contextes de roche dure. Lors de crues extrêmes, accentuées par les changements climatiques, cette érosion constitue une menace croissante pour la sécurité des barrages, notamment au Québec et au Canada, où l'hydroélectricité représente un pilier majeur de l'approvisionnement énergétique. Cette étude s'amorce par une revue de littérature approfondie sur les mécanismes d'érosion et les méthodes classiques de prédiction. Les approches semi-empiriques traditionnelles s'avèrent souvent insuffisantes, car elles négligent certains mécanismes clés et ignorent des paramètres hydrauliques et géomécaniques propres aux sites. Ces limites entraînent fréquemment des écarts notables entre les profondeurs d'érosion prévues et celles observées sur le terrain, ce qui met en évidence la nécessité de méthodes davantage fondées sur les mécanismes physiques. La recherche se concentre sur les évacuateurs de crues non revêtus, en mettant l'accent sur l'arrachage de blocs rocheux, reconnu comme un mode de défaillance dominant. Une série d'essais physiques à échelle réduite a permis d'analyser l'effet de paramètres clés, le débit, l'ouverture des joints, la saillie des blocs et leur orientation, sur la stabilité et le soulèvement des blocs sous des conditions d'écoulement parallèle. Un modèle pilote, constitué de blocs-modèles représentant un massif fracturé interconnecté, a servi à mesurer en détail les pressions hydrauliques autour d'un bloc central instrumenté selon diverses configurations expérimentales. Les résultats montrent que les fluctuations de pression à la surface du canal, particulièrement en dessus des blocs, jouent un rôle déterminant dans l'initiation du soulèvement. En revanche, les pressions mesurées dans les joints demeurent relativement stables, indépendamment de l'écoulement ou de la géométrie. Un modèle mathématique prédictif a été développé pour estimer les fluctuations extrêmes de pression hydraulique à la surface des blocs et évaluer le risque de soulèvement selon les configurations. Ce modèle a démontré une concordance satisfaisante avec les résultats expérimentaux, avec des erreurs quadratiques moyennes (*RMSE*) de 0,04 à 0,37 et des erreurs quadratiques moyennes normalisées (*NRMSE*) de 18% à 35%, confirmant sa fiabilité. Des essais additionnels ont examiné l'effet de l'orientation des blocs (-45°, 0°, +45°). Les blocs inclinés à contre-courant tendaient à basculer avant de se soulever, avec des facteurs de sécurité (F_s) entre 0,5 et 0,8, tandis que ceux alignés avec le courant se soulevaient plus directement, avec des F_s entre 0,2 et 0,7. Les blocs perpendiculaires au courant ont montré une stabilité accrue. Enfin, une analyse paramétrique a évalué l'influence de la géométrie des blocs, rapport d'aspect, longueur exposée et angle de frottement, sur la stabilité sous diverses sollicitations hydrauliques. Cette étude fournit des coefficients adimensionnels et un modèle prédictif permettant de relier les pressions hydrauliques extrêmes aux modes de rupture par soulèvement et basculement. Les résultats confirment que ces paramètres, combinés à l'orientation, doivent impérativement être intégrés à toute évaluation rigoureuse du potentiel d'érosion. Dans l'ensemble, cette recherche améliore la compréhension de l'interaction complexe entre facteurs hydrauliques et géomécaniques dans l'érosion des massifs rocheux aux évacuateurs de crues de barrages et propose des outils analytiques fiables pour l'évaluation de la stabilité des blocs.

Mots clés: Érosion du massif rocheux, Évacuateurs de crues des barrages, Modèle physique à échelle réduite, Paramètres géomécaniques, Mécanismes d'érosion

ABSTRACT

Although rock masses are generally more resistant to scour than alluvial deposits, severe rock mass scour has been reported at numerous dam spillway sites worldwide, even in hard rock conditions. Under extreme flood events exacerbated by climate change, this rock scour poses a growing threat to dam safety, particularly in regions like Québec and Canada, where hydropower infrastructure plays a significant role. This study begins with a comprehensive literature review to understand the scour mechanisms in dam spillways and traditional scour prediction methods. The conventional semi-empirical approaches are shown to be inadequate in many cases, primarily because they overlook key scour mechanisms and fail to account for critical site-specific hydraulic and geomechanical parameters. As a result, significant discrepancies are often observed between predicted and actual scour depths, highlighting the need for more mechanistically grounded approaches. This study investigates the scour mechanisms in unlined dam spillways, focusing on the plucking of rock blocks, which is recognized as dominant failure mechanism influenced by both hydraulic and geomechanical conditions. A series of reduced-scale physical model tests were conducted to study the effect of key parameters, especially, flow rate, joint opening, block protrusion, and joint orientation, on block stability and uplift in parallel flow spillway conditions. Using a pilot-scale spillway model equipped with model blocks, representing rock mass with continuous connected fractures, detailed measurements of hydraulic pressures around a central instrumented block were obtained under varied test configurations. The test results with blocks arranged in different protrusion configurations consistently revealed that pressure fluctuations on the spillway surface, particularly on the top of the blocks, play a critical role in initiating uplift. In contrast, pressure fluctuations within the joints remained relatively stable across different flow and geometry conditions. A predictive mathematical model was developed to estimate extreme hydraulic pressure fluctuations on the block surface, enabling users to evaluate uplift risk for given block and joint configurations. The model showed good agreement with experimental data, with root mean square errors (*RMSE*) ranging from 0.04 to 0.37 and with normalized root mean square errors (*NRMSE*) ranging from 18% to 35%, confirming its reliability. Subsequent testing focused on the effect of block orientation, where blocks were arranged at different angles (-45°, 0°, +45°) relative to the flow. Joint orientation was found to significantly affect stability outcomes. Blocks inclined against the flow exhibited a tendency to topple before uplift, with factor of safety (F_s) values between 0.5 and 0.8, while blocks aligned with the flow showed a greater susceptibility to direct uplift, with F_s values between 0.2 and 0.7. Blocks oriented perpendicular to flow demonstrated greater stability. This study also presents a parametric study to explore the influence of block geometry, particularly aspect ratio, exposure length and friction angle, on stability under varied hydraulic loading. This study provides dimensionless coefficients and a predictive model linking extreme hydraulic pressures to uplift and toppling failure modes. The findings confirmed that both geometric and orientation parameters must be integrated into any reliable assessment of scour potential. Overall, this research contributes a comprehensive understanding of the complex interaction between hydraulic and geomechanical factors in rock mass scour at dam spillways and offers analytical tools to determine the block stability.

Keywords: Rock scour, Dam spillways, Reduced-scale physical spillway model, Geomechanical parameters, Scour mechanisms

TABLE DES MATIÈRES

LISTE DES TABLEAUX

LISTE DES FIGURES

LISTE DES SYMBOLES

β_f	La largeur de la section d'écoulement mesurée à la surface de l'eau en m (*Width of a flow section measured at the water surface in m*)
ϕ	Angle de frottement en º (*Friction Angle in º*)
σ	L'Écart-type des données de pression (*Standard deviation of the pressure data*)
ρ_w	La masse volumique de l'eau en kg/m^3 (*Density of water in kg/m^3*)
Π_{UD}	Dissipation unitaire de puissance de l'écoulement en kW/m^2 (*Unit stream power dissipation in kW/m^2*)
μ	La Moyenne des données de pression (*Mean of the pressure data*)
λ_H	Rapport d'échelle de pression (*Pressure head scale ratio*)
λ_L	Rapport d'échelle de longueur (*Length scale ratio*)
λ_Q	Rapport d'échelle de débit (*discharge scale ratio*)
λ_v	Rapport d'échelle de vitesse (*Velocity scale ratio*)
λ_T	Rapport d'échelle de temps (*Time scale ratio*)
ψ_1	Pendage des joints en profondeur du bloc en º (*Dip of the joints along the depth of the block in º*)
Ψ_2	Pendage des joints à la surface du bloc en º (*Dip of the joints along the surface of the block in º*)
γ_w	Poids volumique de l'eau en kN/m^3 (*Unit Weight of Water in kN/m^3*)
γ_r	Poids volumique du bloc rocheux en kN/m^3 (*Unit Weight of Rock Block in kN/m^3*)
γ_r'	Poids volumique submergé du bloc rocheux en kN/m^3 (*Submerged Unit Weight of Rock Block in kN/m^3*)
a	Longueur d'exposition en mm (*Exposure length in mm*)
A *(Face)*	Face supérieure du bloc instrumenté (*Top face of the instrumented block*)
Ac	Entrée d'eau sur la face supérieure du bloc instrumenté, près de la face C (*Water inlet on the top of the instrumented block close to face C*)
Ad	Entrée d'eau sur la face supérieure du bloc instrumenté, près de la face D (*Water inlet on the top of the instrumented block close to face D*)
A_f	Aire de la face du bloc en m^2 (*Surface area of the block face in m^2*)
$Actual_i$	i^{ème} valeur réelle de la pression dynamique en m (i^{th} *actual value of dynamic head in m*)
B *(Face)*	Face inférieure du bloc instrumenté (*Bottom face of the instrumented block*)
BP	La saillie du bloc en mm (*Block Protrusion Height in mm*)
C *(Face)*	Face latérale amont du bloc instrumenté (*Upstream lateral face of the instrumented block*)
C *(Point)*	Point de rotation dans l'analyse du basculement (*Point of Rotation in overturning analysis*)
C_A	Pression normalisée sur la face supérieure du bloc (*Normalized pressure head on the top of the block*)
C_p'	Pression dynamique normalisée (*Normalized dynamic pressure*)
C_{pA} *(Journal 1)*	Valeur moyenne de la pression fluctuante normalisée sur la face supérieure du bloc (*Mean value of the fluctuating normalized pressure head data on the top of the block*)

C_{pA}' (Journal 1)	Amplitude de la pression fluctuante normalisée sur la face supérieure du bloc (*Amplitude of the fluctuating normalized pressure head on the top of the block*)
C_{pA}^{+}_max	Valeurs des maximas des données de pression (*Values of maxima of the pressure data*)
C_{pA}^{+}_min	Valeurs des minimas des données de pression (*Values of minima of the pressure data*)
C_{pA}'	Pressions dynamiques normalisées sur la face supérieure du bloc (*Normalized dynamic pressures at the top of the block*)
C_{pA}JOXX	Valeur moyenne correspondant aux différentes *JO*; XX représente la valeur de *JO* (*Mean value corresponding to different JO, XX represents JO value*)
C_{pA}'JOXX	Amplitude correspondant aux différentes *JO*; XX représente la valeur de JO (*Amplitude corresponding to different JO, XX represents JO value*)
$C_{pA}Q_x$	Valeurs moyennes correspondant à différents numéros de débit (1-4) (*Mean values corresponding to different discharge numbers (1-4)*)
C_{pB}'	Pressions dynamiques normalisées sur la face inférieure du bloc (*Normalized dynamic pressures at the bottom of the block*)
C_{px}'	Pression dynamique normalisée; x indique la position de l'entrée de pression (*Normalized dynamic pressure, x represents the pressure inlet position*)
C_{up}'	Coefficient de soulèvement adimensionnel (*Non-dimensional Coefficient of Uplift*)
Conf.	Configuration de la saillie (*Protrusion configuration*)
D (Face)	Face latérale en aval du bloc instrumenté (*Downstream lateral face of the instrumented block*)
e	Excentricité de la force considérée par rapport au point de rotation en m (*Eccentricity of the respective force from the point of rotation in m*)
E (Face)	Face latérale droite du bloc instrumenté (*Right lateral face of the instrumented block*)
E_{doa}	Facteur d'orientation de la discontinuité d'érosion (*Erosion discontinuity orientation factor*)
F (Face)	Face latérale gauche du bloc instrumenté (*Left lateral face of the instrumented block*)
f_d	Fréquence Dominante en Hz (*Dominating Frequency in Hz*)
F_L	Force latérale effective générée par la différence de pression en kN/m (*Effective lateral force generated by pressure difference in kN/m*)
F_R	Force résistante en kN/m (*Resisting force in kN/m*)
F_s / *FS*	Facteur de Sécurité (*Factor of Safety*)
$F_{s,O}$	Facteur de Sécurité contre le basculement (*Factor of Safety against Overturning*)
F_{sh}	Résistance totale de frottement développée le long des faces latérales du bloc en kN/m (*Total frictional resistance developed along the lateral faces of the block in kN/m*)
F_{up} / F_{uplift}	Force de soulèvement exercée sur le bloc en kN (*Uplift force generated on the block in kN*)
$F_{s,Up}$	Facteur de Sécurité contre le soulèvement (*Factor of Safety against Uplift*)

$f(K_h)$	Capacité de resistance du massif rocheaux (*Rock mass resistive capacity*)
Fr_{Pr}	Nombre de Froude du prototype (*Froude number of prototype*)
Fr_{RM}	Nombre de Froude du modèle réduit (*Froude number of reduced-scale model*)
g	Accélération gravitationnelle en m/s^2 (*Acceleration due to gravity in m/s^2*)
H / $h_{dynamic}$	Pression dynamique en m (*Dynamic Pressure Head in m*)
$H_{d,Ch}$ / $h_{channel}$	Charge de vitesse moyenne de l'écoulement dans le canal en m (*Mean Channel Flow Velocity Head in m*)
$H_{d,x}$	Charge dynamique mesurée à la position d'entrée « x » en m (*Dynamic head measured at the inlet position 'x' in m*)
$H_{d,max}$	Valeur maximale de la distribution dynamique de la charge mesurée en m (*Actual maximum value of the measured dynamic head distribution in m*)
$H_{d,min}$	Valeur minimale de la distribution dynamique de la charge mesurée en m (*Actual minimum value of the measured dynamic head distribution in m*)
h_{datum}	Charge de pression de référence (ou de position) en m (*Datum or Position Pressure Head in m*)
H_{Pr}	Pression dynamique caractéristique du prototype en m (*Characteristic dynamic head in prototype in m*)
H_{RM}	Pression dynamique caractéristique du modèle réduit en m (*Characteristic dynamic head in reduced-scale model in m*)
h_{static}	Charge de pression statique en m (*Static Pressure Head in m*)
h_{total}	Charge de pression totale en m (*Total Pressure Head in m*)
H_{up} / h_{uplift}	Charge de pression de soulèvement sur le bloc en m (*Uplift Pressure Head on the block in m*)
J_a	Altération de la surface des joints (*Joint surface alteration*)
J_n	Nombre d'ensembles de joints (*Joint set number*)
J_r	Rugosité des joints (*Joint roughness*)
J_s	Cote de structure relative des blocs (*Relative block structure rating*)
JO	Ouverture des joints en mm (*Joint Opening in mm*)
JOr	Orientation des joints en ^{o} (*Joint Orientation in ^{o}*)
K_b	Cote de taille de bloc (*Rock block size rating*)
K_d	Cote de résistance au cisaillement des joints (*Joint shear strength rating*)
M_{Mo}	Moment de basculement en kN-m/m (*Overturning/Mobilizing moment in kN-m/m*)
M_R	Moment résistant en kN-m/m (*Resisting moment in kN-m/m*)
M_s	Cote de résistance en compression selon l'UCS (*Compressive strength rating depending on UCS*)
N / K_h	Indice de Kirsten (*Kirsten's Index*)
N *(Chiffre)*	Nombre d'observations (*Number of observations*)
p	Une constante arbitraire (*An arbitrary constant*)
P_a	Puissance erosive hydraulique (*Hydraulic erosive power*)
q	Debit unitaire en m^2/s (*Unit discharge in m^2/s*)
Q	Débit dans le canal d'écoulement en m^3/s (*Discharge or Flow Rate in the flow channel in m^3/s*)
Q_{Pr}	Débit du prototype en l/s

	(*Discharge in prototype in l/s*)
Q_{RM}	Débit dans le modèle réduit en l/s (*Discharge in reduced-scale model in l/s*)
r	Rapport d'aspect ou rapport des espacements de joints (S_1/S_2) (*Aspect ratio or ratio of joint spacing*)
Re_{Pr}	Le nombre de Reynold's dans le prototype (*Reynold's number in prototype*)
Re_{RM}	Le nombre de Reynold's dans le modèle réduit (*Reynold's number in reduced-scale model*)
S_1	Espacement des joints le long de la face supérieure du bloc en m (*Joint spacing along the top face of the block in m*)
S_2	Espacement des joints le long de la hauteur du bloc en m (*Joint spacing along the depth of the block in m*)
S_f	Pente de frottement ou la pente de la ligne d'énergie totale en radians (*Friction slope or the slope of total energy line in radians*)
$Sinusoidal_i$	i^{ème} valeur sinusoïdale prédite de la charge dynamique en m (i^{th} *sinusoidal predicted value of dynamic head in m*)
t	Temps en s (*Time in s*)
T_{Pr}	Temps caractéristique du prototype en s (*Characteristic time in prototype in s*)
T_{RM}	Temps caractéristique du modèle réduit en s (*Characteristic time in reduced-scale in s*)
v / v_{ch}	Vitesse moyenne de l'écoulement dans le canal en m/s (*Mean Channel Flow Velocity in m/s*)
v_{Pr}	Vitesse d'écoulement dans le prototype en m/s (*Flow velocity in prototype in m/s*)
v_{RM}	Vitesse d'écoulement dans le modèle réduit en m/s (*Flow velocity in reduced-scale model in m/s*)
V_b	Volume du bloc en m^3/m (*Block volume in m^3/m*)
W'	Poids submergé du bloc en kN/m (*Submerged Weight of the block in kN/m*)
W_x'	Composante de W' selon l'axe X en kN/m (*Component of W' in X-direction in kN/m*)
W_y'	Composante de W' selon l'axe Y en kN/m (*Component of W' in Y-direction in kN/m*)

LISTE DES ABRÉVIATIONS

AR	Rapport d'amplitude (*Amplitude Ratio*)
AR-JO	Rapport d'amplitude – *JO* (*Amplitude Ratio – JO*)
ARMA	Moyenne mobile autorégressive (*Autoregressive Moving Average*)
ANOVA	Analysis of variance
CFD	Dynamique des fluides numériques (*Computational Fluid Dynamics*)
CFM	Mécanique de la fracture compréhensive (*Comprehensive Fractue Mechanics*)
CSM	Modèle d'érosion compréhensif (*Comprehensive Scour Model*)
CV	Coefficient de variation (*Coefficient of Variation*)
DEM	Méthode des éléments discrets (*Discrete Element Method*)
DI	L'impulsion dynamique (*Dynamic Impulsion*)
DWF	Direction d'écoulement (*Direction of Water Flow*)
eGSI	Indice de résistance géologique à l'érosion (*Erosion Geological Strength Index*)
FFT	Transformée de Fourier rapide (*Fast Fourier Transform*)
GSI	Indice de résistance géologique (*Geological Strength Index*)
LBM	Méthode de Boltzmann sur réseau (*Lattice Boltzmann Method*)
LF	Facteur de probabilité (*Likelihood factor*)
LVDT	Transformateur différentiel linéaire variable (*Linear Variable Differential Transformer*)
MVR	Rapport de valeur moyenne (*Mean Value Ratio*)
MVR-JO	Rapport de valeur moyenne – *JO* (*Mean Value Ratio – JO*)
NPES	Nature de la surface potentiellement érodable (*Nature of the potentially eroding surface*)
NRMSE	Erreur quadratique moyenne normalisée (Normalized *Root Mean Square Error*)
QSI	Impulsion quasi-statique (*Quasi Static Impulsion*)
RF	Facteur d'importance relative (*Relative importance factor*)
RMEI	Indice d'érodabilité du massif rocheux (*Rock Mass Erodibility Index*)
RMR	Cote de la masse rocheuse (*Rock Mass Rating*)
RMSE	Erreur quadratique moyenne (*Root Mean Square Error*)
RQD	Désignation de la qualité de la roche (*Rock Quality Designation*)
UCS	Résistance à la Compression Uniaxiale (*Unconfined Compressive Strength*)
UDEC	Code universel des éléments distincts (*Universal Distinct Element Code*)
UQAC	Université du Québec à Chicoutimi

DÉDICACE

À mes parents,

Je vous dois tout ce que je suis aujourd'hui. Merci infiniment d'avoir toujours été à mes côtés dans toutes mes décisions de ma vie que j'ai prises.

REMERCIEMENTS

Je tiens à exprimer ma plus profonde gratitude à mon directeur de recherche, le **Dr. Ali Saeidi**, pour son soutien indéfectible, ses conseils éclairés et ses encouragements constants tout au long de mon parcours doctoral. Sa flexibilité, sa patience et son engagement sans faille ont été déterminants pour m'aider à surmonter les nombreux défis de ce projet. Son expertise, sa rigueur scientifique et ses analyses critiques ont joué un rôle essentiel dans l'orientation et la qualité de mes travaux. Je le remercie également pour son appui continu dans mes demandes de bourses, qui m'ont permis de poursuivre ce chemin exigeant, mais enrichissant.

Je suis aussi profondément reconnaissant envers mon co-directeur, le **Dr. Alain Rouleau**, dont les commentaires pertinents et les suggestions précieuses ont grandement contribué à enrichir la clarté et la qualité de ma recherche. Ses critiques constructives, toujours formulées au moment opportun, ont élargi mes perspectives et approfondi mes analyses. Au-delà du cadre académique, son appui dans mon apprentissage du français a été particulièrement significatif. Il m'a constamment encouragé à progresser et m'a offert son aide chaque fois que j'en avais besoin.

Mes remerciements sincères s'adressent également à mon co-directeur industriel, le **Dr. Marco Quirion**, pour avoir stimulé ma curiosité scientifique et contribué à rapprocher mes travaux de la pratique professionnelle. Sa confiance dans mes recherches et son expertise en mécanique des roches ont renforcé la pertinence et la profondeur technique de cette étude.

Je tiens à exprimer ma reconnaissance au **Dr. Rama Vara Prasad Chavali**, mon mentor et collègue senior, pour ses conseils avisés et son soutien constant, surtout durant les premières étapes de ma recherche et mon adaptation à un nouvel environnement. Sa présence bienveillante a grandement facilité ma transition vers un milieu francophone, la rendant moins intimidante et plus stimulante.

Je tiens également à remercier les techniciens **Luc Chatigny** et **Carol Mercier** pour leur soutien technique et leur disponibilité tout au long de ce projet de recherche. Leur expertise et leur aide précieuse lors de la mise en place et de la réalisation des essais expérimentaux ont grandement contribué au bon déroulement de ce travail.

Je souhaite aussi remercier mon collègue et ami **ASM Fahad Hossein**, avec qui j'ai partagé de nombreux défis tout au long de ce doctorat. Nos expériences communes ont contribué de façon significative à mon développement personnel et académique. J'apprécie également le soutien de mes collègues étudiants et des membres du groupe de recherche **R2Eau**, à l'UQAC, dont les commentaires constructifs lors des présentations et des discussions ont été précieux à différentes étapes de ce projet.

Des remerciements particuliers vont au **Dr. Krishnaiah Sankranthi** (ancien professeur au baccalauréat) et au **Dr. Kalyan Kumar Gonavaram** (directeur de recherche à la maîtrise), dont l'encadrement m'a donné la confiance nécessaire pour m'engager dans une carrière de recherche et d'enseignement. J'exprime aussi ma reconnaissance envers mes aînés, qui n'ont cessé de m'inspirer et de soutenir mes ambitions académiques.

Enfin, je suis profondément redevable à ma **famille** pour leur amour inconditionnel, leur patience et leur foi inébranlable en moi. Leurs sacrifices et leur soutien moral ont constitué le socle de cette réussite. À mes **amis**, je dis merci pour avoir été une source constante de force, de motivation et d'encouragement tout au long de ce parcours.

Cette expérience m'a enseigné la valeur des perspectives diverses et l'importance de la persévérance dans la quête du savoir. Je suis sincèrement reconnaissant envers toutes les personnes qui, de près ou de loin, ont contribué à mon cheminement académique et personnel.

AVANT-PROPOS

La présente thèse s'inscrit dans le domaine du génie civil et du génie géotechnique, et plus particulièrement dans l'étude des mécanismes d'érosion hydraulique des massifs rocheux au droit des ouvrages hydrauliques. Les évacuateurs de crues, éléments essentiels à la sûreté des barrages, sont soumis à des sollicitations hydrauliques extrêmes pouvant entraîner des phénomènes d'érosion et d'instabilité des blocs rocheux, avec des conséquences potentiellement majeures sur la sécurité des infrastructures et des populations. Ce travail de recherche a été réalisé dans un contexte où les méthodes traditionnelles d'évaluation de l'érodabilité des roches, bien que largement utilisées en pratique, montrent certaines limites lorsqu'il s'agit de représenter fidèlement la complexité des interactions entre l'écoulement turbulent, les discontinuités du massif rocheux et la géométrie locale de la surface. Les événements récents observés sur plusieurs ouvrages à travers le monde soulignent la nécessité de mieux comprendre et de mieux quantifier ces phénomènes afin d'améliorer les approches de conception, d'analyse et de réhabilitation des évacuateurs de crues. L'objectif principal de cette thèse est de contribuer à l'amélioration des connaissances sur la distribution des pressions hydrauliques agissant à la surface et à l'intérieur des joints rocheux, en tenant compte de paramètres géométriques et géomécaniques représentatifs tels que l'ouverture des joints, la saillie des blocs et leur orientation. Pour ce faire, une approche expérimentale basée sur des essais en modèle physique a été privilégiée, permettant d'obtenir des données détaillées et de mieux appréhender les mécanismes responsables de l'instabilité des blocs rocheux soumis à des écoulements à haute énergie. Les résultats présentés dans ce manuscrit visent à enrichir la compréhension des processus en jeu et à fournir des éléments utiles tant pour la recherche académique que pour la pratique de l'ingénierie. Ils s'adressent aux chercheurs, aux ingénieurs et aux gestionnaires d'ouvrages intéressés par la sécurité des barrages et par le développement de méthodes d'évaluation plus robustes et mieux adaptées aux conditions réelles rencontrées sur le terrain.

CHAPITRE 1

INTRODUCTION

1.1 CONTEXTE GÉNÉRAL

Les barrages sont des ouvrages hydrauliques érigés sur des cours d'eau afin de répondre à divers besoins tels que l'entreposage de l'eau, la production hydroélectrique, la régulation des crues ou encore l'irrigation. Leur conception et leur construction reposent sur une interaction complexe entre plusieurs disciplines du génie civil, soit le génie structural, la géotechnique et l'hydraulique, afin d'assurer à la fois la rétention sécuritaire de l'eau emmagasinée et son évacuation contrôlée. Chaque barrage est conçu pour contenir un volume maximal de retenue et maintenir un niveau d'eau sécuritaire, ainsi que des seuils à ne pas dépasser pour garantir sa stabilité structurale et son bon fonctionnement. Au Canada, les inondations causées par les précipitations et la fonte des neiges représentent la catastrophe naturelle la plus fréquente et la plus coûteuse, engendrant des dommages dépassant les 2 milliards de dollars par année (NRCan, 2022). Les apports excédentaires associés à ces événements dépassent souvent la capacité de retenue et nécessitent alors le relâchement des eaux par les évacuateurs de crues, tout en préservant l'intégrité des ouvrages. Ces structures sont généralement aménagées dans des massifs rocheux géologiquement stables. Quelques exemples d'évacuateur de crues non revêtu sont présentés dans la figure 1.1. Lorsque le substrat rocheux présente une qualité suffisante, l'évacuateur peut être aménagé par excavation contrôlée (blasting), laissant une surface non revêtue. En revanche, lorsque le massif est trop fracturé ou altéré, les évacuateurs de crues sont recouverts de béton armé et ancrés dans la roche pour en assurer la résistance et la durabilité face aux écoulements à grande vitesse. Bien que ces précautions aient été prises lors de la conception, l'érosion du massif rocheux reste un enjeu persistant (Pells et al. 2015; Rock, 2015). Ce problème est amplifié par la présence de discontinuités naturelles comme les joints, fissures et fractures. Selon les conditions hydrauliques, on distingue deux principaux types d'évacuateurs de crues : les structures à écoulement parallèle et celles à jet plongeant, chacune présentant des mécanismes d'érosion distincts. Des cas réels ont montré que l'érosion du massif rocheux peut causer des dommages majeurs, voire des ruptures catastrophiques, comme ce fut le cas en 2017 avec la défaillance de l'évacuateur de crues du barrage d'Oroville, en Californie (Koskinas et al., 2019;

Stofleth et al., 2023; Zhang et al., 2024). Des ravinements de plusieurs mètres de profondeur ont également été rapportés au barrage Mokolo, en Afrique du Sud, ainsi qu'au barrage Copeton, en Australie (Boumaiza, 2019; Pells, 2016). Les conséquences d'une érosion incontrôlée ne se limitent pas aux dommages structuraux : elles entraînent aussi des coûts de réparation ou de reconstruction colossaux, en plus de menacer la sécurité des populations et des habitats situés en aval (Pells et al., 2017; Sawadogo, 2010).

Le Canada est l'un des plus grands producteurs d'hydroélectricité au monde, Hydro-Québec y occupant une place de premier plan. L'entreprise gère un vaste réseau de barrages et de centrales répartis à travers le territoire québécois. Avec ses 61 centrales hydroélectriques, elle joue un rôle essentiel dans l'approvisionnement en énergie renouvelable, tant au Canada qu'aux États-Unis. Or, dans plusieurs installations d'Hydro-Québec, des signes d'érosion du massif rocheux ont été observés aux évacuateurs de crues, soulignant l'importance de développer une méthode d'évaluation de l'érosion à la fois adéquate et fiable. Le concept d'érosion du massif rocheux est complexe et repose sur deux facteurs principaux : (1) la capacité de résistance du massif et (2) la force érosive hydraulique (Annandale, 1995; Jalili Kashtiban et al., 2021; Pells et al., 2017). La force érosive correspond à l'énergie physique de l'eau en mouvement, laquelle dépend de la vitesse d'écoulement, de la turbulence, de la concentration d'air, de la cavitation et des pressions de soulèvement. Quant à la résistance du massif rocheux, elle correspond à sa capacité à s'opposer à ces forces hydrauliques et dépend de ses propriétés mécaniques ainsi que de son intégrité structurelle. La présence de joints ou de fractures diminue généralement cette résistance, ce qui accroît sa vulnérabilité face aux forces érosives.

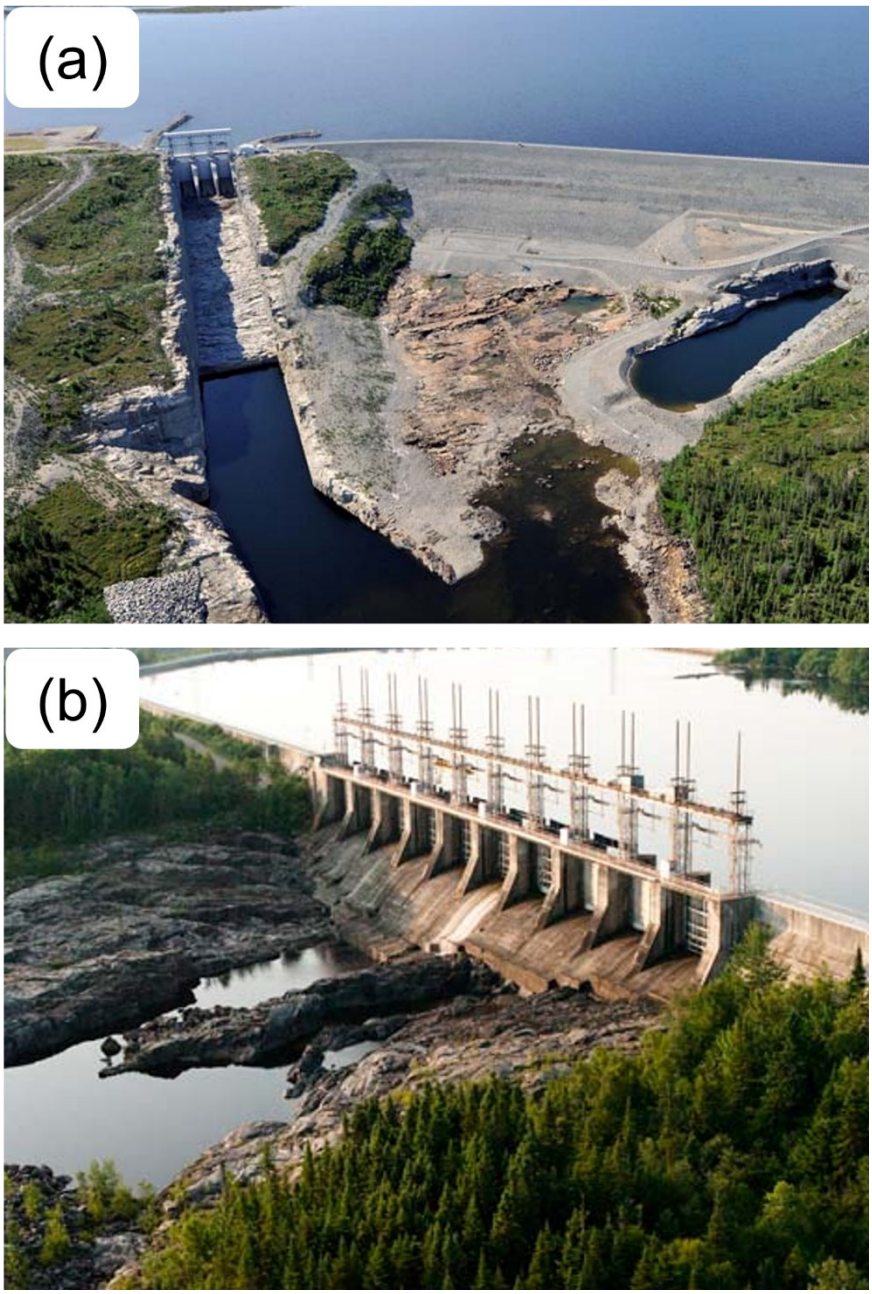

Figure 1.1 Exemples d'évacuateur de crues non revêtu des barrages : (a) Eastmain 1 sur la rivière La Grande; (b) Manic 1 sur la rivière Manicouagan (Source : Hydro-Québec)

Les évacuateurs de crues existants ont été conçus à partir des méthodes d'évaluation de l'érosion disponibles à l'époque. Or, de nombreux cas d'érosion ont néanmoins été observés. Cette situation démontre la nécessité de développer une nouvelle méthode d'évaluation, plus robuste et mieux adaptée, reposant sur l'identification des paramètres hydrauliques et géomécaniques représentatifs qui contrôlent

l'érodabilité des massifs rocheux. Les travaux antérieurs et la littérature scientifique ont servi à dégager les paramètres clés à considérer. Le présent projet met l'accent sur l'aspect géomécanique, en examinant l'effet de paramètres liés aux joints, notamment leur ouverture, la saillie et l'orientation, sur l'érodabilité du massif rocheux à l'aide d'essais en laboratoire. À cette fin, un modèle physique d'évacuateur de crues à l'échelle pilote, développé à l'Université du Québec à Chicoutimi (UQAC), a été utilisé. Ce modèle a été conçu pour reproduire des conditions d'écoulement réalistes, permettant d'étudier la stabilité des blocs à partir de mesures précises des pressions hydrauliques sous diverses configurations géomécaniques. La modélisation physique permet également d'analyser séparément l'effet de plusieurs paramètres et, ainsi, d'identifier les facteurs déterminants. Ce projet vise donc à approfondir la compréhension du phénomène d'érosion du massif rocheux et à contribuer au développement d'outils fiables pour évaluer l'érodabilité dans les conditions réelles d'exploitation des barrages.

1.2 PROBLÉMATIQUE

Au cours des dernières décennies, plusieurs méthodes d'évaluation de l'érodabilité ont été proposées par différents chercheurs. Ces méthodes peuvent être regroupées en trois grandes catégories : les méthodes semi-empiriques, les méthodes semi-analytiques et les méthodes numériques. Les méthodes semi-analytiques reproduisent relativement bien certains mécanismes d'érosion, mais elles n'intègrent pas les effets des paramètres géomécaniques. À l'inverse, les méthodes semi-empiriques les plus courantes tiennent compte de divers paramètres hydrauliques et géomécaniques, mais elles ne représentent pas explicitement les mécanismes particuliers qui gouvernent le processus d'érosion. L'approche la plus couramment utilisée, parmi les méthodes semi-empiriques existantes, demeure celle d'Annandale (2006), fondée sur l'indice de Kirsten (1982), qui avait initialement été développé pour évaluer l'excavabilité des géomatériaux. Toutefois, cet indice ne tient pas compte de l'ensemble des paramètres influençant directement l'érosion. La valeur de résistance du massif qui y est considérée repose sur la résistance à la compression uniaxiale (*UCS*) ainsi que sur des paramètres tels que la désignation de la qualité de la roche (*RQD*). Or, Pells et al. (2017a) ont soutenu que ni l'*UCS* ni le *RQD* ne constituent des paramètres efficaces pour évaluer l'érodabilité d'un massif rocheux. Dans plusieurs cas, des contradictions ont d'ailleurs été relevées entre les prédictions issues de la méthode d'Annandale

et les observations réelles effectuées sur des barrages en exploitation. Concernant les méthodes semi-empiriques développées par Pells, l'indice *eGSI* n'intègre pas les effets de l'ouverture des joints ni ceux de la saillie des blocs, tandis que l'indice *RMEI* repose uniquement sur une approche qualitative. De plus, aucun fondement scientifique rigoureux n'est présenté pour justifier la pondération attribuée aux paramètres. Par conséquent, ces méthodes ne permettent pas d'établir une relation satisfaisante entre les paramètres hydrauliques et géomécaniques qui contrôlent le processus d'érosion. La force érosive de l'eau transmise à la surface du massif rocheux et à l'intérieur des discontinuités est directement influencée par les paramètres géomécaniques. Ainsi, toute variation d'un paramètre géomécanique est susceptible de modifier la distribution de pression hydraulique et le potentiel d'érosion.

Le développement d'une méthode d'évaluation fiable nécessite donc une compréhension approfondie de l'effet individuel des différents paramètres pertinents. Bien que la modélisation numérique constitue une solution prometteuse à cet égard, les limites associées aux modèles couplés actuellement en développement restreignent encore leur applicabilité. Dans l'état actuel des connaissances, les essais sur modèles physiques demeurent l'option la plus crédible et la plus robuste pour analyser ces interactions complexes entre l'hydraulique et la géomécanique. L'effet individuel de plusieurs paramètres géomécaniques pertinents sur la force érosive transmise au massif et sur la profondeur d'érosion doit être étudié. Dans ce contexte, la présente recherche s'articule autour de ces questions scientifiques structurantes :

- Quel est l'effet individuel des différents paramètres géomécaniques sur la distribution de pression hydraulique ?
- Quel est l'effet de ces paramètres sur la stabilité d'un bloc de massif rocheux ?

1.3 OBJECTIFS DE RECHERCHE

L'objectif global du programme de recherche de notre équipe est de développer une méthode prédictive de l'érosion d'un massif rocheux comprenant l'interaction entre les paramètres hydrauliques et géomécaniques. Pour ce projet-ci, l'objectif général consiste à évaluer l'influence de la géométrie des joints et de la rugosité de surface sur les pressions hydrauliques et la stabilité des blocs dans un

évacuateur de crues expérimental à l'échelle du laboratoire. Afin de répondre à cet objectif-général, les objectifs spécifiques suivants ont été définis :

1. Réaliser des essais de modèle physique afin d'analyser l'effet de l'ouverture des joints et de la saillie des blocs sur la distribution des pressions hydrauliques.
2. Développer un modèle mathématique prédictif permettant d'estimer les fluctuations de pression en surface de l'évacuateur de crues en fonction de ces paramètres.
3. Déterminer l'effet de l'orientation des joints sur l'occurrence du soulèvement, à partir des résultats expérimentaux.
4. Évaluer l'influence de la géométrie et de l'orientation des blocs sur la stabilité.

1.4 MÉTHODOLOGIE

La méthodologie de recherche est divisée en quatre volets principaux : la réalisation d'essais de modèle physique avec différentes ouvertures des joints et saillies des blocs pour observer leurs effets sur la pression hydraulique sur les faces des blocs ; le développement d'une prédiction mathématique en fonction des paramètres d'études ; la détermination de l'effet de l'orientation des joints sur le processus d'érosion ; et la détermination de l'effet de la géométrie et de l'orientation des blocs sur leur stabilité. Chacun de ces volets est présenté dans l'organigramme à la figure 1.2.

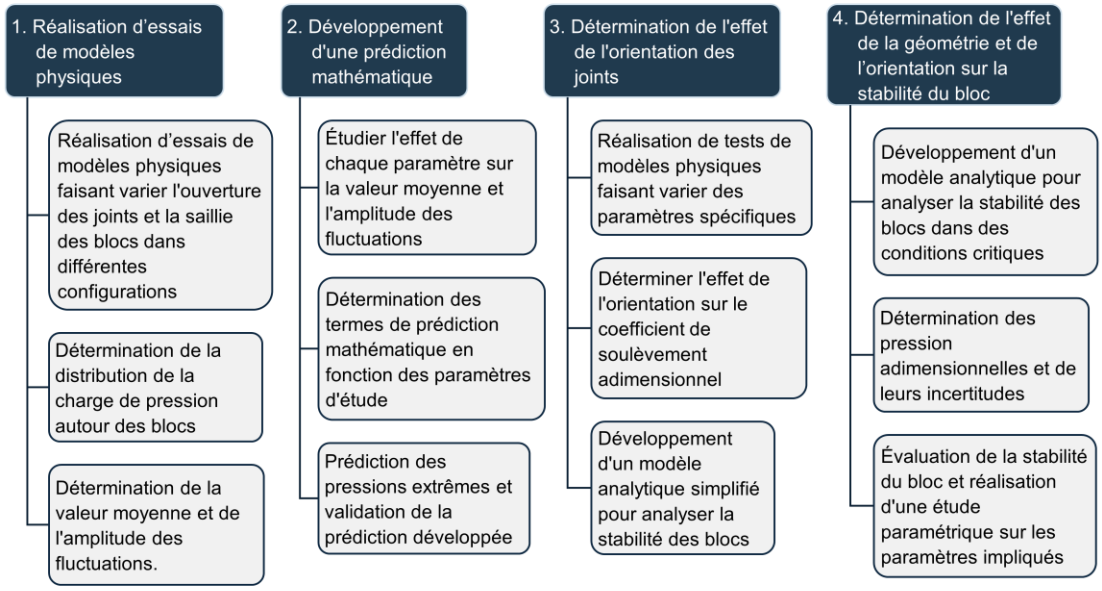

Figure 1.2. La méthodologie appliquée dans cette étude

1.4.1 Essais sur modèle physique avec différentes valeurs d'ouverture de joint et de saillie

Un examen approfondi des essais antérieurs sur modèles physiques et des conditions de terrain a permis de sélectionner des valeurs représentatives d'ouverture de joints, de configurations de saillie et de hauteurs de saillie pour les essais expérimentaux. Les tests ont été effectués sur le modèle réduit construit à l'UQAC, à une échelle de 1:40, simulant l'évacuateur de crues du barrage Romaine-4 d'Hydro-Québec (figure 1.3) (Koulibaly et al., 2023; Wisse et al., 2023). Neuf blocs-modèles en béton (150 × 150 × 300 mm) ont été installés dans une boîte métallique située à l'extrémité aval du canal, permettant de faire varier les paramètres d'essai. Les blocs ont été disposés en configuration 3 × 3, le bloc central étant instrumenté selon la méthodologie proposée par Wisse et al. (2023). Ce bloc central est équipé de tuyaux intégrés dans le béton qui sont attachés par les coudes aux entrées et aux sorties de l'eau. Ces coudes permettent de mieux mesurer la pression dynamique dans les joints. Un total de cinq configurations de saillie, chacune avec deux hauteurs distinctes (sauf la *Conf. 0*), ainsi que trois ouvertures de joints, ont été testés (tableau 1.1) sous différents débits (180, 240, 310 et 340 l/s). Pour chacune des configurations, les trois blocs dans chaque rangée transversale à l'écoulement sont mis au même niveau. La distribution des pressions dynamiques mesurée autour du bloc dans diverses conditions d'essai a permis de calculer la valeur moyenne et l'amplitude des fluctuations. Ces données ont servi à

évaluer l'effet de l'ouverture des joints et de la saillie des blocs sur le processus d'érosion par soulèvement.

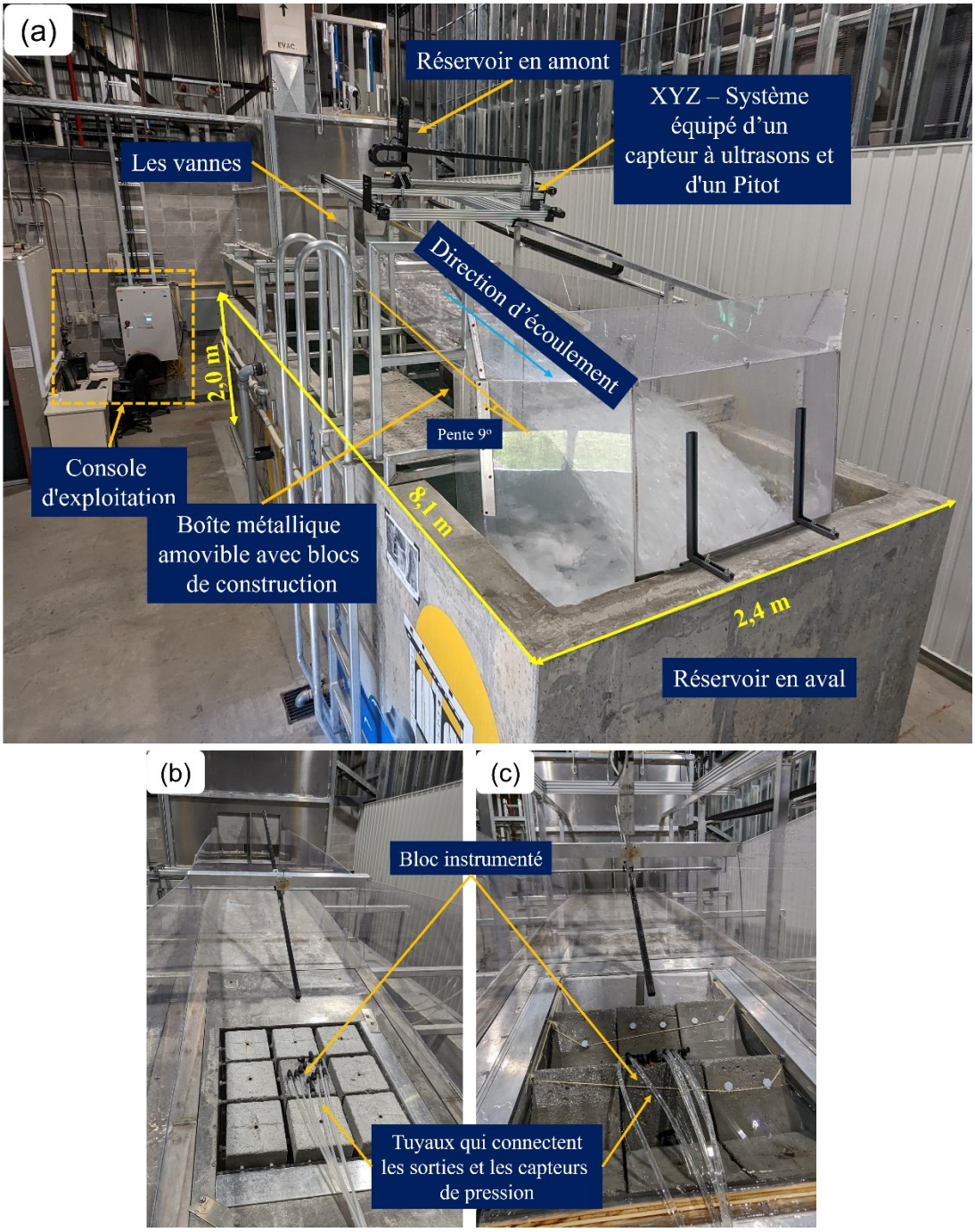

Figure 1.3 Modèle physique d'évacuateur de crues à échelle réduite de l'UQAC : (a) Description de différents éléments du modèle; (b) vue avec le montage des blocs en 0°; (c) Vue avec le montage des blocs en – 45°

Tableau 1.1 Configurations de saillie utilisées dans ce projet avec les hauteurs de saillie et ouvertures de joints correspondantes

Configuration, *Conf.* #	**Installation**	**L'ouverture de joints, *JO* (mm)**	**La saillie du bloc, *BP* (mm)**	**Saillie à la 1ère rangée (mm)**	**Saillie à la 2ème rangée (mm)**	**Saillie à la 3ème rangée (mm)**
0	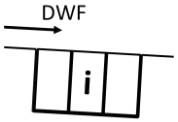	3, 10 et 20	*BP0* = 00	00	00	00
1	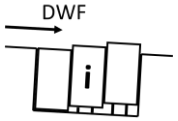	3, 10 et 20	*BP1* = 06 *BP2* = 13	00 00	06 13	12 26
2	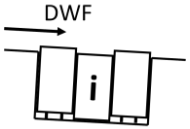	3, 10 et 20	*BP1* = 13 *BP2* = 20	13 20	0 0	13 20
3	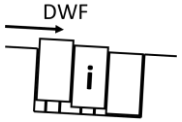	3, 10 et 20	*BP1* = 06 *BP2* = 13	13 26	06 13	0 0
4	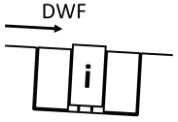	3, 10 et 20	*BP1* = 13 *BP2* = 20	00 00	13 20	00 00

DWF – Direction d'écoulement

1.4.2 Développement d'une prédiction mathématique

La stabilité d'un bloc dépend entièrement des pressions hydrauliques exercées sur ses faces, particulièrement sur la face supérieure et la face inférieure. Une situation critique survient lorsque la pression au-dessus du bloc atteint un minimum tandis que celle en dessous atteint un maximum. Ces pressions varient selon les paramètres géomécaniques étudiés (débit, ouverture des joints, hauteur de saillie et configuration). Il est donc essentiel d'identifier les pressions extrêmes en fonction de ces paramètres afin de mieux évaluer les conditions menant au soulèvement. Pour représenter ces pressions fluctuantes, une équation sinusoïdale a été élaborée. Les termes de cette équation correspondent à la moyenne et à l'amplitude des données de pression, obtenues dans l'étape précédente. Ces grandeurs permettent de traduire les fluctuations mesurées sous forme de variations sinusoïdales en fonction de la saillie des blocs et de l'ouverture des joints. Le modèle sinusoïdal ainsi construit a ensuite été validé au moyen de nouveaux essais réalisés avec un débit et une hauteur de saillie différents de ceux employés lors de son élaboration.

1.4.3 Détermination de l'effet de l'orientation des joints

L'influence de l'orientation des joints sur la distribution des pressions hydrauliques a été étudiée au moyen d'essais sur modèle physique pour trois orientations distinctes (figure 1.4) et pour des ouvertures de joints de 3, 10 et 20 mm. Pour disposer les blocs selon différentes orientations, deux boîtes métalliques distinctes ont été utilisées, tel qu'expliqué par Koulibaly et al. (2023). Dans les conditions inclinées, les blocs forment une surface en zigzag à la base de l'évacuateur, comme déjà observé dans les essais de Reinius (1986) et repris dans le développement du paramètre E_{doa} par Pells (2016). Afin de garantir la précision des mesures de pression, les blocs inclinés ont été fixés empêchant tout mouvement latéral susceptible de biaiser les résultats. Les données de pression obtenues ont permis de calculer les valeurs du coefficient adimensionnel de soulèvement (C_{up}'). La force hydraulique exercée par l'écoulement sur chaque face du bloc (F) a été déterminée comme le produit du poids volumique de l'eau, de l'aire de la face et de la pression dynamique. Une analyse de sensibilité a ensuite été réalisée sur plusieurs variables (pressions dynamiques, coefficients de variation, coefficient de soulèvement), en

fonction du débit et de l'orientation des joints. Enfin, un modèle analytique simplifié a été élaboré pour analyser l'occurrence du soulèvement dans les conditions géométriques étudiées, puis validé à l'aide des mesures expérimentales.

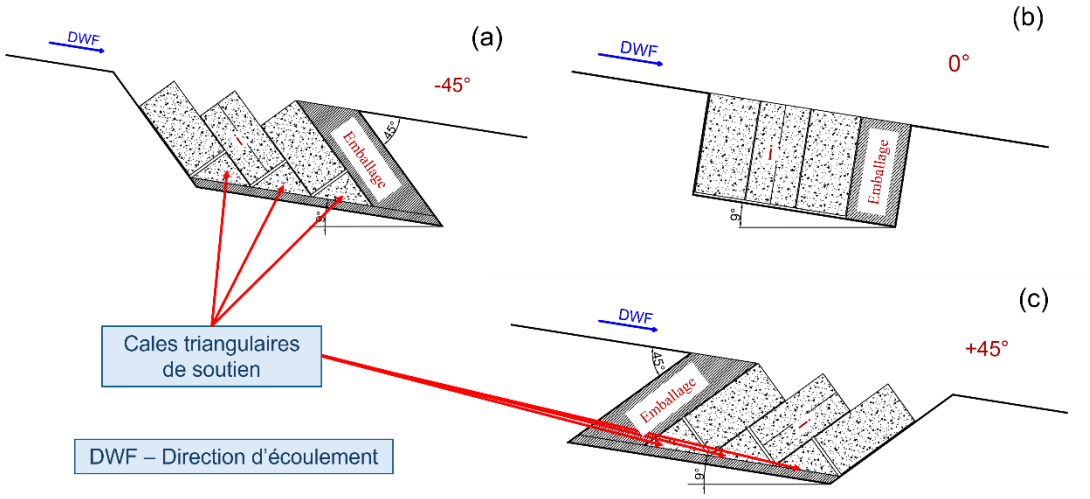

Figure 1.4 Alignement des blocs selon différentes orientations retenues pour les joints: (a) -45°; (b) 0° et (c) +45°

1.4.4 Détermination de l'effet de la géométrie et de l'orientation des blocs sur leur stabilité

Pour étudier l'effet de la géométrie et de l'orientation des blocs sur leur stabilité, le modèle analytique défini précédemment a été utilisé. Comme défini précédemment, les conditions critiques surviennent lorsque la pression hydraulique est minimale au-dessus du bloc et maximale au-dessous. Les pressions dynamiques mesurées dans les étapes antérieures ont servi à identifier les ensembles de valeurs extrêmes (maxima et minima). Un code MATLAB a permis de définir un seuil de 3 % correspondant aux données situées à l'extérieur de l'intervalle $\mu \pm 2\sigma$ (où μ est la moyenne et σ l'écart-type). Ces valeurs extrêmes, normalisées par la vitesse moyenne du canal, ont été utilisées pour analyser la variation des pressions maximales et minimales en fonction de l'ouverture des joints, de la saillie et de l'orientation des blocs. Les coefficients de soulèvement ainsi obtenus ont servi de base à l'analyse de stabilité. Par la suite, une étude paramétrique a permis d'examiner l'effet de la géométrie des blocs, notamment le rapport d'aspect et la longueur exposée, sur l'instabilité. Le rapport d'aspect est défini comme le rapport

entre les espacements caractéristiques des joints qui déterminent la forme géométrique des blocs rocheux. La longueur exposée, dans le cas des blocs orientés à -45°, correspond à la longueur de la face d'un bloc directement exposée à la base du chenal et soumise à l'action de l'écoulement.

1.5 ORIGINALITÉ

Cette recherche apporte une contribution originale à l'étude de l'érosion hydraulique du massif rocheux en évaluant de manière systématique l'influence de paramètres géomécaniques clés – ouverture des joints, saillie des blocs et orientation des joints, sur la distribution des pressions hydrauliques et sur la stabilité des blocs dans les évacuateurs de crues. Elle permet d'abord de déterminer l'effet de l'ouverture des joints et de la saillie des blocs sur la pression fluctuante à la surface de l'évacuateur qui est un point critique du processus d'érosion hydraulique. En analysant ces paramètres de façon individuelle, la recherche met en évidence leur rôle spécifique dans la modification de pression transmise au massif rocheux. Elle permet également d'identifier l'effet de l'orientation des joints sur les principaux mécanismes d'instabilité des blocs, en distinguant explicitement les modes d'instabilité par soulèvement et par basculement. Cette approche contribue à une meilleure compréhension des conditions géométriques favorisant chacun de ces mécanismes d'endommagement. Enfin, l'influence des principaux paramètres géomécaniques sur le processus d'érosion est évaluée à l'aide d'un coefficient adimensionnel de soulèvement, couramment utilisé en pratique. Le modèle analytique développé explique les mécanismes d'instabilité des blocs et présente une étude paramétrique des facteurs influençant leur stabilité. La méthodologie proposée pour isoler l'effet individuel de chaque paramètre constitue une étape centrale vers l'élaboration d'un système de pondération robuste, en vue de définir un indice de résistance du massif rocheux plus représentatif de la réalité.

1.6 PLAN DE LA THÈSE

Cette thèse repose sur trois articles scientifiques, présentés aux chapitres 3 à 5. La structure générale de ces articles comprend : résumé, introduction, description du modèle physique, méthodologie, résultats, discussion et conclusion.

Le CHAPITRE 1 introduit la recherche en présentant l'objectif principal de l'étude et en mettant l'accent sur les questions de recherche. Ce chapitre précise ensuite les objectifs de recherche et donne un aperçu clair de la méthodologie employée pour les atteindre. Il se conclut par un plan général de la thèse, offrant au lecteur une feuille de route des chapitres suivants.

Le CHAPITRE 2 propose une revue de littérature exhaustive sur les méthodes d'évaluation de l'érosion, en mettant l'accent sur les différents paramètres impliqués dans l'analyse du processus d'érosion. Il explore ensuite les mécanismes de défaillance associés à l'érosion à partir des études antérieures. Une analyse comparative des différentes méthodes d'évaluation de l'érosion y est également présentée, soulignant les paramètres essentiels à quantifier pour élaborer une méthode d'évaluation robuste et fiable.

Le CHAPITRE 3 répond aux objectifs spécifiques 1 et 2 de ce projet en examinant l'influence de paramètres géomécaniques spécifiques, soit l'ouverture des joints et la saillie des blocs, sur la distribution des pressions hydrauliques autour des blocs rocheux, à partir d'essais réalisés sur modèle physique. Ce chapitre développe également un modèle mathématique destiné à prédire les fluctuations de pression hydraulique à la surface d'un évacuateur de crues, en fonction de ces paramètres clés. Ce modèle est formulé sous une forme adimensionnelle, facilitant sa comparaison avec les résultats d'autres modèles physiques.

Le CHAPITRE 4 répond à l'objectif spécifique 3 de ce projet et s'intéresse aux effets de l'orientation des joints, combinée à différentes ouvertures, sur la distribution des pressions hydrauliques autour des blocs rocheux, à partir d'essais physiques. Ce chapitre explore aussi les divers modes d'instabilité des blocs observés dans les différentes conditions expérimentales. De plus, un modèle analytique préliminaire est proposé pour étudier les instabilités des blocs observées en lien avec les conditions expérimentales.

Le CHAPITRE 5 répond à l'objectif spécifique 4 de ce projet et affine le modèle analytique développé au CHAPITRE 4 en intégrant des paramètres supplémentaires, comme la saillie des blocs en plus de l'orientation des joints, afin d'évaluer leur influence sur la stabilité des blocs. Les résultats des

essais sur modèle physique, ainsi que les incertitudes associées, sont utilisés pour analyser l'effet de ces paramètres sur la stabilité. Ce chapitre étudie également l'influence de la géométrie des blocs sur la variation du facteur de sécurité en fonction des différents modes d'instabilité identifiés au CHAPITRE 4.

Le CHAPITRE 6 présente une synthèse des principaux résultats obtenus et propose des recommandations pour les recherches futures, en s'appuyant sur les connaissances acquises concernant l'influence des paramètres géomécaniques sur l'érosion du massif rocheux dans les évacuateurs de crues de barrages.

CHAPITRE 2

REVUE DE LITTÉRATURE SUR LES MÉTHODES D'ÉVALUATION DE L'ÉROSION

La compréhension du processus d'érosion d'un massif rocheux constitue un champ de recherche vaste et complexe, qui requiert une analyse approfondie et multidisciplinaire. Dans cette section, les principaux mécanismes d'érosion sont d'abord présentés, suivis d'un survol des méthodes existantes utilisées pour en évaluer l'intensité et les effets. Par la suite, plusieurs travaux de recherche fondés sur des approches analytiques, expérimentales et numériques sont exposés et discutés, afin de mettre en lumière leurs apports et leurs limites.

2.1 MÉCANISMES PRINCIPAUX DE L'ÉROSION DU MASSIF ROCHEUX

Plusieurs mécanismes d'érosion peuvent se manifester à proximité des ouvrages de génie civil. Parmi ceux-ci figurent l'abrasion, la fracturation du massif rocheux, le soulèvement et l'arrachement de blocs, la cavitation, ainsi que le déchaussement (underpinning). Toutefois, quatre mécanismes sont généralement considérés comme les plus significatifs (Bollaert, 2010) et sont illustrés à la figure 2.1 :

i. Abrasion des blocs rocheux (phénomène à long terme)
ii. Fracturation de la roche intacte (rupture fragile ou par fatigue)
iii. Soulèvement ou arrachement de blocs (sous l'effet des pressions hydrauliques dans les joints, de l'écoulement de l'eau ou du cisaillement le long d'un joint)
iv. Soulèvement impulsif ou délamination de blocs

Parmi ces mécanismes, l'arrachement de blocs et la fracturation fragile de la roche intacte se produisent de façon instantanée lorsque l'énergie hydraulique est suffisante. Dans le cas de l'arrachement, des blocs entièrement isolés et distincts peuvent être déplacés de leur position sous l'action des pressions hydrauliques agissant autour d'eux. La fracturation de la roche peut être expliquée à partir de la théorie de l'élasticité : l'amorçage et la propagation des fissures dépendent de l'intensité des contraintes au front d'une fissure et de la résistance à la rupture de la roche. Lorsque les contraintes excèdent cette résistance, une rupture fragile instantanée se produit. Dans d'autres cas, une fracturation

par fatigue peut se développer graduellement en fonction de l'intensité et de la répétition des contraintes (Atkinson, 1987). La littérature rapporte plusieurs exemples de fracturation par fatigue attribuables à la présence de pressions transitoires air-eau intenses à l'intérieur des joints rocheux (Bollaert 2002, 2004). Les conditions d'écoulement peuvent également engendrer des forces quasi-statiques de soulèvement et de traînée, dépendant de divers paramètres hydrauliques et géomécaniques, qui favorisent la délamination des blocs (Bollaert, 2010). Ces différents mécanismes peuvent agir de manière interdépendante ou indépendante, selon les caractéristiques du massif rocheux et les conditions hydrauliques. Enfin, le mécanisme d'abrasion correspond à l'usure progressive des surfaces rocheuses, causée à la fois par l'écoulement et par les particules transportées par celui-ci. Ce processus, bien que réel, peut être considéré comme secondaire dans le contexte des évacuateurs de crues puisqu'il nécessite un temps beaucoup plus long pour se manifester par rapport aux autres mécanismes (Whipple et al., 2000).

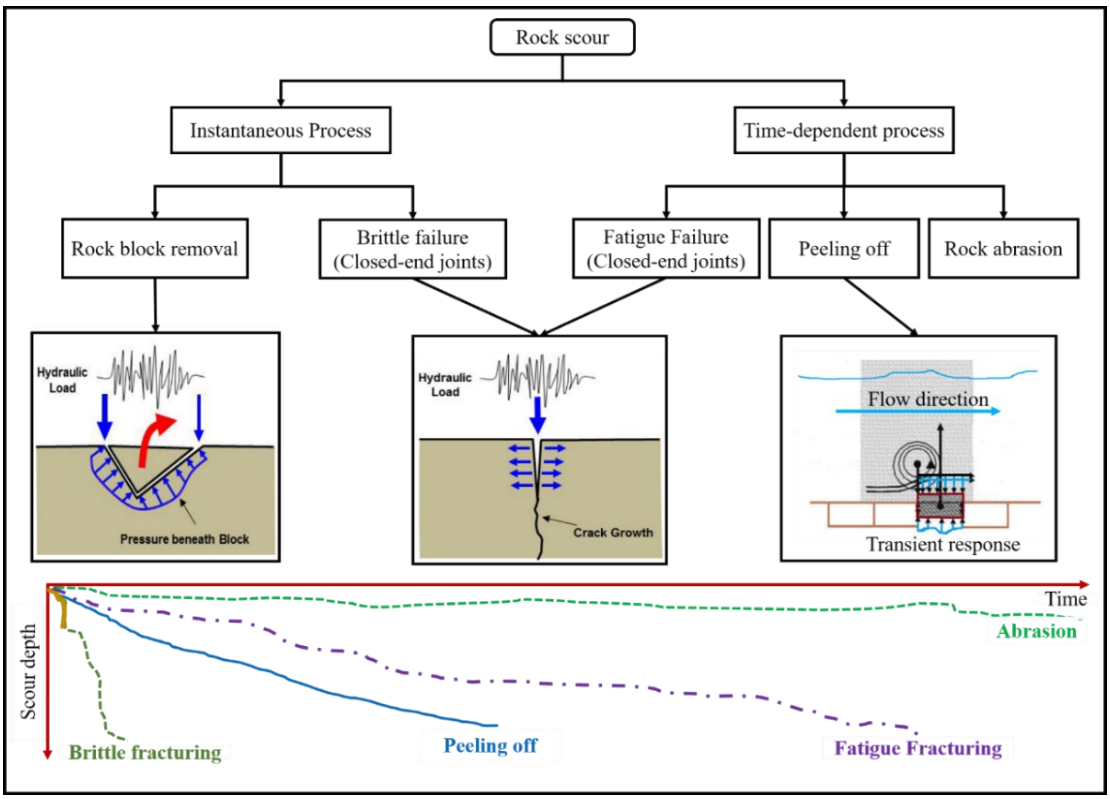

Figure 2.1 Mécanismes principaux de l'érosion du massif rocheux et leurs échelles de temps (Jalili Kashtiban et al., 2021)

2.2 MÉTHODES EXISTANTES D'ÉVALUATION DE L'ÉROSION

De nombreux chercheurs se sont intéressés à l'érosion des massifs rocheux et ont proposé diverses méthodes d'évaluation. Une revue de ces approches a été présentée par Jalili Kashtiban et al. (2021). Dans l'ensemble, la majorité de ces méthodes peut être regroupée en deux grandes catégories : les méthodes semi-empiriques et les méthodes semi-analytiques. Les méthodes semi-empiriques établissent une corrélation entre les forces érosives hydrauliques et la capacité de résistance du massif rocheux, sur la base d'observations de terrain. Les méthodes semi-analytiques, quant à elles, reposent sur des équations classiques dérivées d'essais à échelle réduite, permettant de calculer les profondeurs d'érosion.

2.2.1 Différents indices utilisés dans les méthodes semi-empiriques

Parmi ces approches, les méthodes semi-empiriques demeurent les plus répandues en raison de leur facilité d'application. Elles définissent les seuils d'érosion en fonction de la puissance érosive

hydraulique, P_a et de la capacité de résistance du massif rocheux, $f(K_h)$ (Annandale, 1995; Moren & Sjoberg, 2007; Pells et al., 2015), selon les niveaux d'érosion observés, tel qu'illustré à l'Éq. 2.1. Si $P_a > f(K_h)$, la puissance érosive excède la résistance du massif, entraînant l'érosion du matériau. Si $P_a < f(K_h)$, la puissance érosive est inférieure à la résistance du massif, garantissant sa stabilité (Annandale et al., 1998; Kirsten et al., 2000; Pells, 2016). La force érosive de l'eau est liée aux pressions hydrauliques fluctuantes, représentant le taux de dissipation d'énergie dans l'écoulement. Cette énergie hydraulique est généralement désignée sous le terme de puissance spécifique disponible (P_a) ou de dissipation unitaire de puissance (Π_{UD}), exprimée en kW/m² (Éq. 2.2). Le taux de dissipation d'énergie dépend de la turbulence : une turbulence accrue entraîne des taux de dissipation plus élevés et, en conséquence, des pressions fluctuantes d'amplitude plus importante. La figure 2.2 illustre la variation des propriétés de l'écoulement dans un canal ouvert entre deux sections (figure 2.2a), ainsi qu'une coupe transversale du canal (figure 2.2b).

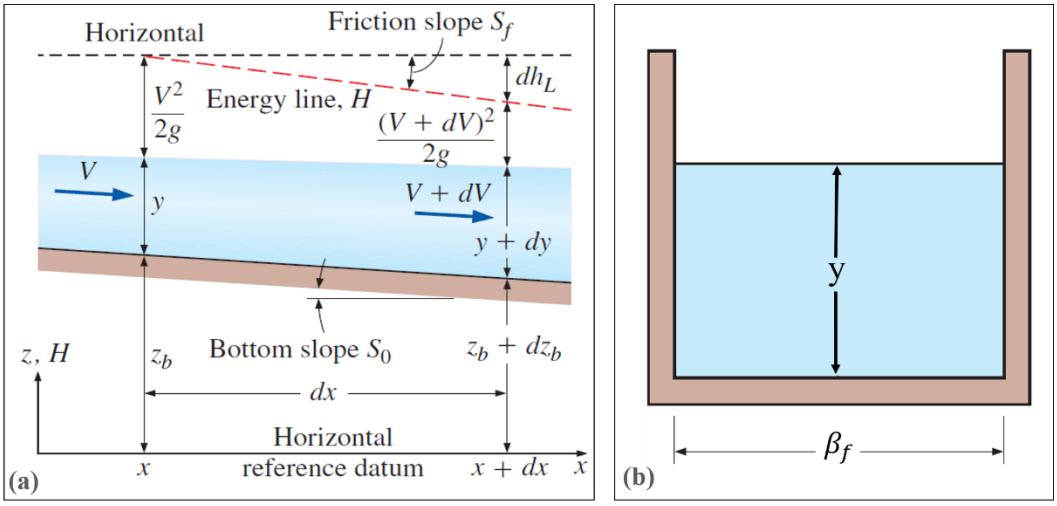

Figure 2.2 Variation des propriétés de l'écoulement dans un canal ouvert (Jalili Kashtiban et al., 2021)

$$P_a = f(K_h) \qquad \text{Éq. 2.1}$$

$$\Pi_{UD} = \gamma_w q \frac{dE}{dx} = \rho_w g \frac{Q}{\beta_f} \frac{dE}{dx} = \rho_w g \frac{Q}{\beta_f} \frac{dh_l}{dx} = \rho_w g q(S_f) \qquad \text{Éq. 2.2}$$

Où,

γ_w représente le poids volumique de l'eau (en kN/m^3) = $\rho_w.g$,

ρ_w représente la masse volumique de l'eau (en kg/m^3),

g représente l'accélération gravitationnelle (en m/s^2),

q représente le débit unitaire (en m^2/s) = le débit par unité de largeur = $\frac{Q}{\beta_f}$,

Q représente le débit total (en m^3/s),

β_f représente la largeur de la section d'écoulement mesurée à la surface de l'eau (en m), et

$S_f = \frac{dh_l}{dx}$ représente la pente de la ligne d'énergie totale ou la pente de frottement (référez à la figure 2.2).

Ces équations ont servi de base à l'estimation de la dissipation unitaire de puissance. Annandale (1995) les a adaptées afin d'évaluer la capacité érosive dans divers contextes : canaux ouverts, seuils, ressauts hydrauliques, entailles (head cuts) et fosses de dissipation (plunge pools). Toutefois, ces équations s'appliquent à des surfaces lisses d'évacuateurs de crues et ne tiennent pas compte des irrégularités liées au dynamitage lors de la construction. Plus récemment, Jalili Kashtiban et al. (2023a, b) ont étudié l'effet de ces irrégularités géométriques sur l'énergie hydraulique de l'écoulement. Jalili Kashtiban (2023) a proposé une modification de l'équation de dissipation unitaire afin d'y intégrer les pertes associées aux irrégularités de surface et à la géométrie.

Pour estimer la capacité de résistance du massif rocheux, certains chercheurs ont d'abord proposé l'utilisation de systèmes de classification existants tels que le *Rock Mass Rating* (*RMR*) (Bieniawski, 1973), le Q-System (Barton et al., 1974) et le Geological Strength Index (*GSI*) (Hoek et al., 1995), qui tiennent compte de plusieurs paramètres liés à l'érodabilité (Moore, 1991; Pitsiou, 1990). Ces méthodes ont toutefois été critiquées, car elles avaient été conçues initialement pour des contextes différents (excavations souterraines, stabilité des pentes, conception de soutènements). Kirsten (1982) a proposé un indice destiné à évaluer l'excavabilité des géomatériaux, intégrant plusieurs paramètres du système *Q* de Barton. Cet indice, connu sous le nom d'indice de Kirsten, a ensuite été adapté à l'étude de l'érodabilité hydraulique en remplaçant la direction d'excavation par celle de l'écoulement. Van Schalkwyk et al. (1994) ont testé ces indices de classification et montré que leurs résultats étaient généralement cohérents, l'indice de Kirsten offrant une meilleure précision. Plus récemment, Pells (2016) a proposé deux nouveaux indices : l'Erodibility Geological Strength Index (*eGSI*) et le Rock

Mass Erodibility Index (*RMEI*). Pells (2016) a rassemblé une vaste base de données sur les massifs rocheux situés sous des évacuateurs de crues non revêtus dans plusieurs pays (Australie, Afrique du Sud, États-Unis). Cette base de données comprend des informations détaillées sur l'ampleur de l'érosion, la géologie des massifs, les conditions hydrauliques et les événements de crues historiques. Un survol de ces indices est présenté dans les sections suivantes.

a. Indice de Kirsten

L'indice de Kirsten est exprimé par l'Éq. 2.3 ci-dessous. Il est déterminé à partir de certains paramètres de la roche liés à la résistance à la compression simple (UCS) de la roche intacte, à la taille des blocs rocheux, à la résistance au cisaillement des joints et à la structure relative des blocs.

$$N = M_s \,.\, K_b \,.\, K_d \,.\, J_s \qquad \text{Éq. 2.3}$$

Où

N: Indice de Kirsten,

M_s: Cote de résistance en compression, dépend de l'UCS (0.87 - 280),

K_b: Cote de taille de bloc (1 - 100) = $\frac{RQD}{J_n}$;

RQD: *Rock Quality Designation* (5% - 100%);

J_n: Nombre d'ensembles de joints (1 - 5),

K_d: Cote de résistance au cisaillement des joints (0.03 – 5.33) = $\frac{J_r}{J_a}$;

J_r: Rugosité des joints (0.5 - 4);

J_a: Altération des surfaces de joints (0.75 - 18) et

J_s: Cote de structure relative des blocs (0.37 – 1.5).

La valeur de J_s a été modifiée par Annandale (1995). Ces valeurs de J_s ont été établies pour des réseaux de joints orthogonaux. Boumaiza et al. (2019) ont proposé une modification de ces valeurs en considérant les réseaux de joints non orthogonaux (0,09 – 1,38). Cependant, l'applicabilité de cet indice demeure incertaine, puisqu'il a été initialement conçu pour évaluer l'excavabilité des matériaux et ne tient pas compte de l'ensemble des paramètres pertinents pour représenter fidèlement la résistance du massif rocheux à l'érosion.

b. Indice *eGSI* de Pells

L'indice de résistance géologique à l'érosion (*eGSI*) a été proposé par Pells (2016) comme première tentative de développer un indice spécifiquement destiné à l'érodabilité. Cet indice (Éq. 2.4) constitue une modification du Geological Strength Index (*GSI*) proposé par Hoek et al. (1995) pour la caractérisation des massifs rocheux. Le GSI est déterminé à l'aide des tableaux de référence de Marinos et Hoek (2000, 2001), à partir d'une évaluation visuelle de la lithologie, de la structure et de l'état des surfaces de joints. Pells (2016) a introduit un facteur d'ajustement supplémentaire, l'*Erosion discontinuity orientation adjustment*, E_{doa}, afin d'intégrer l'effet de la forme des blocs (rapport d'espacement des joints) et de leur orientation par rapport à la direction d'écoulement, sous différents régimes hydrauliques (Pells et al., 2017).

$$eGSI = GSI + E_{doa} \qquad \text{Éq. 2.4}$$

Les valeurs de E_{doa} ont été établies pour des réseaux orthogonaux, ce qui ne reflète pas nécessairement les conditions réelles. Pells (2016) a toutefois suggéré que leur application à des réseaux non orthogonaux ne modifiait pas significativement les résultats. Boumaiza et al. (2019) ont néanmoins souligné l'importance de considérer explicitement ces réseaux dans l'évaluation de la structure relative des blocs, paramètre auquel il conviendrait d'accorder davantage de poids. Il faut toutefois rappeler que l'*eGSI* demeure un paramètre semi-qualitatif, puisqu'il repose sur le *GSI* de Marinos et Hoek, lequel est lui-même semi-qualitatif et fortement dépendant du jugement de l'analyste sur le terrain. De plus, ni l'ouverture des joints ni la saillie des blocs n'y sont intégrées. En conséquence, l'*eGSI* ne peut être considéré comme un indice parfaitement adapté pour représenter la résistance d'un massif rocheux à l'érosion hydraulique.

c. Indice *RMEI* de Pells

Le deuxième indice proposé par Pells (2016) est le *Rock Mass Erodibility Index* (*RMEI*), conçu pour intégrer différents facteurs géologiques influençant directement l'érosion. Cet indice, inspiré du Q-System de Barton et al. (1974), repose sur des observations de terrain effectuées sous des évacuateurs de crues non revêtus. Le *RMEI* est défini par l'Éq. 2.5 où *RF* représente le facteur d'importance relative

(pondération) et *LF* le représente facteur de probabilité (*likelihood factor*) représentant les conditions favorables au détachement des blocs de la surface de l'évacuateur de crues. Les préfixes *P1* à *P5* représentent plusieurs paramètres, soit mécanisme cinématiquement possible de détachement, nature de la surface potentiellement érodable (*NPES*), nature des joints, espacement des joints et forme des blocs. Parmi ces paramètres, le mécanisme de détachement et la *NPES* reçoivent un poids plus élevé (*RF = 3*), comparativement à la nature des joints (*RF = 2*), à l'espacement des joints (*RF = 1*) et à la forme des blocs (RF = 1).

$$RMEI = [(RF_{P1}.LF_{P1}).(RF_{P2}.LF_{P2})].[(RF_{P3}.LF_{P3}) + (RF_{P4}.LF_{P4}) + (RF_{P5}.LF_{P5})] \quad \text{Éq. 2.5}$$

Bien que le *RMEI* constitue probablement l'indice le plus représentatif du phénomène d'érosion, son application soulève plusieurs limites. D'abord, l'importance relative des paramètres est dérivée uniquement d'études de cas et repose donc largement sur le jugement de l'analyste. Ensuite, la taille des blocs n'est pas considérée directement, mais uniquement de manière indirecte à travers l'espacement et la forme des blocs, alors que ces paramètres sont interdépendants. Leur pondération devrait ainsi mieux refléter leurs effets combinés. Par ailleurs, la résistance au cisaillement des joints est intégrée au paramètre « nature des joints », auquel une pondération relativement faible (*RF = 2*) est attribuée. Or, Boumaiza et al. (2021) ont montré, par une analyse de sensibilité basée sur les données de Pells, que ce paramètre exerce une influence beaucoup plus déterminante que ce qui est suggéré. Ces ambiguïtés dans la pondération et l'évaluation de l'importance relative des paramètres rendent l'indice *RMEI* discutable. Elles soulignent la nécessité de développer un nouvel indice intégrant l'ensemble des paramètres critiques du phénomène d'érosion, appuyé sur une pondération scientifiquement justifiée et validée.

2.2.2 Méthodes d'évaluation semi-empiriques de l'érosion

a. Méthodes basées sur l'indice de Kirsten

En utilisant l'indice de Kirsten (1982), plusieurs chercheurs ont proposé des méthodes de prévision de l'érosion en établissant une relation entre cet indice et l'énergie hydraulique (Π_{UD}). Des courbes seuils d'érosion ont ainsi été développées à partir de données de terrain, afin de distinguer différents niveaux de dommages. Moore et al. (1994) ont été les premiers à exploiter les données

compilées par le U.S. Department of Agriculture pour proposer une ligne seuil distinguant simplement les conditions « avec » et « sans » érosion. Toutefois, cette classification binaire a été jugée insuffisante. Van Schalkwyk et al. (1994b) ont alors établi plusieurs lignes seuils, à partir de 18 évacuateurs de crues non revêtus, permettant de définir divers niveaux d'érosion en fonction de la profondeur atteinte. La même année, Van Schalkwyk et al. (1994a) ont mis à jour leurs résultats en intégrant les données de Moore et al. (1994), redéfinissant les classes d'érosion à partir de profondeurs révisées. Annandale (1995) a, pour sa part, analysé l'ensemble des données de Moore et al. (1994), une partie de celles de Van Schalkwyk et al. (1994b), ainsi que des données issues du barrage Bartlett (Arizona). Il a proposé une nouvelle ligne seuil en considérant uniquement comme « érodés » les cas où la profondeur d'érosion excédait 2 m. Selon lui, les deux premiers mètres d'érosion observés correspondaient surtout au retrait de blocs mobiles à la surface et ne devaient donc pas être attribués à une véritable érosion hydraulique. Kirsten et al. (2000) ont repris ce concept de seuil de 2 m et ont proposé une nouvelle ligne seuil à partir des données de (1993) et Moore et al. (1994). Les classes d'érosion définies par ces différents auteurs sont résumées au tableau 2.1. Les lignes seuils correspondantes ont été comparées par Jalili Kashtiban et al. (2021) (sauf celle de Moore et al., 1994), en tenant compte de la limite de 2 m proposée par Annandale (1995), comme illustré à la figure 2.3. Les équations des lignes seuils de première classe sont présentées au tableau 2.2.

Tableau 2.1 Classes d'érosion proposées par divers auteurs (Jalili Kashtiban et al., 2021)

Van Schalkwyk et al. (1994b)		Van Schalkwyk et al. (1994a)		Annandale (1995), Kirsten et al. (2000)	
Profondeur d'érosion (m)	**Classe de l'érosion**	**Profondeur d'érosion (m)**	**Classe de l'érosion**	**Profondeur d'érosion (m)**	**Classe de l'érosion**
0	Aucune	< 0,2	Aucune	< 2	Pas d'érosion
0 – 1	Faible	0,2 – 0,5	Mineure		
1 – 5	Modérée	0,5 – 2	Modérée	> 2	Érosion
> 5	Extensive	> 2	Extensive		

Tableau 2.2 Équations des lignes seuils d'érosion proposées par différents auteurs (Jalili Kashtiban et al., 2021)

Auteur(s)	**Équation**
Van Schalkwyk et al. (1994b)	$\Pi_{UD} = 0.05\ K_h^{0.8}$
Van Schalkwyk et al. (1994a) (après inclusion des données de Moore et al., 1994)	$\Pi_{UD} = 1.5 \times 10^{-16}\ K_h^{5.36}$
Annandale (1995)	$\Pi_{UD} = K_h^{0.75}$
Kirsten et al. (2000)	$\Pi_{UD} = 9\ K_h^{0.5}$

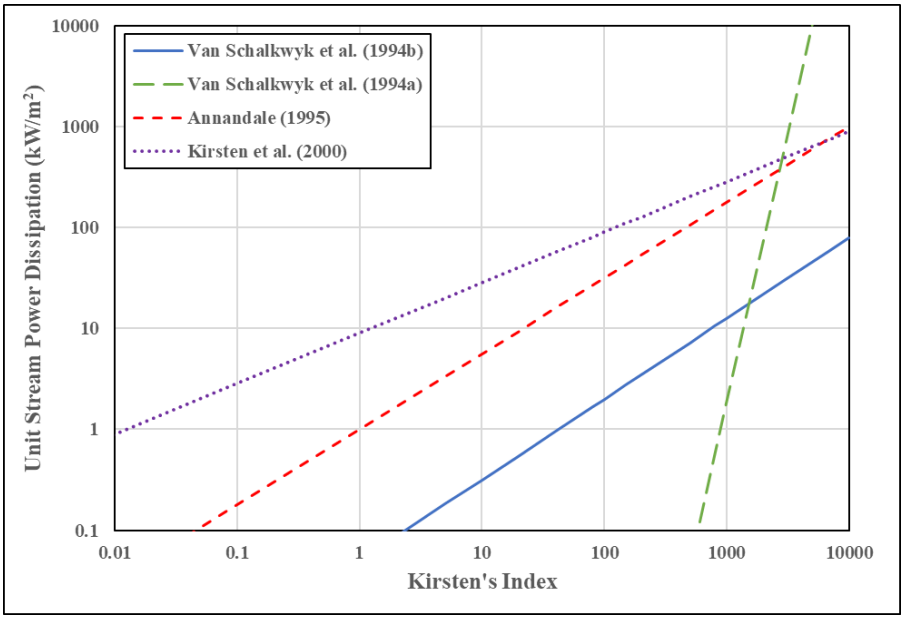

Figure 2.3 Comparaison des lignes seuils proposées par différents auteurs (Modifié de Pells, 2016)

b. Méthodes basées sur les indices de Pells

Pells (Pells et al., 2017; Pells, 2016) a repris le concept de Van Schalkwyk en proposant une classification de l'érodabilité en différentes classes. Contrairement aux travaux précédents, sa classification tient compte non seulement de la profondeur d'érosion, mais aussi de l'ampleur de la zone affectée. Les classes proposées sont présentées au tableau 2.3. L'évaluation de l'érosion fondée sur les indices *eGSI* (Éq. 2.4) et *RMEI* (Éq. 2.5), proposée par Pells (2016), est illustrée à la figure 2.4 : la figure 2.4(a) présente l'évaluation basée sur l'*eGSI*, et la figure 2.4(b) celle basée sur le *RMEI*.

Tableau 2.3 Classes qualitatives d'érosion proposées par Pells (2016)

Profondeur maximum (m)	**Étendue de l'érosion (m^3/100 m^2)**	**Classe**	**Description**
< 0,3	< 10	I	Négligeable
0,3–1	1–30	II	Mineure
1–2	30–100	III	Modérée
2–7	100–350	IV	Grande
> 7	> 350	V	Extensive

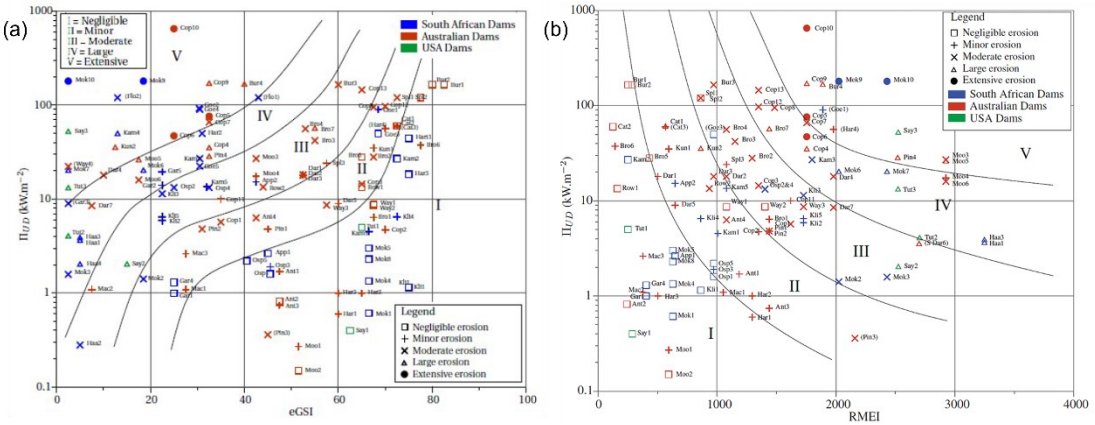

Figure 2.4 Méthodes d'évaluation de l'érosion basées sur les indices de Pells : (a) *eGSI* versus puissance hydraulique (Pells, 2016) et (b) *RMEI* versus puissance hydraulique (Douglas et al., 2018)

c. Comparaison de différentes méthodes semi-empiriques

Jalili Kashtiban et al. (2021) ont utilisé les données compilées pas Pells (2016) afin de comparer l'efficacité des différentes méthodes semi-empiriques. Les résultats de cette analyse comparative sont présentés à la figure 2.5. Il en ressort que la plus faible erreur globale est associée à la méthode basée sur *RMEI*, tandis que les erreurs les plus élevées sont observées pour les méthodes basées sur l'indice de Kirsten et Annandale. L'analyse par classes d'érosion (figure 2.5(b)) montre que la performance est relativement satisfaisante pour les faibles niveaux d'érosion sauf pour la méthode basée sur *eGSI*. À

l'inverse, pour les classes d'érosion grande à extensive, la méthode basée sur *eGSI* présente les erreurs les plus faibles. Cela traduit une capacité limitée à prédire correctement pour différents niveaux d'érosion. Figure 2.5(c) met en évidence une tendance marquée à la sous-estimation du degré d'érosion pour la plupart des méthodes. Une telle sous-estimation peut avoir des conséquences critiques sur la sécurité des ouvrages hydrauliques (Jalili Kashtiban et al., 2021).

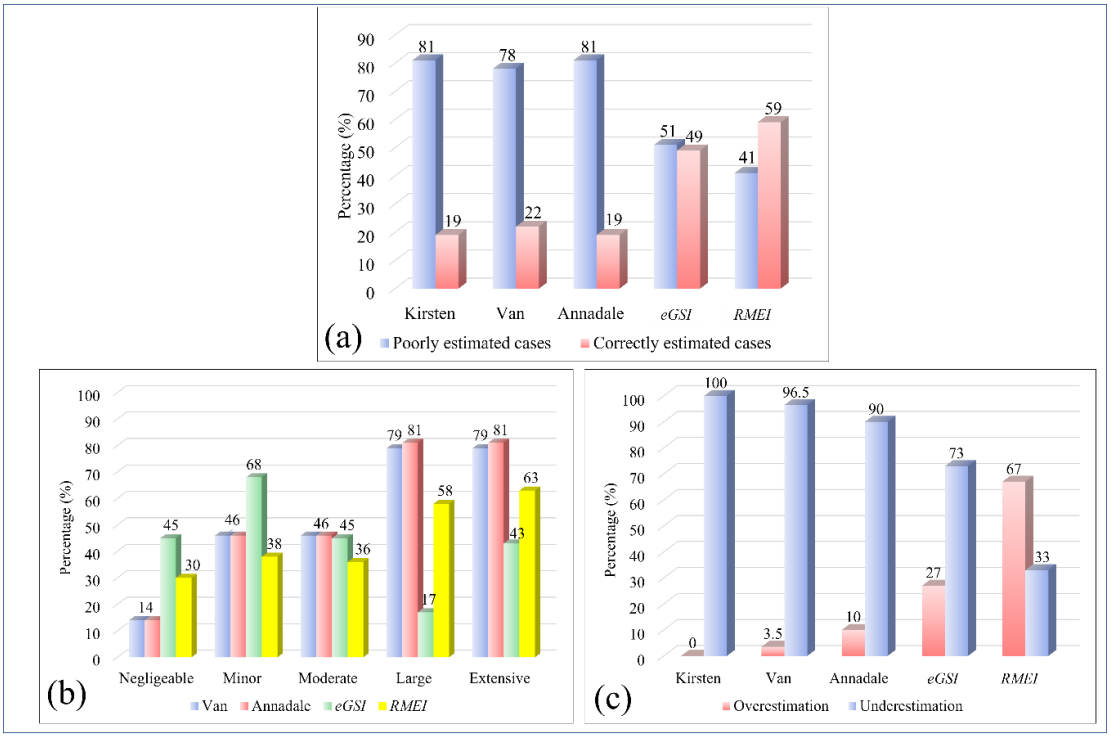

Figure 2.5 Comparaison de la performance de différentes méthodes semi-empiriques : (a) Proportion des cas estimés correctement et incorrectement; (b) Répartition des erreurs selon les classes d'érosion; (c) Tendances à la surestimation et à la sous-estimation du degré d'érosion (Jalili Kashtiban et al., 2021)

2.2.3 Méthodes semi-analytiques

Les méthodes semi-analytiques s'appuient sur des concepts de mécanique des matériaux, des lois hydrauliques et sur des résultats expérimentaux. Elles ont été principalement développées pour évaluer l'érosion dans les fosses d'érosion (plunge pools). Ces fosses se forment lorsqu'un jet d'eau, issu d'un évacuateur de crues, plonge dans l'eau en aval et entraîne le détachement et le transport de blocs rocheux.

La vitesse élevée du jet génère des pressions dynamiques fluctuantes ainsi qu'une pression moyenne au fond de la fosse. L'introduction d'air par le jet dans la zone d'impact réduit cependant la pression dynamique moyenne (Bollaert, 2012; Bollaert et al., 2013; Duarte, 2014; Ervine et al., 1997). En ce qui concerne l'érosion dans les fosses, le modèle semi-analytique le plus abouti est le *Comprehensive Scour Model* (*CSM*) proposé par Bollaert (2002) et modifié par la suite pour les cas de lits de rivières (Bollaert, 2010). Le *CSM* inclut trois phénomènes : la mécanique de fracture complète (*CFM*), l'impulsion dynamique (*DI*) et l'impulsion quasi-statique (*QSI*). Les principaux processus physiques de ce modèle sont présentés à la figure 2.6. Dans le *CFM*, les principes de base de la mécanique de la rupture (théorie élastique linéaire) sont appliqués pour étudier la propagation des fissures dans le massif rocheux. Dans le *DI*, l'éjection verticale des blocs est analysée sous l'action de pressions dynamiques fluctuantes, en appliquant la deuxième loi de Newton (impulsion). Dans l'approche *QSI*, les blocs en saillie sont étudiés lorsqu'ils subissent des forces de soulèvement et de traînée causées par la turbulence de l'écoulement le long des parois de la fosse.

Le module du jet en chute (figure 2.6) décrit la transformation des caractéristiques hydrauliques et géométriques du jet depuis sa sortie du barrage jusqu'à son impact au sommet de la fosse. Le module de la fosse caractérise les interactions hydrauliques entre le jet et l'eau accumulée en aval, ainsi que le transfert des contraintes vers le massif rocheux. Enfin, le module du massif rocheux représente le transfert des contraintes et le processus d'érosion via les mécanismes *CFM*, *DI* et *QSI*. Pour un massif intact, les processus *DI* et *QSI* découlent directement du *CFM* ; pour un massif fracturé, ce sont plutôt les mécanismes *DI* et *QSI* qui contrôlent la profondeur d'érosion. Une revue détaillée de ces méthodes et de l'importance de l'aspect hydraulique dans le phénomène d'érosion est présentée par Jalili Kashtiban et al. (2021).

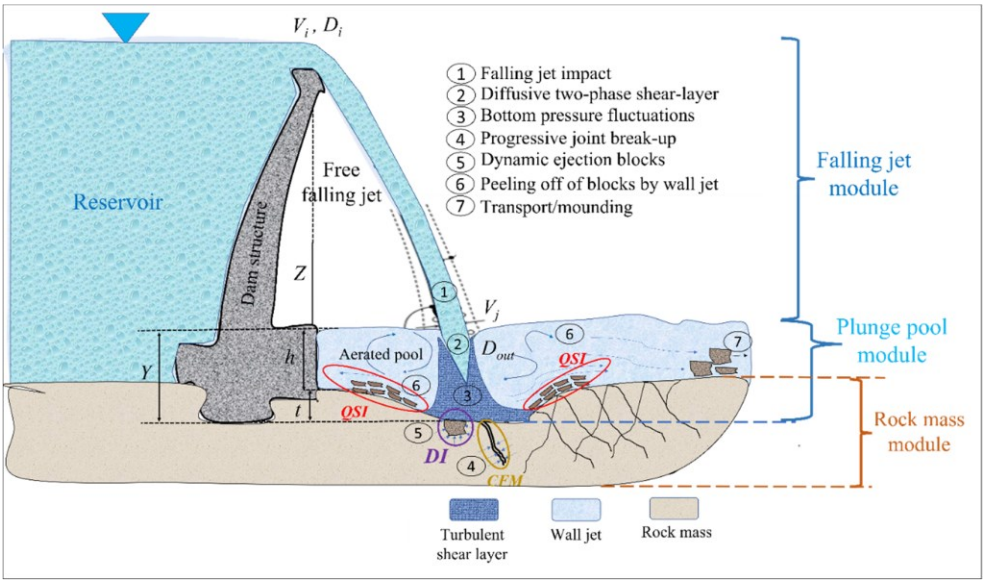

Figure 2.6 Principaux processus physiques intégrés dans le *CSM* (Jalili Kashtiban et al., 2021)

Bollaert et Schleiss (2005) ont proposé un critère d'évaluation de l'érosion des massifs rocheux basé sur la hauteur de soulèvement d'un bloc unique, considérée dans la catégorie *DI*. Ils ont formulé des équations permettant de calculer cette hauteur en appliquant la deuxième loi de Newton, tout en intégrant un coefficient adimensionnel représentant l'intensité des pressions hydrauliques dynamiques fluctuantes. Selon ce critère, un bloc peut être soulevé uniquement si les pressions fluctuantes atteignent une intensité suffisante pour générer un soulèvement équivalant à au moins la moitié de la hauteur du bloc. Cependant, cette approche néglige le phénomène d'accumulation de petits soulèvements successifs, qui peut, à terme, provoquer le détachement complet du bloc. Ce mécanisme progressif a été mis en évidence par Pan et al. (2014), qui ont montré qu'il est particulièrement probable dans un massif rocheux présentant un coefficient de frottement élevé. De son côté, Reinius (1986) a étudié les pressions de stagnation responsables du soulèvement net dans différentes configurations, en faisant varier la saillie des blocs et l'angle des jets soumis à un écoulement parallèle à grande vitesse. Ses travaux ont permis de déterminer des valeurs du coefficient adimensionnel de soulèvement (C_{up}'), défini comme la différence de charge de pression dynamique entre le sommet et la base du bloc, normalisée par la charge de vitesse moyenne de l'écoulement au niveau du bloc. Ces recherches ont ensuite été élargies par Bollaert (2012), qui a étudié le soulèvement de blocs à partir de l'approche *QSI*. Cette approche décrit l'action de l'écoulement parallèle au lit rocheux, en dehors de la zone d'impact direct du jet. Dans ce

cadre, la force totale de soulèvement agissant sur un bloc est définie comme la somme de trois composantes : la poussée d'Archimède, la force de soulèvement quasi-statique liée à l'accumulation de la pression de stagnation sous le bloc en saillie, et les forces turbulentes issues des fluctuations de pression. Toutefois, ces dernières sont généralement considérées comme négligeables, car la vitesse critique de l'écoulement diminue rapidement en dehors de la zone d'impact du jet. Cette conclusion a été confirmée par George (2015), qui a étudié plusieurs conditions d'écoulement et montré que la force de soulèvement quasi-statique constitue le facteur dominant dans les cas d'écoulement parallèle. Cette force peut d'ailleurs être directement utilisée pour calculer la hauteur de soulèvement d'un bloc selon le modèle proposé par Bollaert (catégorie *DI*).

2.2.4 Autres méthodes (expérimentales et numériques)

Boumaiza et al. (2019b) ont utilisé les données de terrain collectées par Pells (2016) afin d'étudier les paramètres les plus pertinents parmi les indices existants. Boumaiza et al. (2021) ont ensuite mis en évidence l'importance relative de ces paramètres. Ceux-ci incluent l'ouverture des joints, le volume des blocs, la résistance au cisaillement des joints, le paramètre lié à l'orientation des discontinuités d'érosion, ainsi que la nature des surfaces potentiellement érodables. Ces paramètres constituent les facteurs géomécaniques individuels pouvant être testés à l'aide d'un modèle physique : ouverture des joints, volume des blocs, orientation des joints, saillie des blocs et configurations de saillie. Wisse (2022) a présenté une revue de différents modèles expérimentaux portant sur l'érosion dans divers types d'évacuateurs de crues (à écoulement parallèle, à jet plongeant et autres), ainsi que sur les paramètres étudiés par différents auteurs (voir tableau 2.4). La plupart de ces modèles sont de petite taille, et les essais les plus marquants incluent les travaux de Reinius (1986), George (2015) et Pells (2016). Tous ces auteurs ont souligné l'importance d'examiner la saillie des blocs et l'orientation des joints. Les essais de George et Pells portaient sur un seul bloc et n'intégraient pas l'effet des blocs environnants. Bien que Reinius ait étudié un ensemble de blocs, ses travaux présentent certaines limites, notamment des mesures de pression insuffisantes et la position du bloc instrumenté. Les essais sur modèles physiques posent leurs propres difficultés, en particulier lorsqu'il s'agit de reproduire le comportement dynamique de massifs rocheux fracturés réels. Pour simplifier ce défi, la plupart des modèles supposent que le massif

est entièrement fracturé et ne considèrent que des blocs individuels pour le représenter. La majorité des modèles physiques recourent à des blocs instrumentés munis de capteurs de pression, les mesures étant prises perpendiculairement à la direction de l'écoulement. Cette configuration peut entraîner des erreurs dans l'évaluation de la vitesse d'écoulement dans les joints, car les pressions dynamiques ne peuvent être mesurées avec précision (Wisse et al., 2023). Ces essais ont permis d'analyser la variation d'un seul paramètre à la fois, mais l'effet combiné de plusieurs paramètres reste encore à étudier. En outre, la plupart des études se sont limitées à un bloc unique ou à un petit groupe de blocs en raison de la faible échelle des modèles réduits (1:50 à 1:100), ce qui restreint la possibilité d'examiner l'ensemble des paramètres du massif rocheux influençant les pressions hydrauliques responsables du soulèvement ou de l'arrachement des blocs, que ce soit à la surface de l'évacuateur de crues, sur le lit rocheux ou sous les blocs.

Tableau 2.4 Différents modèles physiques d'évacuateurs de crues et paramètres étudiés (D'après Wisse, 2022)

Auteur(s)	**Type de modèle**	**Paramètres fixes et variables**	**Débit**	**Pente**	**Méthode d'analyse - Quantitative**
Montgomery (1984)	Écoulement en canal ouvert, ensemble de blocs	**Variables :** inclinaison des blocs; ouverture des joints. **Fixes :** taille et forme des blocs	**Élevé** 250 L/s	Horizontale	Pression mesurée sur une face de bloc
Reinius (1986)	Écoulement en canal ouvert, ensemble de blocs	**Variables :** inclinaison des blocs. **Fixes :** ouverture des joints; taille et forme des blocs	**Élevé** 311 L/s	Horizontale	Pression mesurée sur une face de bloc
Annandale et al. (1998)	Jet plongeant dans une fosse, deux couches de blocs	**Fixes :** disposition des blocs; caractéristiques du jet	**Très élevé** 3400 L/s	Jet à 15°	Blocs dans un bassin horizontal. Pression mesurée sur la surface du canal et entre les couches de blocs
Lieu et al. (1998)	Modèle à l'échelle 1:100 du jet de l'évacuateur du barrage des Trois-Gorges, un bloc	**Variables :** taille et forme du bloc; caractéristiques de l'écoulement. **Fixes :** orientation et ouverture des joints	**Moyen** 174 L/s	Verticale	Pression mesurée sous le bloc
Bollaert et Schleiss (2002)	Jet vertical dans un bassin, joints en acier	**Variables :** caractéristiques de l'écoulement; types de joints.	**Moyen** 120 L/s	Verticale	Pression mesurée dans les joints et sur la surface du canal

		Fixes : orientation des joints			
Wang et Jiang (2010)	Écoulement en canal ouvert et modèle 1:100 de l'évacuateur en marches du barrage de Xiluodu	**Variables :** pente du canal **Fixes :** configuration de l'évacuateur; débit	**Vitesse** 38 m/s	1.44% - 2.62%	Pression mesurée sur la surface du canal, avec accent sur le frottement du canal
George et al. (2015)	Écoulement en canal ouvert, un bloc tétraédrique	**Variables :** orientation du bloc **Fixes :** pente du canal; taille et forme du bloc	**Élevé** 300 L/s	21^{o}	Mesures de pression et forces sur les faces du bloc
Pells (2016)	Écoulement en canal ouvert, un bloc cubique	**Variables :** orientation et saillie du bloc; caractéristiques de l'écoulement **Fixes :** ouverture des joints	**Élevé** 350 L/s	4.6^{o} et 11.1^{o}	Gradient de pression

D'autres études se sont penchées sur la modélisation numérique, une approche complexe puisque les phénomènes hydrauliques et mécaniques ne peuvent être représentés dans un même code. Simões et al. (1997) ont proposé une méthodologie combinant la méthode des éléments finis pour les paramètres hydrauliques et la méthode des éléments discrets pour la modélisation mécanique, afin d'analyser le phénomène d'érosion dans des massifs fracturés. Toutefois, aucune analyse détaillée n'a été réalisée pour appliquer cette approche couplée et en déduire la profondeur d'érosion. Velloso et Vargas Jr (2011) ont repris cette méthodologie en y intégrant des résultats expérimentaux pour étudier les fluctuations de pression hydraulique, lesquelles ont été appliquées aux joints dans un modèle mécanique élaboré avec le logiciel *Universal Distinct Element Code* (*UDEC*), dans le but d'analyser l'accélération des blocs. Bien que les résultats numériques et expérimentaux aient été comparés, les écarts importants observés ont rendu l'approche peu concluante. D'autres chercheurs ont également utilisé le logiciel *UDEC* en 2D

pour modéliser le processus d'érosion à partir de pressions hydrauliques obtenues lors d'essais sur modèles physiques (Moren & Sjoberg, 2007; Wibowo & Lin, 2009). Ces modèles souffrent toutefois de la limite d'un apport hydraulique constant, alors qu'en réalité les conditions hydrauliques évoluent simultanément avec le déplacement des blocs. Dasgupta et al. (2011) ont proposé une méthodologie couplée utilisant les logiciels *ANSYS FLUENT (Computational Fluid Dynamics - CFD)* et *UDEC (Discrete Element Method - DEM)*, mais son application concluante n'a pas encore été démontrée. Plus récemment, Gardner et Sitar (2018, 2019) ont proposé une approche couplée *3D DEM-LBM*, dans laquelle la partie *Lattice Boltzmann Method* (*LBM*) représente l'écoulement hydraulique et la partie *DEM*, la réponse géomécanique. L'application réussie de cette méthode à la modélisation du processus d'érosion a été présentée par Gardner (2023), bien que ce modèle demeure préliminaire et limité à l'analyse d'un seul bloc. Teng et al. (2023a, b) ont pour leur part proposé une approche couplée *CFD-DEM* pour modéliser le processus d'érosion en utilisant un seul bloc, validée par les données expérimentales de George (2015). Un aperçu des différents modèles numériques est présenté au tableau 2.5. Ces modèles nécessitent encore des améliorations, notamment pour intégrer l'interaction avec le massif rocheux environnant, comme l'ont souligné Lamb et al. (2015). Enfin, l'applicabilité de ces méthodes à l'évaluation de la profondeur d'érosion des massifs rocheux demeure conditionnée par l'amélioration de leur efficacité computationnelle. En raison de ces limites, la modélisation physique constitue toujours une approche plus fiable pour l'étude des mécanismes d'érosion.

Tableau 2.5 Différents modèles numériques développés pour évaluer l'érosion du massif rocheux

Auteur(s)	**Type de modèle**	**Type de modélisation**	**Limitations**
Simoẽs et al. (1997)	FEM – paramètres hydrauliques DEM – paramètres géomécaniques	**Non couplé**	Analyse préliminaire seulement
Velloso et Vargas Jr (2011)	Résultats expérimentaux – pressions hydrauliques DEM – UDEC	**Non couplé**	Analyse préliminaire seulement
Moren et Sjoberg (2007)	Résultats expérimentaux – pressions hydrauliques DEM – UDEC	**Non couplé**	Analyse préliminaire seulement
Wibowo et Lin (2009)	Résultats expérimentaux – pressions hydrauliques DEM – UDEC	**Non couplé**	Une seule analyse, sans application du couplage
Dasgupta et al. (2011)	CFD – ANSYS FLUENT DEM – UDEC	**Non couplé**	Une seule analyse, sans application du couplage
Gardner et Sitar (2018, 2019) Gardner (2023)	LBM – portion hydraulique DEM – portion géomécanique	**Couplé – complet**	Analyse d'un seul bloc, modèle encore en développement
Teng et al. (2023b)	CFD – portion hydraulique DEM – portion géomécanique	**Couplé – complet**	Analyse d'un seul bloc tétraédrique, modèle encore en développement

CHAPITRE 3

ARTICLE 1: FLUCTUATING PRESSURES ON SPILLWAY SURFACES AS A FUNCTION OF JOINT OPENING AND BLOCK PROTRUSION

Vineeth Reddy Karnati [a*], Ali Saeidi [a], Alain Rouleau [a], Marco Quirion [b], Fethi Meghnefi[a]

[a] Département des sciences appliquées, Université du Québec à Chicoutimi, Saguenay, QC G7H 2B1, Canada.

[b] Expertise, intégrée - Géologie, Hydro-Québec, 75 Boulevard René-Lévesque Ouest, Montréal, QC H2Z 1A4, Canada.

Accepted for publication in Geotechnical and Geological Engineering (12 December 2025)

Ce chapitre reprend un article dont le premier auteur est l'auteur de cette thèse. Le chapitre présente les détails des essais sur le modèle réduit avec différentes valeurs de saillie et ouvertures des joints. Les résultats sont utilisés pour développer un modèle prédictif afin de déterminer les pressions fluctuantes sur la surface d'un évacuateur de crues.

Credit authorship contribution statement

Vineeth Reddy Karnati: Experimental work, Methodology, Data analysis, Investigation, Spectral analysis, Preparation of original manuscript, review & editing. **Ali Saeidi:** Supervision, Conceptualization, Methodology, Funding & Resource acquisition, Overall project administration, Spectral analysis, Review & editing the manuscript. **Alain Rouleau:** Supervision, Review & editing the manuscript. **Marco Quirion:** Supervision, Funding acquisition, Review & editing the manuscript. **Fethi Meghnefi:** Spectral analysis, Manuscript review.

Competing interests

The authors declare that they have no known competing financial interests or personal relationships that could have appeared to influence the work reported in this paper.

Funding

The project was supported by the Natural Sciences and Engineering Research Council of Canada and Hydro-Québec (NSERC, Hydro-Québec) [CRDPJ 537350 – 18] and NSERC [RGPIN-2019-06693]. The authors also acknowledge the Fonds de Recherche du Québec Nature et technologies for granting the programme de bourses d'excellence pour étudiants étrangers (PBEEE) scholarship (Grant No.: 2023-2024 - 1I - 334721) for this research.

Résumé

Les changements climatiques actuels représentent une menace importante pour la sécurité des évacuateurs de crues des barrages face à l'érosion du massif rocheux, en raison de l'augmentation des précipitations. L'arrachement des blocs rocheux constitue le mécanisme dominant de ce processus d'érosion et est influencé par divers facteurs hydrauliques et géomécaniques propres au site de l'évacuateur. Cet article étudie l'effet de paramètres spécifiques - le débit, l'ouverture des joints et la saillie des blocs - sur les pressions hydrauliques, à l'aide d'un modèle physique d'évacuateur de crues à l'échelle de pilote. Les résultats des essais en modèle réduit montrent que les fluctuations de pression hydraulique au sommet du bloc instrumenté, c'est-à-dire à la surface de l'évacuateur, gouvernent le processus de soulèvement, puisque les fluctuations de pression à l'intérieur des joints demeurent similaires pour l'ensemble des conditions d'essai. Un modèle mathématique est développé afin de prédire les fluctuations extrêmes de pression représentant les conditions critiques menant au soulèvement des blocs. Ce modèle permet à l'utilisateur final d'estimer rapidement les pressions hydrauliques critiques à la surface de l'évacuateur afin d'évaluer la vulnérabilité des structures, contribuant ainsi à l'amélioration de la résilience et à la réduction des risques de catastrophe dans un contexte de changements climatiques. De manière notable, l'erreur quadratique moyenne (*RMSE*) entre la majorité des fluctuations extrêmes de pression mesurées et modélisées se situe entre 0,04 et 0,37, ce qui demeure dans des limites acceptables. De plus, les valeurs de l'erreur quadratique moyenne normalisée (*NRMSE*), normalisées par l'écart entre les pressions maximale et minimale des données mesurées, varient entre 18 % et 35 %, indiquant un ajustement de qualité modérée des données de pression.

3.1 ABSTRACT

The current climate change poses a significant threat to the safety of dam spillways against the rock scour due to increased precipitation. The plucking of rock blocks is the dominating mechanism in this scouring process, which is influenced by various hydraulic and geomechanical factors at the spillway site. This article studies the impact of specific parameters – flow rate, joint opening and block protrusion on the hydraulic pressure, using a pilot plant scale spillway model. The model test results reveal that the hydraulic pressure fluctuations on the top of the instrumented block, i.e., on the spillway surface, govern the uplift process as the pressure fluctuations within the joint remain similar across varying test conditions. A mathematical model is developed to predict the extreme pressure fluctuations that represent the critical conditions for block uplift. This model enables the end user to readily estimate the critical hydraulic pressure on the spillway surface to assess the vulnerability of spillway structures, contributing to improved resilience and disaster risk reduction in the context of a changing climate. Remarkably, the margin of error (*RMSE*) between most of the measured and modelled extreme pressure fluctuations is found to be between 0.04 to 0.37, well within acceptable limits. Also, the normalized *RMSE* (*NRMSE*) values, normalized with difference between maximum and minimum pressure values of the measured data, are lying 18 to 35% which defines a moderate fitting of the pressure data.

Keywords: Rock scour; Block uplift; Joint opening; Block protrusion; Dominating frequency

3.2 INTRODUCTION

The climate change results in significant increase in flood risk, especially in the Nordic countries, associated with ice melting and huge rainfall (Capobianco et al., 2024; Thistlethwaite et al., 2018). Rock mass is generally considered stronger than alluvial deposits against the hydraulic rock mass erosion or rock scour[1] (Baudson et al., 2024; Mir et al., 2018). The devastating 2017 scouring disaster at the Oroville Dam in California, USA, where both lined primary spillway and the unlined emergency spillway suffered severe damage, serves as an indicator of substantial losses and repair costs in millions

[1] The terms “hydraulic rock mass erosion” and “rock scour” are used synonymously in this article which represents the disintegration and removal of rock mass under the action of hydraulic forces.

of dollars (Koskinas et al., 2019; Stofleth et al., 2023; Zhang et al., 2024b). There are numerous types of spillways based on the hydraulic behavior (Afaridegan & Amanian, 2025; Hager et al., 2020) and these can be broadly categorized into plunging jet and straight reach (parallel flow) types based on the flow pattern and interaction with the rock mass (Afaridegan et al., 2024; Wisse et al., 2023). The scour mechanism is completely different between these two spillway types. Jalili Kashtiban et al. (2021) presents a review of existing erosion assessment methods which are majorly classified into semi-empirical (Annandale, 2012; Pells, 2016), for the straight reach spillways, and semi-analytical (Bollaert, 2002, 2010), for the plunge pool scour scenarios. The applicability of the existing methods is limited by discrepancies between predicted and observed scour depths, highlighting the need for improved understanding of the underlying scour mechanisms including hydro-geomechanical interactions (Boumaiza, 2019).

Rock scour involves various mechanisms, including cavitation, rock mass fracturing, abrasion and dissolution (in bedrock conditions with limestones) (Ferrill & Ferrill, 2021; Liu et al., 2021), which can occur simultaneously. Plucking or block uplift becomes the major erosion mechanism in highly fractured rock masses, especially when the blocks are of dimensions less than one meter (Li et al., 2016; Pan et al., 2014). This mechanism results in the ejection of blocks (instantaneous or time-dependent) depending on the interaction between the water flow and the block matrix and is highly dependent on the uplift force that a block is subjected to (Jalili Kashtiban et al., 2021). The block may remain stable, may move upward, vibrate or even be completely dislodged depending on the magnitude of the generated uplift forces and the resisting forces (Bollaert & Schleiss, 2003a). The magnitude of uplift force generated depends on the instantaneous pressure differences generated by the pressure fluctuations between the top and the bottom of the block (Pan et al., 2014), which depend on various factors that include hydraulic, geomechanical and spillway geometrical parameters. These parameters constitute flow rate, spillway inclination, spillway surface irregularities or roughness, joint aperture or opening, joint orientation and block volume (Boumaiza et al., 2019a; Jalili Kashtiban et al., 2021).

Field determination of this pressure distribution is not often feasible due to the associated complex instrumentation and costs. As a result, physical and numerical modelling are recognized as more reliable

means of obtaining the hydraulic pressure fluctuations while allowing controlled variation of specific parameters (Whittaker & Schleiss, 1984). Some coupled numerical models have been developed recently to model the scouring process (Gardner, 2023; Teng et al., 2023; Wang et al., 2018); however, they are based on the single block assessments and requires further understanding to include the interaction with the surrounding rock mass as highlighted by Lamb et al. (2015). Recently, Zhang and Zhang (2025) used a coupled CFD-DEM-VOF framework to predict the sediment erosion under submerged jets, which could be modified to study the rock scour in parallel flow conditions. Applicability of these methods to assess rock scour depth requires further development and improvement of the computational efficiency. Given these limitations, physical modelling remains a reliable approach to study the scour mechanisms. To simplify the difficulty associated with simulating the dynamic behavior of actual fractured rock masses, most physical model tests assume that the rock mass is entirely fractured, using only individual blocks to represent the rock mass.

Several researchers carried out the physical model testing to study the hydraulic pressures by varying specific geomechanical parameters that affect the scouring process (Boumaiza et al., 2019a). The hydraulic conductivity of a fractured rock mass is governed by its discontinuity characteristics such as aperture, filling, spacing and roughness (Ajalloeian & Azimian, 2013; Safari et al., 2025). The block protrusion, representing excavation/blast induced surface irregularities, can severely affect the hydraulic pressure on the spillway surface and within the joints due to the formation of loosened blocks and irregular surfaces (Jalili Kashtiban et al., 2023a; Qi et al., 2025). Reinius (1986) studied the pressures around an instrumented hollow block under varying protrusion heights and joint orientation and presented the normalized pressure heads as a function of block inclination. Coleman et al. (2003) highlighted that even a slight block protrusion could substantially reduce the block stability and recommended incorporating the effects of protrusion in stream power based erosion assessment methods such as Annandale's semi-empirical method (Annandale, 2006). Frizell (2007) and Wahl and Heiner (2024b) studied various protrusion heights and edge configurations and observed the increased uplift pressures associated with offset height due to stagnation pressures. Dubinski (2009) reported that scour starts at knickpoints, and migrates upstream over time, with the removal of key block(s) (one to three blocks), before rapid scour ensues.

George (2012, 2015) focused on the orientation of tetrahedral block with respect to the flow direction and concluded that orientation of the block governs the erosion process. George and Weidner (2025) recently presented the importance of digital rock mass generation and high-resolution remote sensing to characterize rock scour and block kinematics in unlined spillways. Most physical models employed the instrumented blocks equipped with pressure sensors with pressure measurement made perpendicular to the flow direction, which can misrepresent joint flow velocities as the dynamic pressures cannot be accurately captured (Wisse et al., 2023). Most studies used either single block or a group of very small blocks given the smaller size of the reduced-scale model (ranging from 1:50 to 1:100) (Wisse, 2022), which limits the ability to study the full range of rock mass parameters governing the hydraulic pressures and block uplift/plucking. To overcome these difficulties, the current article focuses on understanding the scouring process through block uplift in parallel flow spillways using a relatively large physical model with multi-block configuration to accurately quantify the dynamic pressure fluctuations. Bollaert and Schleiss (2003b) presented the relationship between the pressures at the top of the block (rock surface) and at the end of the joint (bottom of the block) based on the laboratory model under the plunging jet conditions. However, this analysis does not consider the effect of various geomechanical parameters and cannot be directly applicable to the erosion analysis in the parallel flow spillway conditions.

In this context, the objective of this study is to evaluate the combined effects of the selected important parameters, joint opening and block protrusion (including protrusion height and block arrangement configuration) under varying flowrates on these fluctuating pressures on the spillway surface (under parallel flow conditions) which is one of the most important parameters in the evaluation of uplift force. Consequently, a practical approach is developed to determine the extreme pressure fluctuations as a function of these parameters. This approach allows the end-user to directly estimate the fluctuations under given conditions which enables the uplift analysis.

3.3 EXPERIMENTAL PILOT PLANT SCALE SPILLWAY MODEL

Reduced-scale spillway models offer a means to measure the hydraulic pressures above the key block and within the joints, that govern the plucking mechanism of scour. While these models cannot replicate the actual field velocities, they always provide a valuable opportunity to study several parameters influencing the scour process. In this study, physical model tests have been conducted using a pilot plant scale spillway model located at the Université du Québec à Chicoutimi (UQAC) in Québec, Canada. This model, depicted in Figure 3.1, is scaled down (1:40) from Hydro-Québec's Romaine IV Dam spillway following the Froude number similarity. Detailed design and similarity information of the model can be found in Koulibaly et al. (2023). The scaling relationships and Froude similarity considerations are explained in Annexe A.

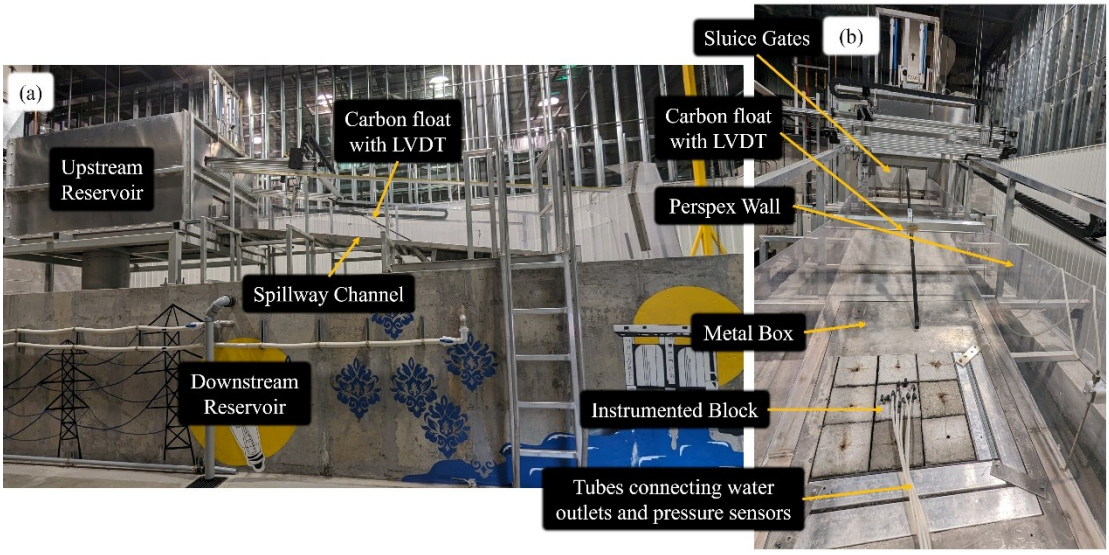

Figure 3.1 Pilot plant scale spillway physical model at Université du Québec à Chicoutimi; (a) Side view of the entire set up over a length of about 8 meters and (b)View along the channel looking upstream

The model comprises a downstream reservoir, from which the water is pumped into an upstream reservoir via a submersible pump. The upstream reservoir is equipped with two gates to control the water release into a parallel-flow smooth spillway channel, inclined at an angle of 9^{o} relative to the ground level. The flowing water ultimately returns to the downstream reservoir. The end of spillway channel is

designed to support a metal box containing 9 concrete blocks, as shown in Figure 3.1. These concrete blocks, each of size 15 cm x 15 cm x 30 cm, represent intact rock blocks delimited by a fully connected fracture network. The channel is also equipped with a carbon rod, acting as a float, with a Linear Variable Differential Transformer (*LVDT*) mounted on it to record the changes in the flow height in proximity to the metal box. The static head over the instrumented block is approximated based on *LVDT* measurements close to the blocks.

The spillway channel is also equipped with XYZ system that allows for the measurement of flow depth and flow velocity at every point in the spillway channel. By adjusting the operating frequency of the motor of submerged pump and keeping the gate opening constant, the discharge and subsequently the flow velocity in the channel can be varied. Throughout the tests, a constant gate opening of 25cm is used as shown in Figure 3.1(b). Among the 9 blocks, the central block is instrumented with internal copper tubes, allowing for the measurement of hydraulic pressure distribution around the block. One end of these copper tubes serves as water inlet and the other as outlet, facilitating the pressure measurement at specific points of interest around the block. Further instrumentation details are available in Wisse et al. (2023). The instrumented block is detailed in Figure 3.2.

The instrumented block's top and bottom faces are labeled *A* and *B*, respectively, while the vertical faces are designated as *C*, *D*, *E*, and *F*. This block features multiple water inlets, with two water inlets on each face except at the top of block, which has a single inlet. All the outlets are located at the top of the block (Figure 3.1(b) and Figure 3.2(a)). Measuring dynamic pressures within the channel presents challenges, particularly when determining flow velocity in the joints. This can only be achieved when the water inlet is positioned opposite to the flow direction, resembling a pitot tube setup. The copper tubes incorporated into the instrumented block are equipped with elbows at each end.

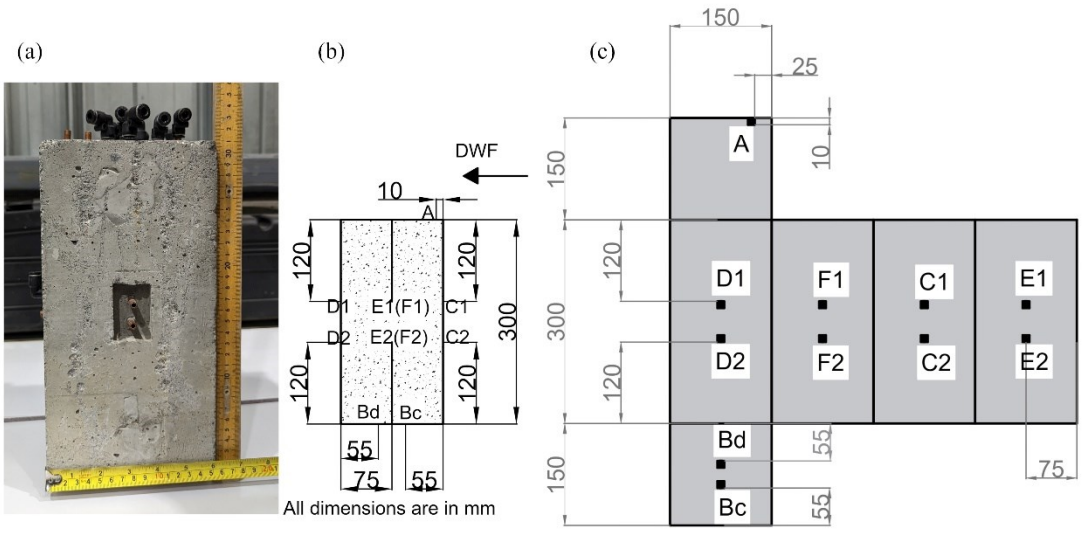

Figure 3.2 Instrumented block showing the position of water inlets: (a) Concrete block with water inlets and outlets; (b) Schematic diagram of the instrumented block with letters indicating the water inlets; (c) Development of the six faces of the instrumented block

These inlet-side elbows function as mini pitot tubes, enabling the measurement of both static and dynamic pressures. On each vertical face of the block (*C*, *D*, *E*, and *F*), two water inlets are strategically placed near the center. One inlet faces upward, while the other faces downward. At the bottom of the block, one inlet points in the direction of the flow within the channel, while the other faces in the opposite direction. The top inlet on the block is positioned near the edge to minimize flow disturbances caused by the water outlets, as illustrated in Figure 3.2. Water inlets are indexed according to their respective faces, as shown in Figure 3.2. For the outlets, elbows are connected to airtight plastic tubes, the other ends of which are connected to the calibrated pressure sensors. Six pressure sensors are employed, each featuring a measurement range of 0 – 70.31 mH_2O (0 – 100 psi). The sensors have been calibrated to ensure an accuracy of up to 4 decimal places in the pressure head measured in meters.

3.4 METHODOLOGY

This study focuses on investigating the impact of two key parameters, namely Joint opening (*JO*) and Block protrusion, on hydraulic pressures at the top of the block and within the joints under varying discharge conditions. Inside the metal box, the blocks are positioned to align the top of a block with the

spillway surface level, creating a consistent 7 mm gap below the blocks. This gap is maintained by three adjustable metal bolts arranged in a triangular pattern. To explore the effect of *JO*, three different joint openings – 3 mm, 10 mm and 20 mm, are selected, representing distinct gapped and open features according to the ISRM aperture classification for joints (ISRM, 1978). *JO* adjustments, maintained to an accuracy of 0.5 mm, are achieved through four Teflon bolts positioned between the blocks on each face, and the opening within the metal box is fine-tuned using packing plates. The study of protrusion comprises two parameters: protrusion height (*BP*) and configuration or pattern of block protrusion (*Conf.*) relative to the surrounding blocks.

The selected protrusion configurations (*Conf.*) and corresponding protrusion heights (*BP*) adopted in this study are outlined in Table 3.1. These configurations are selected to represent the realistic scenarios of positive and negative protrusions (Jalili Kashtiban et al., 2021; Reinius, 1986). The maximum *BP* is determined based on practical considerations of maximum achievable metal bolt adjustment and the water spill caused by the hydraulic jump at the protruded surface. Four different discharge levels: Q_1 = 0.18 m^3/s, Q_2 = 0.24 m^3/s, Q_3 = 0.315 m^3/s and Q_4 = 0.34 m^3/s, are selected, corresponding to various operating frequencies of the pump motor. These discharges include the minimum and maximum possible discharges in the model, along with two intermediate discharges. The flow is essentially a rapidly varying flow with fluctuations in height of water in the channel at all the discharge conditions that result in fluctuations in the pressures around the instrumented block with time. The pressure data is collected for 60 s at a data collection frequency of 100 Hz[1].

The turbulent pressure data recorded during the physical model tests exhibit stochastic behavior, characterized by random or probabilistic variations that are not characterized by deterministic formulas. Although inherently unpredictable, such data can be analyzed using statistical methods to understand the likelihood of certain outcomes. Block removal by uplift is highly influenced by extreme pressure conditions at the top and bottom surfaces of the block, with the critical condition arising when the pressure beneath the block exceeds that above it. While the pressure beneath the block remains relatively

[1] The data is collected by the sensors at an actual frequency of 10,000 Hz which is averaged to obtain a final data collection frequency of 100Hz.

stable, the pressure on the upper surface shows considerable temporal fluctuations. Given this behavior, representing the occurrence of extreme pressures on the top of the block using a sinusoidal distribution (parameterized by key variables influencing the scour process) offers a simplified yet insightful approach to characterize this phenomenon. The pressure fluctuations are approximated using a sinusoidal equation, as presented in Eq. 3.1.

$$H = \left(C_{pA} + C'_{pA}\, cos(2\pi f_d t)\right) * \frac{v_{ch}^2}{2g} \qquad \text{Eq. 3.1}$$

Where C_{pA}, C_{pA}' and f_d are arbitrary terms.

H = Dynamic head (m)

C_{pA} = Mean value of the fluctuating normalized pressure head data

C_{pA}' = Amplitude of the fluctuating normalized pressure head data

f_d = Dominating frequency (Hz)

v_{ch} =Mean channel flow velocity (m/s)

t = Time (s)

To create a standard equation for physical model studies that provides the necessary pressure fluctuations, we express the terms C_{pA}, C_{pA}', and f_d as functions of the study parameters. The methodology adopted in this study is visualized in Figure 3.3. The pressure fluctuations are observed to be composed of different frequencies and the kinematic resistance of the block determines the range of frequency in a spectrum at which the displacements could be observed (Bollaert & Schleiss, 2003b; George & Sitar, 2016). For each test case, we measured the dominating frequency, mean and amplitude of the normalized fluctuating pressure head at the top of the block. The dominating frequency is determined first, as it represents the frequency of the sinusoidal fluctuation with the highest energy in a signal which promotes highest displacements. We achieve this by transforming time-domain data into frequency-domain data using the Fast Fourier Transform (*FFT*) function of MATLAB. The dominating frequency corresponds to the frequency with the highest intensity in the frequency-domain data.

The mean channel velocity head (H_{ch}) at the center of the channel width measured at the instrumented block position using the XYZ-system is presented in Table 3.2. The fluctuating pressure data (H) is normalized with H_{ch} for the corresponding discharge. C_{pA} is derived by averaging all the normalized pressure data recorded over 60 seconds, equivalent to the average of 6000 data values. To

estimate C_{pA}', defined as half of the difference between maxima and minima of the data, we first employ the following approaches to determine the maxima ($C_{pA}^{+}\_max$) and minima ($C_{pA}^{-}\_min$) of the data:

i. The data is divided into three zones with two boundaries, namely ($\mu + 2\sigma$) and ($\mu - 2\sigma$), where μ and σ represent respectively the mean and the standard deviation of the pressure head data. The maxima is defined as the average of data in the zone above the boundary ($\mu + 2\sigma$), whereas minima is defined as the average of those in the zone below the boundary ($\mu - 2\sigma$). (Presented in Figure 3.4)

ii. The time domain is divided into several intervals of time and maximum & minimum values are identified for each time interval. The average of maximum and minimum values gives the maxima and minima respectively. This process is carried out at several time intervals, i.e., 0.5 s, 1 s, 2 s, 5 s, 10 s, 30 s and 60 s (total data).

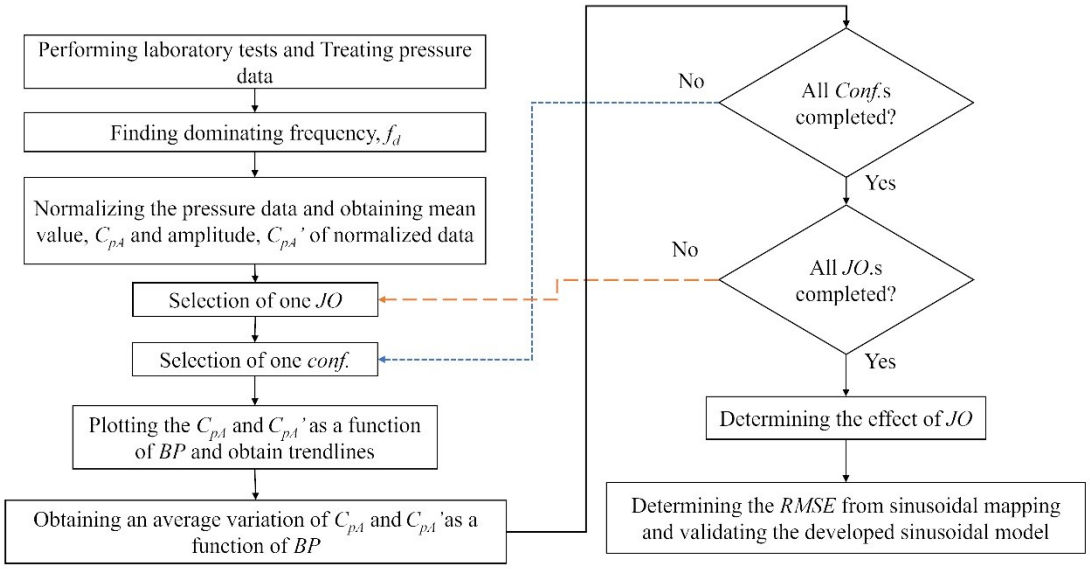

Figure 3.3 Methodology adopted for the development of sinusoidal equation

Table 3.1 Protrusion configurations adopted along with protrusion heights.

Configuration, *Conf.* #	**Setup**	**Block Protrusion Height, *BP* (mm)**	**Protrusion in 1st row (mm)**	**Protrusion in 2nd row (mm)**	**Protrusion in 3rd row (mm)**
0	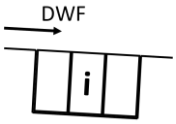	*BP0* = 00	00	00	00
1	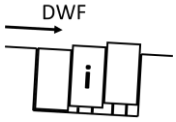	*BP1* = 06 *BP2* = 13	00 00	06 13	12 26
2	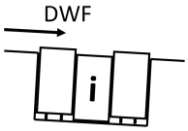	*BP1* = 13 *BP2* = 20	13 20	0 0	13 20
3	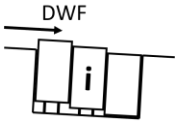	*BP1* = 06 *BP2* = 13	13 26	06 13	0 0
4	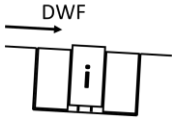	*BP1* = 13 *BP2* = 20	00 00	13 20	00 00

DWF – Direction of Water Flow

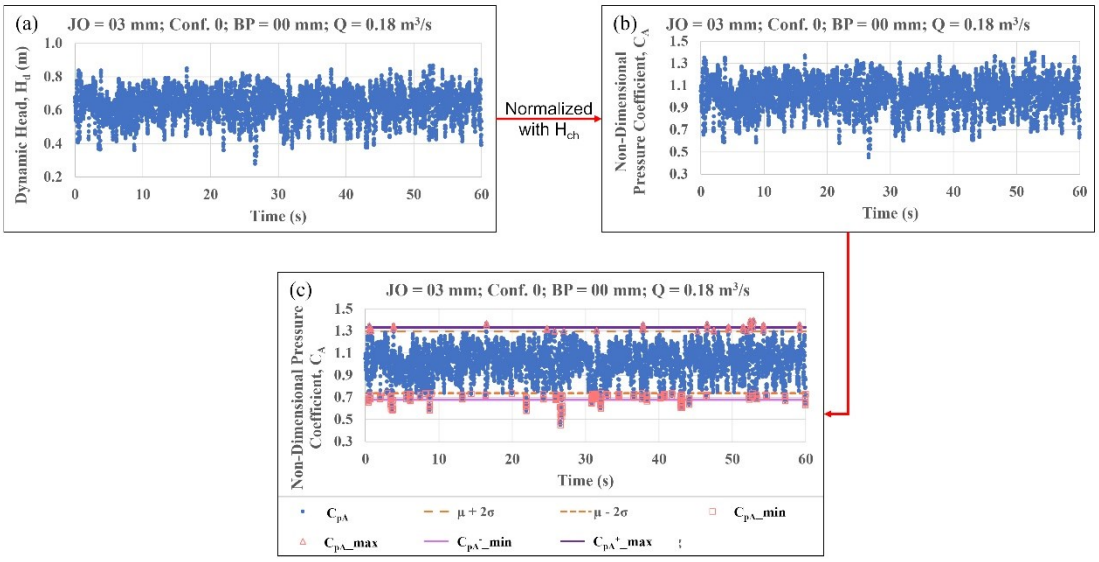

Figure 3.4 Description of the process of obtention of C_{pA} and C_{pA}': (a) Sample test dynamic head data; (b) Normalized pressure head (C_A) and; (c) Maxima and minima of the normalized pressure head (approach i)

Table 3.2 Mean channel velocity head for various test discharges at the instrumented block level

Discharge, Q (m^3/s)	0.18	0.24	0.29	0.315	0.34
Mean channel velocity, v_{ch} (m/s)	3.49	3.98	4.36	4.53	4.70
Mean channel velocity head, H_{ch} (m)	0.62	0.81	0.97	1.05	1.13

The objective of the sinusoidal equation is to accurately determine both the mean pressure head value and the possible extreme values as a function of the study parameters. Among the mentioned approaches, the first approach yielded the most satisfactory results including a range of extreme pressure fluctuations. As a result, this approach is employed to determine the amplitude of fluctuations. This approach (Figure 3.4(c)) considers about 95% of the data within these boundaries and the rest 5% as the extreme values representing the maxima and minima. Once these terms (C_{pA}, C_{pA}' and f_d) are determined for each test case, the procedure illustrated in Figure 3.3 is executed to establish a relationship between these terms and the study parameters (*JO* and *BP*).

First, a specific *JO* is selected. To explore the effect of protrusion, the results are made specific to the *Conf.*, as the outcomes shall vary with different Conf. settings. The variation of C_{pA} and C_{pA}' (Eq. 3.1) with Block Protrusion height (*BP*) is plotted for different discharges (*Q*). For each *Conf.*, *Conf. 0* is employed to represent *BP* = 0 mm and trendlines are derived for each discharge. These trendlines represent approximately the same equations for a given *JO* and *Conf.* as they are normalized with H_{ch}, which in turn is a function of *Q*. This indirectly eliminates the effect of discharge on the pressure determination.

Consequently, an average trendline is obtained from these equations for each *JO* and *Conf.* In the next step, the effect of *JO* is studied for each *Conf.* To achieve this, the average trendline obtained in the earlier step is used to calculate the C_{pA} and C_{pA}' for different arbitrary *BP* values. These values are obtained for different *JO* and are normalized with the values corresponding to *JO* value of 3 mm. Two new terms, namely, Mean Value Ratio (*MVR-JO*) and Amplitude Ratio (*AR-JO*) are introduced, which are defined as ($C_{pA}JO/C_{pA}JO03$) and ($C_{pA}'JO/C_{pA}'JO03$) respectively. $C_{pA}JO$ and $C_{pA}'JO$ represent the value of C_{pA} and C_{pA}' at a joint opening *JO*. *MVR-JO* and *AR-JO* values, that serve as normalisation factors, are plotted against the *JO* to examine the variation of these terms as a function of joint opening. This process is repeated for all the *Conf.* tested. Finally, a relationship is established between the study parameters (*JO*, *BP* and *Q*) and arbitrary terms of Eq. 3.1 (f_d, C_{pA} and C_{pA}').

3.5 DEVELOPMENT OF A MATHEMATICAL EQUATION FOR PRESSURE FLUCTUATIONS

3.5.1 Pressure fluctuations on the top and bottom of the block

The pressure data recorded by the sensors consists of datum head, static head and dynamic head components. The static and dynamic pressure head is isolated by removing the datum head of each water entry to the sensor level. By removing the static head (measured using the float mounted with *LVDT*), dynamic head (velocity head) can be obtained. Since the flow in the spillway channel is unsteady, the static head of the water exhibits slight variations with time. However, these variations are very minimal,

as observed from Figure 3.5-3.7[1], that depict the static head variations for *Conf. 0* across different *JO*s. One noteworthy observation that could be made from the static head is that the mean head value initially experiences a slight decrease from Q_1 to Q_2, followed by an increase for Q_3 and Q_4 in all *JO* cases.

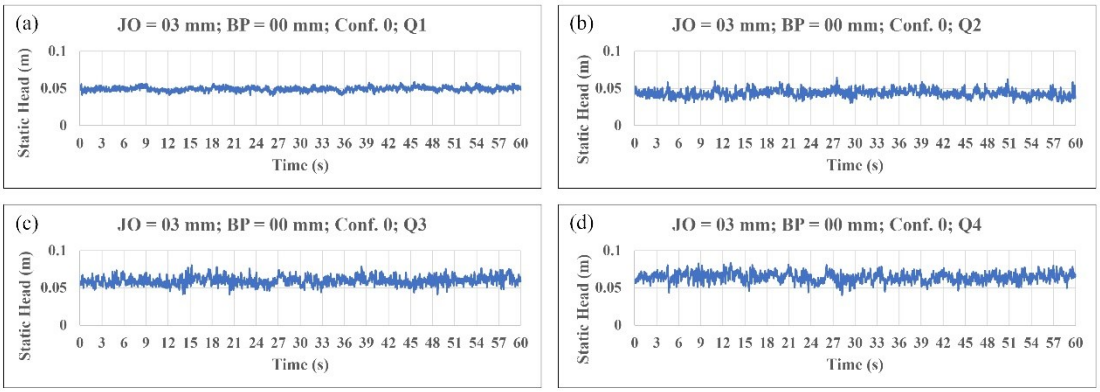

Figure 3.5 Static pressure head fluctuations for *Conf. 0* and *JO* = 03 mm for discharges: (a) Q_1 = 0.18 m^3/s; (b) Q_2 = 0.24 m^3/s; (c) Q_3 = 0.315 m^3/s; (d) Q_4 = 0.34 m^3/s

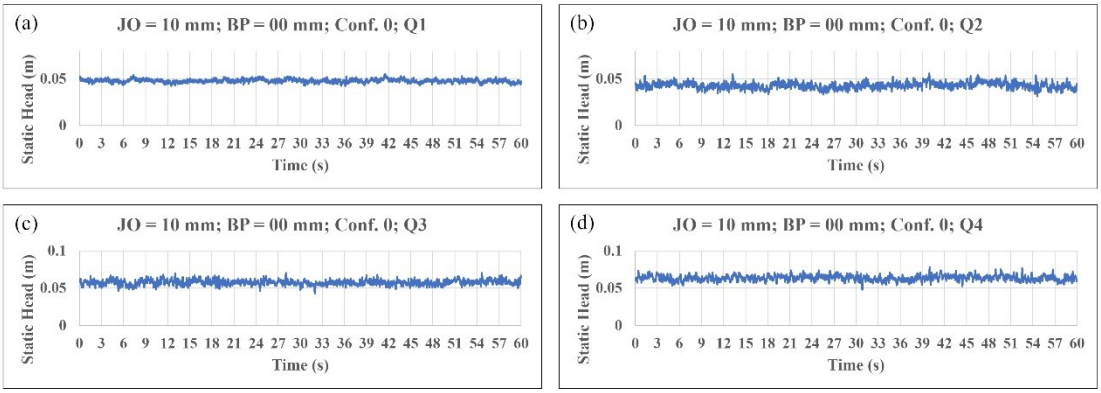

Figure 3.6 Static pressure head fluctuations for *Conf. 0* and *JO* = 10 mm for discharges: (a) Q_1 = 0.18 m^3/s; (b) Q_2 = 0.24 m^3/s; (c) Q_3 = 0.315 m^3/s; (d) Q_4 = 0.34 m^3/s

[1] The static head is also measured for other test configurations which is found to be similar as the measurement of static head is not exactly above the instrumented block and is a little ahead of the blocks. Hence the results for other configurations are not presented in this article.

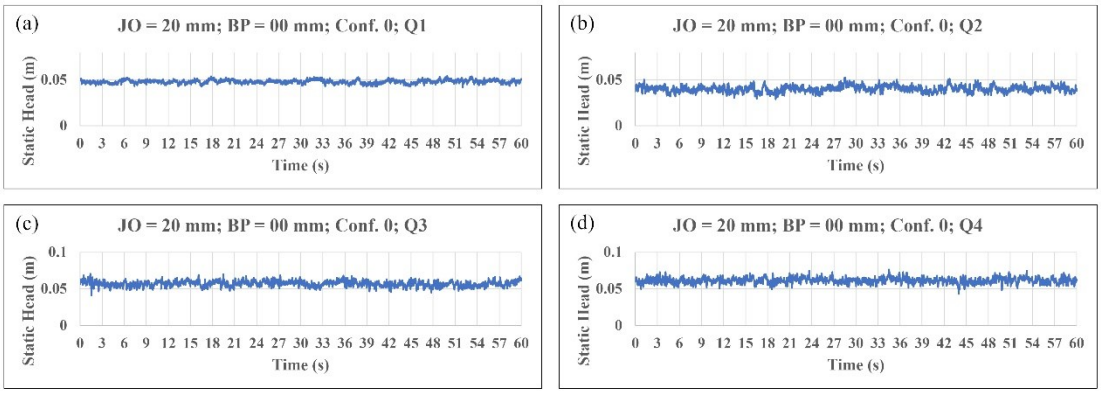

Figure 3.7 Static pressure head fluctuations for *Conf. 0* and *JO* = 20 mm for discharges: (a) Q_1 = 0.18 m^3/s; (b) Q_2 = 0.24 m^3/s; (c) Q_3 = 0.315 m^3/s; (d) Q_4 = 0.34 m^3/s

The variation of dynamic head in *Conf. 0* across different JOs is presented in Figure 3.8-3.10. These figures reveal that the pressure fluctuations are significantly more pronounced at the top of the block compared to those inside the joint at the bottom of the block. The amplitude of fluctuations is observed to be reducing with the increasing *JO*. Within each *JO* scenario, an increase in discharge (*Q*) is associated with an increase in dynamic head, which is attributed to the elevated flow velocity within the channel. Interestingly, the velocities of flow inside the joint at the bottom of the block, measured in both the flow direction and the opposite direction of flow in the channel, appear to be similar. This underscores the significance of pressure head fluctuations at the top of the block, as they govern the uplift mechanism of the block in parallel flow spillways. When these fluctuations fall below the pressure at the bottom of the block, they can trigger the uplift process. Further sections will delve into the influence of test configurations on dynamic head variations at the top of the block, including variations in mean pressure head and fluctuation amplitude.

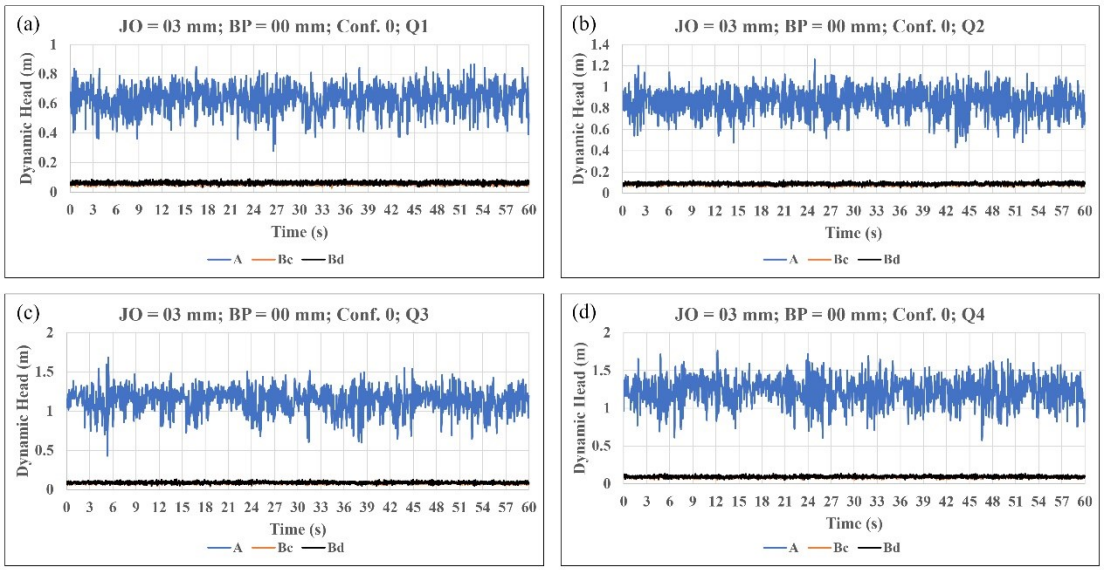

Figure 3.8 Dynamic pressure head fluctuations for *Conf. 0* and *JO* = 03 mm at the top and bottom of the instrumented block for discharges: (a) Q_1 = 0.18 m^3/s; (b) Q_2 = 0.24 m^3/s; (c) Q_3 = 0.315 m^3/s; (d) Q_4 = 0.34 m^3/s

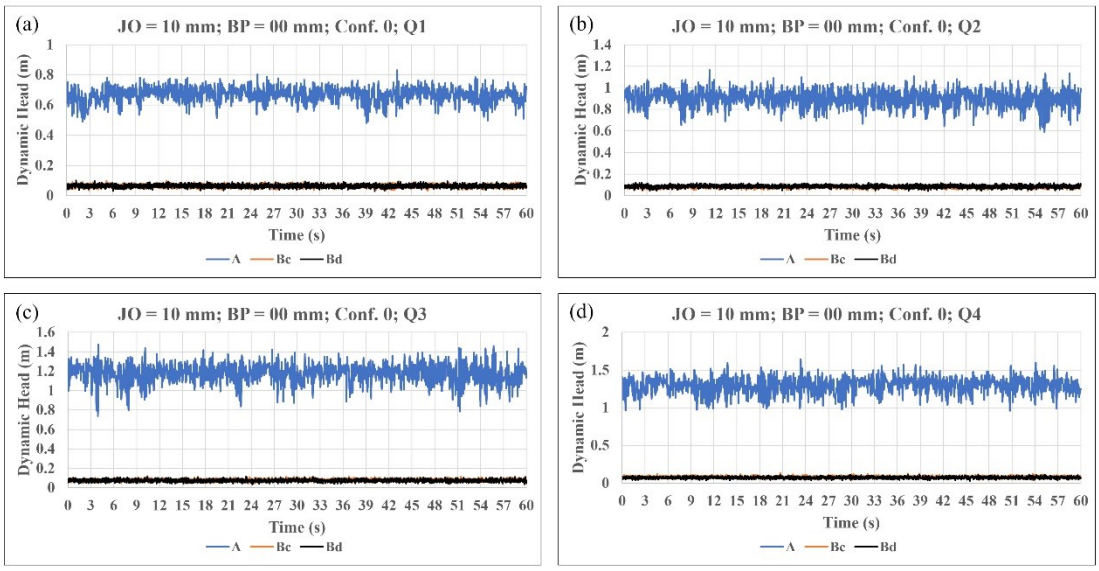

Figure 3.9 Dynamic pressure head fluctuations for *Conf. 0* and *JO* = 10 mm at the top and bottom of the instrumented block for discharges: (a) Q_1 = 0.18 m^3/s; (b) Q_2 = 0.24 m^3/s; (c) Q_3 = 0.315 m^3/s; (d) Q_4 = 0.34 m^3/s

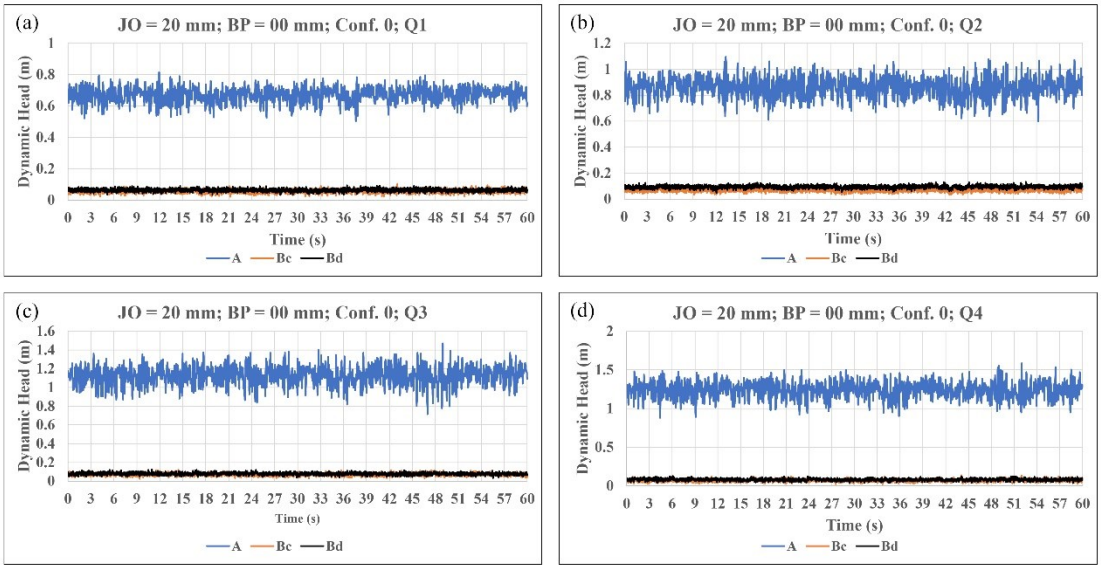

Figure 3.10 Dynamic pressure head fluctuations for *Conf. 0* and *JO* = 20 mm at the top and bottom of the instrumented block for discharges: (a) Q_1 = 0.18 m^3/s; (b) Q_2 = 0.24 m^3/s; (c) Q_3 = 0.315 m^3/s; (d) Q_4 = 0.34 m^3/s

3.5.2 Variation of dominating frequency, f_d, for different test conditions

Any fluctuating signal can be represented by a sum of sinusoidal signals. The dominating frequency, f_d represents the frequency of the sinusoidal signals with highest energy. This point suggests that f_d can be used to represent the frequency of the sinusoidal equation to predict the fluctuating dynamic pressures acting on the rock mass. Given the data collection frequency of 100 Hz used during the tests, the frequency domain obtained from the *FFT* function ranges from 0 to 100. However, it's worth noting that the dominating frequency for all the tests was consistently observed to be below 10 Hz. To provide better clarity, the frequency domain results for various tests are displayed only up to 10 Hz, as shown in Figure 3.11-3.13.

The dominating frequency from each frequency domain data is identified and presented in Table 3.3. Notably, the frequency spectra for *Conf.* 3 with 13 mm BP value in 10 mm and 20 mm *JO* values are found to be different from other spectra [Figure 3.12(b-d) and Figure 3.13(b)]. However, it's essential to highlight that the f_d values do not exhibit a clear trend with any of the study parameters. They predominantly fall within the range of 3-6 Hz, disregarding the erroneous results of *Conf.* 3 with a 13

mm *BP* value. To verify the correlation between f_d and study parameters, single factor analysis of variance (*ANOVA*) has been performed, the results of which are present in Annexe B. The *ANOVA* results show that *JO* has a statistically significant effect on f_d, whereas *Conf.*, *BP* and *Q* do not exhibit significant influence.

Though *JO* is statistically significant, the practical variation in f_d remains minor (the mean f_d for different *JO* are 4.43, 4.72 and 5.25 Hz respectively). The primary objective behind developing the sinusoidal equation is to identify the potential extreme values responsible for triggering the uplift. The value of f_d in Eq. 3.1 determines how many times the amplitude can be observed in $1/2\pi$ s. Consequently, for further analysis, a constant f_d value of 4 Hz is chosen.

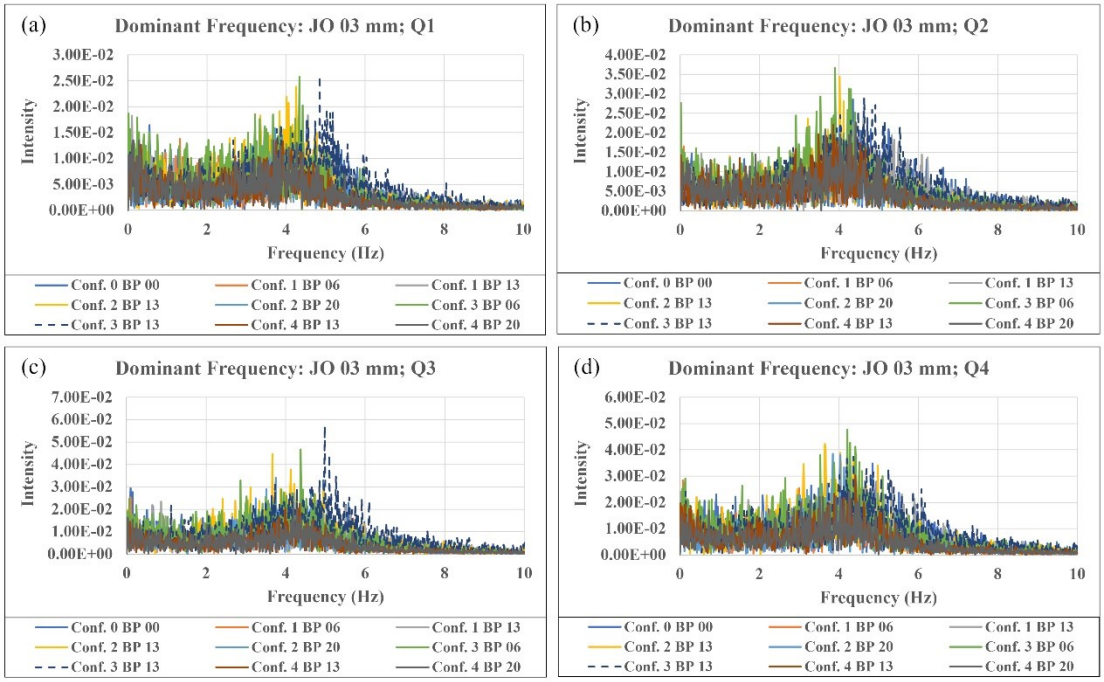

Figure 3.11 Frequency domain of the dynamic head data for 3 mm *JO* value for (a) Q_1 = 0.18 m^3/s, (b) Q_2 = 0.24 m^3/s, (c) Q_3 = 0.315 m^3/s and (d) Q_4 = 0.34 m^3/s

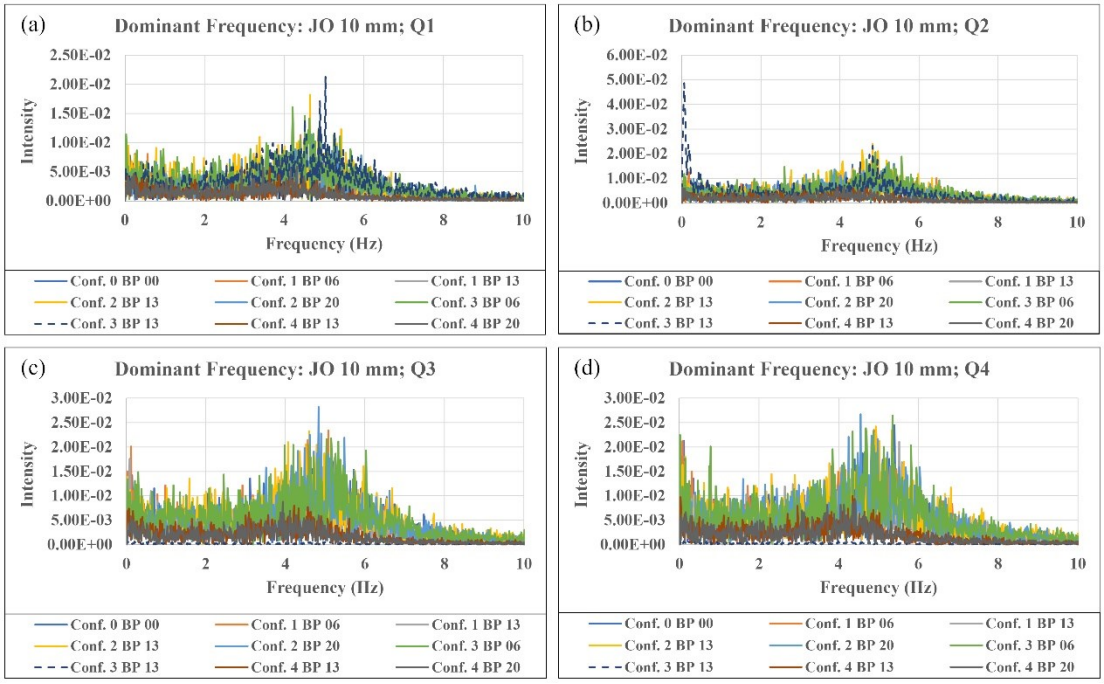

Figure 3.12 Frequency domain of the dynamic head data for 10 mm *JO* value for (a) Q_1 = 0.18 m^3/s, (b) Q_2 = 0.24 m^3/s, (c) Q_3 = 0.315 m^3/s and (d) Q_4 = 0.34 m^3/s

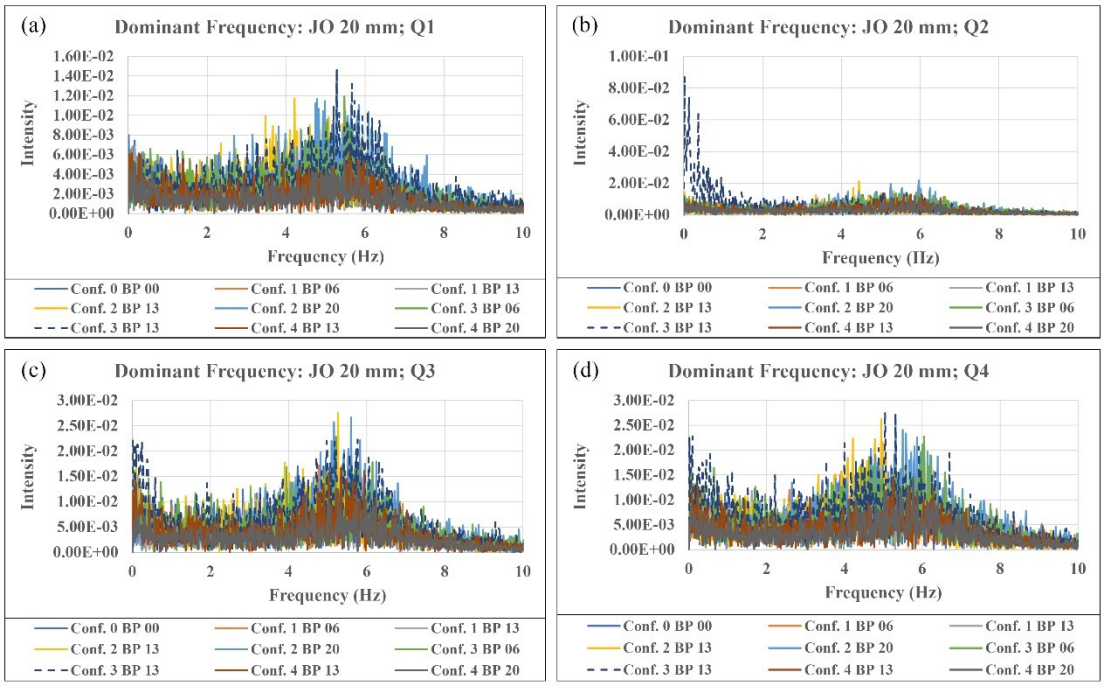

Figure 3.13 Frequency domain of the dynamic head data for 20 mm *JO* value for (a) Q_1 = 0.18 m^3/s, (b) Q_2 = 0.24 m^3/s, (c) Q_3 = 0.315 m^3/s and (d) Q_4 = 0.34 m^3/s

Table 3.3 Dominating frequency data for all the tests performed

Joint Opening		***JO 03***				***JO 10***				***JO 20***			
Conf.	***BP* (mm)**	Q_1	Q_2	Q_3	Q_4	Q_1	Q_2	Q_3	Q_4	Q_1	Q_2	Q_3	Q_4
0	0	4.32	4.35	4.95	4.85	4.88	5.37	5.23	5.40	5.05	5.27	4.95	4.97
1	6	4.30	4.28	4.12	4.52	4.42	5.20	5.08	4.88	5.45	5.63	4.77	5.42
1	13	4.55	4.62	5.05	4.18	4.78	5.22	4.82	4.92	5.23	6.00	5.83	5.87
2	13	4.25	4.02	3.67	3.65	4.65	4.83	4.60	4.93	4.22	4.45	5.27	4.95
2	20	3.45	4.22	3.75	3.85	4.68	4.83	4.83	4.55	5.28	5.97	5.60	5.32
3	6	4.33	3.90	4.38	4.22	4.22	4.90	5.15	5.35	5.48	5.90	5.22	6.05
3	13	4.85	4.63	4.98	4.37	5.03	0.07	4.93	0.03	5.28	0.02	5.77	5.05
4	13	3.75	3.85	4.35	4.42	3.63	3.95	4.22	4.35	5.60	5.10	5.35	5.25
4	20	3.68	4.42	4.20	4.27	3.47	4.12	3.93	4.42	5.48	5.87	5.27	5.77

3.5.3 Effect of block protrusion on C_{pA}

Figure 3.14-3.16 present the results of C_{pA}, computed as described in section 3.4, as a function of *BP* values for various *Conf.*s across different *JO*s. These figures show that the influence of *BP* on C_{pA} varies systematically with *Conf.* For the case of 3 mm *JO*, the positive protrusion cases, i.e., *Conf. 1* and *Conf. 4* [Figure 3.14(a) and Figure 3.14(d)], exhibit slight or no reduction in the dynamic head. In contrast, the negative protrusion cases, i.e., *Conf. 2* and *Conf. 3* [Figure 3.14(b) and Figure 3.14(c)], each one shows a reduction of about 50-60% for the highest *BP* value used in the respective configuration.

This reduction can be attributed to the development of stagnation pressure at the protruded surface and the development of a hydraulic jump. Similar observations hold for the cases of positive protrusion in both 10 mm and 20 mm *JO* values, however, in *Conf. 2*, only about 25-35% reduction in mean dynamic head is observed for the highest *BP* value.

In the case of *Conf. 3* in 10 mm *JO* value, the results show that the mean dynamic head values decrease with increase in discharge for a *BP* value of 13 mm. Similarly, for the same *Conf.* in 20 mm *JO*, similar results are obtained only for Q_2; for other discharges this reduction is not observed. This behavior could be attributed to the water entry position within the instrumented block. *Conf. 3* with 13 mm *BP* value results in a protrusion height of 26 mm in the first row of blocks, leading to a development of a hydraulic jump (Figure 3.17(c)) that reduces the velocity of flow recorded at the water inlet *A*. A comparison of the flow conditions (normal and one with hydraulic jump) at selected test arrangements along with corresponding time-domain pressure variations is presented in Figure 3.17. To better understand the flow patterns, please refer to the attached supplementary video files (JO 10mm Conf. 3 BP 06mm Q3.mp4 and JO 10mm Conf. 3 BP 13mm Q3.mp4), for the test arrangements presented in Figure 3.17, attached along with this article.

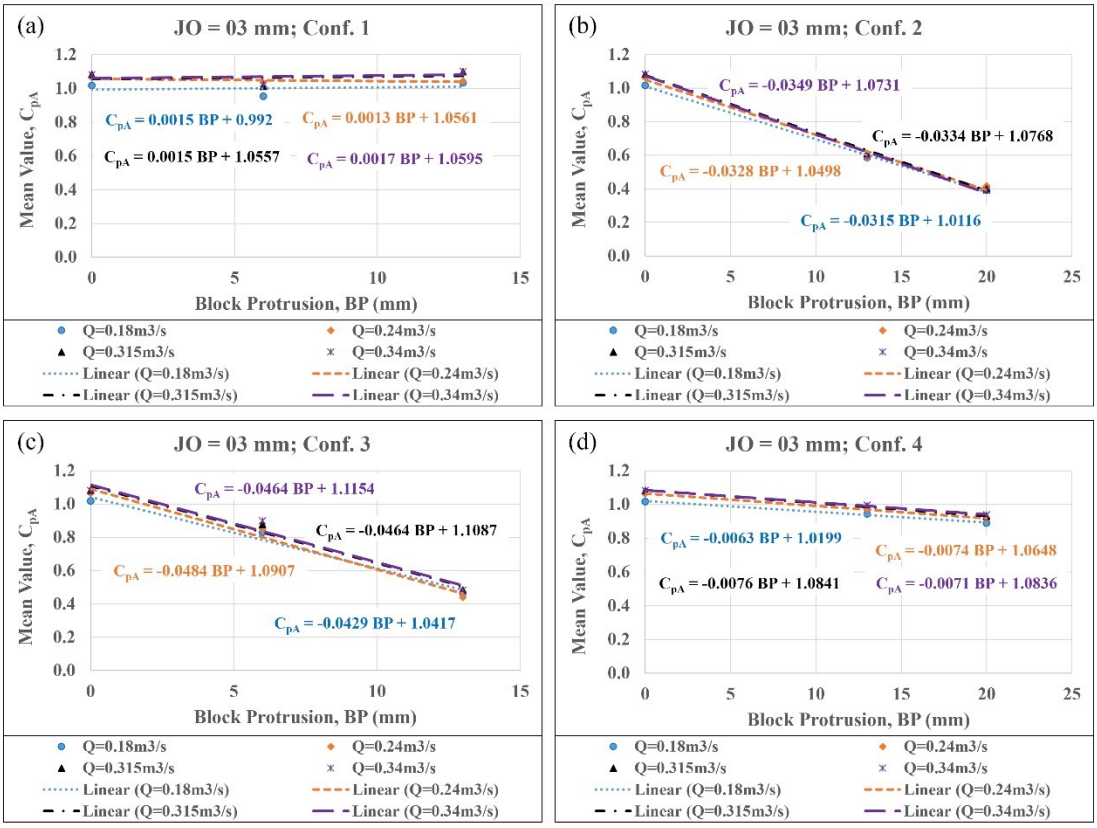

Figure 3.14 Variation of mean value (C_{pA}) with block protrusion height (BP) for JO = 03 mm in (a) *Conf. 1*, (b) *Conf. 2*, (c) *Conf. 3* and (d) *Conf. 4*

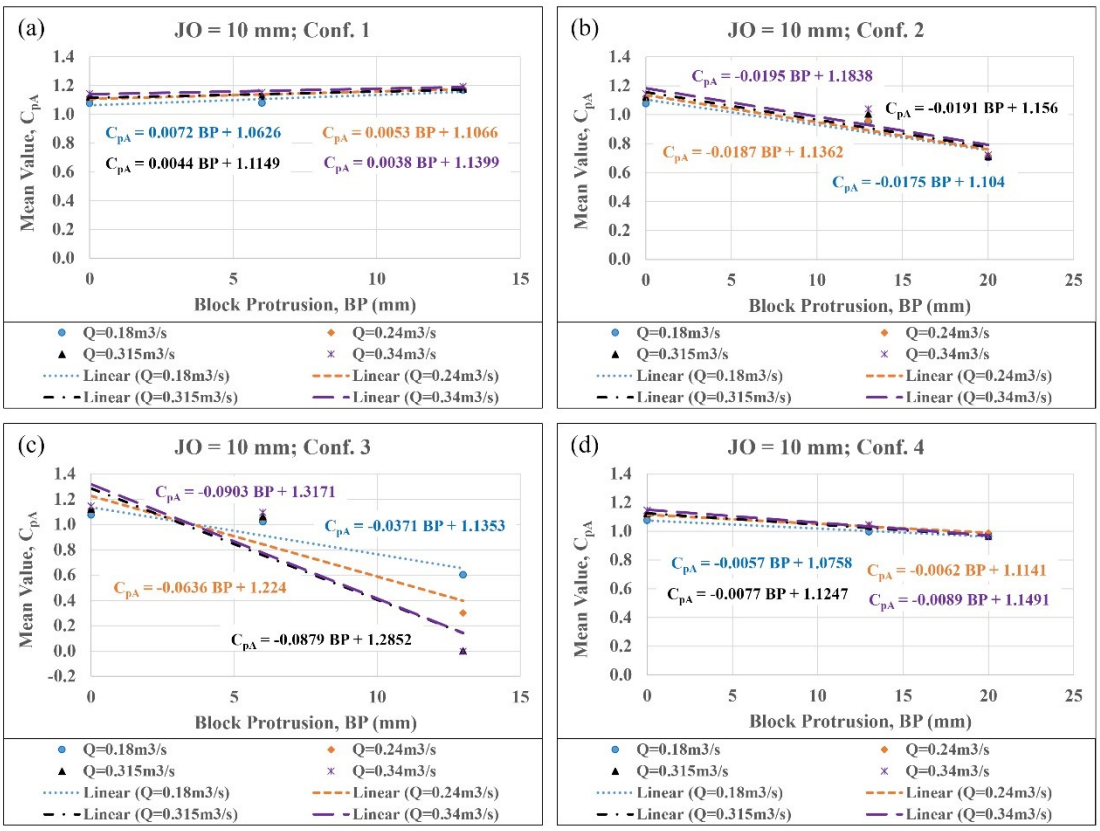

Figure 3.15 Variation of mean value (C_{pA}) with block protrusion height (BP) for JO = 10 mm in (a) *Conf. 1*, (b) *Conf. 2*, (c) *Conf. 3* and (d) *Conf. 4*

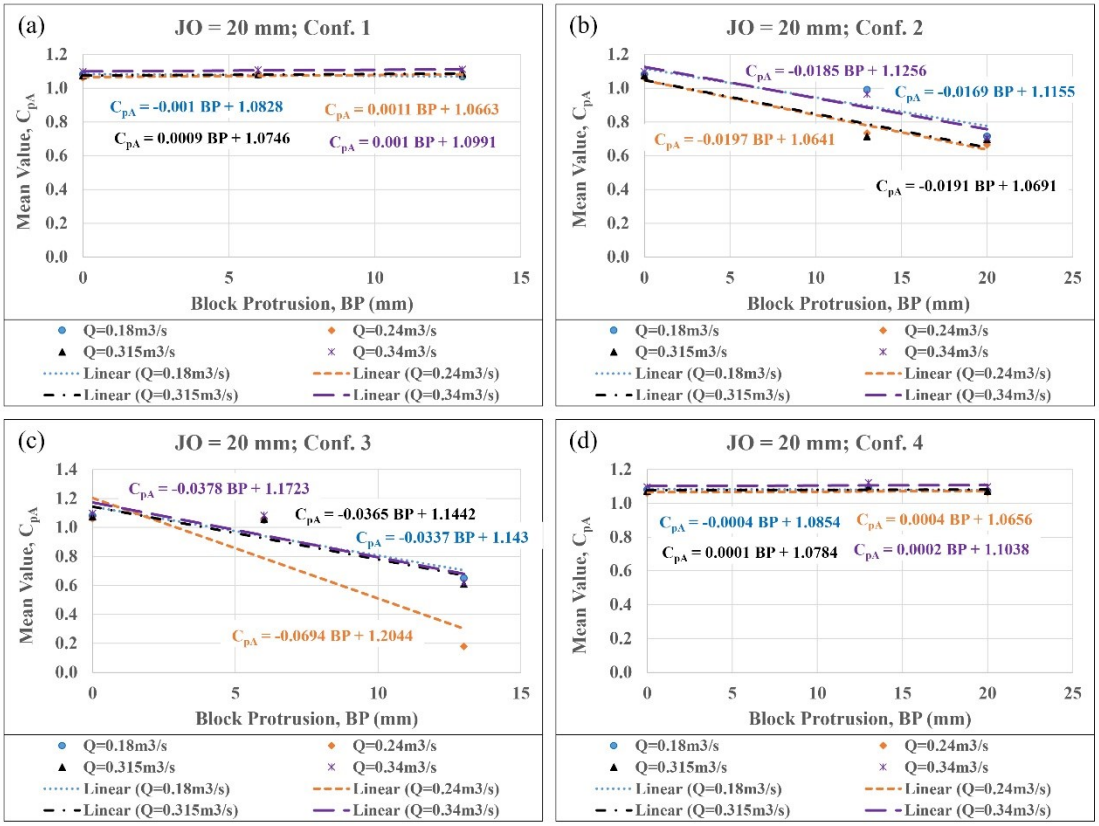

Figure 3.16 Variation of mean value (C_{pA}) with block protrusion height (BP) for JO = 20 mm in (a) *Conf. 1*, (b) *Conf. 2*, (c) *Conf. 3* and (d) *Conf. 4*

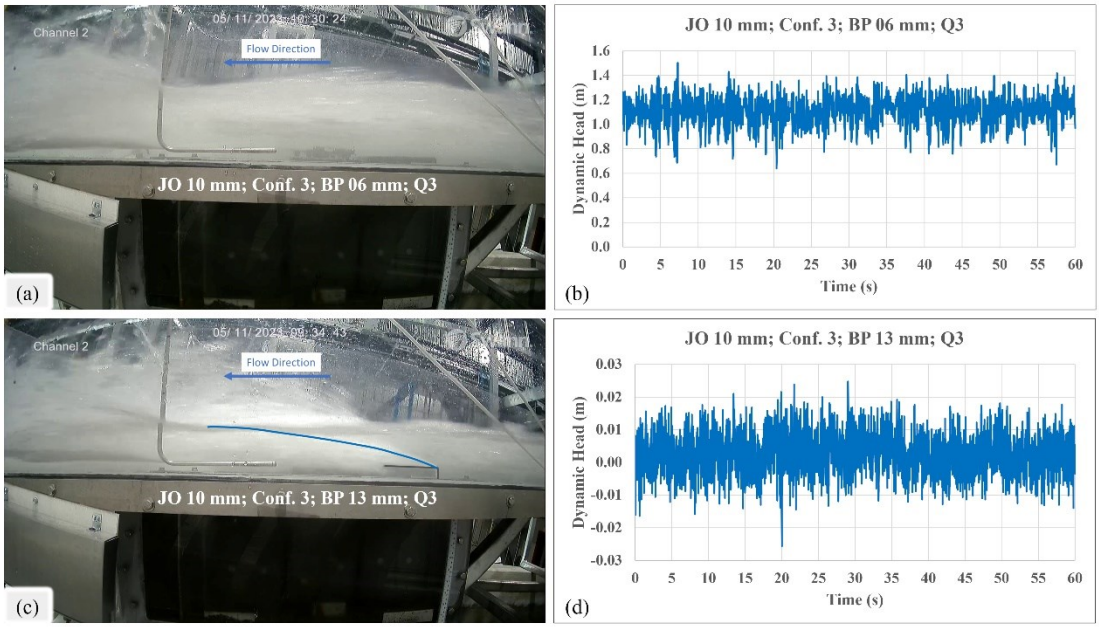

Figure 3.17 Hydraulic jump formation at the protruded surface in negative protrusion configuration (*Conf. 3*)

The probability of development of a negative pressure zone arises in this situation that results in the lower pressure. Thus, the results obtained under the hydraulic jump are considered erroneous and removed while forming the trendlines. These corrected figures for *Conf. 3* are presented for C_{pA} in Figure 3.18. Another noteworthy observation is that, in each of the other configurations, the trendlines plotted for different discharges are approximately similar, suggesting the possibility of obtaining a unique variation as a function of *BP*.

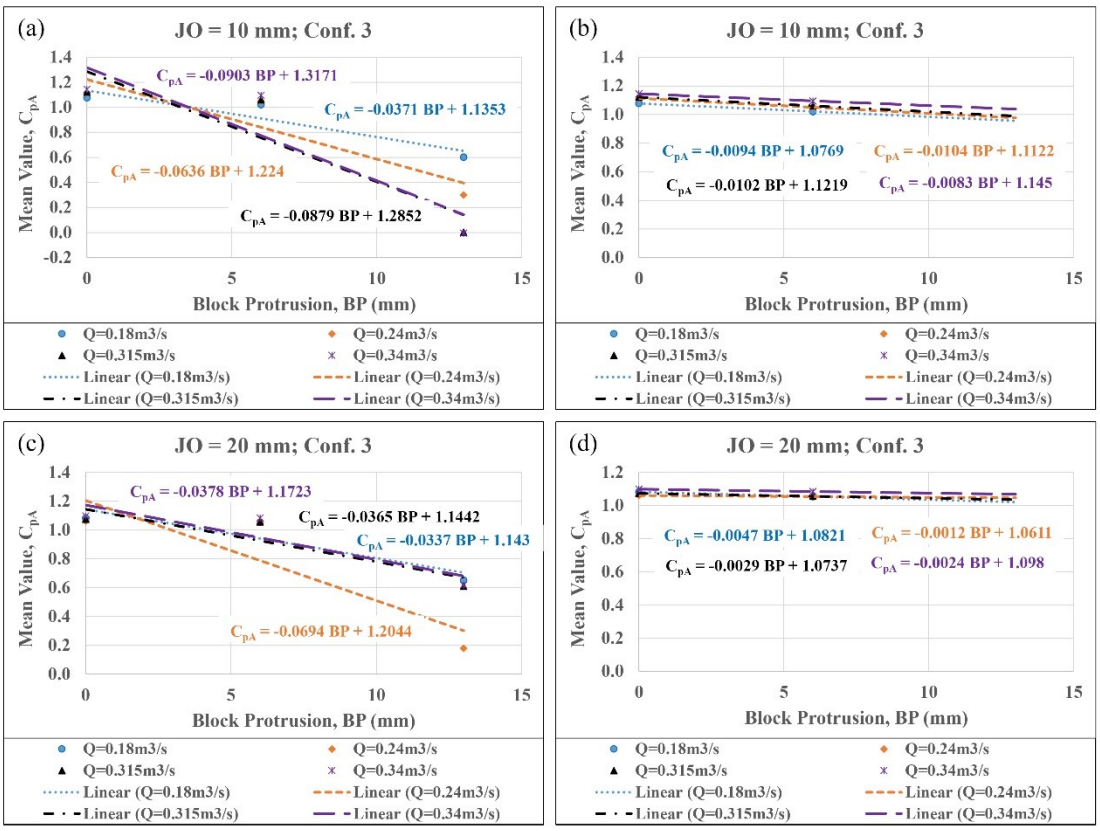

Figure 3.18 Corrected variation of mean value (C_{pA}) with block protrusion height (*BP*) for *Conf. 3*: (a) Original variation for *JO 10*, (b) Corrected variation for *JO 10*, (c) Original variation for *JO 20*, and (d) Corrected variation for *JO 20*

3.5.4 Effect of block protrusion on C_{pA}'

Figure 3.19-3.21 display the results of amplitude values, C_{pA}', computed as mentioned in section 3, as a function of *BP* values across different *JO* values, for various configurations. A comparison of these figures conclude that the amplitude of fluctuations is highest for 03 mm *JO* value, i.e., gapped joints, whereas for the bigger *JO* values, i.e., more open joints, a similar amplitude of fluctuations is observed which is about 60-70% of that observed for 3 mm *JO* values. For a given configuration, different *JO* values exhibit a consistent variation pattern as a function of *BP* values. Figure 3.19-3.21 also reveal that the positive protrusion configurations exhibit a reduction in the amplitude of fluctuations, whereas the negative protrusion configurations show an augmentation except for *Conf. 2* of 3 mm *JO*

value [Figure 3.19(b)]. This peculiar behavior can once again be attributed to the position of water entry point *A*, which is close to the protruded surface and thus reduces the velocity of flow entering the inlet.

Across all *JO* values, Conf. *1* [Figure 3.19-3.21(a)] displays mild negative slope with *BP* values, while *Conf. 4* [Figure 3.19-3.21(d)] exhibits a slightly steeper slope. For *Conf. 2* in 10 mm and 20 mm *JO* values [Figure 3.20-3.21(b)], a mild negative slope is observed, whereas *Conf. 3* in all *JO* values, [Figure 3.19-3.21(c)], exhibit a steeper positive slope compared to other configurations. As mentioned for the C_{pA} values, the results obtained under the hydraulic jump are considered erroneous and removed while forming the trendlines. These corrected figures for *Conf. 3* are presented for C_{pA}' in Figure 3.22. Overall, consistent discharge-independent C_{pA}' - *BP* variations across *Conf.*s enable the derivation of unique relationship between amplitude and *BP* for each *Conf.* and *JO*.

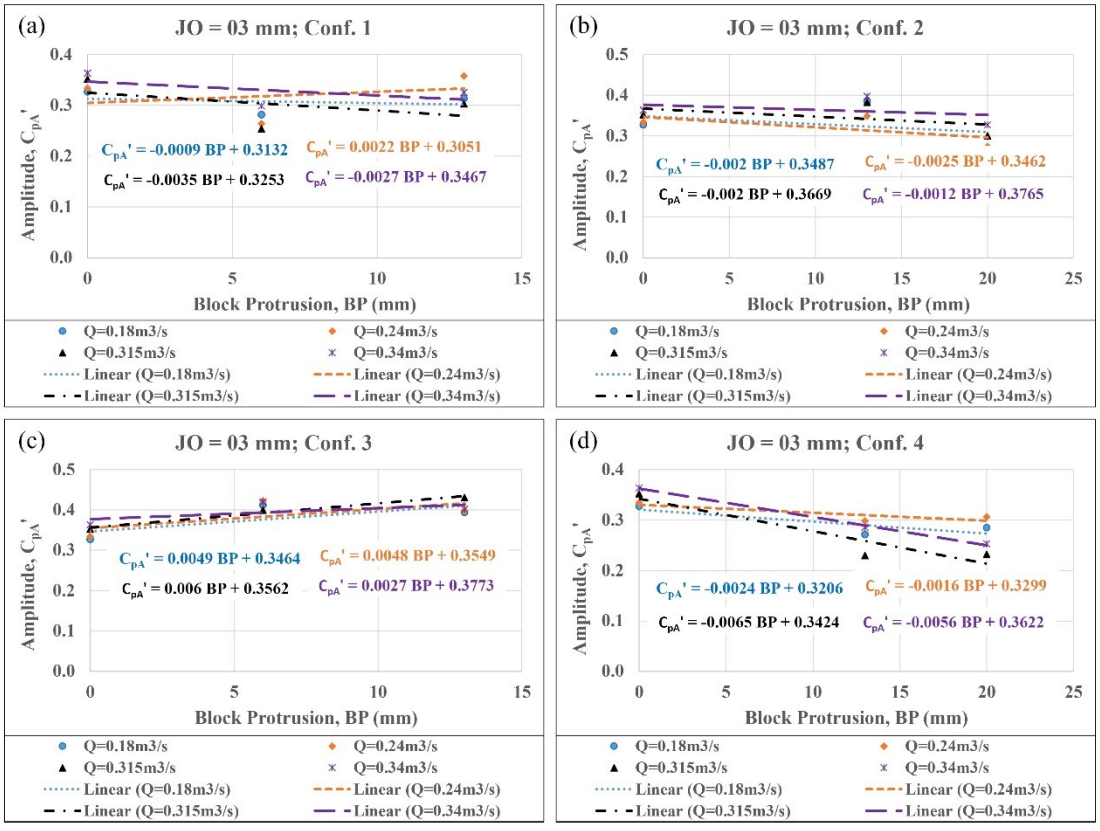

Figure 3.19 Variation of amplitude of fluctuations (C_{pA}') with block protrusion height (*BP*) for *JO* = 3 mm in: (a) *Conf. 1*; (b) *Conf. 2*; (c) *Conf. 3*; (d) *Conf. 4*

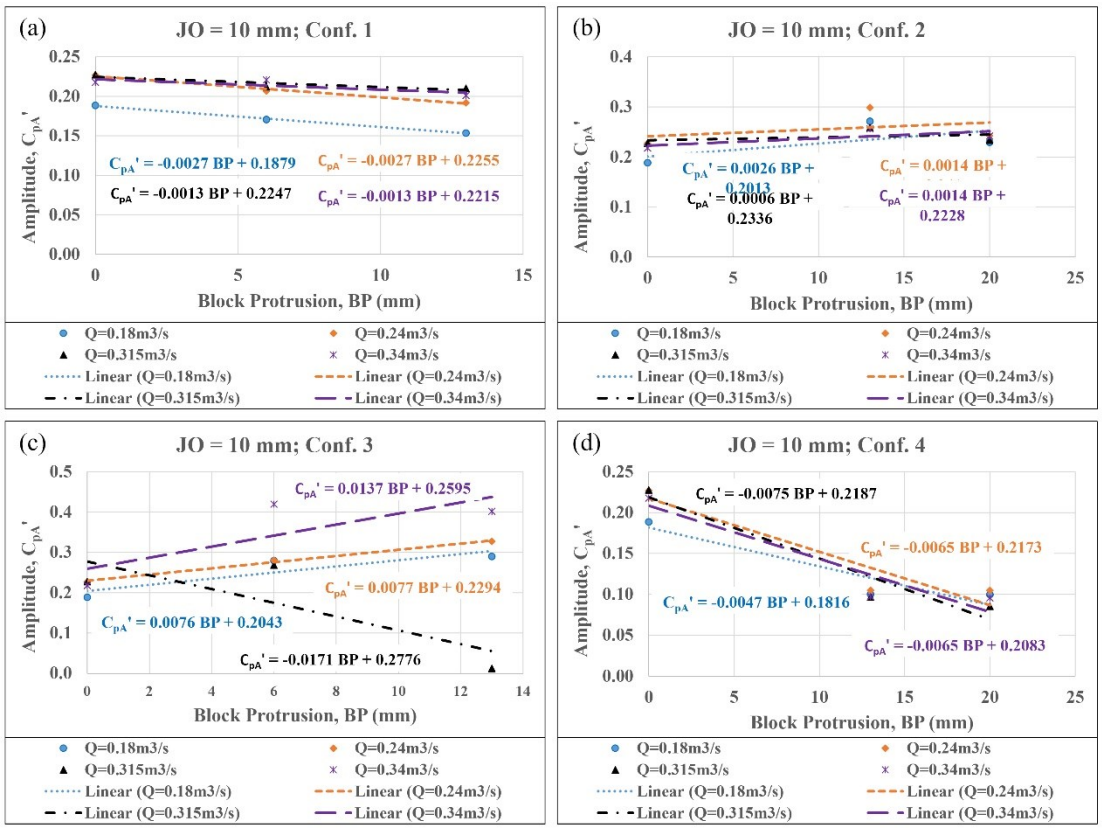

Figure 3.20 Variation of amplitude of fluctuations (C_{pA}') with block protrusion height (BP) for JO = 10 mm in (a) *Conf. 1*, (b) *Conf. 2*, (c) *Conf. 3* and (d) *Conf. 4*

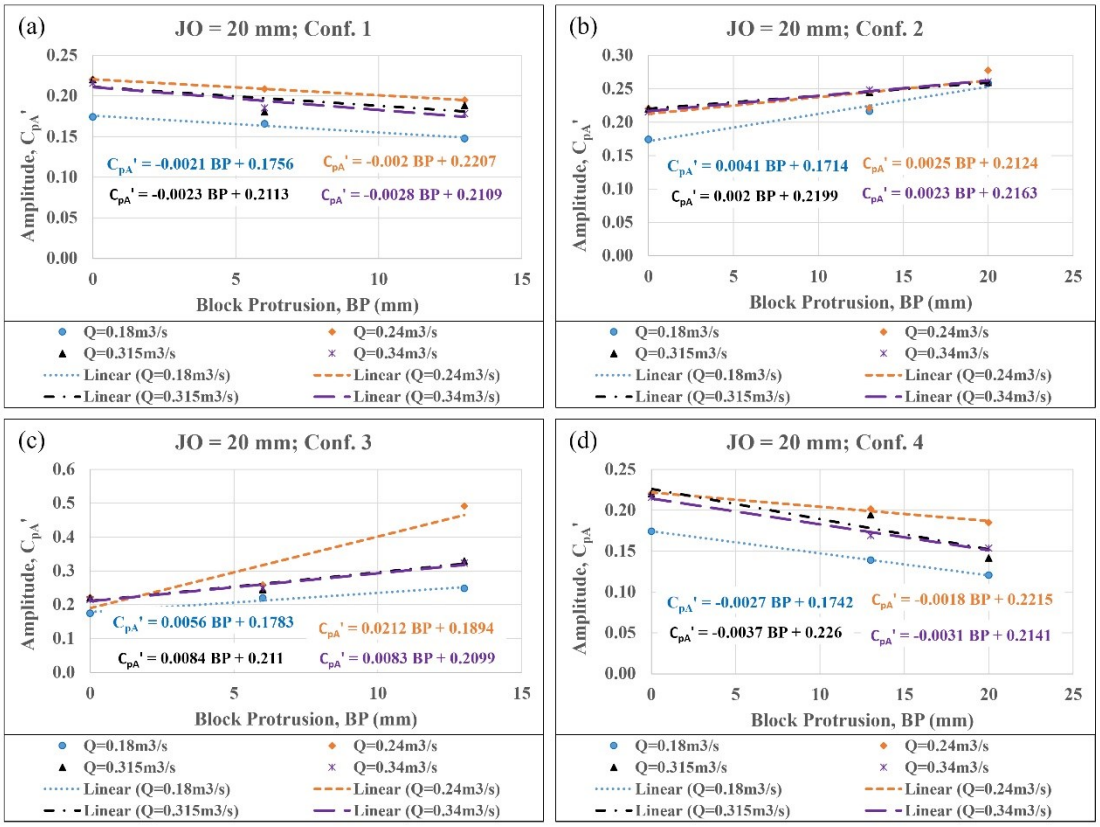

Figure 3.21 Variation of amplitude of fluctuations (C_{pA}') with block protrusion height (BP) for JO = 20 mm in (a) *Conf. 1*, (b) *Conf. 2*, (c) *Conf. 3* and (d) *Conf. 4*

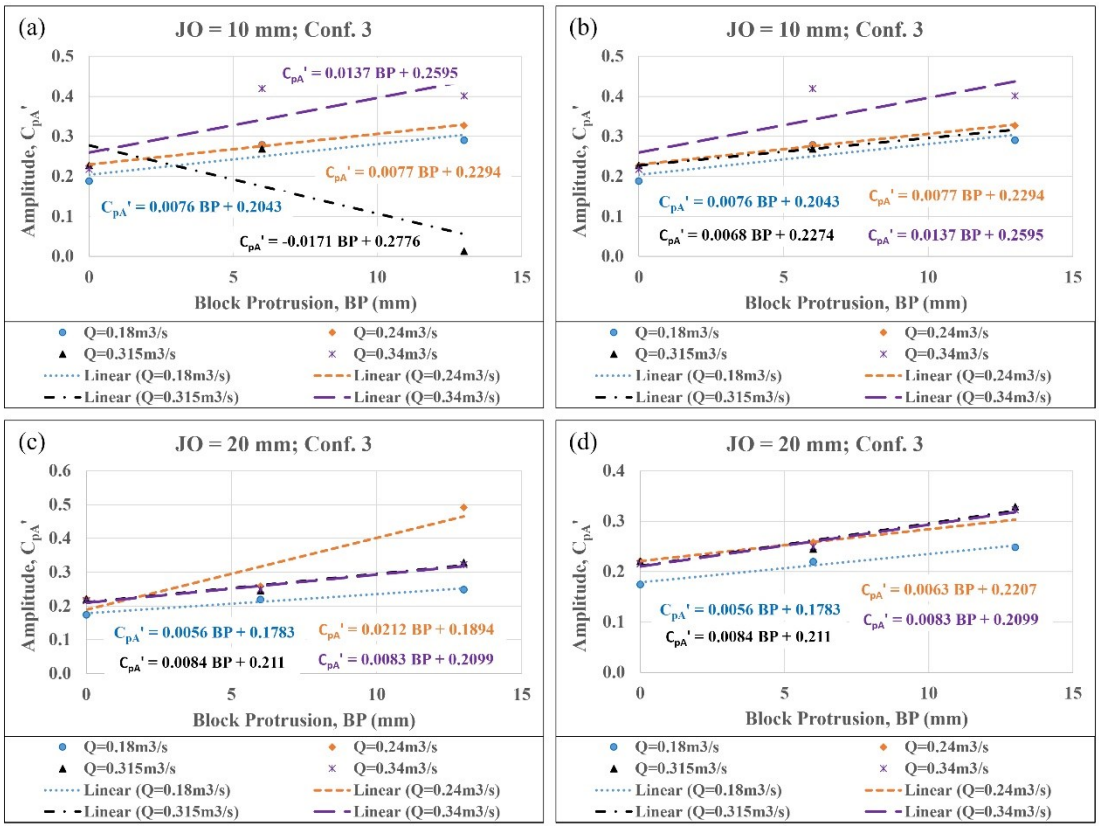

Figure 3.22 Corrected variation of amplitude (C_{pA}') with block protrusion height (*BP*) for *Conf. 3*: (a) Original variation for *JO 10*, (b) Corrected variation for *JO 10*, (c) Original variation for *JO 20*, and (d) Corrected variation for *JO 20*

3.5.5 Determination of unique variation of C_{pA} and C_{pA}' with *BP*

As explained in sections 3.5.3 and 3.5.4, the variation of C_{pA} and C_{pA}' with *BP* values for a given *Conf.* and *JO* is consistent for different discharges. Hence, we have obtained a unique variation of these terms with *BP*. Depending on the configuration (*Conf.*), a range of block protrusion (*BP*) values is chosen. For *Conf. 1* & *Conf. 3*, the range is 0-13 mm, while for *Conf. 2* and *Conf. 4*, it's 0-20 mm. This process is depicted in Figure 3.23 for C_{pA} for the case of *JO 03* and *Conf. 1*. Using the trendline equations from Figure 3.14(a), the mean values, $C_{pA}Q_x$ (x refers to the corresponding discharge numbers 1-4) are calculated for different discharges within the chosen *BP* range as depicted in Figure 3.23(b). Average of these values is calculated for each *BP* value and are plotted against *BP* to obtain the average mean value variation with *BP* (Figure 3.23(c)). This process is repeated for different *Conf.*s and *JO*s studied. These

variations for different *Conf.*s and *JO*s studied are presented in Figure 3.24. This process is also adopted for the amplitude variations to obtain the average amplitude variations with *BP*, which are presented in Figure 3.25. The trendline equations determined from Figure 3.24-3.25 are presented in Table 3.4.

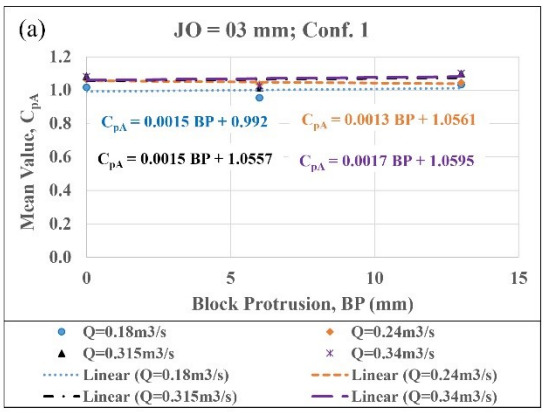

(b)

BP	$C_{pA}Q_1$	$C_{pA}Q_2$	$C_{pA}Q_3$	$C_{pA}Q_4$	$C_{pA}Q_{avg}$
mm	-	-	-	-	-
0	0.992	1.0561	1.0557	1.0595	1.0408
2	0.995	1.0535	1.0587	1.0629	1.0425
4	0.998	1.0509	1.0617	1.0663	1.0442
6	1.001	1.0483	1.0647	1.0697	1.0459
8	1.004	1.0457	1.0677	1.0731	1.0476
10	1.007	1.0431	1.0707	1.0765	1.0493
12	1.01	1.0405	1.0737	1.0799	1.0510
13	1.0115	1.0392	1.0752	1.0816	1.0519

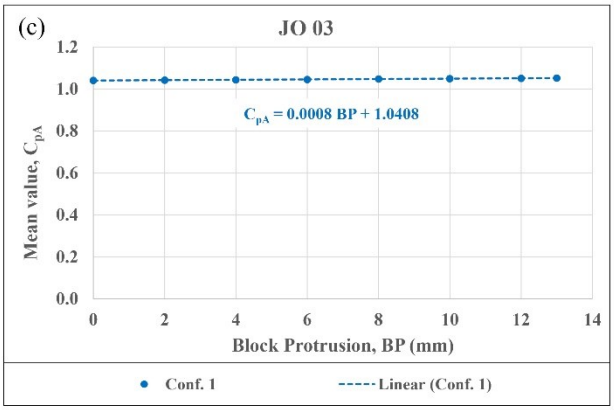

Figure 3.23 Depiction of the process of obtaining the average variation adopted in this study: (a) Variation of C_{pA} with *BP*, (b) Determination of C_{pA} values from the regression trendlines for different *BP* values and (c) Average mean value variation with *BP* for various discharges

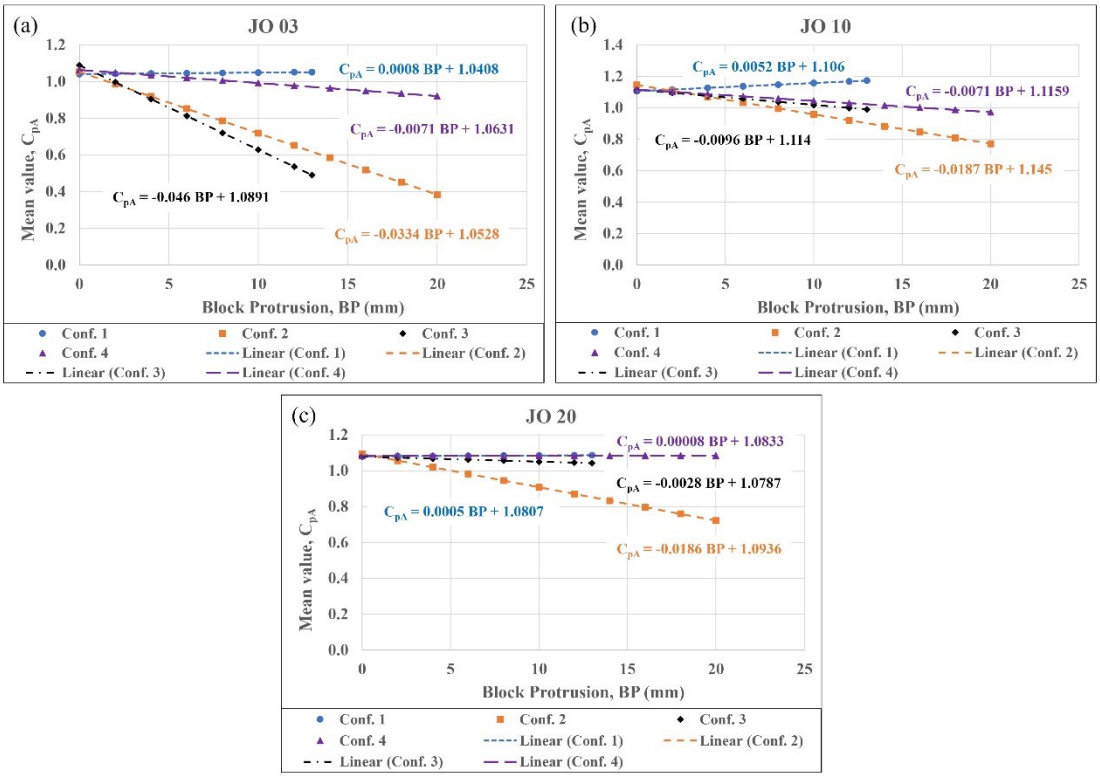

Figure 3.24 Average mean value variations with *BP* for different test *Conf.*s: (a) *JO* = 3 mm, (b) *JO* = 10 mm and (c) *JO* = 20 mm

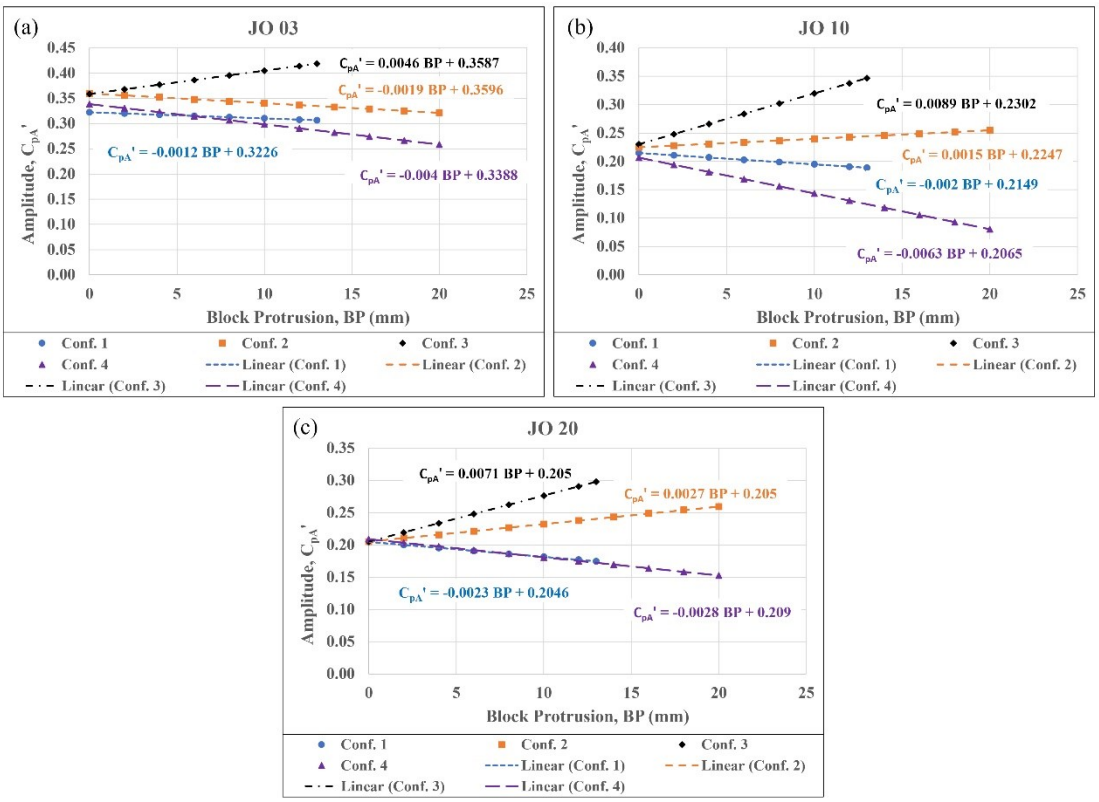

Figure 3.25 Average amplitude variations with *BP* for different test *Conf.*s: (a) *JO* = 3 mm, (b) *JO* = 10 mm and (c) *JO* = 20 mm

Table 3.4 Average mean value and amplitude equations

JO	*Conf.*	Mean value equation	Amplitude equation
3	1	$C_{pA} = 0.0008\,BP + 1.0408$	$C'_{pA} = -0.0012\,BP + 0.3226$
3	2	$C_{pA} = -0.0334\,BP + 1.0528$	$C'_{pA} = -0.0019\,BP + 0.3596$
3	3	$C_{pA} = -0.046\,BP + 1.0891$	$C'_{pA} = 0.0046\,BP + 0.3587$
3	4	$C_{pA} = -0.0071\,BP + 1.0631$	$C'_{pA} = -0.004\,BP + 0.3388$
10	1	$C_{pA} = 0.0052\,BP + 1.106$	$C'_{pA} = -0.002\,BP + 0.2149$
10	2	$C_{pA} = -0.0187\,BP + 1.145$	$C'_{pA} = 0.0015\,BP + 0.2247$
10	3	$C_{pA} = -0.0096\,BP + 1.114$	$C'_{pA} = 0.0089\,BP + 0.2302$
10	4	$C_{pA} = -0.0071\,BP + 1.1159$	$C'_{pA} = -0.0063\,BP + 0.2065$
20	1	$C_{pA} = 0.0005\,BP + 1.0807$	$C'_{pA} = -0.0023\,BP + 0.2046$
20	2	$C_{pA} = -0.0186\,BP + 1.0936$	$C'_{pA} = 0.0027\,BP + 0.205$
20	3	$C_{pA} = -0.0028\,BP + 1.0787$	$C'_{pA} = 0.0071\,BP + 0.205$
20	4	$C_{pA} = 0.00008\,BP + 1.0833$	$C'_{pA} = -0.0028\,BP + 0.209$

3.5.6 Effect of *JO* on C_{pA} and C_{pA}'

The equations determined presented in Table 3.4 are used to determine the effect of *JO*. In the first step, a *Conf.* is selected (Average mean value equations in *Conf. 1* are chosen for explanation of this procedure). As carried out in section 3.5.5, a similar range of block protrusion (*BP*) values is chosen. In the next step, the mean values corresponding to different *JO*s are calculated ($C_{pA}JOXX$, where *XX* stands

for corresponding *JO*), see Table 3.5. In the next step, these mean values are normalized with those obtained for *JO 03* for corresponding *BP* value to obtain the normalization factors. These normalization factors are averaged, and are termed as "Mean Value Ratio-JO", (*MVR-JO*). Thus, by multiplying the *MVR-JO* values to the C_{pA}*JO03* values, we can obtain the C_{pA} values for the required *JO*.

The predicted values (C_{pA}*JOXX Pre*, where *XX* stands for corresponding *JO*), are calculated and compared with the original values (C_{pA}*JOXX*, where *XX* stands for corresponding *JO*) as presented in Figure 3.26(a). The *MVR-JO* values are then plotted against the *JO* values, and a linear regression line is generated as presented in Figure 3.26(b). This process is repeated for different *Conf.*s and the variations of *MVR-JO* values with *JO* are presented in Figure 3.27. The similar process is repeated for Amplitude values to determine the normalization factors termed as "Amplitude Ratio-JO", (*AR-JO*). The variations of *AR-JO* values with *JO* for different test *Conf.*s are presented in Figure 3.28.

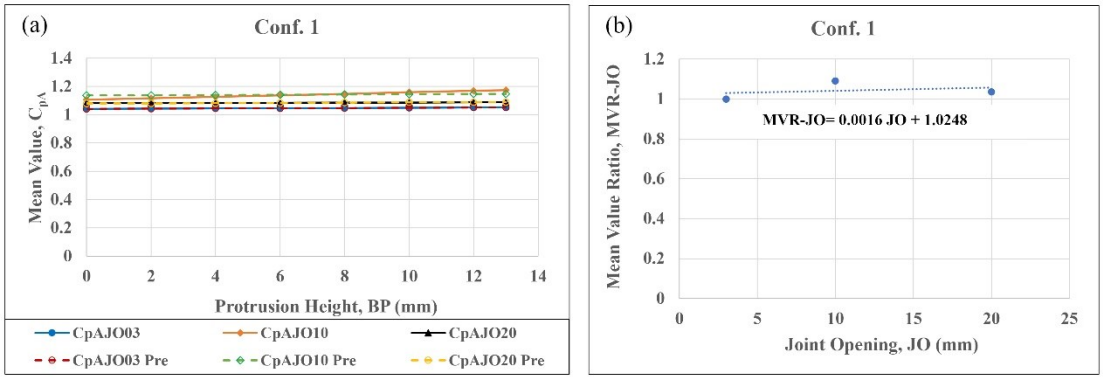

Figure 3.26 Description of the procedure to determine the effect of *JO*: (a) Comparison of actual and predicted C_{pA} values and (b) Variation of *MVR-JO* with *JO*

The goal of the normalization process adopted is to interpret them physically to obtain a reliable trend with *JO*. This is achieved using the minimum tested *JO* (3 mm), which resulted in a monotonically increasing normalizing factors with increasing *JO*. Besides, a 3 mm joint represents a tight or nearly closed joint, and it is frequently reported in field inspections (1-5 mm). Thus, *JO 03* serves as a natural and meaningful normalization baseline. A comparison of normalization results using different baselines is presented in Annexe C. As explained in Annexe C, the change of baseline does not have a significant effect on the trend.

Table 3.5 Calculation of the normalization factors (*MVR-JO*) as a function of *JO*

BP (mm)	**C_{pA}JO03**	**C_{pA}JO10**	**C_{pA}JO20**	**(C_{pA}JO03) / (C_{pA}JO03)**	**(C_{pA}JO10) / (C_{pA}JO03)**	**(C_{pA}JO20) / (C_{pA}JO03)**	**C_{pA}JOXX Pre = C_{pA}JO03 * MVR-JO**		
							C_{pA}JO03 Pre	**C_{pA}JO10 Pre**	**C_{pA}JO20 Pre**
0	1.0408	1.106	1.0807	1	1.0626	1.0383	1.0408	1.1357	1.0784
2	1.0424	1.1164	1.0817	1	1.0710	1.0377	1.0424	1.1374	1.0801
4	1.044	1.1268	1.0827	1	1.0793	1.0371	1.0440	1.1392	1.0818
6	1.0456	1.1372	1.0837	1	1.0876	1.0364	1.0456	1.1409	1.0834
8	1.0472	1.1476	1.0847	1	1.0959	1.0358	1.0472	1.1427	1.0851
10	1.0488	1.158	1.0857	1	1.1041	1.0352	1.0488	1.1444	1.0867
12	1.0504	1.1684	1.0867	1	1.1123	1.0346	1.0504	1.1462	1.0884
13	1.0512	1.1736	1.0872	1	1.1164	1.0342	1.0512	1.1470	1.0892
Average (Normalization factors)				1	1.0912	1.0362			
***JO* (mm)**				3	10	20			

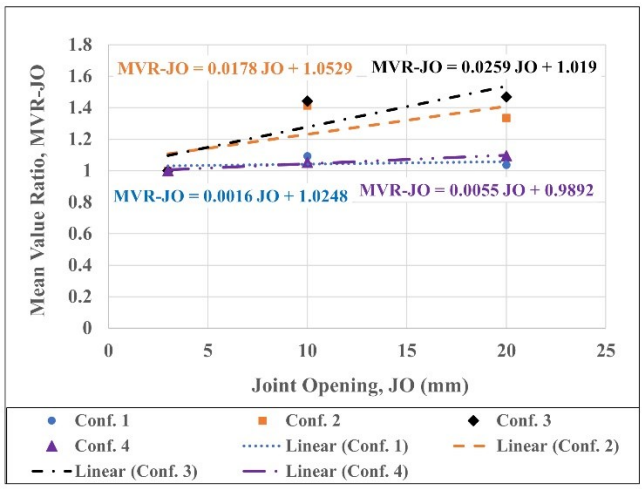

Figure 3.27 Mean Value Ratio variations with *JO* for different test configurations: (a) *Conf. 1*, (b) *Conf. 2*, (c) *Conf. 3* and (d) *Conf. 4*

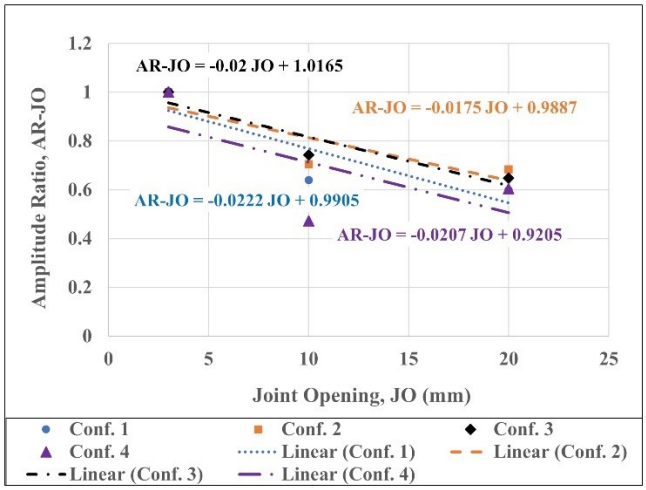

Figure 3.28 Amplitude Ratio variations with *JO* for different test configurations: (a) *Conf. 1*, (b) *Conf. 2*, (c) *Conf. 3* and (d) *Conf. 4*

Figure 3.27-3.28 present that the variations of *MVR-JO* and *AR-JO* do not follow a linear trend with *JO*. Attempting to establish a non-linear relationship is complex with only three *JO* values and could lead to erroneous results. With only three *JO* values (3 mm, 10 mm, and 20 mm) available, it's difficult to accurately capture the complex relationship between dynamic head parameters and *JO*. An important observation is that while mean dynamic head equations are similar for gapped joint features (10 mm and 20 mm *JO* values) within respective configurations, this similarity doesn't hold for

amplitude equations. Given these challenges, it's not currently feasible to develop a direct and robust mathematical relationship between the dynamic head parameters of Eq. 3.1 and *JO* values.

3.5.7 Sinusoidal fitting of a random fluctuating pressure data

For a given *JO*, *Conf.* and *BP*, C_{pA} and C_{pA}' values are calculated using the average mean value and amplitude equations presented in Table 3.4 respectively. With the known values of f_d (4 Hz), C_{pA} and C_{pA}', the dynamic head fluctuations (H) are predicted by using Eq. 3.1, in which the values of v_{ch} are obtained from Table 3.2 for the required discharge, Q. The error between the observed test data and the predicted sinusoidal data was quantified using Root Mean Square Error (*RMSE*), in m, calculated as presented in Eq. 3.2. Table 3.6 presents the *RMSE* values for all tests, with most values falling between 0.04 to 0.37 with an exception for *Conf. 3* of *JO 10* and *JO 20*. This exception is due to the correction applied to these cases due to the erroneous data collection. In order to compare the datasets with different units and/or magnitudes, the *RMSE* values are normalized to obtain normalized RMSE (*NRMSE*) values. While there are numerous methods to determine *NRMSE* values (Azadi et al., 2020; Rathinasamy et al., 2014; Wang et al., 2013), they are normalized with the difference between maximum and minimum values of the measured time-domain dynamic head ($H_{d,max}$ and $H_{d,min}$ respectively) as shown in Eq. 3.3.

$$RMSE = \sqrt{\frac{\sum_{i=1}^{N}(Sinusoidal_i - Actual_i)^2}{N}} \quad \text{Eq. 3.2}$$

$$NRMSE = \frac{RMSE}{H_{d,max} - H_{d,min}} \quad \text{Eq. 3.3}$$

Where,

$Sinusoidal_i$ = ith sinusoidal predicted value of dynamic head (m)
$Actual_i$ = ith actual value of dynamic head (m)
N = Number of observations

Figure 3.29-3.31 visually compares the observed and predicted sinusoidal data for different *JO* values, for no protrusion condition (*BP* = 00 mm) and highest discharge tested (i.e. Q_4). These comparisons illustrate the accuracy of the sinusoidal fitting method and demonstrate that it effectively captures the dynamic head fluctuations. Some minor differences are noticed in a few cases which can be

raised from the errors of fitting and normalization process. This resulted in higher *RMSE* values in such cases. While *RMSE* values are relatively high in such cases, they are considered acceptable, as the primary objective of predicting minimum pressures on top of the block has been achieved. The *NRMSE* values calculated for different test conditions (except for the cases of *BP 13* in *Conf. 3* in *JO 10* and *JO 20*) are presented in Table 3.7, which vary between 18 - 35 %, which demonstrates a moderate fitting.

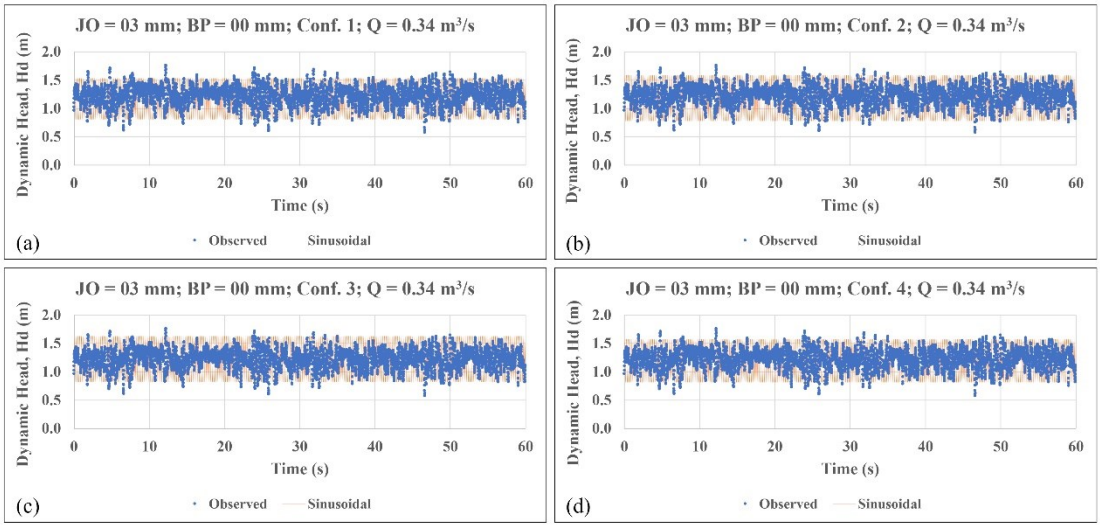

Figure 3.29 Observed and predicted sinusoidal dynamic head data in 3 mm *JO* value for selected cases

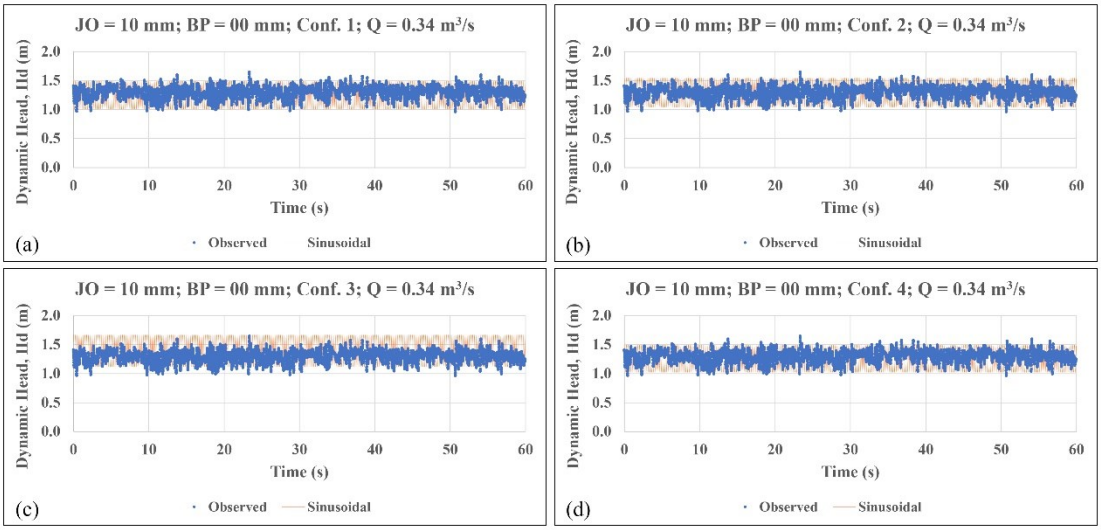

Figure 3.30 Observed and predicted sinusoidal dynamic head data in 10 mm *JO* value for selected cases

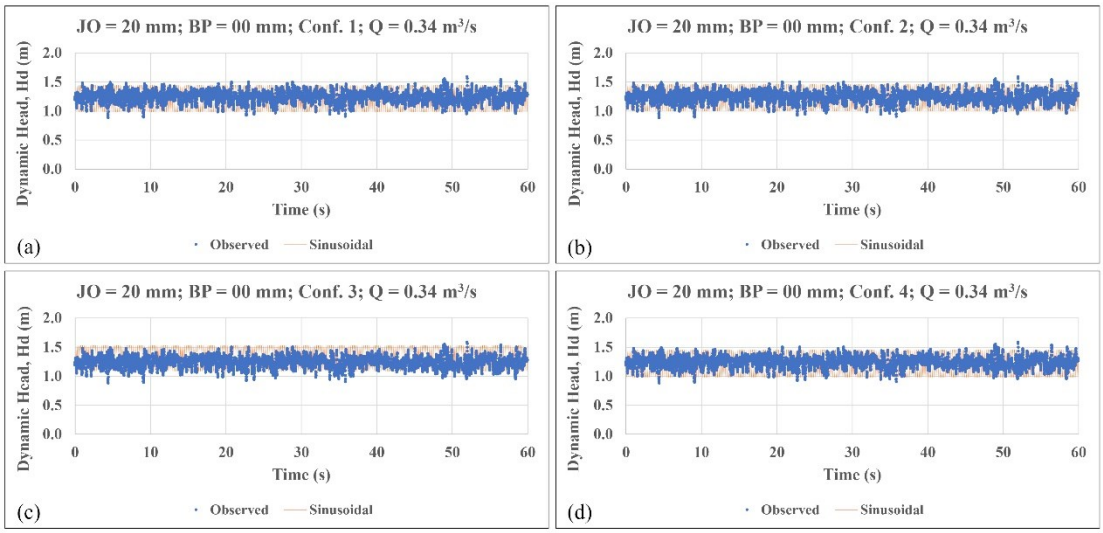

Figure 3.31 Observed and predicted sinusoidal dynamic head data in 20 mm *JO* value for selected cases

Table 3.6 *RMSE* values between the observed and predicted results for all the test cases

Joint Opening		***JO 03***				***JO 10***				***JO 20***			
Conf.	***BP* (mm)**	Q_1	Q_2	Q_3	Q_4	Q_1	Q_2	Q_3	Q_4	Q_1	Q_2	Q_3	Q_4
1	0	0.17	0.22	0.29	0.31	0.11	0.15	0.19	0.21	0.10	0.14	0.18	0.19
1	6	0.17	0.20	0.26	0.28	0.11	0.13	0.18	0.19	0.09	0.13	0.17	0.17
1	13	0.16	0.21	0.27	0.29	0.09	0.13	0.17	0.18	0.09	0.12	0.15	0.17
2	0	0.18	0.24	0.31	0.33	0.12	0.15	0.19	0.21	0.10	0.14	0.18	0.19
2	13	0.17	0.22	0.30	0.33	0.13	0.18	0.24	0.28	0.15	0.18	0.24	0.26
2	20	0.15	0.21	0.27	0.30	0.13	0.18	0.22	0.24	0.13	0.18	0.23	0.24
3	0	0.19	0.24	0.31	0.33	0.11	0.15	0.20	0.22	0.10	0.14	0.18	0.19
3	6	0.20	0.26	0.35	0.37	0.15	0.19	0.24	0.26	0.12	0.17	0.21	0.23
3	13	0.21	0.27	0.36	0.37	0.29	0.60	1.06	1.15	0.28	0.74	0.52	0.56
4	0	0.18	0.23	0.30	0.32	0.11	0.14	0.18	0.20	0.10	0.14	0.18	0.19
4	13	0.15	0.19	0.22	0.26	0.06	0.08	0.10	0.11	0.08	0.12	0.15	0.16
4	20	0.14	0.18	0.22	0.23	0.04	0.06	0.07	0.08	0.07	0.10	0.13	0.14

Table 3.7 *NRMSE* values between the observed and predicted results for all the test cases

Joint Opening		***JO 03***				***JO 10***				***JO 20***			
Conf.	***BP* (mm)**	Q_1	Q_2	Q_3	Q_4	Q_1	Q_2	Q_3	Q_4	Q_1	Q_2	Q_3	Q_4
1	0	29%	27%	23%	26%	31%	25%	25%	31%	33%	28%	23%	27%
1	6	34%	30%	31%	29%	32%	29%	26%	25%	29%	26%	30%	28%
1	13	27%	23%	26%	29%	30%	29%	25%	28%	30%	28%	27%	29%
2	0	31%	29%	25%	28%	34%	26%	26%	31%	33%	28%	24%	27%
2	13	27%	26%	25%	26%	23%	23%	29%	32%	35%	33%	28%	34%
2	20	35%	32%	28%	31%	31%	32%	28%	32%	29%	25%	30%	27%
3	0	32%	29%	25%	28%	33%	26%	27%	32%	33%	28%	23%	27%
3	6	29%	27%	25%	27%	29%	31%	28%	30%	29%	28%	28%	26%
3	13	30%	25%	29%	30%	-	-	-	-	-	-	-	-
4	0	30%	27%	24%	27%	30%	24%	24%	30%	33%	28%	24%	28%
4	13	29%	25%	30%	24%	31%	35%	35%	33%	33%	26%	25%	30%
4	20	24%	24%	28%	29%	24%	24%	25%	21%	34%	18%	24%	25%

3.5.8 Validation of the sinusoidal prediction

The developed sinusoidal equation is subjected to validation to ensure its accuracy before applying it to different protrusion heights or discharges. To validate the discharge parameter, a different discharge (0.29 m^3/s), and a protrusion height (*BP* = 06 mm in Conf. *4*), other than those used in equation's development, are used in several test *Conf.*s as detailed in Table 3.8. The dynamic pressure head data observed during the physical model testing and the pressure head predicted with sinusoidal equation developed are compared. Since *Conf. 0* is tested, this test data can be validated for all the test configurations as presented in Figure 3.32. The validation figures are presented for other test conditions in Figure 3.33. We can clearly notice that a good match has been obtained between the observed and

predicted results, which signifies that the developed model is accurate to determine the fluctuating pressures under the given set of test conditions. While a few deviations are observed in some cases, the accuracy is considered sufficient for predicting minimum pressures on the top of the block, which is critical for uplift analysis.

Table 3.8 Parameters used for the validation of sinusoidal prediction

***JO* (mm)**	***Conf.* #**	***BP* (mm)**	***Q* (m^3/s)**
3	0	0	0.29
3	1	13	0.29
3	3	13	0.29
3	4	6	0.18, 0.29

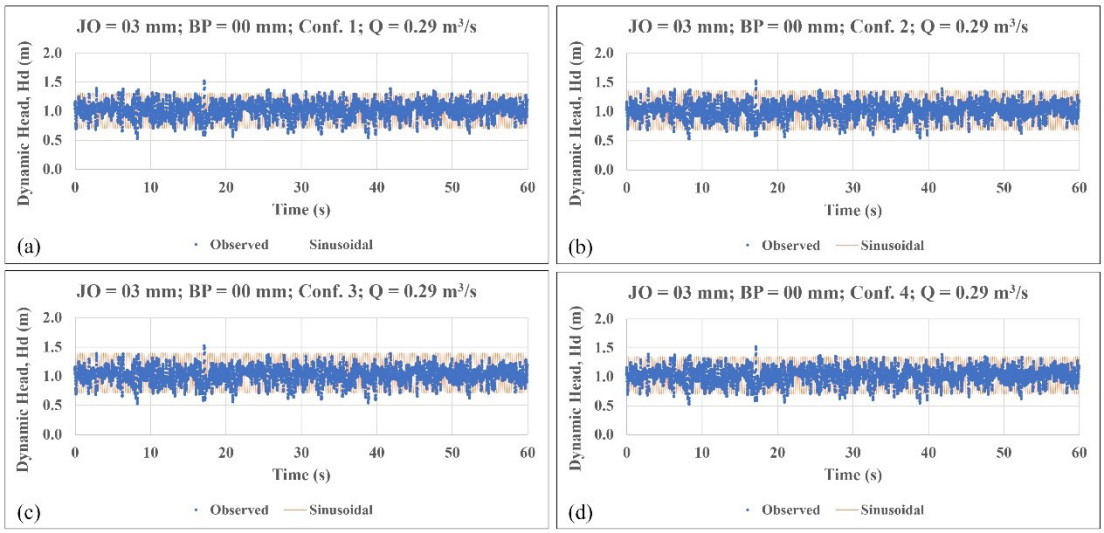

Figure 3.32 Observed and predicted sinusoidal dynamic head data for: (a) *JO* = 3 mm, *BP* = 0 mm, *Conf.* = 1, *Q* = 0.29 m^3/s, (b) *JO* = 3 mm, *BP* = 0 mm, *Conf.* = 2, *Q* = 0.29 m^3/s, (c) *JO* = 3 mm, *BP* = 0 mm, *Conf.* = 3, *Q* = 0.29 m^3/s and (d) *JO* = 3 mm, *BP* = 0 mm, *Conf.* = 4, *Q* = 0.29 m^3/s

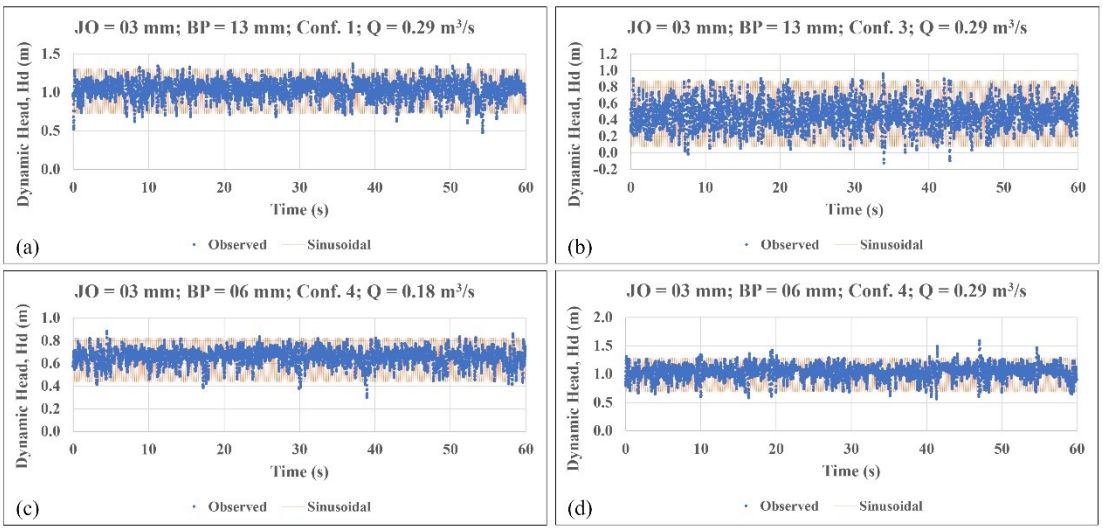

Figure 3.33 Observed and predicted sinusoidal dynamic head data for: (a) *JO* = 3 mm, *BP* = 13 mm, *Conf.* = 1, *Q* = 0.29 m^3/s, (b) *JO* = 3 mm, *BP* = 13 mm, *Conf.* = 3, *Q* = 0.29 m^3/s, (c) *JO* = 3 mm, *BP* = 06 mm, *Conf.* = 4, *Q* = 0.18 m^3/s, and (d) *JO* = 3 mm, *BP* = 06 mm, *Conf.* = 4, *Q* = 0.29 m^3/s

3.6 DISCUSSION

- To present the limitations of previous physical models and contributions of the present study, previous studies on rock mass erosion in dam spillways using small-scale physical models, that are typically in the scale of 1:50 – 1:100, have provided important insights, however, they also exhibit several key limitations. Due to their small size, they inherently restrict the block size, joint geometry, and flow velocity. Accordingly, they limit the ability to reproduce representative three-dimensional joint network. This, in turn, affects the reliability of measured dynamic pressures, especially, within the joints where the flow mechanisms are highly sensitive to sensor inlet orientation. Furthermore, the models employing single block do not capture the interaction between adjacent blocks or the compound effects of neighboring protrusions, joint patterns, and surface irregularities. On the contrary, the relatively large 1:40 scale physical model used in this study with multiple blocks, each of size 15 x 15 x 30 cm, better reproduces the realistic joint conditions, and improved spatial resolution of pressure fluctuations and allows realistic simulation of block interactions. The use of elbows, representing mini-pitot tubes, is a major advancement by

our team (Wisse et al., 2023), which permits reliable quantification of the velocity head. While most previous studies have varied a single parameter, this study simultaneously evaluates the effect of two parameters, i.e., *JO* and *BP*, under various flow conditions. Finally, development of a sinusoidal prediction as a function of *JO*, *BP*, and *Conf.* to characterize extreme dynamic pressures offers a practical approach to estimate the worst-case scenarios. These combined advancements enhance the comprehensive understanding of block uplift mechanisms in parallel-flow spillways, addressing the key gaps in previous studies.

- The results of the hydraulic pressures from the pilot plant-scale spillway model exhibit significantly lower pressures with minimal fluctuations within the joints, as compared to those on the top surface of the block which represents the hydraulic pressures at the spillway surface under different test conditions. The block uplift shall be more pronounced when the hydraulic pressure above the block becomes less than that at the bottom of the block at a given instant which is occurring due to the pressure fluctuations at the top of the block under certain block configurations. Thus, the fluctuations in the pressures on the top of the block are identified as an important governing factor for the block uplift process.
- The hydraulic pressures measured on the rock block surface are exhibiting inherently stochastic nature due to the chaotic behavior of fluid turbulence. A sinusoidal model is employed to predict the extreme pressures of this stochastic turbulent data as this model lets us define clear maximum and minimum values which represents the worst-case analysis. This approach enables the identification of extreme pressure conditions critical for uplift analysis, while simplifying the computational modeling process. This model reflects the amplitude and frequency characteristics observed in the turbulent signal. The limitations due to simplification of random fluctuations are acknowledged which include loss of randomness and over-simplification. These limitations will be addressed in future studies by employing a Fourier series instead of a simple sinusoidal curve.
- Although turbulent pressures are stochastic, the frequency-domain analysis performed using *FFT* (Figure 3.11-3.13) consistently show that the pressure signals are dominated by a single

frequency, typically between 3 and 6 Hz. This dominant peak corresponds to largest energy-containing motions within the flow and therefore has the strongest influence on the extreme pressures that contribute to block uplift. While higher-frequency components are present, they possess much lower amplitudes and hence do not meaningfully affect the extreme pressures. Given this spectral structure, a single sinusoidal representation offers a meaningful approximation to predict these pressures. The three parameters used in the sinusoidal model directly correspond to measurable hydraulic characteristics and allow engineers to estimate relevant pressures without needing to reconstruct the whole time series. While other models like multi-term Fourier series or Autoregressive Moving Average (ARMA) model, could reproduce the detailed temporal variability of the pressure signal, these approaches require estimating numerous additional parameters. Also, they provide limited practical advantage for predicting extreme pressures, which is the main objective of this study. Besides, the ARMA models use the past values of a series to predict the current value, and they require huge time history for high accuracy. Thus, a single sinusoidal function is deliberately chosen to represent the balance between physical relevance, model simplicity and engineering utility. More complex representations (like multi-term Fourier series or ARMA models) will be explored in future work. The RMSE results in Table 3.6 demonstrate that the sinusoidal model captures the magnitude and timing of the extreme fluctuations with acceptable accuracy across discharges and configurations.

- The individual influence of the study parameters, i.e., *JO* and *BP* is studied by carrying out Pearson correlation analysis (Kirch, 2008) using the values of *Conf. 0* as base. The correlation coefficients between *JO*/*BP* and C_{pA}/C_{pA}*'* for different *Conf.*s are presented in Table 3.9. These coefficients indicate that *BP* has significant impact on C_{pA} for negative protrusion configurations (*Conf. 2* and *Conf. 3*) and comparable impact in other configurations, whereas *JO* has significant impact on C_{pA}*'* than *BP* in all the configurations.

Table 3.9 Pearson correlation coefficients between the study parameters and pressure parameters

	Conf. 1		***Conf. 2***		***Conf. 3***		***Conf. 4***	
	***JO* (mm)**	***BP* (mm)**	***JO* (mm)**	***BP* (mm)**	***JO* (mm)**	***BP* (mm)**	***JO* (mm)**	***BP* (mm)**
Mean Value, C_{pA}	0.238	0.231	0.362	-0.808	0.112	-0.850	0.610	-0.593
Amplitude, C_{pA}'	-0.777	-0.157	-0.698	0.110	-0.424	0.187	-0.531	-0.451

- Among the various block protrusion configurations, the positive protrusion cases, i.e. *Conf. 1* and *Conf. 4*, present a minimal variation in the mean dynamic head with a considerable variation in its fluctuating pressures (as observed from the variation of amplitude) as a function of block protrusion height. However, the negative protrusion cases, i.e. *Conf. 2* and *Conf. 3*, presents significant variations in both the mean dynamic head and its fluctuations as a function of block protrusion height. This could be the effect of the hydraulic jump formed by the protruded surface of the leading blocks that develops a reduced pressure conditions at the trailing blocks. Overall, *Conf. 2* is determined to be most critical for the potential block uplift, as the fluctuation in dynamic head is leading to the favourable conditions for uplift to occur at many instants. In all these protruding configurations, the fluctuations arising from the block protrusion height presents the possibility of a minimal pressure on the top of the block being less than that at the bottom, resulting in block uplift conditions.
- The results of Reinius (1986) point out the increase in the values of non-dimensional coefficient of uplift with the introduction of block protrusion. However, the results obtained from those tests are doubtful as they did not clearly show the accurate measurements of dynamic pressures (measurements from piezometric tubes). The Quasi-Static Impulsion (*QSI*) method proposed by Bollaert (2012) could be applicable to the case of parallel flow spillways, however, this method is dependent on the coefficient of uplift values observed from the tests of Reinuis (1986). Due to the discrepancies observed in the tests of Reinuis,

the current method of determination of dynamic pressures placing the elbows is more prominent. Though the current study does not present the determination of non-dimensional coefficient of uplift directly, an indirect means to achieve this objective is proposed by the determination of fluctuating pressures on the spillway surface as a function of study parameters, i.e., joint opening, block protrusion (configurations and protrusion height) and flowrate.

- The development of a sinusoidal equation to represent the fluctuating pressures aids us in the prediction of these extreme pressure fluctuations. The dominating frequency representing the frequency of the pressure fluctuations in the sinusoidal equation is found to be lying in the range of 3 – 6 Hz across various tests and is found to be independent of the study parameters. Hence a constant most suitable value of 4 Hz is chosen to represent the frequency in the sinusoidal equation for all the tests. Mean dynamic head and amplitude of the pressure fluctuations show a consistent variation with the block protrusion height for each protrusion configuration and with the discharge which allowed for the development of uniform mean value ratio and uniform amplitude ratio. The pressure parameters (mean head and amplitude) are not exhibiting a consistent linear variability with the joint opening and fitting a non-linear relationship using only 3 different joint opening values is deemed inconsistent.
- Given the limitations with physical modelling, only limited number of joint openings are studied using our physical model. Numerical modelling of the physical model tests which is currently under development shall aid to the further development of a non-linear relationship of the sinusoidal equation parameters as a function of joint opening. The developed sinusoidal equation as a function of the block protrusion and discharge for different protrusion configurations and joint openings demonstrates an ability to predict the extreme pressure fluctuations observed during the physical model testing. The Root Mean Square Error (*RMSE*) values between the observed and predicted results are within acceptable limits. In summary, this research contributes valuable insights into the factors influencing hydraulic pressures and fluctuations in spillway models, particularly those

related to block protrusion and joint opening. These findings pave the way for more comprehensive analyses and modeling in the future.

- The procedure to link the hydraulic pressure data from reduced-scale model to prototype is explained in Annexe A, which explains another limitation with physical modeling, i.e., scale effect. Applicability of the results obtained with physical models requires the determination of scale effect on different parameters, especially with the geomechanical parameters. Determination of scale effect requires more modeling (physical and/or numerical) at different scales which is under the future scope of this study. Further studies shall be carried out for the results to be applicable to actual spillway cases.

3.7 CONCLUSIONS

The current study presents a comprehensive analysis of fluctuating hydraulic pressures acting around the rock blocks in an unlined parallel-flow spillway using a relatively large-scale physical model with multi-block 3D joint geometry. The study focused on aiming at investigating the combined impact of joint opening (*JO*) and block protrusion conditions on hydraulic pressure distribution. The test results show that the pressures within the joints remain comparatively stable, while the pressures at the upper block surface (spillway surface) exhibit pronounced fluctuations capable of triggering block uplift. The dominating frequency of these pressure signals consistently lies between 3 - 6 Hz, which has been taken as 4 Hz for predictive purposes. A simplified sinusoidal equation is developed to predict extreme pressure fluctuations with its parameters varying as a function of the study parameters (*JO*, *Conf.* and *BP*).

Block protrusion has been identified to produce systematic and configuration dependent variation in the mean and amplitude of the pressure head (C_{pA} and C_{pA}'), while joint opening primarily influences the amplitude of pressure fluctuations as observed from the Pearson correlation values. The sinusoidal model significantly reproduces the pressure data, especially the extreme pressure values. The robustness of the model has been validated using independent test conditions. The low *RMSE* and *NRMSE* values demonstrate the moderate fitting of the pressure data, except for *Conf. 3* with 13 mm block protrusion

which created a flow separation due to the formation of a hydraulic jump. The results provide a new insight into how rock mass conditions (*JO*, *Conf.* and *BP*) shape the spillway hydraulic loading on fractured rock masses. The methodology established here offers a practical insight into estimating critical pressures in engineering assessments.

Future testing combined with coupled numerical modelling will incorporate a broader range of aperture values and joint conditions, address scale effects and extend the model to prototype scale. The parameters of the sinusoidal equation show a consistent variation with the block protrusion height and the flow rate; however, with the joint opening, a consistent linear variation is not observed. The gapped joint features (10 mm and 20 mm openings) exhibited similar pressure results, and the open joint features (3 mm opening) exhibited different results. More testing with respect to the joint opening shall be necessary to confirm this observation; however, given the limitations of the physical model testing, a limited opening values can be tested maintaining their accuracy without affecting the pressure measurement.

CHAPITRE 4

ARTICLE 2: EVALUATION OF THE EFFECT OF JOINT ORIENTATION ON ROCK MASS EROSION USING A PILOT-PLANT SPILLWAY MODEL

Vineeth Reddy Karnati [a*], Ali Saeidi [a], Alain Rouleau [a], Marco Quirion [b]

[a] Département des sciences appliquées, Université du Québec à Chicoutimi, Saguenay, QC G7H 2B1, Canada.

[b] Expertise, intégrée - Géologie, Hydro-Québec, 75 Boulevard René-Lévesque Ouest, Montréal, QC H2Z 1A4, Canada.

Published, Rock Mechanics and Rock Engineering, Volume 58, Issue 7, P. 8351-8372

https://doi.org/10.1007/s00603-025-04565-x

Ce chapitre reprend un article dont le premier auteur est l'auteur de cette thèse. Le chapitre présente les résultats des essais sur modèle réduit avec différentes orientations des joints. À la fin, un modèle analytique est présenté pour déterminer la stabilité des blocs en utilisant les résultats des essais.

Credit authorship contribution statement

Vineeth Reddy Karnati: Experimental work, Methodology, Data analysis, Investigation, Preparation of original manuscript, review & editing. **Ali Saeidi:** Supervision, Conceptualization, Methodology, Funding & Resource acquisition, Overall project administration, Review & editing the manuscript. **Alain Rouleau:** Supervision, Review & editing the manuscript. **Marco Quirion:** Supervision, Funding acquisition, Review & editing the manuscript.

Competing interests

The authors declare that they have no known competing financial interests or personal relationships that could have appeared to influence the work reported in this paper.

Funding

The project was supported by the Natural Sciences and Engineering Research Council of Canada and Hydro-Québec (NSERC, Hydro-Québec [CRDPJ 537350 – 18] and NSERC [RGPIN-2019-06693]. The authors also acknowledge the Fonds de Recherche du Québec Nature et technologies for granting the

programme de bourses d'excellence pour étudiants étrangers (PBEEE) scholarship (Grant No.: 2023-2024 - 1I - 334721) for this research.

Résumé

L'érosion du massif rocheux est observée dans de nombreuses structures hydrauliques et constitue une menace pour leur stabilité. L'orientation des blocs rocheux joue un rôle déterminant dans le processus d'érosion du massif rocheux au niveau des évacuateurs de crues des barrages. La détermination de l'effet individuel des différents paramètres influençant l'érosion aux sites de barrages demeure complexe; dans ce contexte, les essais sur modèles physiques à l'échelle de laboratoire constituent un outil particulièrement pertinent. Dans cette étude, des essais en modèle réduit ont été réalisés sur des blocs modélisés de dimensions 15 cm × 15 cm × 30 cm afin d'évaluer l'influence de l'orientation des joints. Trois orientations de joints différentes ont été testées sous trois ouvertures de joint distinctes et quatre conditions de débit, permettant d'obtenir la distribution des pressions autour du bloc central instrumenté. Ce bloc a été conçu pour mesurer avec une grande précision les pressions statiques et dynamiques. Les coefficients de soulèvement obtenus à partir des résultats expérimentaux sont positifs, variant entre 0,2 et 0,6 pour les blocs disposés à contre-courant, et entre 0,1 et 0,6 pour les blocs orientés dans le sens de l'écoulement, indiquant ainsi un potentiel de soulèvement. L'analyse de stabilité réalisée à partir des résultats de pression montre que les blocs disposés à contre-courant ont tendance à basculer (facteur de sécurité variant de 0,5 à 0,8) et à s'aligner dans le sens de l'écoulement avant d'être soulevés, tandis que les blocs orientés dans le sens de l'écoulement présentent principalement un mécanisme de soulèvement (facteur de sécurité variant de 0,2 à 0,7). Les blocs disposés perpendiculairement à la direction de l'écoulement se révèlent plus stables que ceux placés en conditions inclinées, ce qui met en évidence l'importance de l'orientation des joints dans le processus d'érosion du massif rocheux.

4.1 ABSTRACT

Rock mass erosion has been prevalent in many hydraulic structures which endangers their stability. Rock block orientation plays an important role in the rock mass erosion process in dam spillways. Determining the effect of individual parameters on the erosion process at dam sites is very complicated and hence laboratory scale model testing becomes a powerful tool in this scenario. In this study, model tests are performed on modelled blocks of size 15cm x 15cm x 30cm to understand the effect of joint orientation. Three different joint orientations are tested under three different joint apertures and four different flow rate conditions to obtain the pressure distribution around the central instrumented block. This block is designed to capture the static and dynamic pressures together with high accuracy. The coefficient of uplift values obtained from the test results are found to be positive ranging from 0.2 to 0.6 and 0.1 to 0.6 for blocks arranged against and towards the flow respectively which exhibited the possibility of uplift occurrence. Stability analysis carried out using the pressure results revealed that the blocks arranged against the flow direction tend to topple (FS ranging from 0.5 to 0.8) and align towards the flow before being uplifted whereas the blocks arranged towards the flow direction exhibit uplift occurrence (FS ranging from 0.2 to 0.7). The blocks arranged perpendicular to the flow direction are found to be stable compared to those in the inclined conditions which underlines the importance of joint orientation on the erosion process.

Keywords: Rock mass erosion; Block uplift; Joint opening; Joint orientation; Pilot-plant spillway model

4.2 INTRODUCTION

The process of removal of the geomaterial by various natural elements like wind, water, and gravity is termed as erosion. The erosion process of a rock mass with water as the principal element is termed hydraulic rock mass erosion[1]. This process has been prominent in various dam spillway sites, especially with soft rock and heavily jointed hard rock masses, in the past few decades during both the

[1] The terms “hydraulic rock mass erosion” and “rock scour” both represent the removal of rock mass from its position under the action of hydraulic forces and hence are used synonymously throughout the current article.

normal operating conditions and the flood events, as observed in the case of Oroville dam in California (Wahl et al., 2019; Zhang et al., 2024b), Spaulding dam in California (George, 2015), Ricobayo dam in Spain (Annandale, 2006), Kariba dam in Zambia (Bollaert et al., 2013), Mokolo dam in South Africa and Copeton dam in Australia (Pells, 2016). The main concern with spillway erosion is associated with the stability of the dam structure whereas the secondary effects are associated with loss of stored water, severe damage to property and infrastructure downstream of the spillways, loss of habitat and considerable repair costs as observed from the Oroville Dam incident (Koskinas et al., 2019; Stofleth et al., 2023; X. Zhang et al., 2024b) and Kentucky's state-owned dam repair (Pittman et al., 2023). These historic incidents urge the comprehension of the mechanisms of this erosion process to design and develop erosion prevention measures for the existing spillways and new ones in the future, especially when the spillways are unlined.

There are several types of spillways such as overflow, ogee, side channel, labyrinth, syphon, tunnel smooth and stepped chute spillways, etc. (Coleman et al., 2004; Hager et al., 2020). These spillway types can be broadly classified as either parallel flow (straight reach) or plunging jet spillways based on the interaction between the flowing water and the rock mass. The dissipation of hydraulic energy and the mechanism influencing the erosion are respective to each type. The major mechanisms of rock mass erosion include: rock bed abrasion, fracturing (brittle or fatigue), cavitation and plucking (also known as quarrying) (Jalili Kashtiban et al., 2021; Whipple et al., 2000). Abrasion occurs in the rock mass due to the bed shear stresses and the damage due to the friction caused by the sediments transported by water which is usually a time taking phenomenon (Bollaert et al., 2014; Jalili Kashtiban et al., 2021; Y. Liu et al., 2021). Cavitation occurs close to the rock bed surface causing a localized damage due to flow separation at irregularities and knickpoints resulting in the reduction of pressures below the local water vapour pressure (Annandale & George, 2011; Bollaert, 2002). Cavitation results in the formation of pressure pulses that could fracture even very hard rock masses initiating the erosion process (Salmasi et al., 2023; Schleiss et al., 2023; Zanial et al., 2023). Fracturing of rock masses occurs within the existing joints when hydraulic pressure exceeds the fracture toughness of intact rock mass that can be either instantaneous (brittle fracture) or through repeated loading (fatigue fracture) (Maleki & Fiorotto, 2021). Plucking, though being less frequent than abrasion, could lead to high erosion rates

depending on the joint and block conditions (Lamb et al., 2014; Whipple et al., 2000). This phenomenon is observed to be more pronouncing in the sub-metric blocks (Pan et al., 2014; Li et al., 2016). All of these phenomena can be mutually exclusive or simultaneous depending on the pressure distribution in the actual site conditions, thus creating a challenge in accurately modelling the erosion phenomenon (Annandale, 1995).

Determination of the hydraulic pressures on the spillway surface and in joint set is crucial for the determination of block uplift, but obtaining this data in an actual spillway site is highly complicated. Therefore, the use of reduced-scale physical spillway models is very useful for the evaluation of the effect of these parameters on the hydraulic pressures and in turn on the erosion process. Many researchers have used reduced-scale models to study the variation of hydraulic pressures; however, most of the studies involve the use of single large block (Pells, 2016) or a group of very small blocks (Dubinski, 2009; Sawadogo, 2010). These model studies include studying the effect of block protrusion (Coleman et al., 2003; Frizell, 2007), the effect of joint opening and block size (Dubinski, 2009), and the effect of block orientation using a single tetrahedral block in varied flow conditions (George & Sitar, 2016; George et al., 2015; George, 2015) using parallel flow type spillway models. Studies based on single model block lack the understanding of the hydraulic pressure variations due to the presence of joints between the individual blocks and studies with small blocks do not essentially replicate the flow conditions within the actual rock mass. Though the studies of George offer a comprehensive understanding of the importance of joint orientation, the use of tetrahedral block suffers from pressure measurement in realistic prismatic blocks. The loose tetrahedral blocks, formed due to the inclined joint sets at the spillway surface, escape easily at the early stages of the flow leaving an undulating flow surface. The extent of the erosion is purely dependent on the hydraulic pressure distribution around the most common prismatic blocks. Other set of model studies have used plunging jet condition to study various hydraulic parameters on the effect of erosion (Bollaert & Schleiss, 2003b; 2005; Umumararungu, 2016). Numerical modelling of the erosion process is complicated as it requires integration of hydraulic (computational fluid dynamics, *CFD*) and geomechanical models like Discrete Element Methods (*DEM*). Teng et al. (2023a; 2023b) presents a coupled *CFD-DEM* approach to model the erosion process using a single block, which is validated by the physical experimental data of George (2015). Some

researchers tried to implement the coupling process using Lattice Boltzmann Method to model the hydraulic phase and *DEM* to model the solid phase (Gardner, 2023; Gardner & Sitar, 2018; 2019; Wang et al., 2018). These numerical modelling techniques provide a valuable means to achieve the coupling process. However, these models involve only the use of single block models which are validated using the experiments performed using single block. The surrounding rock mass can significantly determine the removal of the rock block (Lamb et al., 2015).

Several semi-empirical (Annandale, 1995; Pells, 2016) and semi-analytical (Bollaert, 2016) methods have been developed for the erosion assessment as compiled by Jalili Kashtiban et al. (2021). Semi-empirical methods try to relate the erosive power parameter with an index representing the rock mass resistance against the erosion to present various threshold levels. The existing indices are developed from several field erosion case studies and they depend on various geomechanical parameters (Boumaiza, 2019). Semi-empirical methods are developed from the analytical formulations based on the laboratory experiments. Either of these methods implicitly specify that the joint orientation is one of the critical factors in rock mass erosion assessments, as it directly influences the interaction of hydraulic flow with the rock mass structure. The orientation of joints determines whether a block can be kinematically detached under the influence of hydraulic forces. The rock mass with its joints oriented in a manner that allows easy penetration of water and exploiting the weaknesses in rock mass leads to higher erosion levels. The Kirsten's index (Kirsten, 1982) incorporates the joint orientation indirectly using the "Relative block structure rating" parameter, J_s which is based on joint spacing ratio and the dip angle of the closely spaced joint. Boumaiza et al. (2019a) tried to extend the rating values developed by Kirsten to accommodate non-orthogonal joint sets. The erosion discontinuity orientation adjustment (E_{doa}) factor introduced by Pells (2016) addresses the influence of joint inclination with the direction of flow for various joint set spacing ratios and flow conditions. The rock mass erodibility index (*RMEI*) proposed by Pells (2016) emphasizes the joint orientation implicitly through "Kinematically viable mechanism for detachment" parameter. The comprehensive scour model (*CSM*) developed by Bollaert (2010, 2016) do not explicitly involves studying the joint orientation; however, the experiments carried by Bollaert involves minor variations in the direction of impinging jet. Besides, the quasi-static impulsion (*QSI*) module of the *CSM* is based on the uplift force acting on the block, which essentially

depends on the hydraulic pressure difference between the top and bottom of the block. These pressures in turn depend on the geomechanical parameters like joint opening, block protrusion and joint orientation.

As shown in different erosion assessment methods, rock block orientation and shape play an essential role in the rock mass erosion, especially in dam spillways. The current article is focussing on the parallel flow spillways and erosion process in the plunging jet model necessitates modification to apply for the parallel flow conditions which in turn requires studying the hydraulic pressures around the block. In this context, the objective of this paper is to evaluate the effect of joint orientation on the erosion process by plucking/uplift mechanism in unlined parallel flow spillways by studying the hydraulic pressure distribution at different faces of the prismatic block in a group of modelled blocks under different joint aperture conditions and several flow rates. This article firstly provides a detailed description of the reduced-scaled model, then the methodology employed is described followed by the presentation of experimental data to explain the effect of the joint orientation parameter. Finally, the key findings are summarized, describing the role of joint orientation in the evaluation of rock mass erosion.

4.3 PRESENTATION OF THE PILOT-PLANT SCALE REDUCED SPILLWAY MODEL

A pilot plant scale spillway model scaled down from the Romaine IV Hydro-Québec dam spillway (parallel flow type) is built at the Université du Québec à Chicoutimi (UQAC), Canada using the Froude Similitude Criterion. The spillway channel in the reduced-scale model is of 4.2 m long with a width of 0.68 m at the channel entrance which is varied to a width of 0.87 m over a length of 1.6 m from the channel entrance after which the width remained constant. The technical design details and comprehensive specifications of the model are available in (Koulibaly et al., 2023; Wisse et al., 2023). This model permits studying the individual effects of various important hydraulic and geomechanical parameters. The physical description of various components of the model is presented in Figure 4.1. In the model setup, a submersible pump is used to pump water from a downstream reservoir to an upstream reservoir which is equipped with two sluice gates that control the release of water into a smooth surface parallel flow spillway inclined at about 9^{o} to the horizontal and finally allowed to reach the downstream

reservoir. The end of the channel is provided with an opening to support an exchangeable metal box that can accommodate nine light weight concrete blocks of size 15 cm x 15 cm x 30 cm in a 3 x 3 matrix as shown in Figure 4.1(b). The spacing between the blocks is maintained using the Teflon bolts with an accuracy of 0.5 mm. These isolated concrete blocks at a constant specified joint opening represents the rock mass with a fully connected fracture system. The use of fixed number of Teflon bolts helps us in calculating the resisting shear force against the uplift occurrence in the stability analysis and maintaining controlled test conditions. The central block in the 3 x 3 matrix is instrumented to measure the hydraulic pressures at the top and within the fractures. This arrangement of central instrumented block surrounded by 8 non-instrumented blocks allows for the free circulation of water within the modelled fractures. The technical details of the instrumented block used are provided in our previous articles (Karnati et al., 2023a; Wisse et al., 2023). The isometric drawing of the instrumented block is presented in Figure 4.2 for better understanding. This block is equipped with 11 water inlets with elbows to allow the measurement of both static and dynamic pressure heads serving as a mini pitot tube. The top and bottom faces of the block are termed as faces "*A*" and "*B*" respectively. The vertical faces towards the upstream and downstream of flow are termed as faces "*C*" and "D*"* respectively. The lateral vertical faces towards the right and left of the flow direction are termed as faces "*E*" and "*F*" respectively. On each face of the block, two water entries are provided. The water entries on the top and bottom of the block are termed as "*Ac*", "*Ad*"[1], "*Bc*" and "*Bd*" such that the first letter indicates the face on which the entry is available, and the second letter indicates the nearest vertical face along the flow direction. The water entries on the vertical faces are termed using the indices '1' and '2' where they are having elbows facing faces "*A*" and "*B'* respectively (for example, the entries on vertical face "*C*" are termed as "*C1*" and "*C2*" respectively). All the water outlets are provided on the top of the block as presented in Figure 4.1(b), which are connected to the pressure sensors of measuring range of 0 – 10.54 mH_2O (0 – 15 psi) placed outside of the channel using airtight connecting tubes. The sensors are calibrated to ensure an accuracy of 0.0001m.

[1] For 0^o inclination condition, only one water inlet is used on the top face of the block (*A*) close to u/s side (face C), i.e., inlet *Ac* as both the inlets (*Ac* and *Ad*) are giving the similar results in the preliminary tests the results of which are not presented in this article.

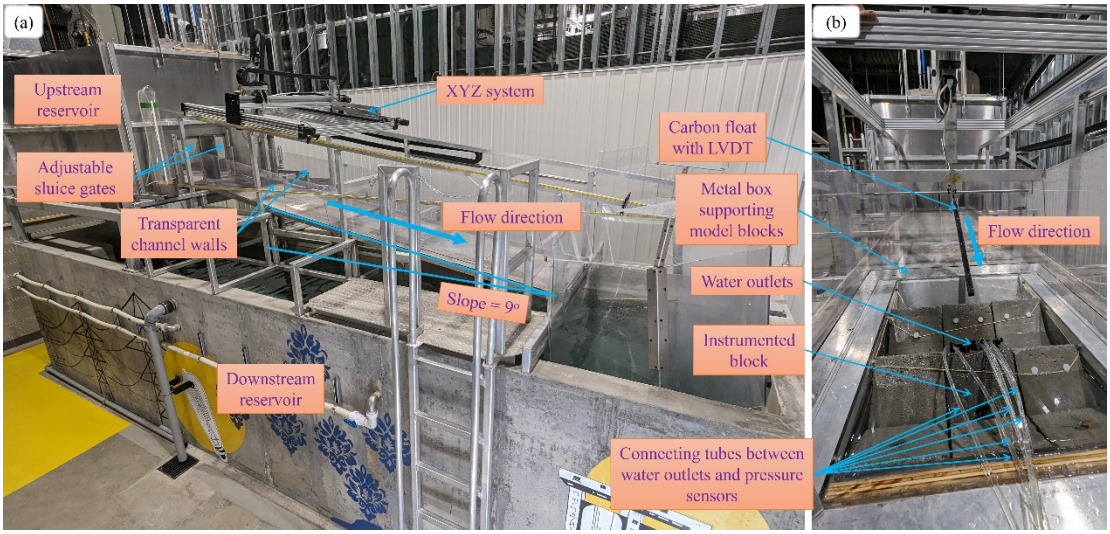

Figure 4.1 Scaled down experimental spillway model: (a) Channel side view and (b) Channel view from the downstream

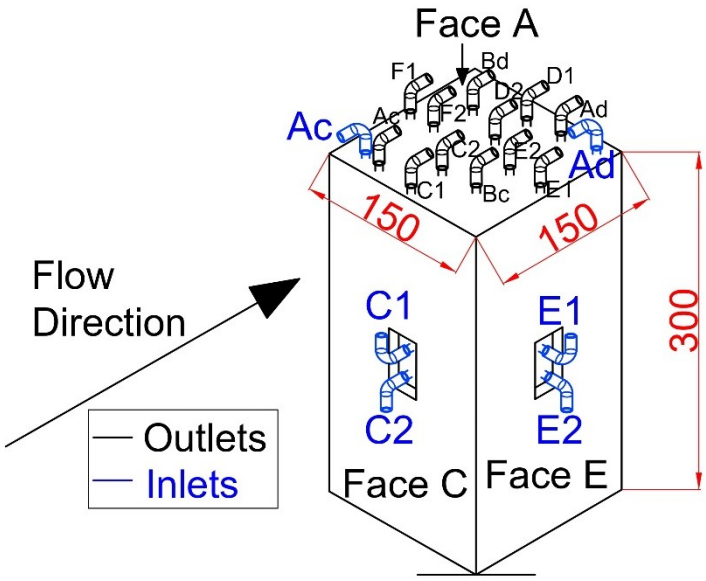

Figure 4.2 Isometric view of the instrumented block presenting the hydraulic inlets and outlets

The flowrate in the channel is controlled by varying the sluice gate opening and the operating frequency of the submersible pump. During the tests, four different flowrates within the channel are used: 0.180 m^3/s (*Q1*), 0.240 m^3/s (*Q2*), 0.315 m^3/s (*Q3*) and 0.340 m^3/s (*Q4*). The model is also equipped with a robotic XYZ system that can measure the flow velocity and depth at all the locations within the

channel using a pitot tube and an Ultrasound sensor. A carbon float is mounted in the channel which is placed close to the metal box to allow the measurement of flow depth near the blocks using a Linear Variable Differential Transformer (*LVDT*).

4.4 METHODOLOGY

4.4.1 Testing program

The study focuses on investigating the effect of the joint orientation on the hydraulic pressures around the block under a given joint opening and varied discharge conditions. The model consists of two exchangeable metal boxes that allow the placement of blocks in vertical direction (0^o), i.e., the height dimension of the blocks is placed perpendicular to the flow direction and inclined at 45^o to the flow direction. By rotating the metal box by 180^o, we shall be able to test the blocks oriented in the direction of flow (-45^o) and against the direction of flow ($+45^o$) as presented in Figure 4.3. These inclinations represent the conditions in which the height dimension in the direction of uplift is higher than the length or width of the block. The blocks are arranged in different orientations at three different joint openings, i.e., 3 mm, 10 mm and 20 mm using 4 Teflon bolts as spacers. These aperture values are chosen keeping in mind the ease of placing the blocks and the limitations of the metal box dimensions and the bolt lengths. The chosen aperture values may create very loose block conditions (open joint conditions, (ISRM, 1978)), however, the objective is the determination of water pressure distribution within the joint under different joint apertures as a function of water pressure in the channel which is made possible by the presence of elbows. The presence of elbows necessitates a minimum aperture of 10 mm and hence the elbows are not used in the lateral faces for the tests with 3 mm aperture. The additional space within the metal box is covered with packing material which is represented with shading in Figure 4.3. The top surfaces of the blocks in inclined condition represent the undulations formed during the blasting process resulting in the development of a protruded surface as observed in Figures 4.3(a) and 4.3(c). The inclined block conditions always forms a zig-zag surface in the spillway base as observed in the model tests of Reinius (1986) and the development of Edoa parameter presented by Pells (2016). The formation of this zig-zag surface on the spillway base produces different flow conditions compared to the flushed ones as observed in 0^o inclination presented in Figure 4.3(b). This in-turn modifies the hydraulic force

transferred to the rock mass as studied by Jalili Kashtiban et al. (2023) indicating the effect of surface irregularities on the energy gradient along the flow. Under these conditions, at the zig-zag surfaces stagnation pressures develop on the thrust side of the block and the eddy currents on the leeside of the block contributing to the increase in the lift force acting on the block (Li et al., 2016; Reinius, 1986). Reinius (1986) quantified the total lift force acting on the block in these conditions by measuring the pressures recorded at different positions along the block and this procedure is adopted in this study to quantify the effect of the different flow conditions arose by the zig-zag surface. The metal boxes are designed such that joint opening under the blocks is maintained 10 mm under all the test conditions allowing the top of the blocks coincide with the spillway surface. In each test condition, the hydraulic pressures at each water entry level are recorded for a period of 60 s with a data collection frequency of 100 Hz[1] for each flowrate tested starting from lowest discharge (0.180 m^3/s) to highest discharge (0.340 m^3/s). During the testing, the blocks are fixed in their position using thin jute fibres to avoid their lateral movement in inclined condition and to obtain the exact pressures in each arrangement which would be erroneous if the movement of blocks is allowed.

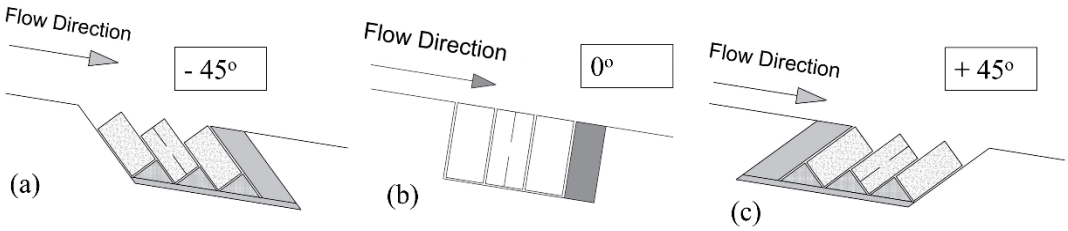

Figure 4.3 Schematic diagram of arrangement of rows of blocks in the metal boxes: (a) Blocks oriented in the flow direction (- 45°), (b) Blocks oriented perpendicular to the flow direction (0°) and (c) Blocks oriented against the flow direction (+ 45°)

[1] The testing program is designed such that the sensors collect the pressure data at 10,000 Hz and it is averaged to a final data collection frequency of 100 Hz to avoid data handling issues.

4.4.2 Interpretation of results

The pressures measured with the sensors include the sum of position/datum head, static head and dynamic head (Eq. 4.1) as depicted in Figure 4.4. The datum head (h) is the vertical distance between the positions of sensors and the water inlet. The static head (h_w) is the vertical distance between the positions of the water inlet and the water surface level (measured with the help of LVDT and ultrasound sensor). The dynamic head corresponds to the respective flow velocity (v) at the water inlet level. Removing the datum head results in the total pressure at each water entry level that includes only the static and dynamic heads that could result in the block uplift process. The role of static pressure head is solely reflected in the reduction of the weight of the block and hence the resistive shear forces. Hence only the dynamic heads at each water inlet are calculated by removing the static and datum head values from the recorded pressure data. In turn the effective weights can be used in the analysis of uplift to balance the removal of static pressure head. The uplift pressure head applied on the block can be thus measured as the difference between dynamic pressure heads at the bottom and top of the block at the critical condition (Eq. 4.2). The non-dimensional coefficient of uplift, C_{up}' is calculated as the ratio of the uplift pressure head and the average dynamic head of flow in the channel (Eq. 4.3). The hydraulic force due to the flow velocity, $F_{dynamic}$ applied on each face of the block can be calculated as the product of the unit weight of water, the area of the face and the dynamic head (Eq. 4.4). The friction resistance, F_{sh} shall be developed along the surfaces of Teflon bolts in the lateral faces due to the differences in hydraulic forces in the lateral direction and the normal force due to the weight component of the block. The frictional resistance developed shall be calculated as presented in Eq. 4.5. A sensitivity analysis is carried out for several variables studied (dynamic head at different water inlets, coefficient of variation of the dynamic heads, and coefficient of uplift) as a function of discharge and joint orientation, for different apertures (joint opening). Finally, a simplified analytical model is developed to analyze the uplift occurrence under the geometric conditions studied, which is validated using the pressure measurements recorded.

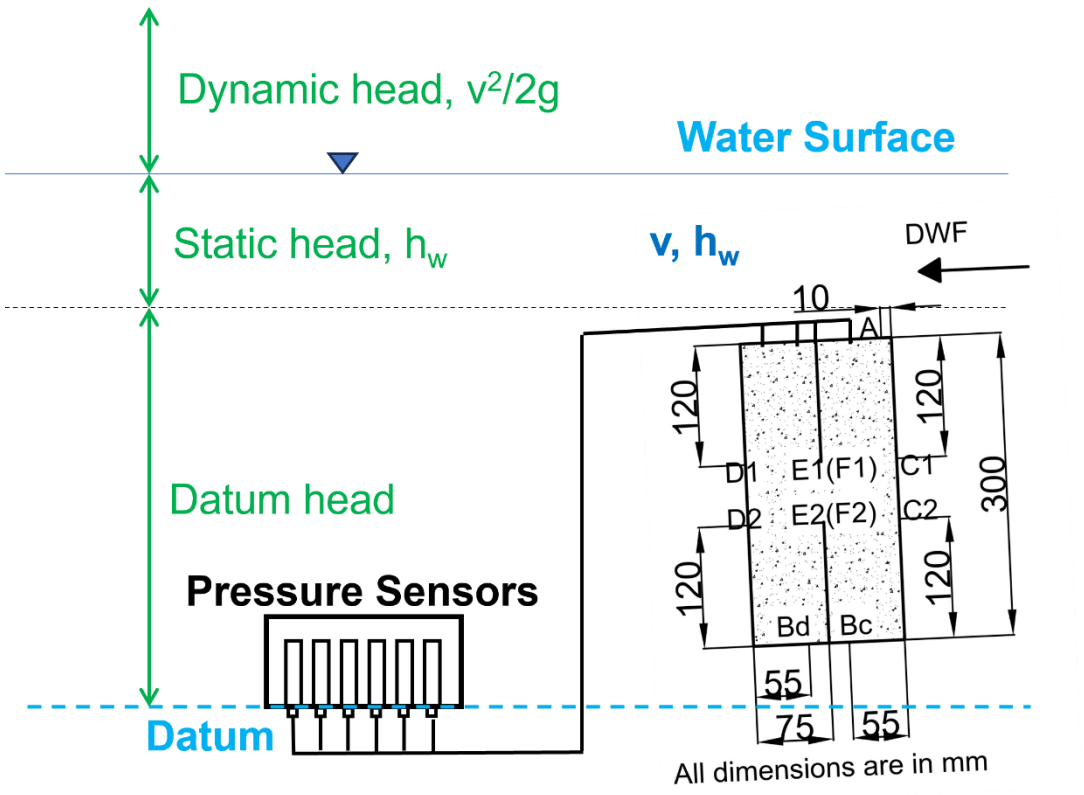

Figure 4.4 Description of various pressure heads included in the hydraulic flow

$$h_{\text{total}} = h_{\text{datum}} + h_{\text{static}} + h_{dynamic} = \text{h} + \text{h}_{\text{w}} + \frac{v^2}{2g} \quad \text{Eq. 4.1}$$

$$\text{h}_{\text{uplift}} = h_{dynamic,B} - h_{dynamic,A} \quad \text{Eq. 4.2}$$

$$\text{C}'_{\text{up}} = \frac{h_{uplift}}{\left(\frac{v^2_{channel}}{2g}\right)} = \frac{h_{uplift}}{h_{channel}} \quad \text{Eq. 4.3}$$

$$\text{F}_{dynamic} = \gamma_{\text{w}} * A_f * h_{dynamic} \quad \text{Eq. 4.4}$$

$$\text{F}_{sh} = F_L * \tan\emptyset \quad \text{Eq. 4.5}$$

Where h_{total} is the total pressure head, h is the datum head, h_w is the static head, v is the average flow velocity, $h_{dynamic,B}$ is the dynamic head on face B, $h_{dynamic,A}$ is the dynamic head on face A, γ_w is the unit weight of water, A_f is the surface area of a face of the block, F_L is the effective lateral force generated by the pressure difference and the weight component of the block, and ϕ is the friction angle (measured to be about 30° for the Teflon bolts using an inclinometer).

4.5 PRESENTATION OF MODEL TEST RESULTS

4.5.1 Analysis of model tests data

The raw data obtained from the model tests include the pressure head data obtained from each water inlet, water level in the channel, and the corresponding flow rates for a period of 60 s (i.e., 6000 data with 100 Hz data collection frequency). The XYZ system in the model setup is used only to obtain the water level above the instrumented block which is similar to the data obtained from the *LVDT* record. The pressure head data recorded at the sensor level for each inlet includes the static water head, h_{static}, dynamic water head, $h_{dynamic}$, and the datum head, h_{datum}. The sample total head, static head and dynamic head data obtained for the vertical blocks (i.e., 0° inclination) at 0.180 m^3/s flow rate for water inlet at face *A* in 3 mm joint opening are presented in Figure 4.5. The static head results presented in Figure 4.5 indicate negligible fluctuations compared to the dynamic head fluctuations. Similar variations in the static head results are observed in all the test conditions and hence only corresponding mean static head data is subtracted from the total head to obtain the dynamic head. The mean dynamic head at the top of the block in 0° inclined condition represents the average flow velocity in the channel as the top of the blocks is matching the spillway bottom. The variation of mean dynamic head and the corresponding velocity of the flow at the top of blocks with the flow rate for different joint openings in 0° inclination is presented in Figure 4.6. Figure 4.6 presents that the variation of mean dynamic head and mean velocity at the top of the blocks, i.e., in the channel is negligible for different joint openings. The position of the instrumented block in the spillway channel remains approximately similar in different inclinations and different joint opening conditions. Hence the average dynamic head in the spillway channel at the instrumented block level for each flow rate is taken as the average of the mean dynamic head at different joint openings. Table 4.1 presents the mean dynamic head and the average flow velocity in the channel at the top of instrumented block for different discharges.

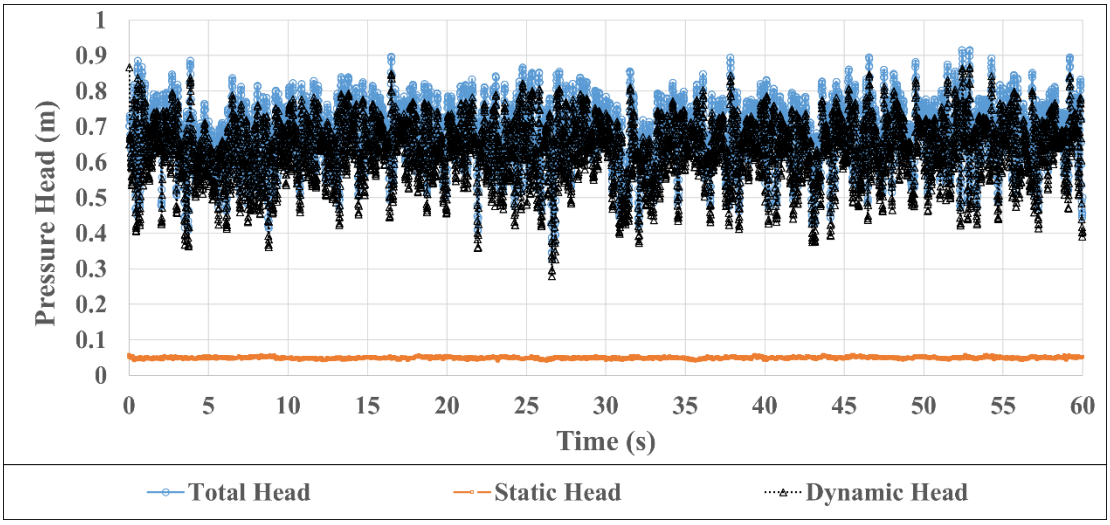

Figure 4.5 Sample temporal variation of pressure head data for water inlet at face *A* in 3 mm joint opening for 0° inclination condition

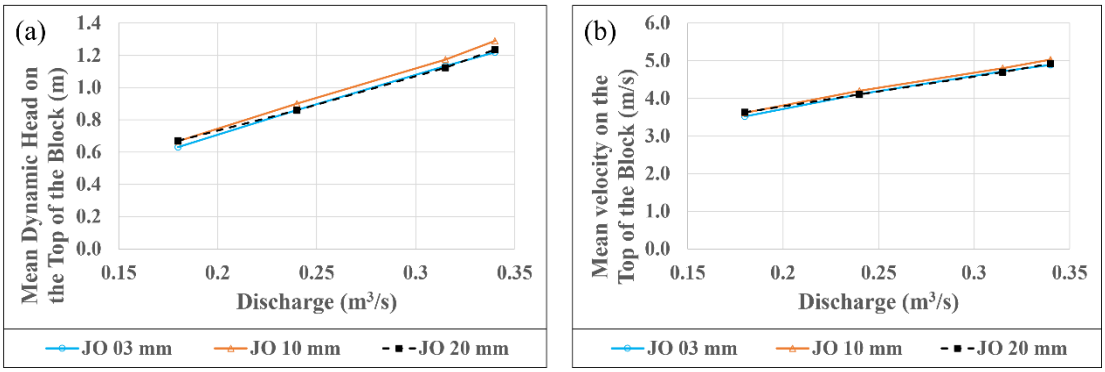

Figure 4.6 (a) Mean dynamic head and (b) Mean velocity at the top of the instrumented block for different joint openings at 0° inclination condition

Table 4.1 Mean dynamic head and the average flow velocity in the channel at the level of instrumented block

Flow rate (m^3/s)	**Mean Dynamic Head, $h_{dynamic,\ channel}$ (m)**	**Average flow velocity, $v_{channel}$ (m/s)**
0.180	0.6560	3.6
0.240	0.8732	4.1
0.315	1.1439	4.7
0.340	1.2476	4.9

4.6 EFFECT OF JOINT ORIENTATION ON THE PRESSURE FLUCTUATIONS

The dynamic head data obtained at each water entry is analyzed to obtain the mean, standard deviation, minimum and maximum values. Inspiring from the work of Wisse et al. (2023b), the relative variability of the dynamic head data is measured using the coefficient of variation, *CV*. The *CV* is defined as the ratio of the standard deviation, σ to the mean, μ of the corresponding dynamic head data (expressed as a percentage). The higher *CV* value, the higher is the dispersion of pressure data around the mean value. The *CV* values greater than 100% is mostly observed in the case of highly skewed distribution conditions or with a few extreme eccentricities (Bendel et al., 1989; Forkman, 2006). The variation of *CV* values for pressures on different faces of the instrumented block as a function of joint orientation with the spillway surface is presented in Figures 4.7 – 4.11. The *CV* values of the dynamic head on the top and bottom of the block lies below 20% in all the cases of 0° inclination (Figures 4.7 – 4.9) indicating the lower dispersion of the dynamic head data, whereas higher *CV* values are observed in the - 45° and + 45° inclined conditions. Higher *CV* values are induced by the protrusion height and the turbulence introduced by the triangular portion of the block in inclined conditions. The *CV* values of more than 100% are observed for 0.180 m^3/s flow rate for the water inlet *Ac* in + 45° inclined condition (Figures 4.7(a) and 4.9(a)). This could be understood from the higher dispersion of data observed in the dynamic

head data under these conditions. The *CV* values of the dynamic head values within the lateral faces of the instrumented block (Figure 4.10) exhibits similar results as those of the bottom face of the block in the 10 mm joint opening condition. Higher *CV* values are observed in the lateral faces especially in the 20 mm joint opening which could be attributed to the higher turbulence with the higher joint opening values. In all the conditions, the *CV* values for the dynamic heads in lateral faces for the + 45° inclination are found to be higher than those of the - 45° and 0° inclinations.

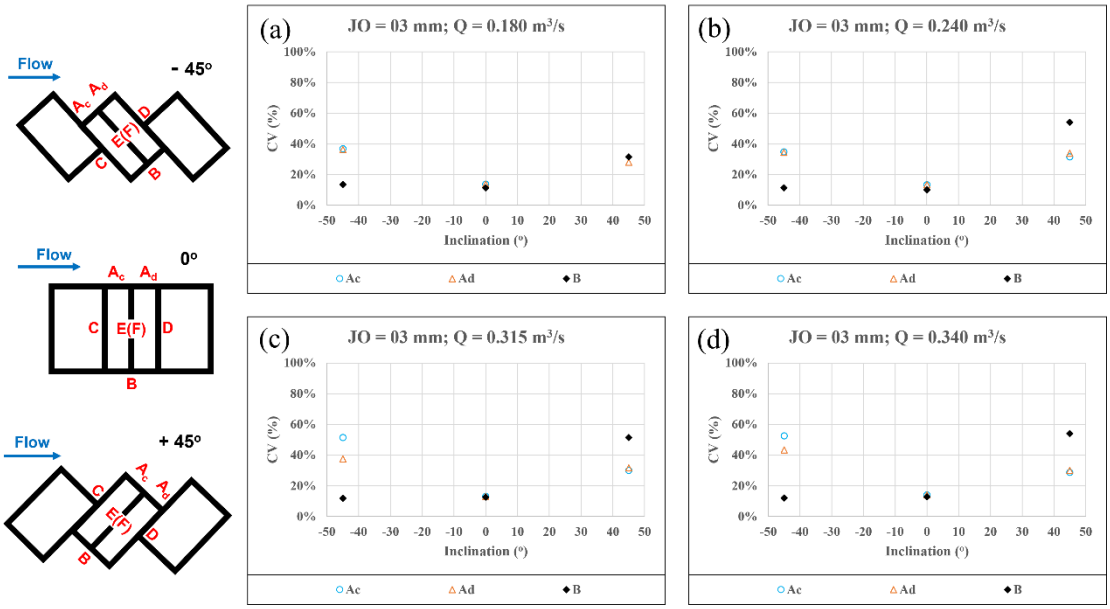

Figure 4.7 Variation of *CV* with inclination on faces *A* and *B* (top and bottom respectively) in joint opening 3 mm for flow rates of: (a) 0.180 m^3/s; (b) 0.240 m^3/s; (c) 0.315 m^3/s; (d) 0.340 m^3/s

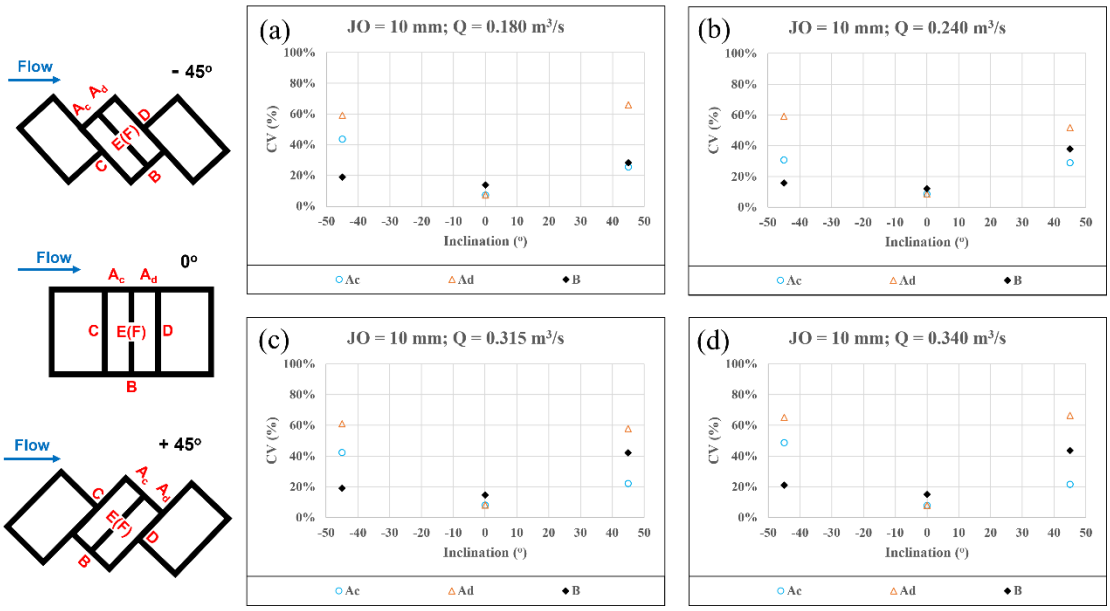

Figure 4.8 Variation of *CV* with inclination on faces *A* and *B* (top and bottom respectively) in joint opening 10 mm for flow rates of: (a) 0.180 m^3/s; (b) 0.240 m^3/s; (c) 0.315 m^3/s; (d) 0.340 m^3/s

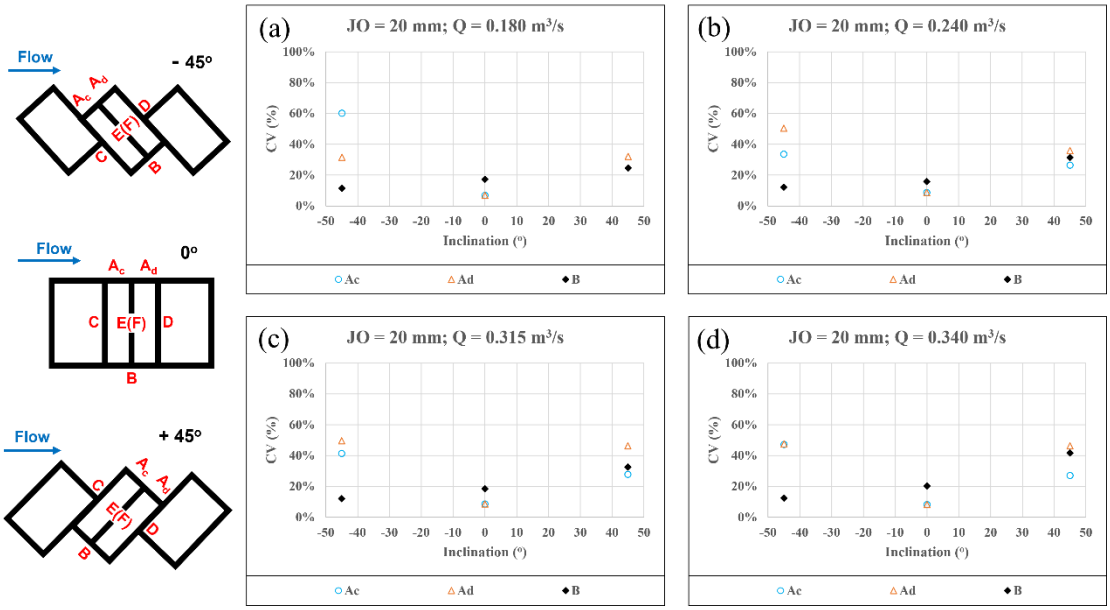

Figure 4.9 Variation of *CV* with inclination on faces *A* and *B* (top and bottom respectively) in joint opening 20 mm for flow rates of: (a) 0.180 m^3/s; (b) 0.240 m^3/s; (c) 0.315 m^3/s; (d) 0.340 m^3/s

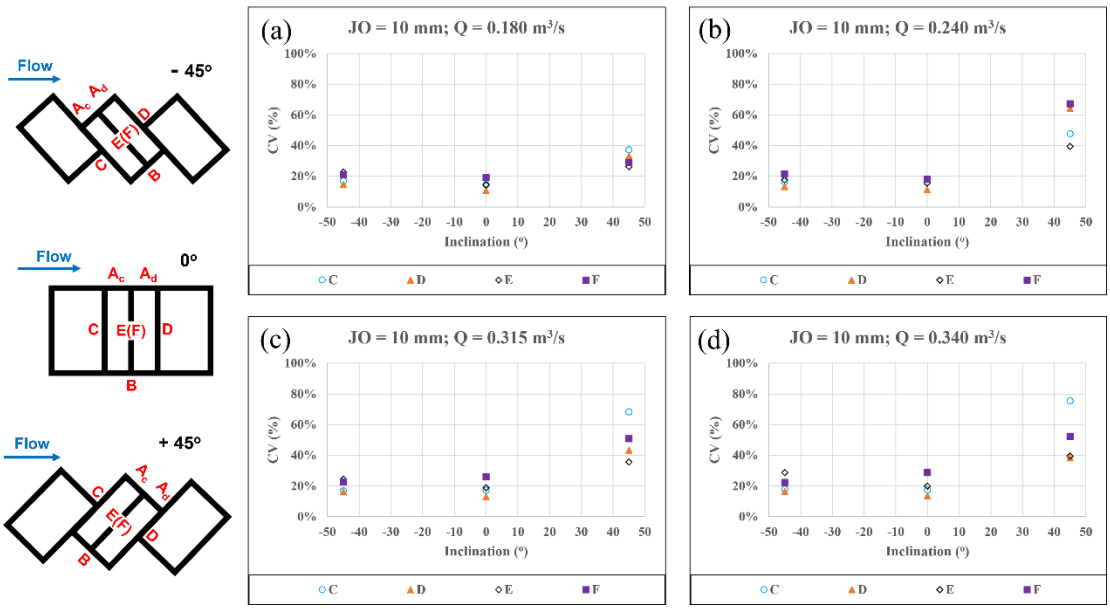

Figure 4.10 Variation of *CV* with inclination on faces *C*, *D*, *E* and *F* (Lateral faces) in joint opening 10 mm for flow rates of: (a) 0.180 m^3/s; (b) 0.240 m^3/s; (c) 0.315 m^3/s; (d) 0.340 m^3/s

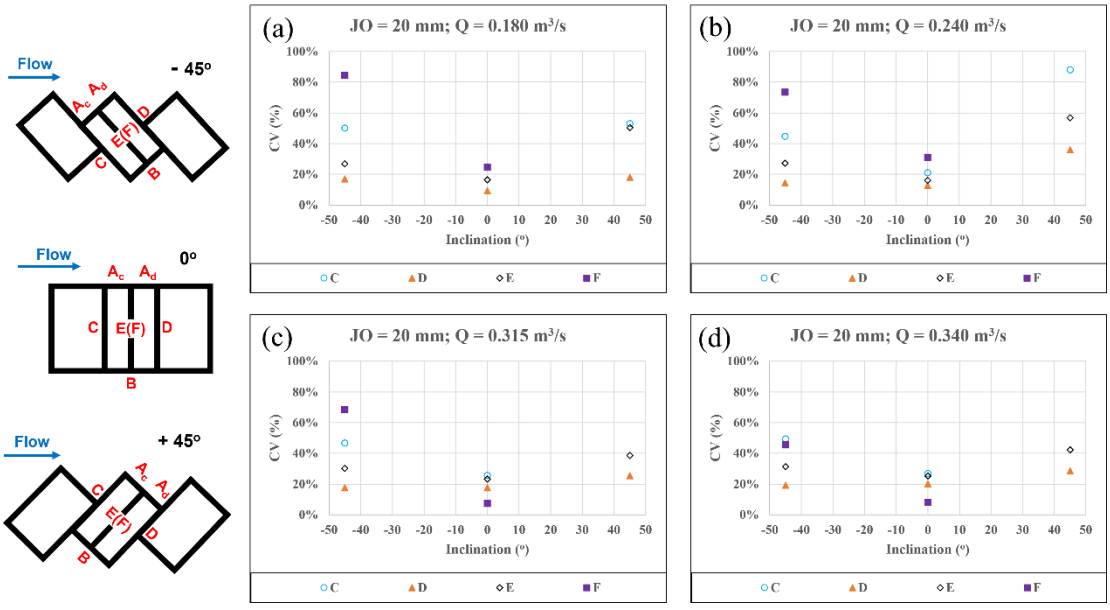

Figure 4.11 Variation of *CV* with inclination on faces *C*, *D*, *E* and *F* (Lateral faces) in joint opening 20 mm for flow rates of: (a) 0.180 m^3/s; (b) 0.240 m^3/s; (c) 0.315 m^3/s; (d) 0.340 m^3/s

The fluctuating pressure data is presented for different joint openings as the centralised mean value with error bars pointing the maximum and minimum values obtained from the pressure data in Figures 4.12 – 4.13 which are mostly self explanatory. The results of inlet *Ac* are used to plot the variation of results of inlet *Ad* for the case of 0º inclination in Figures 4.12 – 4.14. Figures 4.12 – 4.14 present that the mean dynamic head at the bottom of the block (Face *B*) is close to zero at all inclination conditions with a little increment in the inclined conditions, however, significant fluctuations have been observed in the case of inclined blocks (both - 45º and + 45º inclinations) as noticed from the error bars pointing the minimum and maximum values of the dynamic head distribution. In the contrary, the mean dynamic head is found to be maximum when the blocks are arranged in 0º inclination. The mean dynamic head at the top of the block at both the inlets *Ac* and *Ad* is found to be reducing with inclined blocks with higher values recorded at the inlets placed close to the spillway surface (i.e., inlet *Ad* in - 45º inclination condition and inlet *Ac* in + 45º inclination condition). Significant pressure fluctuations have been observed in the pressure data of the inlets placed close to the spillway surface and a lower fluctuation in the other inlets on the top of the block. A significant observation is that the fluctuations are exchanged almost entirely between the inlets *Ac* and *Ad* between the - 45º and + 45º conditions. The negative dynamic head results indicate the formation of eddy currents and flow separation on the top of the block. The mean dynamic head along the lateral faces of the instrumented block within the joints is found to be approximately similar with a little higher value in the inclined block conditions (Figures 4.15 – 4.16). Significant pressure fluctuations are also recorded in the lateral faces for inclined block conditions with higher fluctuations for + 45º inclination condition. The significant pressure fluctuations within the lateral faces and at the bottom of the block could be attributed to the development of the stagnation pressures at the protrusion formed by the inclined blocks and the corresponding flow separations.

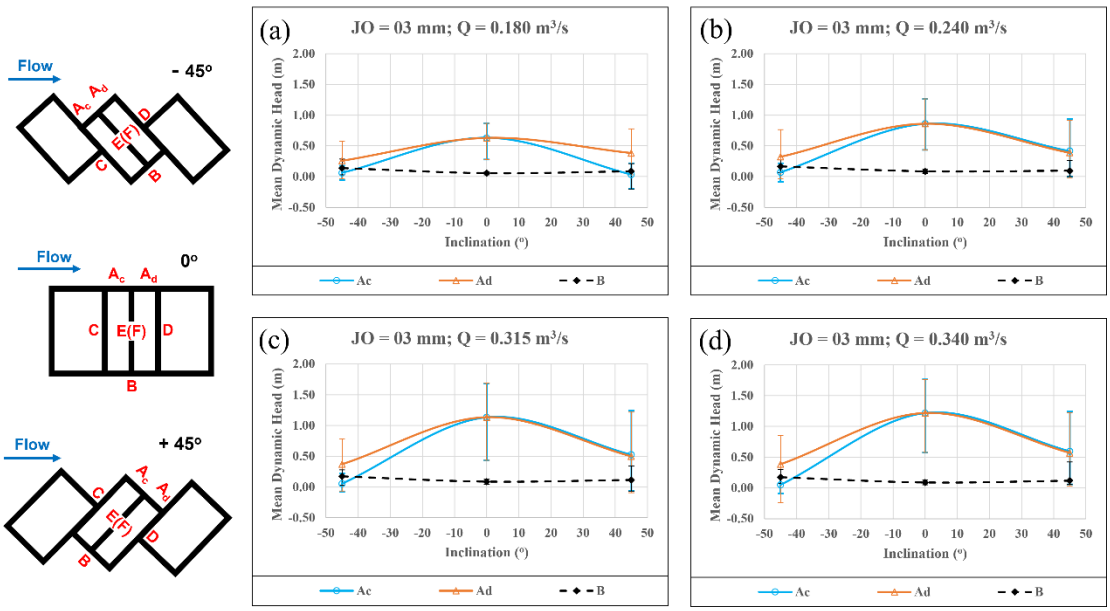

Figure 4.12 Variation of dynamic head with inclination on faces *A* and *B* (top and bottom respectively) in joint opening 3 mm for flow rates of: (a) 0.180 m^3/s; (b) 0.240 m^3/s; (c) 0.315 m^3/s; (d) 0.340 m^3/s

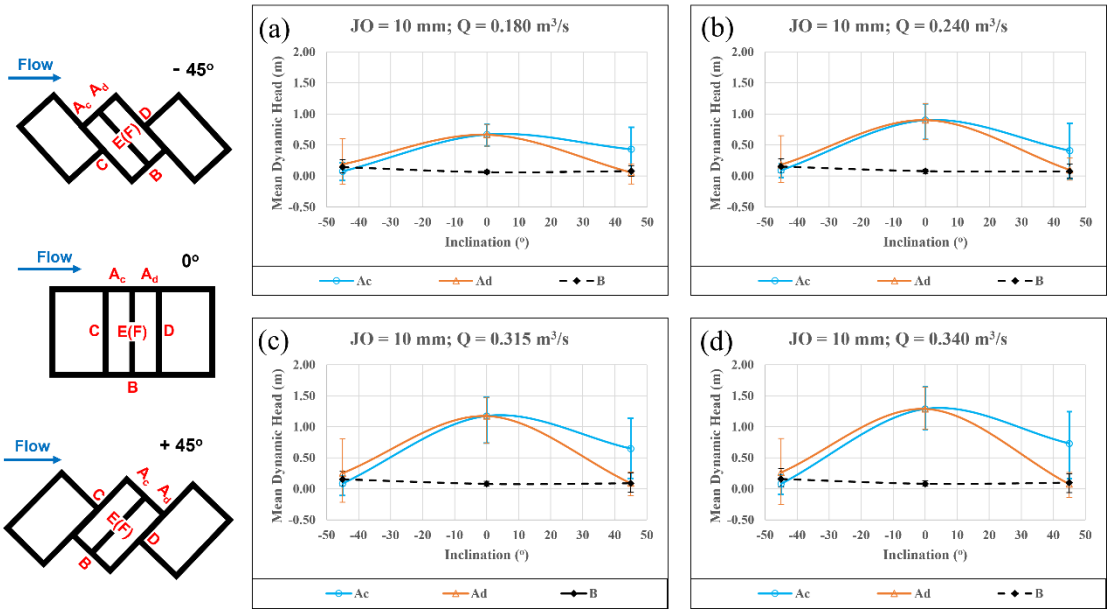

Figure 4.13 Variation of dynamic head with inclination on faces *A* and *B* (top and bottom respectively) in joint opening 10 mm for flow rates of: (a) 0.180 m^3/s; (b) 0.240 m^3/s; (c) 0.315 m^3/s; (d) 0.340 m^3/s

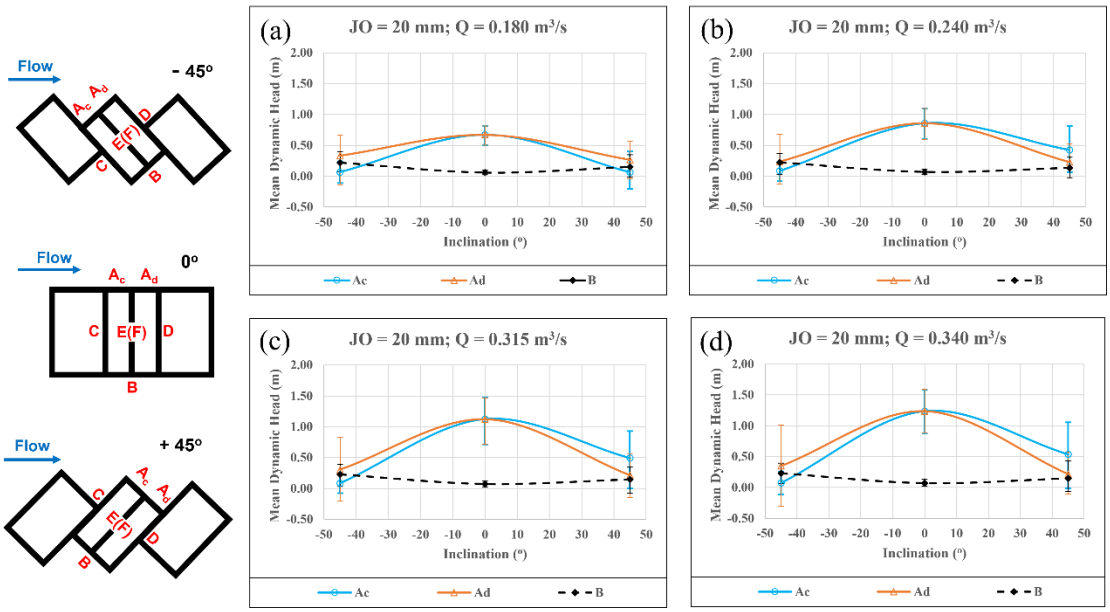

Figure 4.14 Variation of dynamic head with inclination on faces *A* and *B* (top and bottom respectively) in joint opening 20 mm for flow rates of: (a) 0.180 m^3/s; (b) 0.240 m^3/s; (c) 0.315 m^3/s; (d) 0.340 m^3/s

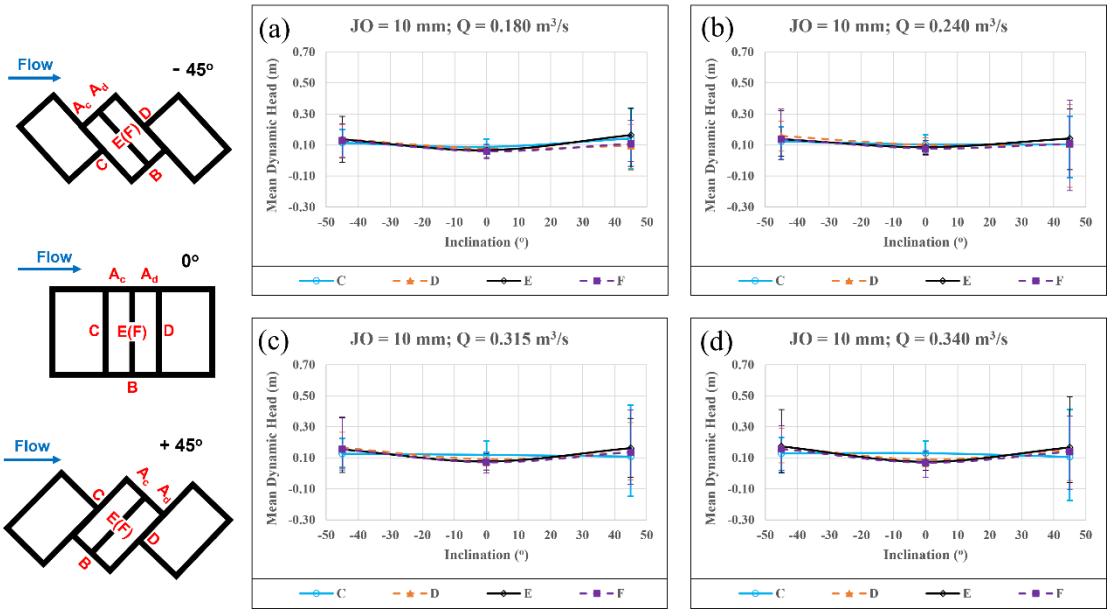

Figure 4.15 Variation of dynamic head with inclination on faces *C*, *D*, *E* and *F* (Lateral faces) in joint opening 10 mm for flow rates of: (a) 0.180 m^3/s; (b) 0.240 m^3/s; (c) 0.315 m^3/s; (d) 0.340 m^3/s

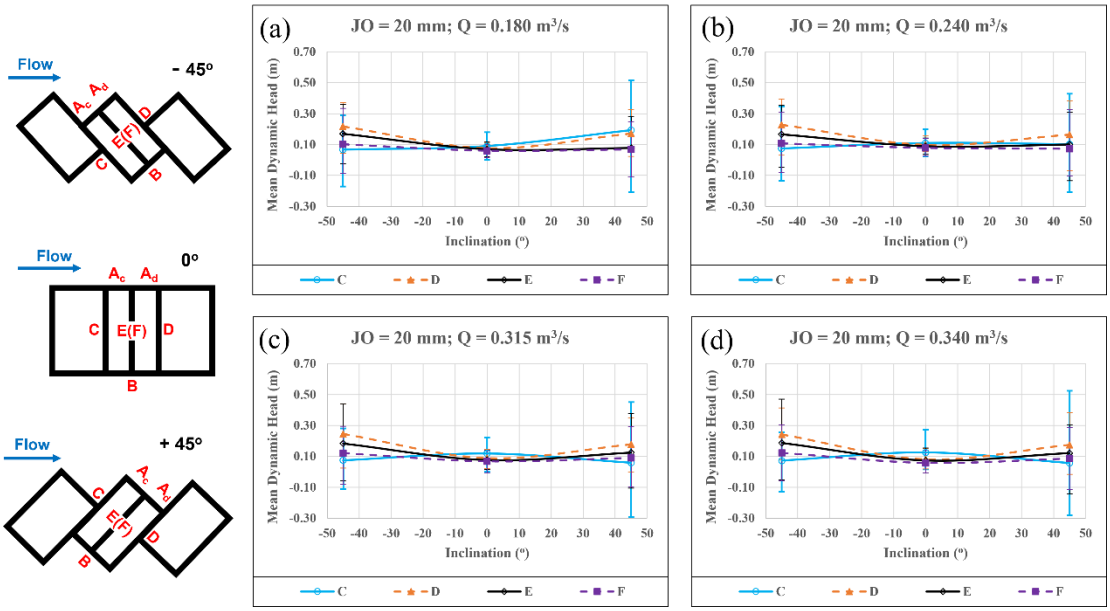

Figure 4.16 Variation of dynamic head with inclination on faces *C*, *D*, *E* and *F* (Lateral faces) in joint opening 20 mm for flow rates of: (a) 0.180 m^3/s; (b) 0.240 m^3/s; (c) 0.315 m^3/s; (d) 0.340 m^3/s

4.7 EFFECT OF JOINT ORIENTATION ON THE NON-DIMENSIONAL COEFFICIENT OF UPLIFT

The non-dimensional coefficient of uplift, C_{up}' is defined as the ratio of the dynamic head difference between the bottom and top of the block for the critical condition to the average dynamic head of the flow in the channel. The pressure on the top of the blocks is not uniform for the inclined block conditions. Reinius (1986) suggested the use of parabolic increase of pressure after the lower water inlet level during his tests. However, in these tests, the inlets are placed very close to the block edges and hence a linear variation is assumed between the pressure heads. The critical conditions exist when the pressure on the top is minimal and on the bottom maximal. Hence for the calculation of C_{up}', the average of the minimum dynamic head values is used on the top of the block[1] and the maximum dynamic head value is used on the bottom of the block. The variation of the C_{up}' with joint orientation for different joint openings is presented in Figure 4.17. Figure 4.17 presents that the C_{up}' values are high in the case

[1] Since variation is observed on the top of the block at two different inlets under inclined joint conditions, the average minimum value observed at both inlets is considered as the minimum dynamic head on the top of the block. The value of the average dynamic head on the top is assumed zero if the value is found negative to be conservative.

of inclined block conditions as compared to the non-inclined blocks presenting the possibility of block uplift. The uplift conditions exist when the uplift force exceeds the weight of the block, and the shear resistance developed along the shear face. The C_{up}' values are following a similar trend for different flow rates under the laboratory test conditions. These coefficients are found to be higher for *Q1* (0.18 m^3/s) compared to *Q4* (0.34 m^3/s) which is related to the significant increase in the pressure on the top of the block as compared to the pressure within the joints with increase in flow rate. The C_{up}' is an important parameter that enables the possibility of applying the QSI method (Bollaert, 2010; Jalili Kashtiban et al., 2021) to the parallel flow spillway condition. The most important criterion in the QSI method is the identification of the non-dimensional uplift coefficient, i.e., C_{up}' which is used to define the uplift pressure generated by the flowing water on the block.

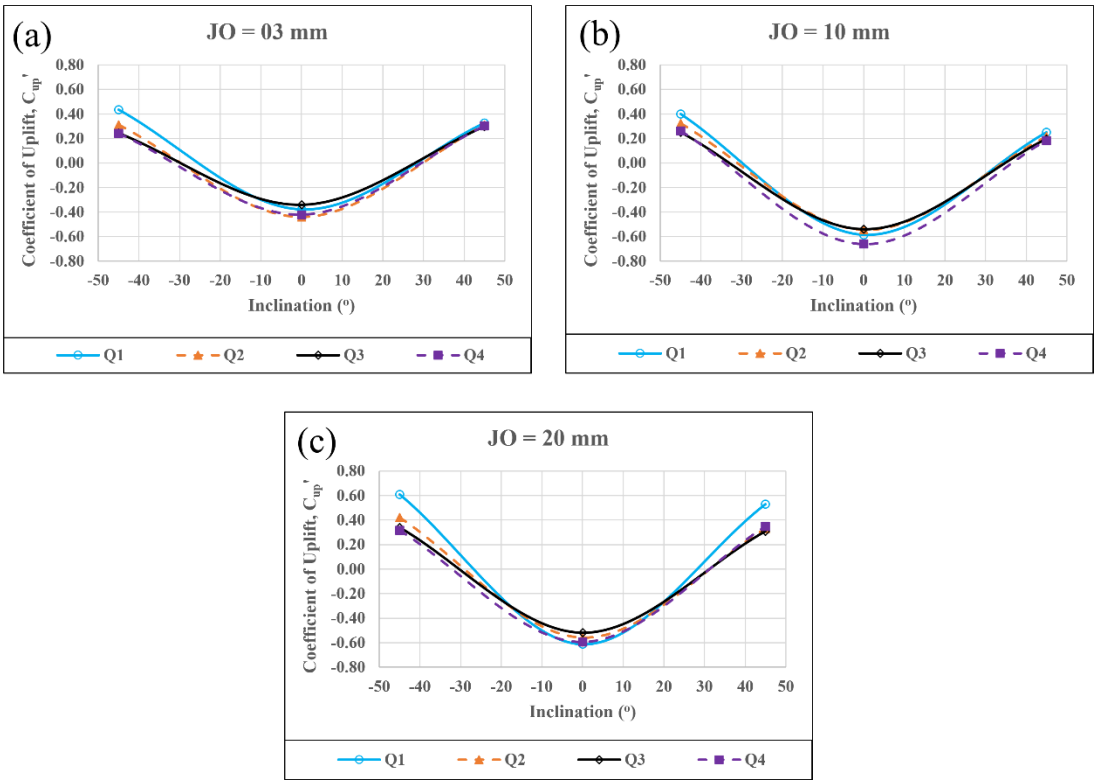

Figure 4.17 Variation of C_{up}' with joint orientation for joint openings of: (a) 3 mm; (b) 10 mm; (c) 20 mm

4.8 COMPARISON OF DIFFERENT CRITERIA FOR EVALUATION OF ROCK BLOCK ORIENTATION

For the model blocks under consideration, the ratio of joint spacing (r) which represents block structure can be taken as 1:2. The C_{up}' values for different joint openings at lowest discharge level ($Q1$) are compared with the block orientation parameters used in other rock erosion assessment techniques as observed from Table 4.2 for a similar joint spacing ratio (r = 1:2). Table 4.2 indicates that the uplift coefficients under different joint apertures (JOs) are exhibiting a similar trend. For the case of blocks dipping in the direction of flow, the rating of the J_s used by Kirsten (1982) for orthogonal joint sets under r of 1:2 tend to reduce from 1 for relative dip angle of 90^o to around 0.47 for the relative dip angle of 45^o. For the similar case, the E_{doa} rating used by Pells (2016) is found to be reducing from -10 to -12.5. In the case of blocks dipping against the flow, the rating of J_s for similar conditions tend to reduce again from 1 to about 0.54 and the E_{doa} rating is found to be increasing from -10 to -5. According to Kirsten (1982), the blocks are more stable when they are arranged perpendicular to the direction of excavation with J_s of 1, whereas according to Pells (2016), the blocks are more stable when they are arranged such that the close spaced joint set has a relative dip angle of 60^o to 70^o oriented against the flow direction (E_{doa} = 0). Hence the values of E_{doa} rating are found to be contradictory to the Kirsten's methods. Under the given testing conditions, the blocks are found to be unstable under both the inclined testing conditions and stable under vertical oriented blocks. The E_{doa} rating is developed to examine the possibility of erosion occurrence by uplift occurrence alone, however, the possible instability in this orientation is observed to be the toppling. The blocks in the vertical alignment with the flow direction are observed to be more stable. The J_s rating of 1 complies with this observation indicating that the blocks are not favourable for the removal whereas the E_{doa} rating does not agree with these results. The uncertainty cannot be completely explained with the current testing conditions alone.

Table 4.2 Comparison of orientation parameters in existing erosion assessment techniques with C_{up}' values

Inclination		**- 45°**	**0°**	**+ 45°**
C_{up}' (for Q1)	***JO 03***	0.4339	-0.3791	0.3256
	JO 10	0.3993	-0.5860	0.2502
	JO 20	0.6084	-0.6123	0.5290
J_s (Kirsten's Index)		0.54	1	0.47
E_{doa} (Pells's Index)		-5	-10	-12.5

4.9 BLOCK STABILITY ANALYSIS USING MODEL TESTS DATA

4.9.1 Blocks oriented against the flow

This orientation of the blocks is usually considered unfavourable for the block uplift to occur as the top of the block becomes the thrust side and the lateral face downstream becomes the leeside. Though Figure 4.17 is presenting the possibility of the uplift in this orientation, the realistic scenario shall be the block trying to overturn along the leeside with the top of adjacent block as the point of rotation (more dominant mechanism due to the thrust forces generated by the flowing fluid). The blocks exhibited the similar behaviour during the trial tests with the physical model, one such example of which is presented in Figure 4.18(a). The other possible scenarios would be (i) Development of a new crack/opening of an existing crack within the protruded portion of the block that shall function as a block oriented towards the flow (favourable condition) and (ii) simultaneous uplift and toppling of the unfavourably oriented block as presented in Figures 4.18(b) and 4.18(c). The possibility of toppling of the block is analyzed by considering the mobilizing and resisting moments generated by the hydraulic pressures and the weight of the block formed by three orthogonal joint sets about the possible point of rotation. The pressure

distribution around the block is assumed to be as presented in Figure 4.18(d). The section *BE* presented in Figure 4.18(d) is assumed to be the leeside of the block where flow separation is expected and hence no pressure distribution is assigned in this section to be conservative. The pressure distribution on the top of the blocks is assumed to be linearly varying with high and low pressures at the edges close to and away from the spillway surface respectively. The pressures along the joints (dynamic head on face *C* along *AD*, dynamic head on face *B* along face *CD* and dynamic head on face *D* along *CE*) are considered to be constant as measured from the model tests. It is assumed that the interaction of the flow from spillway and other lateral joints, the continuity law is not observed at the block corners where interaction is expected. The mobilizing moments are generated by the hydraulic pressures on the surfaces *AD*, *CD* and *CE* and the resisting moments are generated by the hydraulic pressure on the surface *AB* and the weight of the block. Upon the measurement of hydraulic pressures, knowing the unit weight of the rock, the ratio of the resisting moments to the mobilizing moments shall be calculated which determines the stability of the block if the ratio is greater than 1.

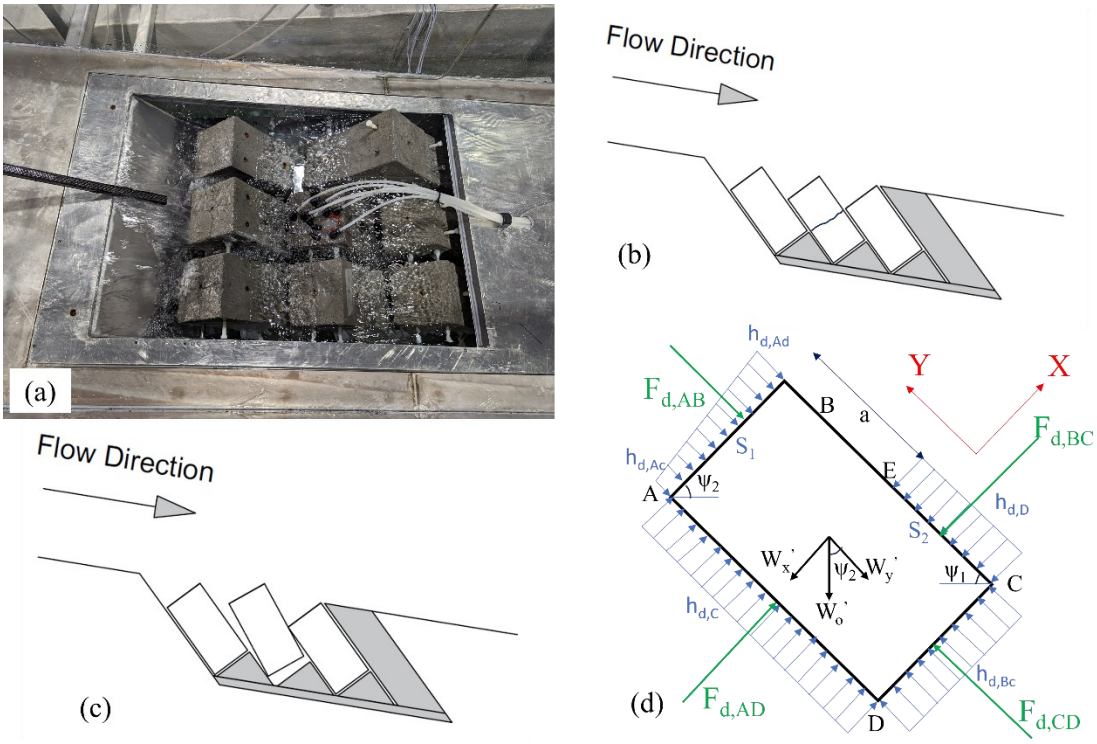

Figure 4.18 Analysis of blocks oriented against the flow: (a) Block aligning in the favorable direction by toppling during the trial tests; (b) Possible block failure by development of a new crack due to interlocking of blocks; (c) Possible block failure by simultaneous uplifting and toppling and (d) Pressure distribution around the block at critical condition

Applying the results of the model tests, the worst-case scenario shall be the minimum and maximum pressures on the top and bottom of the block respectively, with maximum pressures on the lateral surfaces *AD* and *CE*. The minimum pressures on the top are assumed to be zero since the recorded minimum pressures are mostly negative on the top of the block. The possibility of toppling is verified under mean pressure conditions and the critical conditions explained earlier. In the model tests, the spacing S_1 = 0.15 m, S_2 = 0.30 m, the dip of the block, ψ_1 = 54° (45° inclination of blocks to the spillway surface + 9° spillway inclination to the horizontal), $\psi_1 + \psi_2$ = 90° (Orthogonal joint sets), a = 0.15 + joint opening (m) and unit weight of the lightweight block material, γ_r = 13.5 kN/m^3. The submerged weight of the block material, $W_o' = \gamma_r'$ * volume of the block = (13.5-9.81) * 0.15 * 0.15 * 0.30 = 0.0249 kN. The hydraulic force on each face is calculated as described in Eq. 4.4 which is multiplied with respective eccentricity, e from the point of rotation, *C*. The values of eccentricity are presented in Table 4.3 for

respective joint opening values. Since the pressures within the joint are not available for 3 mm joint opening, the analysis can be made only for the 10 mm and 20 mm joint openings. The analysis of the possibility of toppling using the experimental results of 10 mm and 20 mm joint openings are presented in Tables 4.4 and 4.5 respectively. The factor of safety, *FS* results from Tables 4.4 and 4.5 exhibit the possibility of toppling in all the discharges for both 10 mm and 20 mm joint openings. Data in Table 4.4 shows that the instability is observed in both analyses using mean and extreme pressure conditions. Data in Table 4.5 shows that instability is observed in the case of extreme pressure conditions and at the mean pressure conditions, the block is at the verge of instability (FS ~ 1-1.2)). This indicates the probability of block instability by toppling under laboratory test conditions. The important criteria in the block instability are the occurrence of the critical conditions and the frequency of its occurrence which governs the displacement of the block. The blocks oriented against the flow presented higher possibilities of overturning and aligning towards the most favourable direction of uplift rather than uplifting against the flow though the pressure conditions are favourable under critical conditions. The more realistic scenario would be the combination of uplifting and overturning as the joint aperture reduces. Additionally, the analysis considered no pressure distribution on the leeside of the block, which is not following the continuity law, however, given the complexity of the scenario, the pressure distribution is considered as presented in Figure 4.18(d) to be conservative.

Table 4.3 Eccentricity values in meters used in the toppling analysis

Eccentricity about *C*, *e*	**Respective force**	***JO 10***	***JO 20***
e_1	$F_{d,BC}$	0.07	0.065
e_2	$F_{d,AD}$	0.15	0.15
e_3	$F_{d,CD}$	0.075	0.075
e_4	$F_{d,AB}$	$\frac{0.15}{3}\frac{(h_{d,Ad} + 2\,h_{d,Ac})}{(h_{d,Ad} + h_{d,Ac})}$	
e_5	W_x'	0.15	0.15
e_6	W_y'	0.075	0.075

Table 4.4 Analysis of possibility of block toppling in - 45^{o} inclination for 10 mm joint opening

Discharge (m^3/s)	Mean $h_{d,Ac}$ (m)	Mean $h_{d,Ad}$ (m)	Mean $h_{d,Bc}$ (m)	Mean $h_{d,C}$ (m)	Mean $h_{d,D}$ (m)	Mobilizing moments (N-m)		Resisting moments (N-m)				ΣM_{mo} (N-m)	ΣM_R (N-m)	$FS = \Sigma M_R/\Sigma M_{mo}$
						$F_{d,AD} * e_2$	$F_{d,CD} * e_3$	$F_{d,BC} * e_1$	$F_{d,AB} * e_4$	$W_x' * e_5$	$W_y' * e_6$			
Mean Pressure Conditions														
0.180	0.0737	0.1909	0.1425	0.1140	0.1383	7.5493	2.3595	1.9949	1.8670	2.1954	1.5108	9.9088	7.5681	0.76
0.240	0.0941	0.1816	0.1529	0.1243	0.1581	8.2276	2.5313	2.2804	2.0405	2.1954	1.5108	10.7589	8.0272	0.75
0.315	0.0843	0.2537	0.1585	0.1271	0.1644	8.4172	2.6237	2.3701	2.3303	2.1954	1.5108	11.0409	8.4067	0.76
0.340	0.0805	0.2653	0.1595	0.1281	0.1701	8.4842	2.6411	2.4526	2.3525	2.1954	1.5108	11.1253	8.5113	0.77
Critical Conditions														
0.180	-0.0739	-0.1356	0.2453	0.1986	0.2261	13.1475	4.0608	3.2601	0.0000	2.1954	1.5108	17.2083	6.9663	0.40
0.240	-0.0274	-0.1051	0.2589	0.2251	0.2570	14.9030	4.2860	3.7062	0.0000	2.1954	1.5108	19.1890	7.4124	0.39
0.315	-0.1064	-0.2144	0.2676	0.2328	0.2805	15.4141	4.4299	4.0448	0.0000	2.1954	1.5108	19.8440	7.7510	0.39
0.340	-0.0839	-0.2486	0.2825	0.2266	0.2948	15.0059	4.6771	4.2506	0.0000	2.1954	1.5108	19.6830	7.9568	0.40

Table 4.5 Analysis of possibility of block toppling in - 45^{o} inclination for 20 mm joint opening

Discharge (m^3/s)	Mean $h_{d,Ac}$ (m)	Mean $h_{d,Ad}$ (m)	Mean $h_{d,Bc}$ (m)	Mean $h_{d,C}$ (m)	Mean $h_{d,D}$ (m)	Mobilizing moments (N-m)		Resisting moments (N-m)				ΣM_{mo} (N-m)	ΣM_R (N-m)	$FS = \Sigma M_R / \Sigma M_{mo}$
						$F_{d,AD} * e_2$	$F_{d,CD} * e_3$	$F_{d,BC} * e_1$	$F_{d,AB} * e_4$	$W_x' * e_5$	$W_y' * e_6$			
Mean Pressure Conditions														
0.180	0.0657	0.3315	0.1984	0.0667	0.2172	4.4161	3.2846	2.7008	2.5545	2.1954	1.5108	7.7007	8.9615	1.16
0.240	0.0879	0.2362	0.2004	0.0744	0.2287	4.9234	3.3173	2.8442	2.2741	2.1954	1.5108	8.2408	8.8245	1.07
0.315	0.0842	0.3049	0.2071	0.0747	0.2453	4.9468	3.4282	3.0502	2.6116	2.1954	1.5108	8.3750	9.3681	1.12
0.340	0.0765	0.3509	0.2081	0.0721	0.2417	4.7720	3.4444	3.0059	2.7802	2.1954	1.5108	8.2164	9.4923	1.16
Critical Conditions														
0.180	-0.1119	-0.1454	0.3987	0.2770	0.3707	18.3439	6.6005	4.6090	0.0000	2.1954	1.5108	24.9443	8.3153	0.33
0.240	-0.0813	-0.1228	0.3716	0.3470	0.3918	22.9782	6.1514	4.8719	0.0000	2.1954	1.5108	29.1295	8.5781	0.29
0.315	-0.0757	-0.2023	0.3775	0.2617	0.4368	17.3321	6.2489	5.4318	0.0000	2.1954	1.5108	23.5810	9.1380	0.39
0.340	-0.1152	-0.3070	0.3802	0.2600	0.4126	17.2190	6.2933	5.1302	0.0000	2.1954	1.5108	23.5123	8.8365	0.38

4.9.2 Blocks oriented towards the flow

Arrangement of blocks oriented towards the flow is the most favourable for plucking and they tend to slip from their position under suitable hydraulic conditions. The uplift occurrence recorded during the initial trial tests under this arrangement is presented in Figures 4.19(a) and 4.19(b). To obtain the hydraulic pressures under the fixed orientation and joint opening conditions, the uplifting of blocks is prevented using thin jute fibres as done with the case of the blocks oriented against the flow. Under this orientation, the top of the block shall be on the leeside whereas the upstream face is on the thrust side. This increases the pressure within the joints because of the development of stagnation pressure at the upstream face. Analysis of uplift involves the calculation of uplift force, the weight of the block along the direction of movement and the resisting shear forces. The forces around the block are assumed as presented in Figure 4.19(c). Unlike the blocks oriented against the flow, the thrust forces exerted by the flow shall be reflected in the water inlet at face *C*. Hence the dynamic head obtained from inlets of face *C* is assumed throughout the section *AB* in Figure 4.19. Also, the pressures recorded from the inlets of faces *B* and *D* are assumed throughout the sections *AD* and *CD* respectively as they are located within the joint. The component of weight of the block along the opposite direction of uplifting (Negative X-direction) shall be calculates as $W_x' = W * sin(\psi_2)$. The shear resistance shall be calculated as the normal force generated by the hydraulic pressure difference between the faces *C* and *D* (i.e., section *AB* and section *CD* in Figure 4.19(c)) and the weight component in negative Y-direction multiplied by the tangent of angle of friction between the contacts of the block (bolts and concrete in the model tests). The shear resistance due to the lateral forces on the faces E and F are ignored in the current analysis as they are usually similar on both the faces.

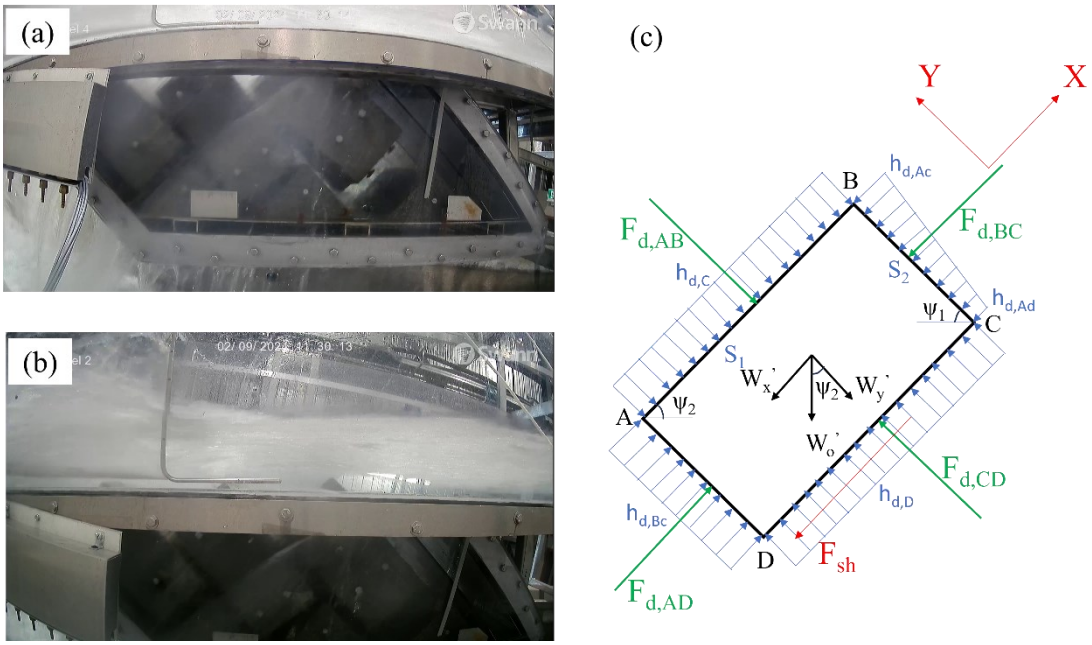

Figure 4.19 Analysis of blocks oriented towards the flow: (a) & (b) Uplift occurrence in the blocks during the trail run and (c) Pressure distribution around the block at critical condition

The resultant force, *R* in the direction of the height axis of the block (i.e., X-axis of Figure 4.19Figure 4.19(c)) is the sum of uplift forces, weight component in the direction of X ($-W_x'$) and shearing resistance ($-F_{sh}$). The block uplift is possible if the resultant *R* is positive, and uplift is not possible if the resultant R is negative. The worst-case scenario for the occurrence of block uplift shall be the case with highest uplift pressure and the minimum shear resistive forces. The shear resistive force is dependent on the weight component of the block and the hydraulic forces on the block faces *C* and *D*. For the uplift to occur, the worst-case scenario shall be the case with equal hydraulic pressures on both faces, *C* and *D*, which offers zero shear resistance due to hydraulic pressures. Applying the hydraulic pressure data obtained from the model tests, the uplift force is calculated as presented in Eq. 4.6. The resultant force, *R* is calculated by ignoring the hydraulic pressures on the lateral faces considering the most probable critical case and is presented in Table 4.6 for various joint openings. The positive resultant force and the lower factor of safety (FS) values from Table 4.6 highlights the possibility of the block uplift under critical conditions that validates the block movement during the initial trial tests. Another remarkable point is that the uplift and hence the resultant forces are less for the 10 mm joint opening. In each joint opening, the resultant force is showing a constant increase with the flowrate (Discharge),

except for Q_1 at 20 mm case, the reason for which could be the fluctuations in pressure leading to block uplift.

Table 4.6 Analysis of possibility of block uplift in + 45° inclination for various joint openings under critical conditions

JO	**Discharge, *Q* (m^3/s)**	**Non-dimensional uplift coefficient, C_{up}'**	**Total uplift force, F_{uplift} (kN)**	**Weight components**		**Shear force, F_{sh} (kN)**	**Total resisting force, $W_x' + F_{sh}$ (kN)**	**Resultant, *R* (kN)**	**$FS = (W_x' + F_{sh})/F_{uplift}$**
				W_x' (kN)	**W_y' (kN)**				
3	0.180	0.3256	0.0472	0.0146	0.0201	0.0116	0.0263	0.0209	0.56
	0.240	0.3077	0.0593	0.0146	0.0201	0.0116	0.0263	0.0330	0.44
	0.315	0.2973	0.0751	0.0146	0.0201	0.0116	0.0263	0.0488	0.35
	0.340	0.3026	0.0833	0.0146	0.0201	0.0116	0.0263	0.0571	0.32
10	0.180	0.2502	0.0362	0.0146	0.0201	0.0116	0.0263	0.0100	0.72
	0.240	0.2147	0.0414	0.0146	0.0201	0.0116	0.0263	0.0151	0.63
	0.315	0.1954	0.0493	0.0146	0.0201	0.0116	0.0263	0.0231	0.53
	0.340	0.1837	0.0506	0.0146	0.0201	0.0116	0.0263	0.0243	0.52
20	0.180	0.5290	0.0766	0.0146	0.0201	0.0116	0.0263	0.0503	0.34
	0.240	0.3312	0.0638	0.0146	0.0201	0.0116	0.0263	0.0376	0.41
	0.315	0.3073	0.0776	0.0146	0.0201	0.0116	0.0263	0.0513	0.34
	0.340	0.3484	0.0959	0.0146	0.0201	0.0116	0.0263	0.0697	0.27

$$F_{uplift} = \gamma_w * C'_{up} * h_{channel} * A_f \quad \text{Eq. 4.6}$$

Where C_{up}' is obtained from Figure 4.17, $h_{channel}$ is mean dynamic head of flow in channel obtained from Table 4.1 and A_f is the surface area of the block bottom or top face, i.e., 0.15 x 0.15 m^2.

4.9.3 Blocks oriented perpendicular to the flow (0° inclination)

The arrangement of blocks perpendicular to the spillway surface with the top of the blocks matching the spillway level without any protrusion is the most stable condition according to the model test studies. The values non-dimensional coefficient of uplift C_{up}' obtained from the model tests are found to be negative in all the joint opening conditions. This could be attributed to the high aspect ratio of 1:2 for the block. With the introduction of even a small amount of protrusion, the C_{up}' can be increased to make the block move from its position (Frizell, 2007; Wahl et al., 2019; Wisse, Saeidi, et al., 2023). Further tests shall be made in near future by varying the aspect ratio of the block under different protrusion conditions that shall aid the development of a relationship between the most important geomechanical parameters concerning the uplift analysis.

4.10 CONCLUSIONS

The primary and emergency spillways of dams, though typically founded on hard rock, can still experience significant rock mass erosion under unfavourable joint conditions. Joint orientation is one of the prominent factors in this regard. This study investigates the hydraulic pressure distribution through physical spillway model tests on modelled prismatic rock blocks oriented at - 45°, 0° and + 45° with respect to the flow. The results obtained from the tests are analyzed to obtain the mean value, coefficient of variation (*CV*) and non-dimensional coefficient of uplift, C_{up}'. The current test results are measured by arresting the movement of the block. However, in the natural erosion process, the block positions alter through translation or rotation which alters the pressure distribution around the block. The current test set-up does not include any means of measuring displacement and hence the movement is arrested to measure the pressure distribution under measured geomechanical conditions, i.e. constant spacing between the blocks. In the near future, installation of accelerometers and extensometers shall allow for

the measurement of the hydraulic pressure distribution around the block during the block toppling or uplifting. Accompanying the measurements by measuring the air concentration during the block displacement could improve the understanding of the erosion process which falls under the limitations of this study. The scope of the future studies involves further in-depth analysis of block instability by varying different key properties of block, including, size, shape (aspect ratio) and orientations. This enables the possible quantification of individual effects of these parameters which helps in development of a rating system to determine the quality of rock masses. Due to physical and technical limitations, the problem of scale effect persists despite of extensive data measurement. This issue could be overcome by numerical modelling which could serve as a useful tool in assessing the scale effects and verifying the effect of wide range of block orientations on the erosion process. The experimental data serves as the basis for the calibration of the numerical model developed at the model scale. The calibrated model can then be used to model real scale erosion conditions.

The following conclusions are drawn from the study:

- Observation of dynamic head variations revealed that the pressure values on the top of the block reduced close to zero whereas the pressures within the joint increased with both the block inclination conditions.
- Introduction of the block protrusion by the wedged portion of the block affected the pressures on the top of the block and within the joints.
- The values of C_{up}' for various tests presented a possibility of uplift in the case of inclined block orientations indicating the importance of joint orientation in the uplift analysis. The results obtained are following similar trend as obtained with the Kirsten's index's orientation parameter (J_s), but the Pells's index's orientation parameter (E_{doa}) is exhibiting a disagreeing trend. Further modelling is necessary to determine the actual effect of joint orientation parameter on the erosion process.
- The blocks oriented against the flow tend to topple and align themselves towards the flow indicating that the uplift is mostly possible with the latter orientation. The factor of safety (FS) values against the toppling failure are found to be in the range of 0.5 – 0.8 for different

joint apertures and flow rates which indicates the possibility of toppling in all these test conditions.

- The blocks arranged in the direction perpendicular to the flow didn't result in any block movement under the given test conditions; however, the introduction of protrusion between the blocks will result in the block uplift.
- The blocks oriented in the direction of the flow readily exhibited the uplift possibility as observed from the positive value of the resultant force and FS (0.2-0.7) under critical conditions of the laboratory test data.

CHAPITRE 5

ARTICLE 3: INFLUENCE OF ROCK BLOCK GEOMETRY AND ORIENTATION ON SCOUR FORMATION IN A DAM SPILLWAY USING PHYSICAL MODEL TESTING

Vineeth Reddy Karnati [a*], Ali Saeidi [a], Alain Rouleau [a], Marco Quirion [b]

[a] Département des sciences appliquées, Université du Québec à Chicoutimi, Saguenay, QC G7H 2B1, Canada.

[b] Expertise, intégrée - Géologie, Hydro-Québec, 75 Boulevard René-Lévesque Ouest, Montréal, QC H2Z 1A4, Canada.

Submitted to Rock Mechanics and Rock Engineering

Ce chapitre reprend un article dont le premier auteur est l'auteur de cette thèse. Le chapitre utilise les résultats des essais sur le modèle physique pour calculer la stabilité des blocs avec différentes valeurs d'ouvertures et d'orientations des joints, ainsi que de saillie des blocs. À la fin, une étude paramétrique est présentée pour déterminer l'effet de chaque paramètre clé.

Credit authorship contribution statement

Vineeth Reddy Karnati: Experimental work, Methodology, Data analysis, Investigation, Preparation of original manuscript, review & editing. **Ali Saeidi:** Supervision, Conceptualization, Methodology, Funding & Resource acquisition, Overall project administration, Review & editing the manuscript. **Alain Rouleau:** Supervision, Review & editing the manuscript. **Marco Quirion:** Supervision, Funding acquisition, Review & editing the manuscript.

Competing interests

The authors declare that they have no known financial or personal conflicts of interest that could have influenced the content or outcomes of this research.

Funding

This research was funded by the Natural Sciences and Engineering Research Council of Canada (NSERC) and Hydro-Québec through the Collaborative Research and Development Grant (CRDPJ 537350–18), as well as an individual NSERC Discovery Grant (RGPIN-2019-06693). The authors also acknowledge the support of the Fonds de recherche du Québec – Nature et technologies (FRQNT) for

awarding the *Programme de bourses d'excellence pour étudiants étrangers* (PBEEE) scholarship (Grant No.: 2023–2024 – 1I – 334721), which contributed to this work.

Résumé

Les évacuateurs de crues non revêtus des barrages ont été, au fil des années, soumis à une érosion sévère du massif rocheux, laquelle est reconnue comme un enjeu critique de sécurité dans la conception de ces ouvrages hydrauliques. Le développement d'une méthode d'évaluation fiable nécessite une compréhension approfondie des mécanismes en jeu dans le processus d'érosion ainsi que des paramètres qui y sont associés. La présente étude examine l'influence de la géométrie des blocs rocheux et de leur orientation sur la stabilité des blocs à l'aide d'essais sur modèles physiques. Un modèle analytique est développé afin d'évaluer la stabilité des blocs à partir des résultats expérimentaux obtenus sous différentes conditions géomécaniques, notamment l'orientation des joints et la protrusion des blocs. L'effet de la géométrie des blocs, telle que le rapport d'aspect et la longueur exposée, sur les mécanismes d'instabilité est également analysé au moyen d'une étude paramétrique approfondie. L'analyse de stabilité met en évidence la possibilité d'un arrachement des blocs par basculement pour des blocs orientés à -45° par rapport à la direction de l'écoulement, avec des facteurs de sécurité inférieurs à 1 sous diverses combinaisons de pression. De plus, un mécanisme de soulèvement est observé pour des blocs orientés à +45° et à 0° sous certaines configurations de protrusion, également associé à des facteurs de sécurité inférieurs à 1 pour des combinaisons de pression spécifiques. L'approche proposée constitue un cadre expérimental et analytique novateur permettant de relier des paramètres hydrauliques et géomécaniques quantifiables à la prédiction des mécanismes probables d'érosion. Les résultats de cette étude fournissent des éléments pratiques pour une meilleure évaluation des risques d'érosion et contribuent à l'amélioration des analyses de sécurité des barrages.

5.1 ABSTRACT

Unlined dam spillways have been subjected to severe rock mass scour/erosion over the years, and this erosion has been considered a critical safety concern in the design of these hydraulic structures. Development of a reliable assessment method necessitates the proper understanding of the mechanisms involved in the scouring process and the associated scour parameters. This study investigates the effect of rock block geometry and its orientation on block stability using physical model testing. An analytical model is developed to evaluate the block stability using the results of model tests under varied geomechanical parameters, especially, joint orientation and block protrusion. The effect of block geometry like aspect ratio and exposure length on the instability is further examined through a comprehensive parametric analysis. The stability analysis presents the possibility of block removal by overturning in blocks oriented at -45^{o} to the flow direction with factor of safety less than 1 under different pressure combinations and by uplift in blocks oriented at +45^{o} and 0^{o} under specific protrusion configurations with factor of safety less than 1 under certain pressure combinations. The proposed approach presents a novel experimental-analytical framework linking quantifiable hydraulic and geomechanical parameters to predict probable scour mechanisms. The findings of this study offer practical insights to better evaluate the erosion risks and enhance dam safety assessments.

Keywords: Rock scour; Pilot-plant spillway model; Block uplift; Block overturning; Block geometry; Parametric study

5.2 INTRODUCTION

Dam spillways are the hydraulic structures that serve the purpose of a safe evacuation of the flood water and can be either lined or unlined depending on the underlying rock mass condition. In either case, severe threats posed by rock scour in the last few decades at numerous spillways sites have been reported (Annandale, 1995; Boumaiza, 2019; Pells, 2016). The threats posed by the extended spillway rock scour have been recently demonstrated by the Oroville spillway incident in 2017 (Koskinas et al., 2019; Stofleth et al., 2023) and Eping dam spillway incident in 2021 (Yu et al., 2025). Rock scour involves the removal of detached intact rock blocks, separated by inherent discontinuities, under the action of

hydraulic forces. Thus, this physical process involves the complex interaction between the geomechanical (rock-mass) parameters and the hydraulic parameters (Jalili Kashtiban et al., 2021; Pells, 2016). The hydraulic force transferred to the rock mass could also vary with spillway geometry and surface irregularities (Jalili Kashtiban et al., 2023b, 2023a).

Many studies have proposed semi-empirical and semi-analytical approaches to assess the scour depth and to prevent these disasters. The methods developed were typical to the flow configurations, i.e., parallel flow and plunging jet spillways (Jalili Kashtiban et al., 2021). While semi-empirical approaches remain popularly employed for scour predictions for their inherent simplicity, severe damages were reported at several instances due to the uncertainties involved in the measurement of field parameters (Boumaiza, 2019). Furthermore, these approaches do not explicitly represent the underlying scour mechanisms. The semi-analytical model developed by Bollaert (2004, 2010) clearly demonstrated specific scour mechanisms, yet it was developed based on small-scale model studies performed at low velocities (Wisse, 2022) limiting its applicability to parallel-flow spillways. Therefore, the development of a reliable scour prediction method integrating important geomechanical and hydraulic parameters addressing different scour mechanisms remains necessary. Boumaiza et al. (2019) compared existing scour indices using the database compiled by Pells (2016) and identified several key parameters influencing the scour phenomenon including joint opening, joint shear strength, block volume, erosion discontinuity orientation adjustment (E_{doa}) and the nature of the potentially eroding surface (*NPES*). The E_{doa} parameter was related to joint orientation and the aspect ratio (Pells et al., 2017; Pells, 2016) and the *NPES* parameter was dependent on the surface roughness defined by block alignment and its protrusion (Douglas et al., 2018; Pells, 2016). Thus, the evaluation of individual effects of these parameters is important for the development of a reliable index to determine the rock mass resistive capacity. Determination of the influence of these parameters under in-situ conditions could be challenging due to complex instrumentation and high costs involved (George, 2015; Karnati et al., 2025). Given these limitations, the practical alternatives to evaluate the individual effect of these parameters include reduced-scale physical modeling and numerical simulation. However, a reliable numerical model requires a coupled interactive modelling of hydraulic and geomechanical processes. Most numerical models that are available (Dasgupta et al., 2011; Li & Liu, 2010; Moren & Sjoberg, 2007;

Saiang et al., 2022) include interactive behavior considering only one level of information exchange, limiting their ability to replicate real scour conditions. Recently, a few coupled interactive models, considering multiple information exchanges, were developed (Gardner, 2023; Teng et al., 2023a; 2023b), however, they still remain under development to incorporate the effects of surrounding blocks. Under such limitations, physical model testing becomes a practical and reliable alternative.

Wisse (2022) presented a review of various physical models used to study the scour phenomenon. Most of these physical models suffer from the limitations of smaller model size, use of a single model block (either tetrahedral or cubical) or use of very small multiple blocks. These limitations result in the improper simulation of the dynamic flow behavior within the joints of a fractured rock mass. Lamb et al. (2015) presented the importance of considering the interaction between the surrounding rock masses, which necessitates the use of multiple blocks. Among various rock mechanisms, rock block removal by plucking or uplift was considered to be more conventional under the action of hydraulic forces (Jalili Kashtiban et al., 2021; Lamb et al., 2014; Whipple et al., 2000), which requires the determination of uplift pressure acting on the block. The uplift pressure acting on the block depends on hydraulic pressures acting on the top and the bottom of the block, which in turn depend on several geomechanical parameters, especially block protrusion, joint aperture/opening, flowrate and joint orientation. Frizel (2007) studied the hydraulic pressures across a slab under varied offset conditions. Wahl and Heiner (2024) expanded on the results obtained by Frizel (2007) using large-scale laboratory tests quantifying the uplift pressures calculated as the increase in the pressure in the chamber below an open joint with the introduction of square-edged offsets varying offset heights and joint apertures (gap widths). The reduced-scale model used by Wahl and Heiner did not incorporate the use of model blocks simulating the three-dimensional joints which may influence the local hydraulic behavior and pressure distribution within the joints. The Quasi-Static Impulsion (QSI) mechanism, presented by Bollaert (2010b) could be applied to the parallel-flow spillways although it was developed to determine block uplift in the plunge pool walls where the flow direction is almost parallel to the surface of the plunge pool. This approach was based on the results of non-dimensional coefficients of uplift (C_{up}') (Refer to Annexe D) calculated from the model test results of Reinius (1986) and Montgomery (1984); however, this approach does not consider other

possible mechanisms of instability. Besides, these studies suffer from the limitations of pressure measurements on one block face and measurements with piezometers.

Despite extensive research on spillway scour, existing experimental and numerical models still lack the ability to simultaneously capture the combined effects of joint orientation, block protrusion and multi-block interaction under realistic pressure distributions. These limitations restrict their applicability for assessing the rock block stability in unlined dam spillways. To address this knowledge gap, the current study develops an integrated experimental-analytical framework using a considerably large-scale physical model capable of measuring dynamic pressures around the rock blocks under varied geomechanical conditions. The measured pressures are used to evaluate the block uplift and overturning mechanisms through a corresponding analytical model formulated, supported by a parametric investigation of block geometry and joint configuration. This approach provides new insights into how these parameters individually influence hydraulic uplift and rock block removal, rendering a more reliable basis for assessing scour risk for unlined spillways.

5.3 PRESENTATION OF THE PHYSICAL MODEL

A reduced-scale physical spillway model at a scale of 1:40 representing the spillway of Romaine-4 Hydro-Québec Dam facility was developed at the Université du Québec à Chicoutimi (UQAC), Québec, Canada using Froude scaling laws. The design details, model specifications and expansion to scaling laws were presented in Koulibaly et al. (2023) and Wisse et al. (2023). Froude similitude is appropriate for high-velocity spillway flows where gravity dominates the inertial forces, and is the standard approach for modelling open-channel and spillway flows (Koulibaly et al., 2023; Wisse, Saeidi, & Quirion, 2022). Using this scaling law, flow velocity and discharge in the model are obtained using the relationships presented in Eq. 5.1-5.2, where v_{RM}, v_{Pr}, Q_{RM} and Q_{Pr} stands for flow velocity in reduced-scale model, flow velocity in prototype, discharge in reduced-scale model and discharge in prototype respectively, thus ensuring kinematic similarity. While Reynold's number similarity cannot be simultaneously achieved with Froude similarity in free-surface flows, the flows in both the prototype and the model were fully turbulent. The Reynold's numbers for the prototype and the 1:40 model were

calculated as 7.3 x 10^7 and 2.9 x10^5 respectively, which were well above the threshold for fully turbulent conditions (R_e > ~ 2000) (Koulibaly et al. 2023). As the hydraulic pressures primarily depend on turbulent stagnation and separation behavior, which scale well when the turbulence is fully developed, the deviation from strict Reynold's similarity has negligible effect on the relative pressure fluctuations and hence on the pressure coefficients (Annandale, 2006; Ervine et al., 1997). The effects of cavitation have not been observed in the model studies as the pressures measured at all block faces remained above vapor pressure. Besides, the prototype cavitation indices are not usually reached at the reduced-scale model velocities (Yusuf & Micovic, 2020). Wahl and Heiner (2024a) mentioned that aeration effects exist in both prototype and reduced-scale models, but were found to be secondary compared to dominant role of turbulent stagnation pressure at the block edges.

$$v_{RM} = \frac{v_{Pr}}{\sqrt{40}} \qquad \text{Eq. 5.1}$$

$$Q_{RM} = \frac{Q_{Pr}}{40^{\frac{5}{2}}} \qquad \text{Eq. 5.2}$$

The physical model at UQAC with its various components is presented in Figure 5.1. The rock scour process involves the removal of intact rock blocks after isolation of blocks through rock mass fracturing. The time required to initiate fracturing depends on the stress intensity applied to the joint and the number of stress cycles. Given the difficulties associated with modelling the stress-dependent fatigue accumulation, most physical models assume that the rock mass is completely fractured and use only the individual model blocks to represent the isolated intact blocks. This relatively large-scale model consists of an opening at the end of the spillway channel supporting exchangeable metal boxes that allow the positioning of the model blocks in different orientations. A total of 9 lightweight concrete blocks each of size 15 x 15 x 30 cm^3 are arranged in a 3 x 3 matrix. The blocks are positioned at the chosen joint opening, *JO* using Teflon bolts allowing a constant aperture between the blocks. The central block is instrumented with internal hollow copper tubes that allow the pressure measurement at different positions on various faces of the block. A schematic of the block arrangement in different orientations is presented in Figure 5.1 (b - d). Wisse et al. (2024) reported that for the proper measurement of both static and dynamic pressures, the inlets should be positioned against the flow direction. To facilitate this,

all the water inlets have been provided with elbows that serve as a mini pitot-tube. The details related to the operation of this model and the details of the instrumented block were presented in our previous article (Karnati et al., 2025). The XYZ system presented in Figure 5.1 allows the measurement of flow properties, i.e., flow height and flow velocity by means of a pitot tube and an ultrasound sensor.

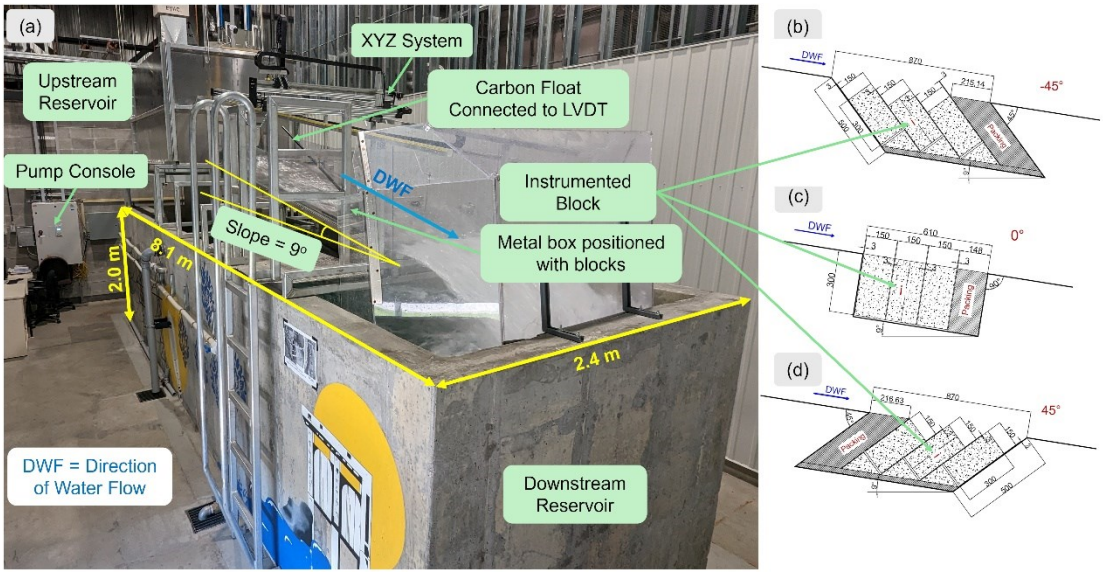

Figure 5.1 Reduced-scale physical model at *UQAC*: (a) Model view from a downstream corner; (b) Schematic of blocks positioned at -45° to the flow direction; (c) Schematic of blocks positioned vertical to the flow direction; and (d) Schematic of blocks positioned at +45° to the flow direction

5.4 METHODOLOGY

The objective of this study is to determine the influence of block geometry and its orientation with respect to the flow direction on the block removal using the results of the physical model tests. The methodology adopted to achieve this study's objective is presented in Figure 5.2. Initially, the fluctuating pressures have been obtained under different test conditions presented in Annexe D. The fluctuating pressures obtained during various testing conditions were presented in our previous articles (Karnati et al., 2023b, 2024, 2025; Wisse et al., 2024). Figure 5.3 presents the temporal variation of a few selected test cases that presented the possibility of block instability by uplift. The conditions in Figure 5.3 where the pressure at the block's bottom is significantly higher than that at its top are recognized as potentially unstable. Under these conditions, the block is subjected to an upward pressure which can result in its

uplift provided that it exceeds the resistive forces generated by the block weight and the shear forces along the sides. Though different *JOs* were tested, this article presents the stability analysis only for 3 mm *JO*. Under this condition, positioning of elbows within the joints is not possible and hence the pressure within the joints has been assumed the same as that at the bottom of the block. This assumption is considered valid as the pressures obtained at different positions along the joints under 10 and 20 mm *JO*s were similar according to the continuity law in fluid mechanics. In the next step, the fluctuating pressures are analyzed to determine the extreme pressures under critical conditions that facilitate the block removal. These conditions represent the scenario where the minimum pressures on the top and maximum pressures on the bottom of a block occur simultaneously, resulting in the maximum uplift pressures. To consider the uncertainty of these extreme values, about 3% of the total data is determined from each measurement, as 95% of the fluctuating data lies within $\mu \pm 2\sigma$, where μ stands for mean and σ stands for standard deviation of the data. This process is explained in Annexe D.

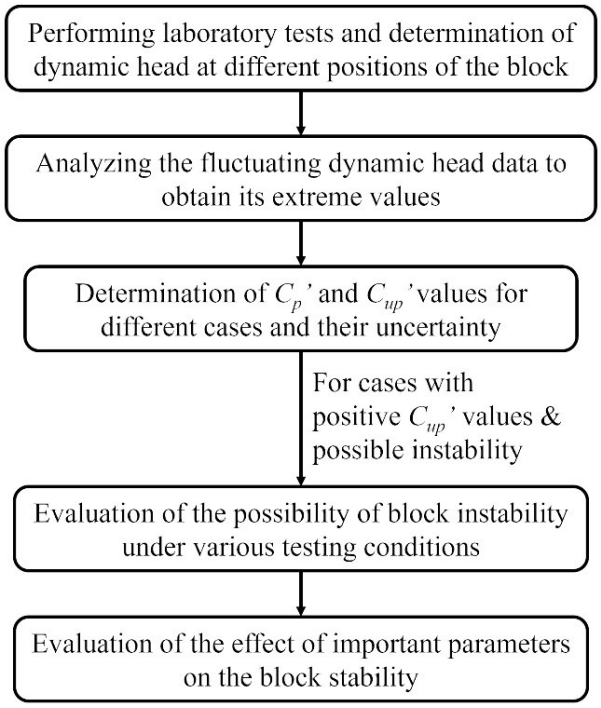

Figure 5.2 Methodology adopted in this study

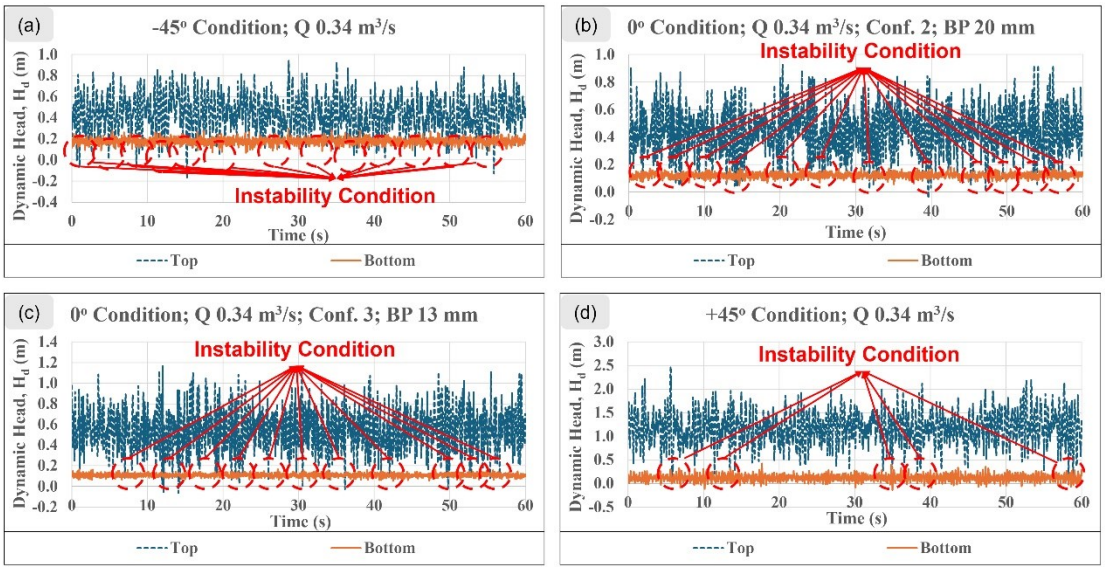

Figure 5.3 Time domain signals of selected test cases at 0.34 m^3/s flowrate: (a) -45° condition; (b) 0° condition in *Conf.* 2 with *BP* 20 mm; (c) 0° condition in *Conf.* 3 with *BP* 13 mm; and (d) +45° condition

These values are normalized with the mean dynamic head observed above the instrumented block in the channel, $H_{d,Ch}$, (Eq. D1 in Annexe D) presented in Table 5.1 for various discharges studied. Then the normalized pressure head values are combined for different discharges in a similar test arrangement, for example, the values obtained in different Q values in the test arrangement of 0° blocks with 3 mm *JO*, *Conf.* 1 and 6 mm *BP*. The minimum, mean and maximum of these values are calculated, and this process is repeated for all the pressure results at the top and bottom of the instrumented block under different test conditions which allows the determination of extreme values and their uncertainties. Using these values, the C_{up}' values as presented in Eq. D2 in Annexe D are determined along with their uncertainties. During their calculation, the individual negative pressure values observed on the top of the block are considered zero to reflect on the fact that their occurrence is due to the formation of eddies at the protruded surface. An explanation for this assumption is presented in the discussion section. The C_{up}' values could be used to determine the uplift forces acting on the block as presented in Eq. 5.3. If these values are negative, this represents that the pressure on the bottom of the block is lower than that on the top of the block indicating that there will not be any possibility of uplift. Under certain conditions, such as protruded configurations and inclined blocks, these values are found to be positive. An analytical

model is developed to analyze the block stability under the action of hydraulic forces and the resistive forces (generated from weight of the block and shear resistance). The details regarding the analytical model are presented in the following section. In the next step, stability analysis is carried out in the cases with positive C_{up}' values to determine the factor of safety against the instability. In the final step, the parameters involved in the factor of safety are varied to carry-out a parametric study.

Table 5.1 Mean dynamic head in the channel above the instrumented block

Discharge, Q (m^3/s)	0.18	0.24	0.315	0.34
Mean dynamic head in the channel, $H_{d,Ch}$ (m)	0.63	0.80	1.00	1.07

Uplift force, $F_{up} = C'_{up} * \gamma_w * H_{d,Ch} * Width\ of\ the\ block$ (kN/m) Eq. 5.3

Where, γ_w represents the unit weight of water in kN/m^3 and $H_{d,Ch}$ represents the mean channel velocity head at the block level in m.

5.5 ANALYTICAL MODEL TO ANALYZE THE BLOCK STABILITY

Different instability conditions are observed during the initial trial tests made under other *JO*s which are recorded and attached as supplementary .gif files along with this article. Snapshots of these instabilities are presented in Figure 5.4 for different block arrangements to point out the possibility of instability occurrence. An analytical model has been developed to evaluate the block stability using the results of physical model tests. The blocks are idealized as two-dimensional elements by assuming unit thickness in the out-of-plane direction as uniform pressure distribution is assumed on the blocks along the width perpendicular to the flow. As mentioned earlier, the dynamic pressure head within the joints is assumed to be same as that at the bottom of the block ($H_{d,Ch} * C_{pB}'$). Thus, along the joints, a rectangular dynamic pressure distribution is assumed. On the top of the block, the dynamic head is measured at two positions, *Ac* and *Ad*, which are located close to the upstream and downstream edges of the block respectively as shown in Figure 5.5. In these two positions, the position close to the channel surface has

exhibited higher dynamic pressure heads compared to that located far from it. Besides, in the case of vertical blocks with 0° condition, the pressure recorded at *Ac* and *Ad* (corresponding normalized pressure heads are determined as C_{pAc}' and C_{pAd}' respectively) were found similar and hence the values of *Ac* have only been considered uniformly over the entire surface. Thus, a linear variation of dynamic pressure distribution at the top is considered for inclined condition and a rectangular distribution for vertical blocks. The actual turbulent pressure fields often tend to exhibit localized reductions caused by fluctuating flow conditions. Thus, assuming rectangular pressure distributions assumed on the joint surfaces tend to slightly overestimate uplift forces which is a conservative assumption. However, the assumption of a linear pressure variation on the top-surface is largely neutral as the interpolation reflects the measured pressure gradient between the two sensors *Ac* and *Ad* which preserves the correct magnitude and trend, and does not affect the resistant forces. The hydraulic forces acting on the block faces are determined based on the pressure distribution and are presented in Figure 5.5. Figure 5.5(a) presents additionally, the distances of these forces from point *C*. In this orientation, blocks have been observed to be overturning/toppling instead of uplifting during the trial tests, which could be understood by the combined action of the uplift forces and the heavy thrust forces generated by the flowing water. Thus, the most common mode of failure in this arrangement is determined to be block overturning. Additionally, in this orientation, the dynamic pressures in the zone *BE* have been recorded negative, that could be due to the eddies developing under the separated flow, which were considered zero. This assumption could be not considered conservative as it would increase the overturning moment and decrease the safety margins. In all the cases of uplift analysis, uplift force acting on the block could be simply presented as the difference between the forces F_{AB} and F_{CD} (acting in the positive Y-direction). The forces acting on different faces of the block (along with their eccentricities for -45° blocks) are presented in Tables E1-E2 in Annexe E. Figure 5.5 illustrates that the forces acting in the X-direction, $F_{X,}$ contribute to the generation of shear resistance (Eq. 5.5) and the remaining forces in the negative Y-direction contribute to the resistive forces.

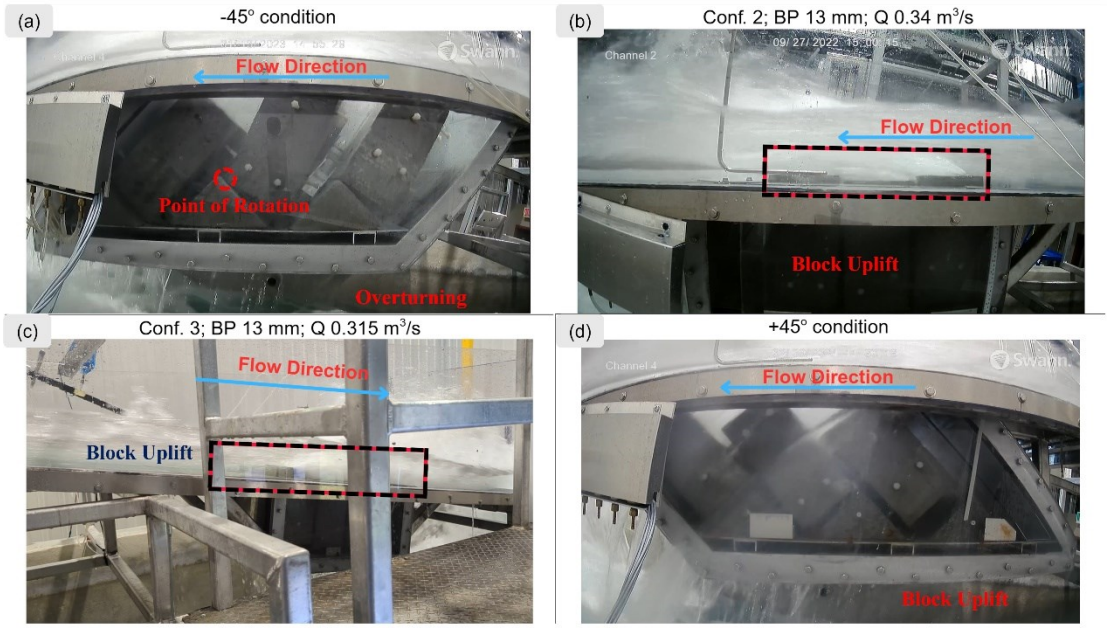

Figure 5.4 Snapshots of different instabilities recorded during trial tests on higher *JO* (10 and 20 mm): (a) -45° condition; (b) 0° condition, Conf. 2, BP 13, Q 0.34 m^3/s; (c) 0° condition, Conf. 3, BP 13, Q 0.315 m^3/s; and (d) +45° condition

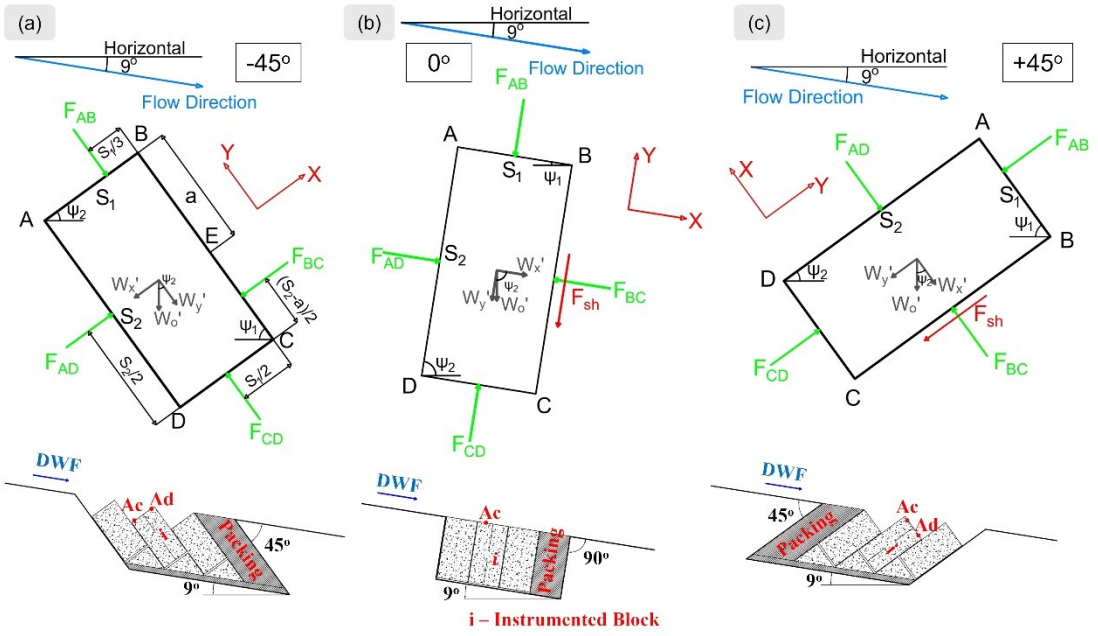

Figure 5.5 Description of the forces acting on the block under: (a) -45° condition; (b) 0° condition; and (c) +45° condition

Hydraulic force, $F = \gamma_w * C_p' * H_{d,Ch} * Width\ of\ the\ block\ face$ (kN/m) Eq. 5.4

Shear Resistance, $F_{sh} = F_X * \tan\phi$ (kN/m) Eq. 5.5

Where F = Hydraulic force acting on a face of the block (with subscripts indicating the block face); C_p' = Non-dimensional pressure coefficient at the corresponding face; ϕ = Friction angle between the blocks.

5.5.1 Stability analysis for blocks oriented against the flow (-45º blocks)

Figure 5.5(a) presents the different forces acting on the block. Under the action of the moments generated by these forces about point *C*, the block could overturn about *C*. Among these forces acting on different faces, F_{CD} and F_{AD} result in mobilizing moments, whereas the other forces offer resistive moments about point *C*. The overall mobilizing and resistive moments (ΣM_{Mo} and ΣM_R respectively) and hence the factor of safety against overturning about point *C* ($F_{s,O}$) are presented respectively in Eq. 5.6 – 5.8.

$$\Sigma M_{Mo} = \frac{\gamma_w C'_{pB} H_{d,Ch}}{2}(S_1^2 + S_2^2) \quad \text{(kN-m/m)} \qquad \text{Eq. 5.6}$$

$$\Sigma M_R = \frac{\gamma'_r S_1 S_2}{2}(S_2 \sin\psi_2 + S_1 \cos\psi_2) + \gamma_w C'_{pB} H_{d,Ch} \frac{(S_2 - a)^2}{2} + \frac{\gamma_w H_{d,Ch} S_1}{6}\left(C'_{pAc} + 2C'_{pAd}\right) \quad \text{(kN-m/m)} \qquad \text{Eq. 5.7}$$

$$F_{s,O} = \frac{\Sigma M_R}{\Sigma M_{Mo}}$$

$$= \frac{\gamma'_r S_1 S_2 (S_2 \sin\psi_2 + S_1 \cos\psi_2) + \gamma_w C'_{pB} H_{d,Ch} (S_2 - a)^2 + \frac{\gamma_w H_{d,Ch} S_1}{3}\left(C'_{pAc} + 2C'_{pAd}\right)}{\gamma_w C'_{pB} H_{d,Ch} (S_1^2 + S_2^2)} \qquad \text{Eq. 5.8}$$

5.5.2 Stability analysis for block uplift

Figure 5.5 (b and c) present different forces acting on the block and under the action of these forces, the block may uplift (Refer to Annexe E for the formulae to calculate these forces). Among the forces acting along the X direction, F_{AD} and F_{BC} are found to be equal and hence discarded in the

subsequent analysis. Thus, only the force W_X' results in the development of shear resistance along *BC*, F_{sh}. The difference between the forces F_{AB} and F_{CD} results in the generation of uplift forces on the block, whereas the other forces act as resistive forces. The total uplift force (ΣF_{up}), resistive force (ΣF_R) and hence the factor of safety against uplift ($F_{s,Up}$) are presented in Eq. 5.9 - 5.11 respectively.

$$\Sigma F_{up} = \gamma_w S_1 H_{d,Ch}\left(C'_{pB} - C'_{pA}\right) = \gamma_w S_1 H_{d,Ch} C'_{up} \text{ (kN/m)} \quad \text{Eq. 5.9}$$

$$\Sigma F_R = \gamma'_r S_1 S_2 (\sin\psi_2 + \cos\psi_2 \tan\phi) \text{ (kN/m)} \quad \text{Eq. 5.10}$$

$$F_{s,Up} = \frac{\Sigma F_R}{\Sigma F_{up}} = \frac{\gamma'_r S_2 (\sin\psi_2 + \cos\psi_2 \tan\phi)}{\gamma_w H_{d,Ch} C'_{up}} \quad \text{Eq. 5.11}$$

5.6 ANALYSIS OF THE NORMALIZED EXTREME VALUES AND C_{UP}' VALUES

The normalized pressure coefficients, C_p' are determined for the pressure inlets on the top and bottom of the instrumented block for different tests as explained in section 5.4. In this section the effect of block protrusion and the joint orientation on the C_p' and C_{up}' are presented.

5.6.1 Effect of block protrusion

The effect of block protrusion on the block removal includes studying the effect of protrusion configuration, *Conf.* and the block protrusion height, *BP*. The variation of C_p' values with *BP* values is presented for different *Conf.*s considering *Conf. 0* as a base for each case in Figure 5.6. Each vertical section of Figure 5.6 includes the C_p' values measured at different flowrates in the model tests. This allows the determination of possible range of extremities of C_p' values at the top and bottom of the block. Considering the minimum (A Min & B Min), mean (A Mean & B Mean) and maximum (A Max & B Max) values of the C_p' values, the range of non-dimensional coefficient of uplift, C_{up}' values is determined. The variations of C_{up}' values with *BP* values for different *Conf.*s are presented in Figure 5.7. As explained in section 5.4, negative C_{up}' values indicate that the pressure on the top is more than that on the bottom of the block resulting in stable conditions, whereas positive values indicate unstable conditions. As *Conf. 0* is considered the most stable condition, the initial C_{up}' values in Figure 5.7 are

negative and with the introduction of *BP*, these values varied, especially for negative protrusion configurations (*Conf. 2* and *Conf. 3*), where there was only a slight variation observed for the other *Conf.*s. Figure 5.6 – 5.7 present the possibility of the development of uplift pressures on the block in *Conf. 2* and *Conf. 3* at protruded conditions which could create instability conditions. Another interesting observation is that the uncertainty has been decreasing with increasing *BP* values in these *Conf.*s.

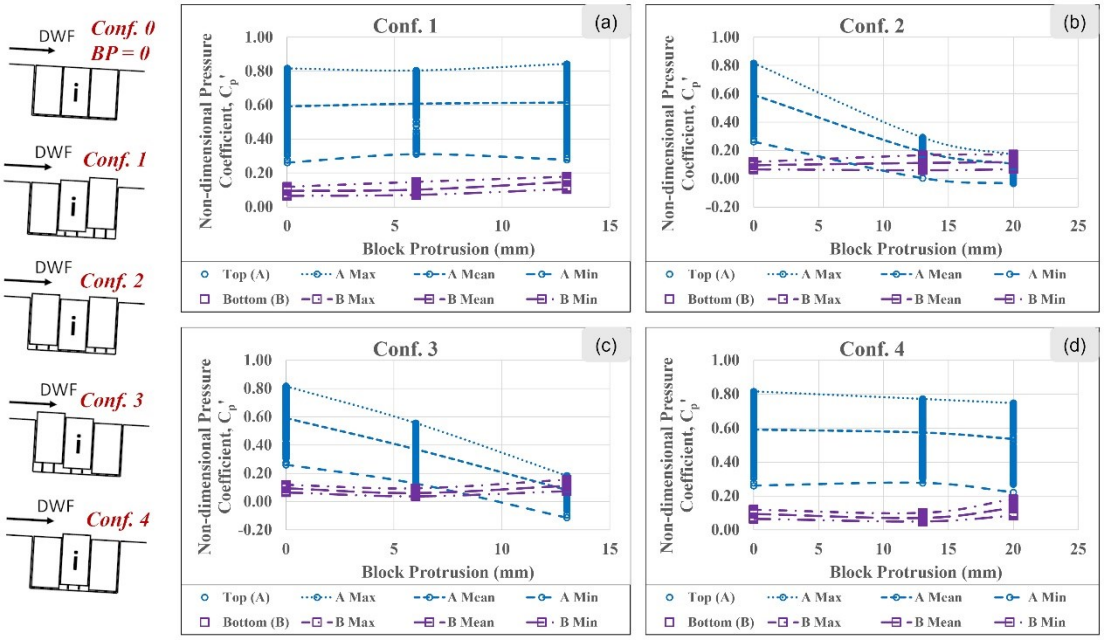

Figure 5.6 Variation of non-dimensional pressure coefficients, C_p' with *BP* for: (a) *Conf. 1*; (b) *Conf. 2*; (c) *Conf. 3*; and (d) *Conf. 4*

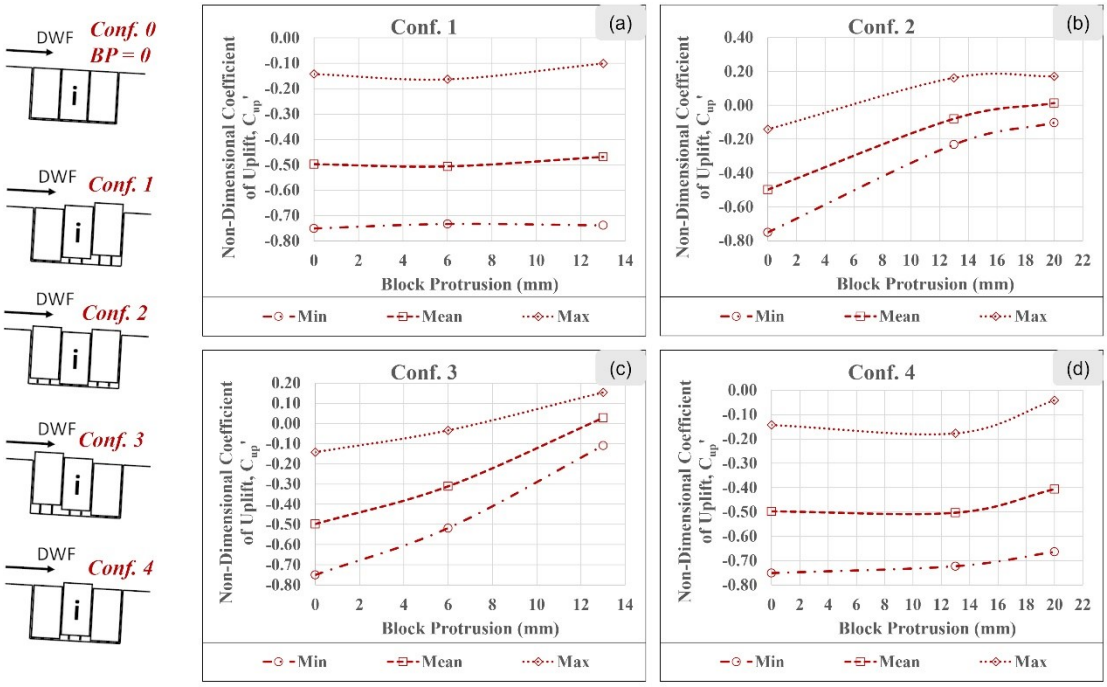

Figure 5.7 Variation of non-dimensional coefficient of uplift, C_{up}' with *BP* for: (a) *Conf. 1*; (b) *Conf. 2*; (c) *Conf. 3*; and (d) *Conf. 4*

5.6.2 Effect of joint orientation

As performed in section 5.6.1, the variations of *Cp'* and *Cup'* values with *JOr* along with their uncertainty are presented in Figure 5.8. The 0° condition represents *Conf. 0* of section 5.6.1 and hence acts as stable condition. Figure 5.8 (a - b) indicate the possibility of development of uplift forces under inclined conditions (-45° and +45°). Figure 5.8 (a) presents that the uncertainty in the extreme pressures is less in the inclined conditions as compared to the 0° block arrangement for the pressure on top of the blocks; whereas for the pressure on the bottom of the blocks is high as observed from the difference between minimum and maximum C_p' values. Figure 5.8 (a-b) demonstrate that the blocks oriented against the flow (-45°) have shown less uncertainty compared to the blocks oriented towards the flow (+45°). This could be due to the highly fluctuating pressure recorded under the miniature hydraulic jump developed on the leeside on the blocks in +45° arrangement.

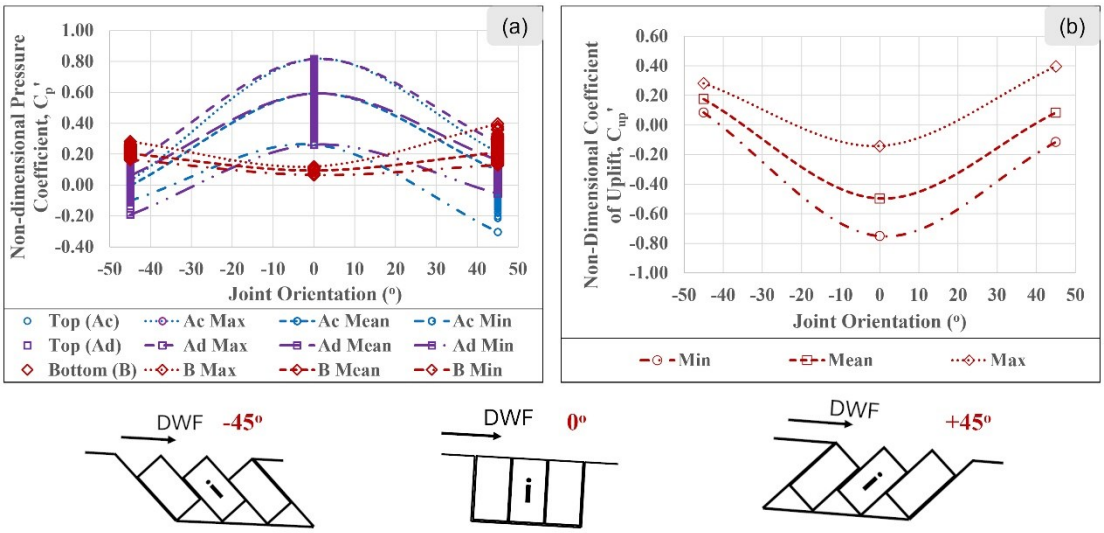

Figure 5.8 Variation of non-dimension coefficients with joint orientation: (a) C_p'; and (b) C_{up}'

5.7 BLOCK STABILITY ANALYSIS ON THE MODEL TEST SCENARIOS

Figure 5.7 – 5.8 have presented the cases with positive C_{up}' values where block uplift could be possible under the action of uplift forces, except for the -45° arrangement where the instability has been determined as block overturning/toppling. The stability analysis has been performed on the cases with positive C_{up}' values under model test scenarios using the Eq. 5.6 – 5.11. The unit weight of the lightweight blocks used in the model tests, γ_r is 13.5 kN/m^3. The friction angle has been measured using an inclinometer. In this process, the blocks were placed one over the other underwater using the Teflon bolts separating them such that the surface of the top block was placed just above the water surface to position an inclinometer. The blocks were slowly lifted along one edge increasing the block inclination until the block positioned on the top begins to slide and the angle at which the block sliding initiated was noted as the friction angle. This process was repeated three times to ensure the repeatability and the friction angle, ϕ, was noted as 30°.

5.7.1 Stability analysis against overturning in -45° blocks

The various terms required for the stability analysis against overturning (Eq. 5-7) in the model testing scenario for -45° blocks are as follows: S_1 = 0.15 m; S_2 = 0.30 m; γ_w = 9.81 kN/m^3; γ_r' = 13.5-9.81 = 3.69 kN/m^3; ψ_2 = 45-9 = 36°; and exposure length, a = 0.153 m. The C_p' values used the analysis

are presented in Table 5.2. The factor of safety against overturning, $F_{s,O}$ could vary depending on the combination of C_p' values used. The lowest $F_{s,O}$ occurs when the maximum C_{pB}' values are used simultaneously with the minimum C_{pAc}' and C_{pAd}' values. Conversely, the highest $F_{s,O}$ occurs when the minimum C_{pB}' values are used with the maximum C_{pAc}' and C_{pAd}' values. The values of total overturning moments (ΣM_{Mo}), total resisting moments (ΣM_R) and hence $F_{s,O}$ for various discharges are presented in Table 5.3. The $F_{s,O}$ values from Table 5.3 have been found to be less always than 1 which shows that the blocks could always overturn in all these combinations of extreme values which was observed during the initial trial tests presented in Figure 5.4(a) and in the supplementary .gif figure (Block overturning in -45° blocks). Additionally, increase in flowrate has shown reduced $F_{s,O}$ values increasing the possibility of instability.

Table 5.2 Extreme C_p' values for the top and bottom of the block obtained from model tests in -45° condition

	C_{pAc}'	C_{pAd}'	C_{pB}'
Maximum	0.028	0.132	0.281
Mean	-0.004	0.060	0.202
Minimum	-0.101	-0.192	0.165

Table 5.3 $F_{s,O}$ analysis in the blocks oriented against the flow (-45°) under model testing conditions

Discharge, Q (m^3/s)	**Minimum $F_{s,O}$**			**Mean $F_{s,O}$**			**Maximum $F_{s,O}$**		
	ΣM_{Mo} (Eq. 5.6)	**ΣM_R (Eq. 5.7)**	**$F_{s,O}$ (Eq. 5.8)**	**ΣM_{Mo} (Eq. 5.6)**	**ΣM_R (Eq. 5.7)**	**$F_{s,O}$ (Eq. 5.8)**	**ΣM_{Mo} (Eq. 5.6)**	**ΣM_R (Eq. 5.7)**	**$F_{s,O}$ (Eq. 5.8)**
0.18	0.197	0.087	0.44	0.142	0.079	0.56	0.115	0.080	0.70
0.24	0.247	0.097	0.39	0.178	0.087	0.49	0.145	0.088	0.61
0.315	0.310	0.109	0.35	0.223	0.097	0.43	0.182	0.098	0.54
0.34	0.331	0.113	0.34	0.238	0.100	0.42	0.194	0.101	0.52

5.7.2 Stability analysis against uplift in +45° blocks

The various terms required for the stability analysis against uplift (Eq. 5.9 – 5.11) in the model testing scenario for +45° blocks are as follows: S_1 = 0.15 m; S_2 = 0.30 m; γ_w = 9.81 kN/m^3; γ_r' = 3.69 kN/m^3; ψ_2 = 45-9 = 36°; and ϕ = 30°. The C_p' values used in the analysis are presented in Table 5.4. As mentioned in section 5.7.1, the factor of safety against uplift, $F_{s,Up}$ depends on the C_{up}' values, which in turn depend on the combination of C_p' values. The C_{up}' values obtained under these combinations are also presented in Table 5.4. It should be noted that the C_p' values have been considered 'zero' when it was observed to be negative during the calculation of C_{up}' values as mentioned earlier. Eq. 5.10 shows that the total resistance force, ΣF_R, shall be due to the weight of the block and shear resistance developed along the sliding surface and depends on the block dimensions, unit weight of the block material, block inclination with horizontal and friction angle. The ΣF_R value will thus remain constant under different pressure conditions which is calculated as 1.17 kN/m. The values of total uplift forces (ΣF_{up}), and hence $F_{s,Up}$ for various discharges are presented in Table 5.5 for the cases with positive C_{up}' values. The $F_{s,Up}'$ values from Table 5.5 show that the blocks could uplift under the action of maximum uplift forces (under maximum C_{up}' values) which was observed during the initial trial tests presented in Figure 5.4(d) and in the supplementary .gif file (Block uplift in +45° blocks). As observed in the case of overturning, the factor of safety against uplift decreases with increasing flowrate, thus increasing the possibility of instability.

Table 5.4 Extreme C_p' values for the top and bottom of the block and C_{up}' values obtained from model tests in +45° condition

	C_{pAc}'	C_{pAd}'	C_{pB}'	C_{up}'
Maximum	0.213	0.277	0.396	0.396
Mean	0.094	0.160	0.210	0.083
Minimum	-0.303	-0.055	0.131	-0.114

Table 5.5 $F_{s,Up}$ analysis in the blocks oriented towards the flow (+45°) under model testing conditions

Discharge, Q (m^3/s)	Using Mean C_{up}'		Using Maximum C_{up}'	
	ΣF_{up} (Eq. 5.9)	$F_{s,Up}$ (Eq. 5.11)	ΣF_{up} (Eq. 5.9)	$F_{s,Up}$ (Eq. 5.11)
0.18	0.52	2.26	2.46	0.47
0.24	0.65	1.80	3.09	0.38
0.315	0.81	1.43	3.88	0.30
0.34	0.87	1.34	4.14	0.28

5.7.3 Stability analysis against uplift in 0° blocks

The various terms required for the stability analysis against uplift (Eq. 5.9 – 5.11) in the model testing scenario for 0° blocks are as follows: $S_1 = 0.15$ m; $S_2 = 0.30$ m; $\gamma_w = 9.81$ kN/m^3; $\gamma_r' = 3.69$ kN/m^3; $\psi_2 = 90\text{-}9 = 81°$; and $\phi = 30°$. As the possibility of block uplift has been observed only in *Conf.2* and *Conf. 3*, the C_p' values of these cases are presented in Table 5.6 and stability analysis has been carried out only for the cases with positive C_{up}' values. As mentioned in section 5.7.2, the factor of safety against uplift, $F_{s,Up}$ depends on the C_{up}' values, which in turn depend on the combination of C_p' values. The C_{up}' values obtained under these combinations are also presented in Table 5.6. As explained earlier, the ΣF_R value will be constant for different cases mentioned whose value is calculated as 1.19 kN/m. The values of total uplift forces (ΣF_{up}), and hence $F_{s,Up}$ for various discharges for selected cases with possibility of block uplift are presented in Table 5.7. The $F_{s,Up}'$ values from Table 5.7 show that the blocks could uplift under the action of maximum uplift forces (under maximum C_{up}' values), except for the flowrate, Q = 0.18 m^3/s. The instabilities observed during the initial trial tests are presented in Figure 5.4(b and c) and in the supplementary .gif files (Block uplift in Conf. 2 BP 13 mm & Block in uplift Conf. 3 BP 13 mm). The factor of safety has always decreased with increasing flowrate, thus increasing the possibility of instability.

Table 5.6 Extreme C_p' values for the top and bottom of the block and C_{up}' values obtained from model tests in 0° condition for *Conf. 2* and *Conf. 3*

	Conf. 0; BP 00 mm			***Conf. 2; BP 13 mm***			***Conf. 2; BP 20 mm***			***Conf. 3; BP 6 mm***			***Conf. 3; BP 13 mm***		
	C_{pA}'	C_{pB}'	C_{up}'	C_{pA}'	C_{pB}'	C_{up}'	C_{pA}'	C_{pB}'	C_{up}'	C_{pA}'	C_{pB}'	C_{up}'	C_{pA}'	C_{pB}'	C_{up}'
Maximum	0.816	0.119	-0.142	0.292	0.166	0.162	0.169	0.171	0.171	0.557	0.094	-0.034	0.184	0.155	0.155
Mean	0.592	0.094	-0.498	0.191	0.111	-0.080	0.105	0.117	0.012	0.371	0.061	-0.311	0.083	0.112	0.029
Minimum	0.261	0.066	-0.751	0.004	0.060	-0.232	-0.034	0.066	-0.103	0.128	0.038	-0.518	-0.113	0.075	-0.110

Table 5.7 $F_{s,Up}$ analysis for selected cases in the blocks oriented perpendicular to the flow (0°) under model testing conditions

Discharge, Q (m^3/s)	**Using Mean C_{up}' for *Conf. 2; BP 20 mm***		**Using Maximum C_{up}' for *Conf. 2; BP 13 mm***		**Using Maximum C_{up}' for *Conf. 2; BP 20 mm***		**Using Mean C_{up}' for *Conf. 3; BP 13 mm***		**Using Maximum C_{up}' for *Conf. 3; BP 13 mm***	
	ΣF_{up} **(Eq. 5.9)**	$F_{s,Up}$ **(Eq. 5.11)**	ΣF_{up} **(Eq. 5.9)**	$F_{s,Up}$ **(Eq. 5.11)**	ΣF_{up} **(Eq. 5.9)**	$F_{s,Up}$ **(Eq. 5.11)**	ΣF_{up} **(Eq. 5.9)**	$F_{s,Up}$ **(Eq. 5.11)**	ΣF_{up} **(Eq. 5.9)**	$F_{s,Up}$ **(Eq. 5.11)**
0.18	0.08	15.56	1.01	1.18	1.06	1.12	0.18	6.71	0.96	1.24
0.24	0.10	12.39	1.26	0.94	1.33	0.90	0.22	5.34	1.21	0.99
0.315	0.12	9.88	1.59	0.75	1.67	0.71	0.28	4.26	1.52	0.79
0.34	0.13	9.25	1.69	0.70	1.78	0.67	0.30	3.99	1.62	0.74

5.8 INDIVIDUAL EFFECT OF THE PARAMETERS INVOLVED IN THE STABILITY ANALYSIS

Eq. 5.9 shows that the parameters defining the factor of safety against block overturning include the pressure coefficients (i.e., C_{pAc}', C_{pAd}' and C_{pB}'), block dimensions or joint spacings (i.e., S_1 and S_2, where S_2 is along the depth direction of the block) submerged block unit weight (i.e., γ_r'), block inclination with flow direction (i.e., ψ_2) and exposure length (i.e., a). Similarly, Eq. 12 presents the parameters defining the factor of safety against block uplift as the pressure coefficients (i.e., C_{pA}' and C_{pB}'), block dimensions or joint spacings (i.e., S_1 and S_2), submerged block unit weight (i.e., γ_r'), block inclination with flow direction (i.e., ψ_2) and friction angle (i.e., ϕ). Clearly, the pressure coefficients depend on the block inclination and studying the effect of inclination requires further model tests than those presented in the current study. The effect of other parameters on the factor of safety is studied by performing a parametric study. This is achieved by varying one parameter at a time while holding the others constant. The pressure coefficients and inclination conditions are maintained as per the initial conditions for factor of safety calculations. Then variation of the factor of safety with respect to these parameters involved is studied to understand its effect. The effect of block dimensions is studied non-dimensionally by varying S_1 and S_2 to represent different aspect ratio, r defined as S_1/S_2, while maintain the same block volume as that of model testing conditions ($V = S_1*S_2*1 = 0.045\ m^3/m$). Different r values are chosen based on the literature (Pells et al., 2017), i.e., 4:1, 3:1, 2:1, 1:1, 1:2, 1:3 and 1:4. Accordingly, the considered values of S_1 *and* S_2 are presented in Table 5.8. The exposure length, a, is varied as a function of the dimension S_2, i.e., a/S_2 (0%, 10%, 20%, ….., 100%). During the uplift calculations, as the triangular portion with the block face is on the thrust side, the face AD experiences pressure along its whole length and hence no exposure zone is considered in this analysis. As the shear resistance is involved in the uplift analysis, a variation of ϕ values is considered (0^o, 5^o, 10^o, 15^o, …... , 50^o) in the factor of safety calculations.

Table 5.8 Variation of block dimensions for parametric study

Aspect ratio, r (S_1/S_2)	**Block dimension, $S_1 = \sqrt{r * V_b}$ (m)**	**Block dimension, $S_2 = \sqrt{V_b/r}$ (m)**
4:1	0.424	0.106
3:1	0.367	0.122
2:1	0.300	0.150
1:1	0.212	0.212
1:2	0.150	0.300
1:3	0.122	0.367
1:4	0.106	0.424

5.8.1 Parameters involved in the stability analysis of -45° blocks

As explained earlier, the parameters involved in the stability analysis against overturning of a -45° block that could affect its stability are the aspect ratio, $r = S_1/S_2$, and exposure length, a, whereas the other parameters like the block orientation and hence the pressure parameters which need further model testing to study the effect of joint orientation, JOr.

a. Aspect ratio, *r*

Keeping the other parameters constant as that of the model testing scenario, except for a which is taken as 0, the $F_{s,O}$ values for different scenarios (Minimum, Mean and Maximum $F_{s,O}$) were determined for different r values chosen. The assumption of $a = 0$ would be appropriate in the actual site conditions with supporting rock mass which creates a stable condition. These values are plotted against aspect ratio, r as presented in Figure 5.9. Figure 5.9 illustrates that the factor of safety is decreasing with increase in aspect ratio under different combinations of the hydraulic forces. This indicates that slender (columnar) blocks possess higher stability compared to the flat blocks against overturning under the combined action of the lift forces and the thrust forces generated by the flowing water. The variation of r presented a reduction of about 20 – 40% in the factor of safety against overturning when it is varied from 1:4 to 1:1

and a reduction of about 60 – 80% when it is varied from 1:1 to 4:1 in different combinations. A major variation in factor of safety is observed between 1:2 to 2:1 after which the variation is found to be minor.

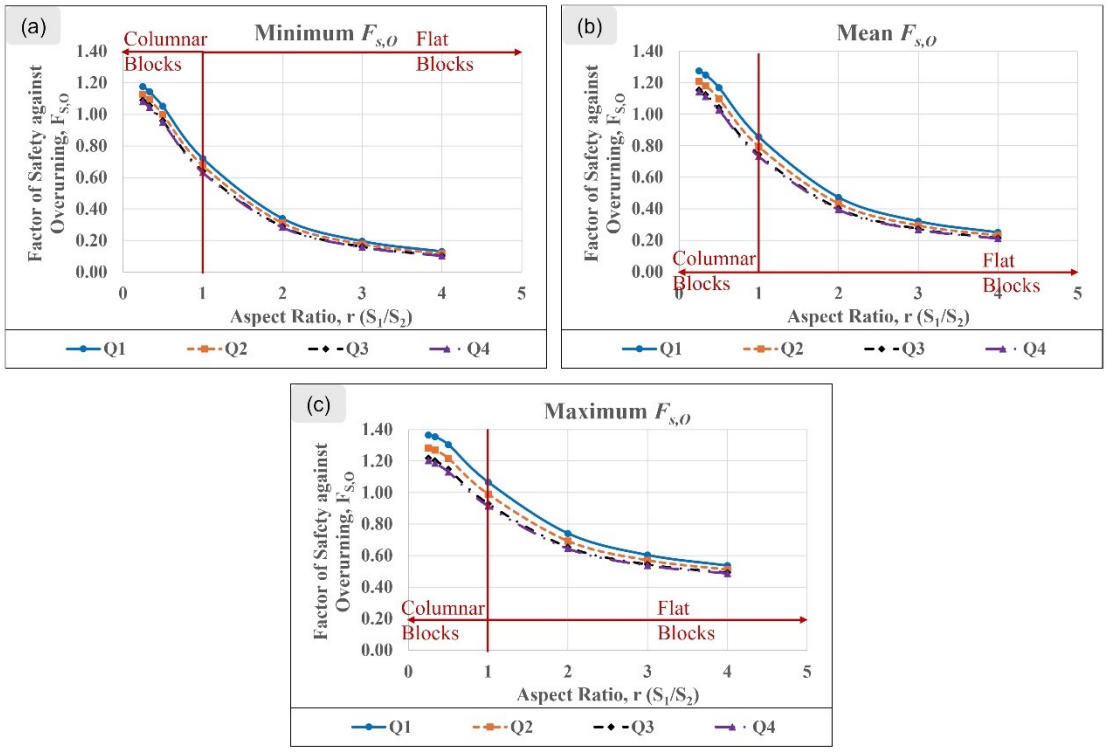

Figure 5.9 Variation of $F_{s,O}$ values with aspect ratio (r) under varying flowrates in -45° blocks: (a) for minimum $F_{s,O}$ condition; (b) for mean $F_{s,O}$ condition; and (c) for maximum $F_{s,O}$ condition

b.* Exposure length, *a

The exposure length is an important parameter that affects the factor of safety against block overturning as it influences the resistive moment. This parameter is varied as a percentage of the block depth, i.e., S_2 (0%, 10%, ……, 100%). Keeping the other parameters constant as those in the model testing conditions, $F_{s,O}$ value for varying a value is calculated for different flowrates considering the minimum, mean and maximum $F_{s,O}$ possibilities explained earlier. The variation of $F_{s,O}$ with a is presented for these conditions in Figure 5.10. Figure 5.10 shows a decreasing trend in $F_{s,O}$ values with exposure length. As a/S_2 values are varied from 0 to 100%, the factor of safety decreases to about 60 - 80% compared to the condition with a = 0. The reduction in factor of safety is higher until a/S_2 = 50% which resulted in about 50 – 60% reduction after which the variation is minor. The results are logical as increased exposure length would reduce the resisting forces on the leeside of the block and provides

more degree of freedom for the block toppling to occur. Though the occurrence of a large amount of exposed surface area is not common, it is possible by removal of loose blocks downstream of the block under consideration.

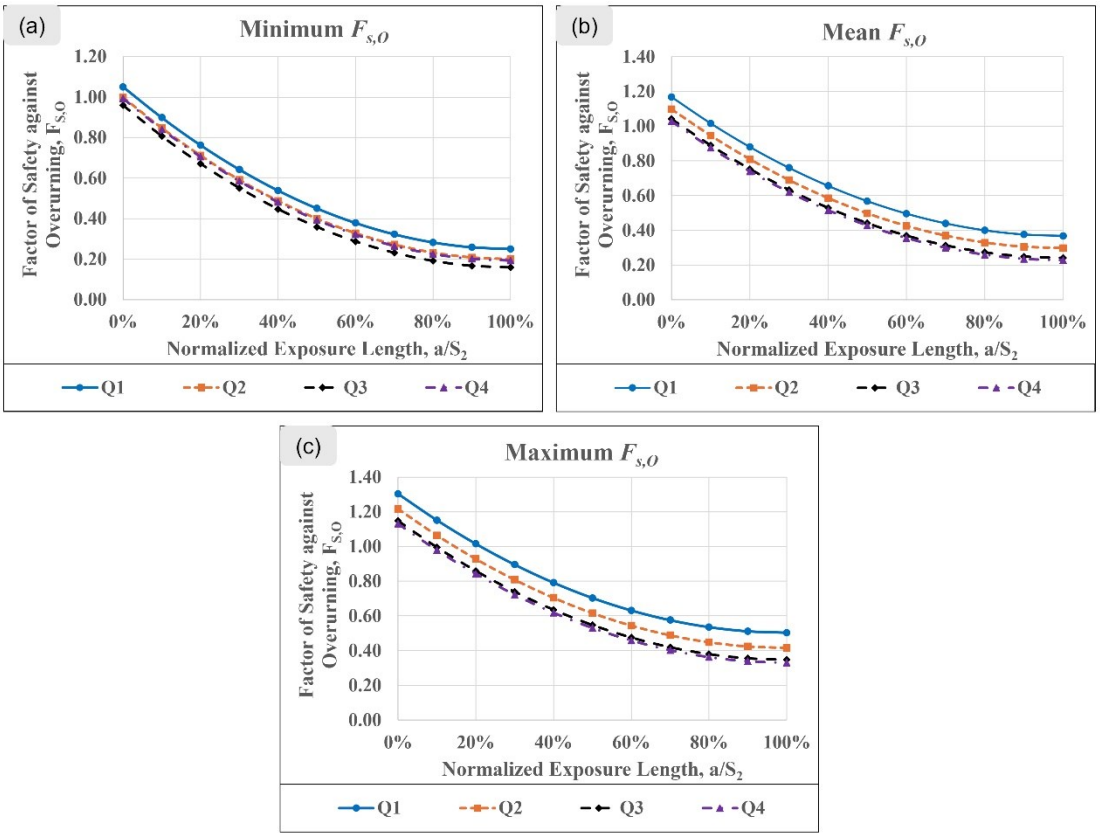

Figure 5.10 Variation of $F_{s,O}$ values with a in -45° blocks under varying flowrates for: (a) minimum $F_{s,O}$ condition; (b) mean $F_{s,O}$ condition; and (c) maximum $F_{s,O}$ condition

5.8.2 Parameters involved in the stability analysis against uplift (in +45° and 0° conditions)

The parameters involved in the stability analysis against uplift that could affect the block stability are the aspect ratio, $r = S_1/S_2$, and friction angle, a, whereas the other parameters like the block orientation and hence the pressure parameters which need further model testing to study the effect of joint orientation, *JOr*.

a.* Aspect ratio, *r

Under these variations considered for aspect ratio, *r*, maintaining other parameters constant as per the model testing, $F_{s,Up}$ values for different conditions are calculated. The variation of $F_{s,Up}$ values with *r* is presented for +45º blocks, 0º blocks with *Conf. 2* and *Conf. 3* in Figure 5.11 – 5.13 respectively. A decreasing trend of $F_{s,Up}$ is observed with *r* in the case of +45º blocks. Eq. 5.11 shows that the factor of safety against uplift is related to *r* as a function of S_2. Thus, as *r* increases, S_2 decreases, thus reducing the factor of safety. As the *r* value varied either from 1:4 to 1:1 or 1:1 to 1:4, a reduction of 50% in factor of safety is recorded in all the conditions presented (+45^0 and 0º blocks).

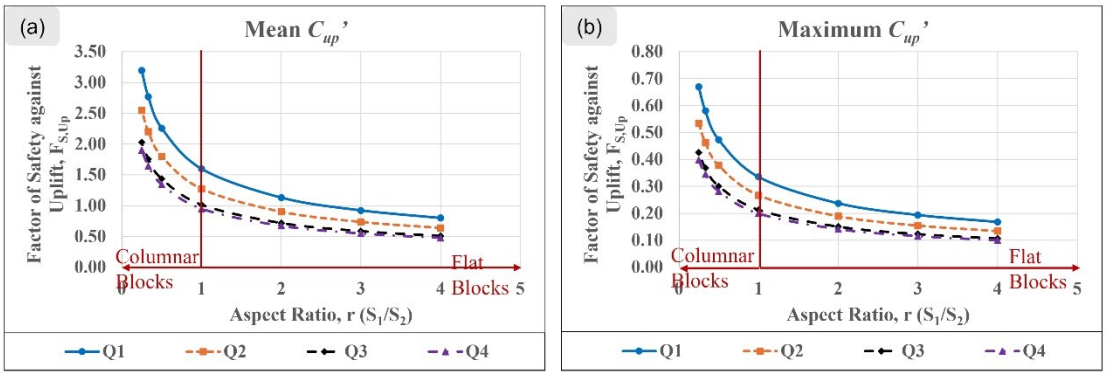

Figure 5.11 Variation of $F_{s,Up}$ values with aspect ratio (*r*) under varying flowrates in +45º blocks: (a) for mean C_{up}' condition; and (b) for maximum C_{up}' condition

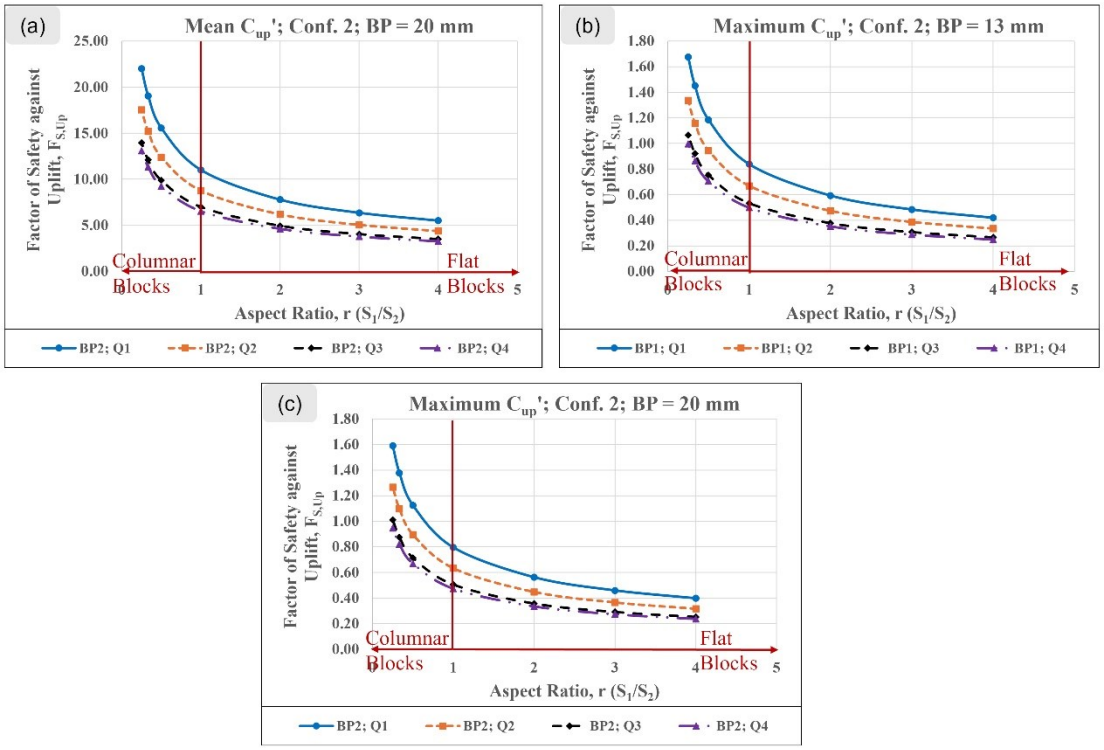

Figure 5.12 Variation of $F_{s,Up}$ values with aspect ratio (r) under varying flowrates in 0° blocks – *Conf. 2*: (a) for mean C_{up}' – *BP = 20 mm*; (b) for maximum C_{up}' – *BP = 13 mm*; and (c) for maximum C_{up}' – *BP = 20 mm*

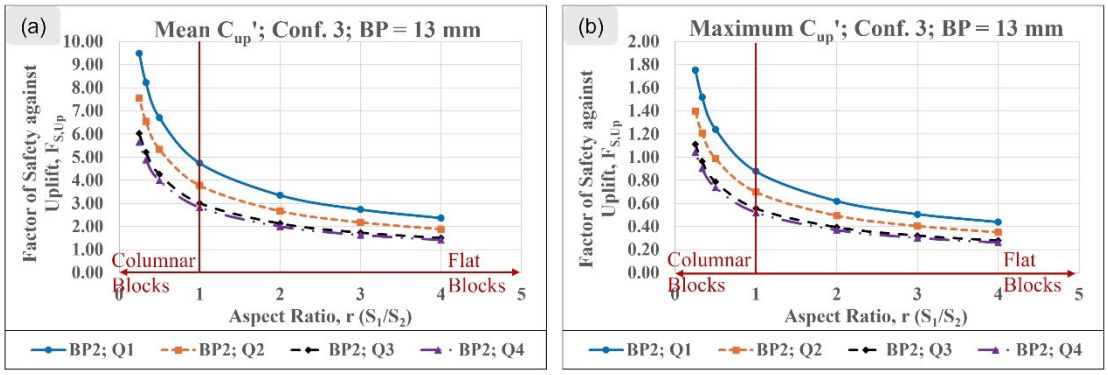

Figure 5.13 Variation of $F_{s,Up}$ values with aspect ratio (r) under varying flowrates in 0° blocks – *Conf. 3*: (a) for mean C_{up}' – *BP = 13 mm*; and (b) for maximum C_{up}' – *BP = 13 mm*

***b.* Friction angle, ϕ**

Keeping all the other parameters constant as those in the model testing, the friction angle, ϕ, is varied from 0° to 50° as explained earlier. The $F_{s,Up}$ values calculated for varied ϕ values are plotted for +45° blocks, 0° blocks with *Conf. 2* and *Conf. 3* in Figure 5.14 – 5.16 respectively. An increase in ϕ value offers higher frictional resistance, thus increasing the factor of safety against block uplift as observed in Figure 5.14 – 5.16, which is found to be approximately linear. It should be noted that ϕ is one of the important parameters affecting the block uplift that depends on the contact between two rock blocks and shear strength characteristics along the joint. The friction angle presents a higher variation of factor of safety with ϕ in +45° blocks compared to those arranged in 0° orientation. As ϕ value is varied from 0 to 50°, an increase of about 60% and 16% is observed in +45° and 0° blocks respectively.

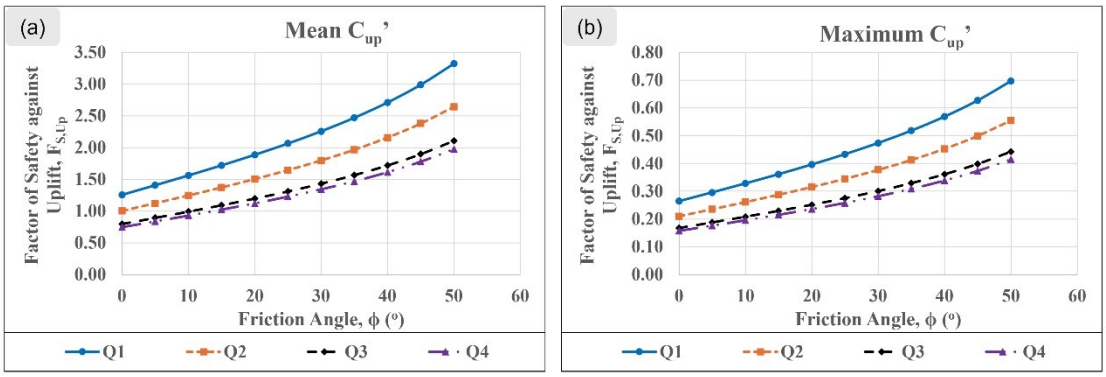

Figure 5.14 Variation of $F_{s,Up}$ values with friction angle (ϕ) under varying flowrates in +45° blocks: (a) for mean C_{up}'; and (b) for maximum C_{up}'

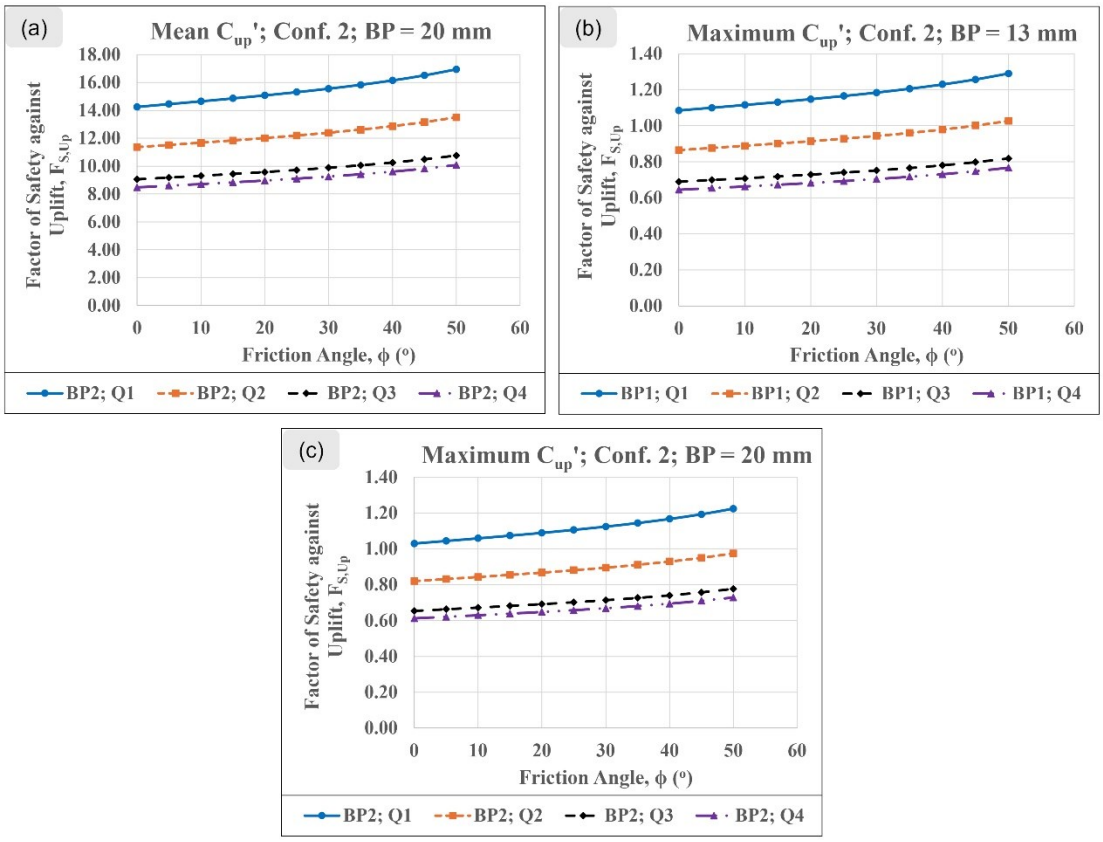

Figure 5.15 Variation of $F_{s,Up}$ values with friction angle (ϕ) under varying flowrates in 0° blocks – *Conf. 2*: (a) for mean C_{up}' – *BP = 20 mm*; (b) for maximum C_{up}' – *BP = 13 mm*; and (c) for maximum C_{up}' – *BP = 20 mm*

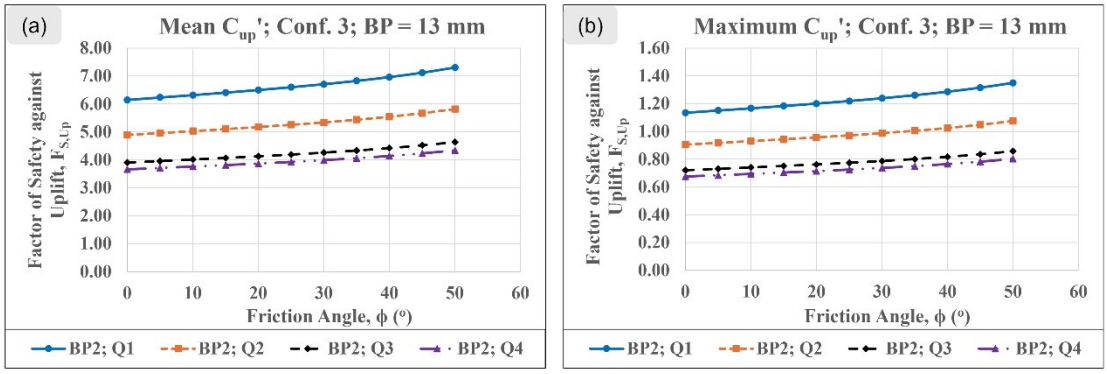

Figure 5.16 Variation of $F_{s,Up}$ values with friction angle (ϕ) under varying flowrates in 0° blocks – *Conf. 2*: (a) for mean C_{up}' – *BP = 13 mm*; and (b) for maximum C_{up}' – *BP = 13 mm*

5.9 DISCUSSION

This article presents the application of the physical model test results to study the stability of a rock block under the action of hydraulic forces that determines the scouring process in rock masses in a parallel flow type spillway. The following observations are made during the analysis of the results.

- Under the various testing conditions proposed, it is observed that the dynamic pressure fluctuations are significantly lower at the bottom of the block compared to those at top of the block. However, other physical model tests, especially those from Reinius (1986) (for parallel flow conditions) and Bollaert (2002) (for plunging jet conditions), reported that the dynamic pressure fluctuations within the joints were amplified compared to the pressures measured at the top of the block. The instrumented block used by physical model studies of Reinius (1986) do not correctly measure the hydraulic pressures around the block as the hydraulic entrance for pressure measurement was not positioned opposite to the flow direction and the pressure measurements were made using piezometric tubes. In addition, both these authors studied the pressures within the closed joints. Under these conditions, the hydraulic pressures were amplified within the joints; however, in this study, the blocks are arranged such that they represent the rock-mass with continuously connected open joints which represent more realistic conditions. Higher pressures were recorded in Bollaert's model studies (Bollaert, 2002) due to the plunging jet conditions where jet flow is in the direction of the joint. Thus, in the model test results presented in this study, the fluctuations in the hydraulic pressure data are more pronounced at the top and more or less constant within the joints. However, certain geomechanical arrangements have presented the conditions with hydraulic pressures within the joints exceeding the minimum pressure acting on the top of the block creating unstable conditions. Further model testing by closing the end of one joint allows the measurement of dynamic pressures in the closed joints and allows for the comparison with open joints.
- The application of C_{up}' in this study builds upon and extends beyond the formulation used by Reinius (1986). In his work, Reinius applied it primarily to identify uplift driven block removal under a limited set of geometries, whereas in the current study, it is interpreted as a

part of multi-directional hydraulic loading system governing multiple block-instability mechanisms relevant to natural fractured rock masses.

- Though the geomechanical conditions change under the action of the hydraulic pressures, they are maintained constant during the physical model tests. The aim of the tests performed is to measure the hydraulic pressures under a given set of physical conditions. This will allow the application of similar conditions using advanced coupled numerical modelling that allow the modelling of the complete scour process.
- Bollaert and Schleiss (2003) and Reinius (1986) presented the importance of expressing the hydraulic pressure data in a non-dimensional domain that allow the applicability of the data to other physical models and for their comparison. Additionally, they mentioned the importance of maximum and minimum pressure coefficients that represent the extreme pressures under critical conditions. These studies considered a single extreme value from a test case. However, the occurrence of these worst-case scenarios simultaneously at different positions of the block creating favourable conditions for block removal is questionable. In such scenarios, determining multiple extreme values in a fluctuating pressure condition would account for uncertainty in the extreme values. Thus, in this study, a range of extreme values are determined as explained in the methodology section. Combining these values with measurements from several tests under similar conditions has allowed us to determine the minimum, mean and the maximum possibilities of the extreme pressure fluctuations.
- With the introduction of block protrusion, a minor flow separation is observed at the edge of the protruded surface with eddies under the separated flow boundary which has resulted in reduced dynamic pressure at the top of the block. In addition, fluctuations in the pressures within the joint increased as the protrusion height increased. The observations are in line with those reported by Wahl and Heiner (2024a, b) for hydraulic-jacking of spillway slabs which demonstrated that flow separation at block edges can generate localized stagnation pressures. Their formulations for uplift head as a function of gap-to-offset ratio and boundary-layer velocity head are conceptually similar to the pressure distributions observed in this study along rock-joint openings. Since both experimental models demonstrated that localized

stagnation and partial drainage control the magnitude of uplift, Wahl and Heiner's findings provide a valuable comparative basis for interpretation of the hydraulic loading conditions governing the block stability under parallel-flow spillway conditions.

- The effect of inclination is similar to that of block protrusion. The inclined block arrangement has created a protruded triangular portion with a high protrusion height that resulted in higher pressure fluctuations within the joint and very low pressures at the top of the block. Similar observations were reported in Reinius (1986). The inclinations presented in this study are only preliminary and require further model testing under different inclinations to study the variation of dynamic pressures with joint orientations. It would be beneficial to obtain the hydraulic pressure data under at least two other inclinations such as 30^o and 60^o in addition to the current data to observe the trend of C_{up}' with the joint orientation. These pressure data could be useful to validate a numerical model and determine the pressure distribution at other inclinations.
- The semi-empirical indices, *Edoa* and *NPES*, introduced by Pells (2016) quantitatively represent how different parameters like joint orientation, block protrusion, block and spillway surface geometry influence the scour susceptibility of a spillway based on field data; however, they do not explicitly quantify the hydraulic forces responsible for block removal. The results of this study provide a mechanistic explanation of these indices by showing that the same geometric features embedded within these indices directly control the stagnation pressures and flow separation. Configurations which result in high *Edoa* or *NPES* values are explicitly exhibiting lower factor of safety values confirming the physical mechanisms implied by these empirical parameters. The mechanics-based stability model results could provide a quantitative foundation that could be used in future to refine or develop erodibility indices with stronger physical basis rather than completely relying on biased field data. To further clarify how the present approach relates to existing empirical and semi-analytical methods used in rock-mass scour predictions, a brief comparison of the three methodological classes is presented in Table 5.9.

Table 5.9 Comparison of semi-empirical, semi-analytical and mechanics-based approaches

Approach	Captured core phenomena	Key limitations	Contribution of the present study
Semi-empirical (George W. Annandale, 2012; Steven Edward Pells, 2016)	Qualitative effects of geomechanical parameters like joint orientation, block protrusion, surface roughness. Qualitatively captures case-history patterns	1. No direct relation of the parameters with hydraulic forces 2. No quantification of individual block displacement	This study presents how the geometric features, linking the indices, produce measurable pressure coefficients and hence stability analysis.
Semi-analytical (E Bollaert, 2010)	Bulk hydraulic intensity Mechanisms representing block instability	Insensitive to variation in geomechanical parameters Requires physical model testing to apply these methods	This study identifies parameter-sensitive mechanisms missing in semi-analytical models
Mechanics-based	Directly quantifies hydraulic forces with respect to different parameters. Identifies key mechanisms affecting the scour intensity.	Requires detailed physical modelling and/or coupled numerical simulations	This study provides a physical basis needed to refine or develop scour indices based on measurable hydraulic entity.

- A preliminary assumption made in the block stability analysis presented in this study is a 2D analysis with one of the block edges placed perpendicular to the flow direction along the channel cross-section. Studying other arrangements, by aligning blocks in different inclinations with the flow direction while keeping the top surface of the block parallel to the flow, would allow us to fully comprehend the effect of edge inclination. George (2015), in his physical model tests, presented the importance of this aspect by varying the alignment of a tetrahedral block. Varying similar inclinations using a cubical or cuboidal shaped block would be important given that they represent more general shapes of the rock blocks. Due to current technical limitations in our physical model, this would be possible in the future using numerical modelling.
- The block stability analysis carried out in this study considers different erosion mechanisms which could act simultaneously as presented in the overturning analysis for -45^{o} conditions. The zone of exposure length has been subjected to highly fluctuating pressures due to the eddy currents generated on the leeside of the triangular surface presented in Figure 5.1(b). Under these conditions, the dynamic pressure measurement made in this zone has exhibited negative pressures. The total pressure (static + datum + dynamic) measured remains positive, and repeated measurements confirmed that the negative values arise from the dynamic component only. Since the magnitude and spatial occurrence of these negative dynamic pressures are highly stochastic, they are set to zero before computing the forces and moments in the factor-of-safety calculations to avoid distorting the pressure fields with uncertain suction effects. A similar assumption is made for the minimum pressure recorded on the top of the block during the uplift analysis when this value is recorded negative. There is a possibility that block uplift could occur upon the block overturning to align itself towards the flow. However, studying this phenomenon requires further numerical modelling as it is complicated to do this during the physical model tests.
- The block stability analysis against uplift presented the possibility of instability under certain critical conditions using extreme mean pressures and their uncertainty. The blocks are found

to undergo uplift in +45° blocks and in 0° blocks under negative protrusion conditions. Even under positive protrusion conditions, the blocks exhibited a reduction in pressure at the top; however, the reduction is not high enough to induce the block uplift. Higher protrusion heights than those used in the physical model tests could induce unstable conditions which would be possible to study with numerical modelling.

- The parametric analysis presented in section 5.8 reveals the effect of several terms involved in the stability analysis. Among different parameters, aspect ratio, *r*, has shown a significant effect on the magnitude of block instability. In -45° blocks, the columnar/slender blocks ($r > 1$) tend to be more stable compared to the flat blocks ($r < 1$) against overturning. Physically, slender blocks result in a lower center of rotation and a larger stabilizing moment arm, requiring significantly higher moment to initiate overturning. Besides, these blocks consist of a narrower exposed top surface, reducing the magnitude and lever arm of the destabilizing pressures acting on it. On the contrary, flat blocks results in higher destabilizing pressures on the upstream surface and lower stabilizing moments due to short depths, making them sensitive to pressure fluctuations. Similar stability behavior is observed in the case of 0° and +45° blocks. In the latter, the rate of reduction in the factor of safety with *r* is higher for blocks with $r < 1$ compared to the blocks with $r > 1$. A value of $r = 1$ in -45° blocks presents a similar condition as that of +45° blocks. In such scenarios, the instability could occur in the mode with lowest factor of safety or as a combination of the two modes. However, modeling such a condition is considered complex in the context of physical modeling, which could be verified in the future using numerical modelling. The exposure length (represented with a/S_2) primarily affects the magnitude of the destabilizing moment in -45° blocks by creating longer protruded surfaces where eddy shedding occurs, increasing fluctuations and decreasing stabilizing moment. From an engineering perspective, the findings of this study suggest preliminary thresholds to identify the potentially vulnerable blocks (with $r < 1$ and large a/S_2).
- The shearing resistance depends on various factors, especially on the roughness of the joints, the availability of rock bridges between two blocks and filling within the joints. Thus, it is an important parameter affecting the block uplift. An increasing trend in $F_{s,Up}$ with friction angle,

ϕ, is observed in almost all the cases with the possibility of block uplift. However, there is little effect on $F_{s,Up}$ compared to other parameters in 0° blocks, given the little increase of about 20% in the factor of safety with change in ϕ from 0° to 50°. However, in +45° blocks, a significant increase of about 160% in the factor of safety with change in ϕ from 0° to 50° is observed. This is due to the higher contribution of the weight component (W_x') to the shear resistance in +45° blocks compared to 0° blocks. Thus, the total shear resistance varies depending on the block inclination, i.e., joint orientation.

- The block stability analysis and the sensitivity analysis are performed under the model testing scenarios where the block unit weight was only 13.5 kN/m^3. However, under realistic conditions with $\gamma_r \sim 27\ kN/m^3$, the factor of safety observed in the stability analysis would be considerably higher given the high volume of the block compared to the flow conditions. Such conditions require higher flowrates to initiate block instability given the higher resistance from the increased weight of the block. The block stability analysis results under the same geomechanical conditions with realistic block unit weight of 27 kN/m^3 for -45°, 0° and +45° blocks are presented in Annexe F. The factor of safety results from Annexe F indicate that the blocks in +45° and 0° blocks are stable as the $F_{s,Up}$ values greater than 1. The blocks with -45° arrangement also show increased factor of safety; however, they can still overturn the blocks at higher flowrates (0.315 and 0.34 m^3/s) under maximum $F_{s,O}$ conditions. These values could be affected by varying the parameters such as aspect ratio, block volume, exposure length (for -45° blocks) and friction angle (for 0° and +45° blocks).

- The findings of this study provide initial guidance for field dam safety evaluation and potential retrofitting of the spillway structures. The sensitivity of block stability to various parameters studied indicates that inspections should focus on identifying the blocks with adverse circumstances, such as critical orientations, significant block protrusions and small aspect ratios, that could result in higher uplift pressures and lower block safety. Several geometric conditions tested in this study align with higher *Edoa* and *NPES* classifications indicating that these results form the mechanistic foundation for future development of quantitative scour predictions. Although the findings point to the conditions alerting the requirement of localized

reinforcements, the current study only represents the first step towards the development of a full-scour prediction tool. It can be used for the calibration of numerical models considering the real scale of spillways, which is the objective of our future work.

- The limitations of this study must be acknowledged while extrapolating the findings to the prototype conditions. Firstly, despite careful design considering geometric Froude similitude, some scale distortions, particularly related to flow turbulence, air entrainment, and energy dissipation at the block edges, inevitably remain. Secondly, the block interfaces used in the model blocks were geometrically simplified and smoother compared to the natural rock blocks forming irregular block interfaces, which may underestimate resistance offered by joint roughness and interlocking between the rock bridges in field conditions. Another limitation associated with fixing the block positions is that the coupled hydro-mechanical process is not included as the geomechanical parameters are maintained constant. The block displacement could seriously influence the pressure distribution over time in realistic scenarios. Another limitation is that the stability analysis is carried out considering the occasional negative dynamic pressures as zero, as their magnitude and spatial distribution are highly stochastic. This assumption removes part of the destabilizing suction effect which represents a non-conservative simplification. Future work will focus on accurately resolving pressure distributions within separation and eddy zones, including quantification of local stagnation and suction pressures through enhanced instrumentation or coupled numerical modelling. Finally, the tested flow conditions only represent a subset of different possible hydraulic scenarios. Nevertheless, the findings provide the essential basis for the future development of robust engineering tools to develop quantitative scour indices capable of assessing safety against scour and supporting decisions regarding retrofitting of existing spillways.

5.10 CONCLUSION

This paper presents an integrated experimental-analytical framework to quantitatively determine how block protrusion, joint opening and block geometry parameters influence important scour

mechanisms, uplift and overturning using the results of physical spillway model tests. The conclusions drawn from this study are described below:

- The use of open joint conditions in the block arrangements have resulted in lower pressure measurements within the joints compared to those in the studies using closed-joints; however, the block instabilities are still observed under inclined block conditions (-45º and +45º) and negatively protruded block conditions of 0º blocks (*Conf. 2* and *Conf. 3*).
- Block stability analysis is carried out using normalized extreme pressures considering uncertainty of these values (minimum and maximum possible values). The results demonstrated that block instability arises from certain hydraulic-geomechanical interactions. For instance, overturning governs in the blocks dipping against the flow, whereas uplift governs in the blocks dipping towards the flow and block protrusion governs in the blocks that are aligned perpendicular to the flow.
- Parametric study carried out presents the impact of different parameters on the block stability. The analysis has shown that the geometric factors, specifically, aspect ratio and exposure length, influence the magnitude and lever arm of destabilizing forces, making them primary indicators of scour susceptibility.
- The framework proposed in this study offers a mechanistic basis for future quantitative scour predictions and, consequently, provides practical guidance for spillway safety inspections by identifying critical combinations of block geometry, orientation and protrusion that warrant priority attention.

Although this study captures dominant hydraulic loading mechanisms, some limitations such as absence of couple hydro-mechanical feedback, probable scale distortion and smooth block interfaces, restrict direct extrapolation to the field conditions currently. Nevertheless, the results provide a robust basis for future advancements integrating additional joint geometries, closed-joint conditions, and coupled numerical modelling to support engineering decisions regarding spillway scour mitigation.

CHAPITRE 6

CONCLUSIONS ET RECOMMANDATIONS

6.1 CONCLUSIONS

Cette étude a permis d'examiner en profondeur, à l'aide d'essais réalisés sur un modèle physique, la problématique complexe de l'influence de divers paramètres géomécaniques sur le processus d'érosion. Les travaux entrepris contribuent à améliorer la compréhension des mécanismes fondamentaux d'érosion dans des évacuateurs de crues et ouvrent la voie au développement d'une méthode plus robuste d'évaluation de l'érodabilité. Les principales conclusions de cette recherche peuvent être résumées comme suit :

- L'effet sur les pressions hydrauliques autour des blocs a été caractérisé pour plusieurs paramètres géomécaniques, en particulier l'ouverture des joints, la saillie des blocs et l'orientation des joints. Les résultats sont exprimés en termes de variation de la charge moyenne et de l'amplitude des fluctuations, en fonction de chaque paramètre analysé individuellement.
- Les valeurs fluctuantes de la pression ont été modélisées à l'aide d'une représentation sinusoïdale, permettant de prédire les pressions extrêmes correspondant aux conditions critiques. Les paramètres du modèle sinusoïdal ont été formulés dans un cadre adimensionnel, ce qui favorise leur applicabilité à divers environnements expérimentaux.
- Les résultats mettent également en évidence que l'introduction d'une saillie de bloc, même minimale, entraîne une modification significative des pressions hydrauliques locales. Cette modification augmente la susceptibilité des blocs au soulèvement instantané, ce qui souligne le rôle critique des irrégularités de surface dans les mécanismes d'érosion observés en conditions réelles.
- L'analyse des coefficients adimensionnels de soulèvement a permis de démontrer que l'orientation des joints contrôle le mode dominant d'instabilité des blocs. À cet égard, un

modèle analytique simplifié a été proposé pour évaluer le facteur de sécurité associé à ce type d'instabilité.

- Les mécanismes d'instabilité observés au cours des essais préliminaires ont montré que les blocs orientés à contre-courant sont davantage sujets au basculement, sous l'effet de forces élevées de poussée, tandis que ceux orientés dans le sens de l'écoulement présentent une tendance accrue au soulèvement. L'augmentation de l'ouverture des joints accentue ce dernier phénomène. Ces résultats apportent une clarification importante quant aux liens entre la géométrie des discontinuités et les mécanismes de rupture observés sur le terrain.
- L'étude paramétrique a révélé l'influence de divers paramètres géométriques, notamment le rapport d'aspect, la longueur exposée et l'angle de frottement, sur la stabilité des blocs. Parmi ces paramètres, le rapport d'aspect s'est avéré être le facteur exerçant l'effet le plus déterminant, confirmant que la forme des blocs, directement liée à la structuration du massif rocheux, joue un rôle majeur dans les mécanismes de rupture.

6.2 LIMITATIONS

Bien que cette recherche apporte des contributions significatives à la compréhension des mécanismes d'érosion hydraulique des massifs rocheux à partir des essais sur le modèle physique à l'échelle réduite, certaines limitations doivent être prises en compte dans l'interprétation et l'application des résultats.

- Tout d'abord, la plage de variation des paramètres étudiés demeure limitée. Les essais ont été conduits pour un nombre restreint de configurations, notamment trois valeurs d'ouverture des joints, deux valeurs de saillie (dans chaque configuration) et trois orientations de blocs. Bien que ces configurations aient été choisies pour représenter des conditions réalistes et critiques, une exploration plus étendue des paramètres pourrait permettre de mieux généraliser les tendances observées.
- Par ailleurs, les essais expérimentaux ont été réalisés en considérant des blocs rigides dont le mouvement est restreint. Bien que cette hypothèse soit nécessaire pour isoler l'effet individuel

des paramètres géomécaniques sur la distribution des pressions, elle ne permet pas de représenter l'évolution en temps réel des pressions induites par le déplacement progressif ou la rotation des blocs, telle qu'elle peut se produire en conditions réelles d'érosion.

- De plus, l'analyse des pressions hydrauliques à la surface de l'évacuateur repose principalement sur la caractérisation des valeurs moyennes et des amplitudes des fluctuations, ainsi que sur l'estimation des pressions extrêmes à partir d'une représentation sinusoïdale. Cette approche ne permet pas de reproduire l'ensemble du spectre fréquentiel des fluctuations de pression.
- En fin, l'applicabilité directe des résultats aux ouvrages à l'échelle réelle demeure conditionnée par les effets d'échelle inhérents aux modèles physiques réduits. Les différences potentielles entre les conditions de laboratoire et les conditions réelles, notamment en ce qui concerne les régimes turbulents et les amplitudes de pression, devront être évaluées afin de déterminer les effets d'échelle et d'assurer une transposition fiable des résultats.

6.3 RECOMMANDATIONS

Les résultats obtenus dans cette recherche ouvrent la voie à plusieurs orientations de travaux futurs, visant à approfondir la compréhension du phénomène d'érosion et à développer des outils plus fiables pour son évaluation.

- **Détermination des effets des joints fermés :** Les blocs utilisés dans cette étude présentaient une distribution relativement stable de la pression hydraulique dans des joints ouverts. Or, en conditions réelles, les blocs peuvent se rapprocher et former des joints fermés, ce qui amplifie les pressions dynamiques internes. L'analyse de ce phénomène est nécessaire pour mieux comprendre l'effet des joints fermés sur le processus d'érosion.
- **Développement d'un modèle basé sur les séries de Fourier :** La distribution fluctuante des pressions peut être représentée par une série de Fourier composée de plusieurs composantes sinusoïdales. La détermination expérimentale des paramètres de ces courbes permettra de proposer une représentation plus fiable et transférable aux conditions réelles.

- **Évaluation de l'impact complet de l'orientation :** Le modèle est actuellement capable de faire des essais uniquement à 3 orientations; notamment 0^o, -45^o et $+45^o$ par rapport à l'écoulement. Pour mieux caractériser l'influence de l'orientation des joints, il sera nécessaire d'explorer un plus grand éventail d'inclinaisons, soit par des essais physiques, soit par des simulations numériques.
- **Développement d'un modèle numérique couplé :** La simulation numérique du processus d'érosion requiert le couplage de la dynamique des fluides computationnelle (CFD) et de la modélisation par éléments discrets (DEM). Les pressions hydrauliques mesurées dans le cadre de cette étude fourniront des données de validation essentielles pour un tel modèle couplé.
- **Évaluation de l'effet d'échelle :** Bien que les modèles physiques fournissent des données réalistes, leur extrapolation aux conditions réelles implique la prise en compte de deux types distincts d'effets d'échelle. Le premier concerne les paramètres hydrauliques et géométriques de l'écoulement. Dans cette étude, cet effet d'échelle est généralement maîtrisé par l'application de la loi de similitude de Froude (comme montré dans l'Annexe A), laquelle assure la reproduction adéquate des phénomènes gouvernés par la gravité, notamment les régimes d'écoulement et les structures de surface. Le second effet d'échelle est associé aux paramètres géomécaniques du massif rocheux. Il concerne la manière dont les variations des caractéristiques géométriques et mécaniques des joints influencent la distribution et l'amplitude des pressions hydrauliques. Cette étape pourra être franchie en comparant les résultats expérimentaux obtenus à différentes échelles, grâce à une approche combinée de modélisation physique et numérique.
- **Développement d'un indice de qualité du massif rocheux :** Une fois l'effet individuel des paramètres hydrauliques et géomécaniques bien défini, il sera possible de concevoir un système de classification attribuant des cotes à différentes plages de valeurs. Cet indice fournirait une mesure intégrée de la résistance du massif rocheux face au processus d'érosion.
- **Développement d'une méthode fiable d'évaluation de l'érosion :** En établissant une relation entre l'indice de résistance proposé et la dissipation unitaire de puissance de l'écoulement, une méthode robuste d'évaluation pourra être développée. Celle-ci devra être validée à partir d'un

ensemble de données expérimentales, numériques et de terrain, afin d’assurer sa pertinence et son applicabilité pratique.

PUBLICATIONS

REVUES AVEC COMITÉ DE LECTURE

1. Karnati, V. R., Saeidi, A., Rouleau, A., Quirion, M., et Meghnefi, F. 2025. Determination of Fluctuating Pressures on the Spillway Surface as a function of Joint Opening and Block Protrusion. *Geoenvironmental Disasters*. (Accepté le 12 décembre 2025).
2. Karnati, V. R., Saeidi, A., Rouleau, A., et Quirion, M. 2025. Evaluation of the Effect of Joint Orientation on Rock Mass Erosion Using a Pilot-Plant Spillway Model. *Rock Mechanics and Rock Engineering*, 58(7): 8351-8372. https://doi.org/10.1007/s00603-025-04565-x
3. Karnati, V. R., Saeidi, A., Rouleau, A., et Quirion, M. 2025. Influence of Rock Block Geometry and Orientation on Scour Assessments in a Dam Spillway Using Physical Model Testing. *Rock Mechanics and Rock Engineering*. (Soumis)

CONFÉRENCES (revus par des pairs)

1. Karnati, V. R., Saeidi, A., Rouleau, A., et Quirion, M. 2025. Impact of Block Geometry on the Rock Mass Erosion: A Laboratory-Scale Model Study. Dans : le 23e Symposium canadien sur la mécanique des roches - RockEng 2025, 17 – 19 août, Montréal, Québec, Canada.
2. Karnati, V. R., Saeidi, A., Rouleau, A., et Quirion, M. 2025. Impact of Joint Orientation on Rock Mass Erosion: Insights from Model Testing. Dans : *ISRM International Symposium 2025 & EUROCK 2025*, 16 – 20 juin, Trondheim, Norvège.
3. Karnati, V. R., Saeidi, A., Rouleau, A., et Quirion, M. 2024. Effect of joint orientation on the non-dimensional uplift pressure coefficient based on spillway model tests. Dans : *ISRM International Symposium 2024 & 13th Asian Rock Mechanics Symposium*, 22 – 27 septembre, Delhi, Inde.
4. Karnati, V. R., Saeidi, A., Rouleau, A., et Quirion, M. 2024. Hydraulic Pressure Distribution on Inclined Rock Blocks using an Experimental Spillway Model. Dans : *la 77e Conférence canadienne de géotechnique et la 16e Conférence AIH-SNC sur les eaux souterraines – GeoMontréal 2024*, 15 – 18 septembre, Montréal, Québec, Canada.

5. Karnati, V. R., Saeidi, A., Rouleau, A., et Quirion, M. 2024. Effect of Joint Orientation on Rock Mass Erosion Based on Experimental Results Using a Pilot Plant Spillway Model. Dans : *ARMA 58th US Rock Mechanics/Geomechanics Symposium*, 23 – 26 juin, Golden, Colorado, États-Unis. https://doi.org/10.56952/ARMA-2024-0753
6. Karnati, V. R., Saeidi, A., Rouleau, A., et Quirion, M. 2023. Effect of Joint Opening and Block Protrusion on the Hydraulic Pressure Around Rock Blocks in Unlined Dam Spillways. Dans : *ARMA 57th US Rock Mechanics/Geomechanics Symposium*, 25th – 28th juin, Atlanta, États-Unis. https://doi.org/10.56952/ARMA-2023-0469

RÉFÉRENCES

Afaridegan, E., & Amanian, N. (2025). Enhanced prediction of energy dissipation rate in hydrofoil-crested stepped spillways using novel advanced hybrid machine learning models. *Results in Engineering*, *25*, 103985. https://doi.org/10.1016/j.rineng.2025.103985

Afaridegan, E., Amanian, N., Shanehsazzadeh, A., & Parsaie, A. (2024). Characteristics of flow passing over Hydrofoil Crested Stepped Spillway. *Alexandria Engineering Journal*, *108*, 897-910. https://doi.org/10.1016/j.aej.2024.09.077

Ajalloeian, R., & Azimian, A. (2013). Geotechnical Engineering Assessment of the Nargesi Damsite, Southwest Iran. *Geotechnical and Geological Engineering*, *31*(4), 1369-1392. https://doi.org/10.1007/s10706-013-9661-3

Annandale, G., Wittler, R., Ruff, J., & Lewis, T. (1998). Prototype validation of erodibility index for scour in fractured rock media (pp. 1096-1101). Communication présentée au Water Resources Engineering'98, ASCE.

Annandale, George W. (2006). Current Technology to Predict Scour of Rock. Dans *Golden Rocks 2006, The 41st U.S. Symposium on Rock Mechanics (USRMS)*. Golden, Colorado, USA. Repéré à https://onepetro.org/ARMAUSRMS/proceedings-abstract/ARMA06/All-ARMA06/ARMA-06-987/116097

Annandale, George W. (2006). *Scour technology : Mechanics and engineering practice*. (S.l.): McGraw Hill Professional.

Annandale, George W. (2012). Current state-of-the-art Rock Scouring Technology, 1-12. https://doi.org/10.1061/40911(230)2

Annandale, George W., & George, M. F. (2011). Closure problem to jet scour. *Journal of Hydraulic Research*, *49*(2), 276-277. https://doi.org/10.1080/00221686.2011.568205

Annandale, G.W. (1995). Erodibility. *Journal of Hydraulic Research*, *33*(4), 471-494. https://doi.org/10.1080/00221689509498656

Atkinson, B. K. (1987). *Fracture Mechanics of Rock*. (S.l.): Academic Press: Cambridge, MA, USA. (Google-Books-ID: FXMSAQAAIAAJ).

Azadi, S., Nozari, H., & Godarzi, E. (2020). Predicting Sediment Load Using Stochastic Model and Rating Curves in a Hydrological Station. *Journal of Hydrologic Engineering*, *25*(8), 05020017. https://doi.org/10.1061/(ASCE)HE.1943-5584.0001967

Barton, N., Lien, R., & Lunde, J. (1974). Engineering classification of rock masses for the design of tunnel support. *Rock Mechanics Felsmechanik M□canique des Roches*, *6*(4), 189-236. https://doi.org/10.1007/BF01239496

Baudson, D. R. S., Ferreira, L. D., & De Almeida Prado Bacellar, L. (2024). Geotechnical analysis on the erodibility of tailings from the Fundão dam collapse. *Geotechnical and Geological Engineering*, *42*(6), 4453-4475. https://doi.org/10.1007/s10706-024-02791-8

Bendel, R. B., Higgins, S. S., Teberg, J. E., & Pyke, D. A. (1989). Comparison of skewness coefficient, coefficient of variation, and Gini coefficient as inequality measures within populations. *Oecologia*, *78*(3), 394-400. https://doi.org/10.1007/BF00379115

Bieniawski, Z. (1973). Engineering classification of jointed rock masses. *Civil Engineering= Siviele Ingenieurswese*, *1973*(12), 335-343.

Bollaert, E. (2004). A comprehensive model to evaluate scour formation in plunge pools. *International Journal on Hydropower & Dams*, *11*(1), 94-101.

Bollaert, E. (2010). The comprehensive scour model : Theory and feedback from practice. Dans *Proceedings of the 5th International Conference on Scour and Erosion* (pp. 7-10). San Francisco, California, USA.

Bollaert, E. (2016). Simplified Comprehensive Scour Model compared to Erodibility Index Method. Communication présentée au ICSE 2016 (8th International Conference on Scour and Erosion), Oxford, UK. Repéré à https://eprints.hrwallingford.com/1028/

Bollaert, E. F. R. (2010). Numerical Modeling of Scour at Bridge Foundations on Rock. Dans *Scour and Erosion* (pp. 767-776). San Francisco, California, United States: American Society of Civil Engineers. https://doi.org/10.1061/41147(392)76

Bollaert, E. F. R. (2012). A quasi-3D prediction model of wall jet rock scour in plunge pools. *Hydropower and Dams*, *19*(4), 1-9.

Bollaert, E.F.R., Munodawafa, M. C., & Mazvidza, D. Z. (2013). Kariba Dam Plunge Pool Scour : Quasi-3D Numerical Predictions. *La Houille Blanche*, (1), 42-49. https://doi.org/10.1051/lhb/2013007

Bollaert, Erik F. R. (2002). *Transient water pressures in joints and formation of rock scour due to high-velocity jet impact*. Ph.D. Thesis. École Polytechnique Fédérale de Lausanne - Laboratory of Hydraulic Constructions (EPFL-LCH), Lausanne, Switzerland. Repéré à https://infoscience.epfl.ch/record/116162/files/Comm_LCH_13.pdf

Bollaert, Erik F. R., & Schleiss, A. J. (2005). Physically Based Model for Evaluation of Rock Scour due to High-Velocity Jet Impact. *Journal of Hydraulic Engineering*, *131*(3), 153-165. https://doi.org/10.1061/(ASCE)0733-9429(2005)131:3(153)

Bollaert, Erik F. R., Stratford, C. S., & Lesleighter, E. J. (2014). Numerical modelling of rock scour : Case study of Wivenhoe Dam (Australia). Dans *Scour and Erosion : Proceedings of the 7th International Conference on Scour and Erosion* (pp. 397-404). Perth, Australia: CRC Press. Repéré à https://www.academia.edu/download/36443757/Numerical_modelling_of_rock_scour_Case_study_of_Wivenhoe_DamBollaertStratfordLesleighter.pdf

Bollaert, Erik, & Schleiss, A. (2003a). Scour of rock due to the impact of plunging high velocity jets Part I : A state-of-the-art review. *Journal of Hydraulic Research*, *41*(5), 451-464. https://doi.org/10.1080/00221680309499991

Bollaert, Erik, & Schleiss, A. (2003b). Scour of rock due to the impact of plunging high velocity jets Part II : Experimental results of dynamic pressures at pool bottoms and in one- and two-dimensional closed end rock joints. *Journal of Hydraulic Research*, *41*(5), 465-480. https://doi.org/10.1080/00221680309499992

Boumaiza, L. (2019). *Rock mass parameters governing the hydraulic erodibility of rock in unlined spillways*. Doctoral dissertation. Université du Québec à Chicoutimi, Chicoutimi. (publisher: Université du Québec à Chicoutimi). Repéré à https://constellation.uqac.ca/id/eprint/5755/1/Boumaiza_uqac_0862D_10682.pdf

Boumaiza, L., Saeidi, A., & Quirion, M. (2019a). A method to determine relevant geomechanical parameters for evaluating the hydraulic erodibility of rock. *Journal of Rock Mechanics and Geotechnical Engineering*, *11*(5), 1004-1018. https://doi.org/10.1016/j.jrmge.2019.04.002

Boumaiza, L., Saeidi, A., & Quirion, M. (2019b). Determining relative block structure rating for rock erodibility evaluation in the case of non-orthogonal joint sets. *Journal of Rock Mechanics and Geotechnical Engineering*, *11*(1), 72-87. https://doi.org/10.1016/j.jrmge.2018.06.010

Boumaiza, L., Saeidi, A., & Quirion, M. (2021). A method to determine the relative importance of geological parameters that control the hydraulic erodibility of rock. *Quarterly Journal of Engineering Geology and Hydrogeology*, *54*(4), qjegh2020-154. https://doi.org/10.1144/qjegh2020-154

Capobianco, V., Palau, R. M., Solheim, A., Gisnås, K., Gilbert, G., Danielsson, P., & Van Der Keur, P. (2024). The potential use of nature-based solutions as natural hazard mitigation measure for linear infrastructure in the Nordic Countries. *Geoenvironmental Disasters*, *11*(1), 27. https://doi.org/10.1186/s40677-024-00287-4

Coleman, H. W., Wei, C. Y., & Lindell, J. E. (2004). Hydraulic design of spillways. Dans *Hydraulic design handbook*. New York, NY, USA: McGraw-Hill.

Coleman, S. E., Melville, B. W., & Gore, L. (2003). Fluvial Entrainment of Protruding Fractured Rock. *Journal of Hydraulic Engineering*, *129*(11), 872-884. https://doi.org/10.1061/(ASCE)0733-9429(2003)129:11(872)

Dasgupta, B., Basu, D., Das, K., & Green, R. (2011). Development of computational methodology to assess erosion damage in dam spillways. Dans *31st Annual United States Society on Dam Conference*. San Diego, California.

Dooge, N. (1993). *Die hidrouliese erodeerbaarheid van rotsmassas in ombelynde oorlope met spesiale verwysing na die rol van naatvulmateriaal*. Dissertation. University of Pretoria. (Accepted: 2014-08-04T08:48:22Z). Repéré à https://repository.up.ac.za/handle/2263/41066

Douglas, K., Pells, S., Fell, R., & Peirson, W. (2018). The influence of geological conditions on erosion of unlined spillways in rock. *Quarterly Journal of Engineering Geology and Hydrogeology*, *51*(2), 219-228. https://doi.org/10.1144/qjegh2017-087

Duarte, R. X. M. (2014). *Influence of air entrainment on rock scour development and block stability in plunge pools*. Ph. D. Dissertation. Laboratory of Hydraulic Constructions. Ecole Polytechnique Federale de Lausanne, Switzerland. Repéré à https://infoscience.epfl.ch/record/201642/files/EPFL_TH6195.pdf

Dubinski, I. M. (2009). *Physical modeling of jointed bedrock erosion by block quarrying*. Ph.D. Thesis. *ProQuest Dissertations and Theses*. Colorado State University, United States -- Colorado. (3385138). Repéré à ProQuest Dissertations & Theses Global. (304861260)

Ervine, D. A., Falvey, H. T., & Withers, W. (1997). Pressure fluctuations on plunge pool floors. *Journal of Hydraulic Research*, *35*(2), 257-279. https://doi.org/10.1080/00221689709498430

Ferrill, N. S. L., & Ferrill, D. A. (2021). Influence of mechanical layering and natural fractures on undercutting and rapid headward erosion (recession) at Canyon Lake spillway, Texas, U.S.A. *Engineering Geology*, *280*, 105897. https://doi.org/10.1016/j.enggeo.2020.105897

Forkman, J. (2006). *Statistical inference for the coefficient of variation in normally distributed data* (Rapport No. Report 2). Sweden: Centre of Biostochastics, Swedish University of Agricultural

Sciences. Repéré à https://www.slu.se/contentassets/5116f4fbceaa42e7817a7a4acb4a24df/report2006_2.pdf

Frizell, W. (2007). *Uplift and Crack Flow Resulting from High Velocity Discharges over Open Offset Joints—Laboratory Studies* (Rapport No. Report 12-2007). Denver, CO, USA: U.S. Dept. of the Interior, Bureau of Reclamation. Repéré à https://www.usbr.gov/damsafety/TechDev/DSOTechDev/DSO-07-07.pdf

Gardner, M. (2023). Toward a Complete Kinematic Description of Hydraulic Plucking of Fractured Rock. *Journal of Hydraulic Engineering*, *149*(7), 04023015. https://doi.org/10.1061/JHEND8.HYENG-13193

Gardner, M. H., & Sitar, N. (2018). Modeling of rock scour using coupled 3-D discrete element and lattice boltzmann methods. Communication présentée au 52nd US Rock Mechanics/Geomechanics Symposium, OnePetro.

Gardner, M., & Sitar, N. (2019). Modeling of Dynamic Rock–Fluid Interaction Using Coupled 3-D Discrete Element and Lattice Boltzmann Methods. *Rock Mechanics and Rock Engineering*, *52*(12), 5161-5180. https://doi.org/10.1007/s00603-019-01857-x

George, M. F., & Sitar, N. (2016). Mechanics of 3D Rock Block Erodibility. Dans *50th U.S. Rock Mechanics/Geomechanics Symposium*. Houston, Texas: OnePetro. Repéré à https://onepetro.org/ARMAUSRMS/proceedings-pdf/ARMA16/All-ARMA16/ARMA-2016-848/1329162/arma-2016-848.pdf

George, M. F., Sitar, N., & Sklar, L. (2015). Experimental Evaluation of Rock Erosion in Spillway Channels. Dans *49th U.S. Rock Mechanics/Geomechanics Symposium*. San Francisco, California, USA. Repéré à https://escholarship.org/uc/item/82s7c2f9

George, Michael F. (2012). *Block theory application to scour assessment of unlined rock spillways*. Masters Thesis. University of California, Berkeley, California, USA. Repéré à https://damfailures.org/wp-content/uploads/2021/08/MichaelGeorge_Thesis.pdf

George, Michael F., & Weidner, L. (2025). Rock erodibility in a digital world : Advancing the state of the art using high-resolution remote sensing technology and digital rock mass generation. *Geomechanics and Tunnelling*, *18*(3), 199-208. https://doi.org/10.1002/geot.202500022

George, Michael Freeman. (2015). *3D Block Erodibility : Dynamics of Rock-Water Interaction in Rock Scour*. Ph.D. Thesis. University of California, Berkeley, Berkeley, USA. Repéré à https://escholarship.org/uc/item/61q7798m

Hager, W. H., Schleiss, A. J., Boes, R. M., & Pfister, M. (2020). *Hydraulic Engineering of Dams* (1re éd.). London, UK: CRC Press. https://doi.org/10.1201/9780203771433

Hoek, E., Kaiser, P., & Bawden, W. (1995). Support of Underground Excavations in Hard Rock AA BALKEMA. *Rotterdam/Brookfield*.

ISRM. (1978). International society for rock mechanics commission on standardization of laboratory and field tests. *International Journal of Rock Mechanics and Mining Sciences & Geomechanics Abstracts*, *15*(6), 319-368. https://doi.org/10.1016/0148-9062(78)91472-9

Jalili Kashtiban, Y. (2023). *Development of an equation for evaluating hydraulic erosive parameter of unlined dam spillways considering surface irregularities and geometrical parameters*. Université du Québec à Chicoutimi.

Jalili Kashtiban, Y., Saeidi, A., Farinas, M.-I., & Patarroyo, J. (2023a). Evaluation of the Effect of Rock Surface Irregularities on Energy Gradient in Unlined Dam Spillways (p. ISRM-15CONGRESS-2023-203). Communication présentée au 15th ISRM Congress.

Jalili Kashtiban, Y., Saeidi, A., Farinas, M.-I., & Patarroyo, J. (2023b). Evaluation of the Effect of Surface Irregularities on the Hydraulic Parameters within Unlined Dam Spillways. *Water*, *15*(16), 3004. https://doi.org/10.3390/w15163004

Jalili Kashtiban, Y., Saeidi, A., Farinas, M.-I., & Quirion, M. (2021). A Review on Existing Methods to Assess Hydraulic Erodibility Downstream of Dam Spillways. *Water*, *13*(22), 3205. https://doi.org/10.3390/w13223205

Karnati, V. R., Saeidi, A., Rouleau, A., & Quirion, M. (2023a). *Effect of Joint Opening and Block Protrusion on the Hydraulic Pressure Around Rock Blocks in Unlined Dam Spillways* (Vol. All Days). (S.l.): (s.n.). https://doi.org/10.56952/ARMA-2023-0469

Karnati, V. R., Saeidi, A., Rouleau, A., & Quirion, M. (2023b). Effect of Joint Opening and Block Protrusion on the Hydraulic Pressure Around Rock Blocks in Unlined Dam Spillways. Dans *57th U.S. Rock Mechanics/Geomechanics Symposium*. Atlanta, Georgia, USA: ARMA. https://doi.org/10.56952/arma-2023-0469

Karnati, V. R., Saeidi, A., Rouleau, A., & Quirion, M. (2024). Effect of Joint Orientation on Rock Mass Erosion Based on Experimental Results Using a Pilot Plant Spillway Model. Dans *58th U.S. Rock Mechanics/Geomechanics Symposium* (p. ARMA-2024-0753). Golden, Colorado, USA: ARMA. https://doi.org/10.56952/ARMA-2024-0753

Karnati, Vineeth Reddy, Saeidi, A., Rouleau, A., & Quirion, M. (2025). Evaluation of the Effect of Joint Orientation on Rock Mass Erosion Using a Pilot-Plant Spillway Model. *Rock Mechanics and Rock Engineering*. https://doi.org/10.1007/s00603-025-04565-x

Kaufmann, J., & Schering, A. (2007). Analysis of Variance ANOVA. Dans R. B. D'Agostino, L. Sullivan, & J. Massaro (Éds), *Wiley Encyclopedia of Clinical Trials* (1re éd.). (S.l.): Wiley. https://doi.org/10.1002/9780471462422.eoct017

Kirch, W. (Éd.). (2008). Pearson's Correlation Coefficient. Dans *Encyclopedia of Public Health* (pp. 1090-1091). Dordrecht: Springer Netherlands. https://doi.org/10.1007/978-1-4020-5614-7_2569

Kirsten, H. A. D. (1982). A classification system for excavating in natural materials. *Civil Engineering = Siviele Ingenieurswese*, *1982*(7), 293-308. https://doi.org/10.10520/AJA10212019_15379

Kirsten, H. A., Moore, J. S., Kirsten, L. H., & Temple, D. M. (2000). Erodibility criterion for auxiliary spillways of dams.

Koskinas, A., Tegos, A., Tsira, P., Dimitriadis, P., Iliopoulou, T., Papanicolaou, P., … Williamson, T. (2019). Insights into the Oroville Dam 2017 Spillway Incident. *Geosciences*, *9*(1), 37. https://doi.org/10.3390/geosciences9010037

Koulibaly, A. S., Saeidi, A., Rouleau, A., & Quirion, M. (2023). A Reduced-Scale Physical Model of a Spillway to Evaluate the Hydraulic Erodibility of a Fractured Rock Mass. *Rock Mechanics and Rock Engineering*, *56*, 933-951. https://doi.org/10.1007/s00603-022-03101-5

Lamb, M. P., Finnegan, N. J., Scheingross, J. S., & Sklar, L. S. (2015). New insights into the mechanics of fluvial bedrock erosion through flume experiments and theory. *Geomorphology*, *244*, 33-55. https://doi.org/10.1016/j.geomorph.2015.03.003

Lamb, M. P., Mackey, B. H., & Farley, K. A. (2014). Amphitheater-headed canyons formed by megaflooding at Malad Gorge, Idaho. *Proceedings of the National Academy of Sciences*, *111*(1), 57-62. https://doi.org/10.1073/pnas.1312251111

Li, A., & Liu, P. (2010). Mechanism of rock-bed scour due to impinging jet. *Journal of Hydraulic Research*, *48*(1), 14-22. https://doi.org/10.1080/00221680903565879

Li, K.-W., Pan, Y.-W., & Liao, J.-J. (2016). A comprehensive mechanics-based model to describe bedrock river erosion by plucking in a jointed rock mass. *Environmental Earth Sciences*, *75*(6), 517. https://doi.org/10.1007/s12665-015-5113-0

Liu, Y., Wu, J., Wei, J., Hao, T., & Liu, X. (2021). Erosion Wear Characteristics of Rock Eroded Using Abrasive Air Jet at 90° Impingement Angle. *Rock Mechanics and Rock Engineering*, *54*(3), 1565-1582. https://doi.org/10.1007/s00603-020-02335-5

Maleki, S., & Fiorotto, V. (2021). Hydraulic Brittle Fracture in a Rock Mass. *Rock Mechanics and Rock Engineering*, *54*(9), 5041-5056. https://doi.org/10.1007/s00603-021-02533-9

Mir, B. H., Lone, M. A., Bhat, J. A., & Rather, N. A. (2018). Effect of Gradation of Bed Material on Local Scour Depth. *Geotechnical and Geological Engineering*, *36*(4), 2505-2516. https://doi.org/10.1007/s10706-018-0479-x

Montgomery, R. A. (1984). *Investigations into rock erosion by high velocity water flows* (Masters Thesis). Royal Institute of Technology.

Moore, J. (1991). The characterization of rock for hydraulic erodibility. *Technical Release; USDA: Washington, DC, USA*, *78*.

Moore, J. S., Temple, D. M., & Kirsten, H. a. D. (1994). Headcut advance threshold in earth spillways. *Bulletin of the Association of Engineering Geologists; (United States)*, *31*(2). Repéré à https://www.osti.gov/biblio/7231905

Moren, L., & Sjoberg, J. (2007). Rock Erosion In Spillway Channels-A Case Study of the Ligga Spillway. Dans *11th ISRM congress*. Lisbon, Portugal: OnePetro.

NRCan, C. (2022, 28 janvier). Flood Hazard Identification and Mapping Program. Repéré à https://natural-resources.canada.ca/science-data/science-research/natural-hazards/flood-mapping/flood-hazard-identification-mapping-program

Pan, Y.-W., Li, K.-W., & Liao, J.-J. (2014). Mechanics and response of a surface rock block subjected to pressure fluctuations : A plucking model and its application. *Engineering Geology*, *171*, 1-10. https://doi.org/10.1016/j.enggeo.2013.12.008

Pells, P. J., Bieniawski, Z. T., Hencher, S. R., & Pells, S. E. (2017). Rock quality designation (RQD) : Time to rest in peace. *Canadian Geotechnical Journal*, *54*(6), 825-834. https://doi.org/10.1139/cgj-2016-0012

Pells, Steven E., Douglas, K., Pells, P. J. N., Fell, R., & Peirson, W. L. (2017). Rock Mass Erodibility. *Journal of Hydraulic Engineering*, *143*(5), 06016031. https://doi.org/10.1061/(ASCE)HY.1943-7900.0001243

Pells, Steven E, Pells, P. J., Peirson, W. L., Douglas, K., & Fell, R. (2015). Erosion of unlined spillways in rock–does a "scour threshold" exist? *Proceeding of Australian National Committee on Large Dams, Brisbane, Queensland, Australia*, *1*(9).

Pells, Steven Edward. (2016). *Erosion of Rock in Spillways* (Ph.D. Thesis). University of South Wales, Australia.

Pitsiou, S. (1990). *The effect of discontinuities on the erodibility of rock in unlined spillways of dams*. M.S. Thesis. University of Pretoria. (Accepted: 2014-04-01T09:11:14Z). Repéré à https://repository.up.ac.za/handle/2263/37300

Pittman, J., Lloyd, F., & Alexander, G. (2023). Kentucky's State-Owned Dam Repair Program in Action : Bullock Pen Lake Dam Rehabilitation. *Journal of Dam Safety*, *20*(1), 22-39.

Qi, F., Zhou, W., Bao, J., Lou, X., Hu, C., & Liang, R. (2025). Fracture Damage Analysis of Rock Near Blastholes in High-Slope Throw Blasting. *Geotechnical and Geological Engineering*, *43*(6), 269. https://doi.org/10.1007/s10706-025-03241-9

Rathinasamy, M., Khosa, R., Adamowski, J., Ch, S., Partheepan, G., Anand, J., & Narsimlu, B. (2014). Wavelet-based multiscale performance analysis : An approach to assess and improve hydrological models. *Water Resources Research*, *50*(12), 9721-9737. https://doi.org/10.1002/2013WR014650

Reinius, E. (1986). Rock erosion. *International Water Power and Dam Construction*, *38*(6), 43-48.

Rock, A. J. (2015). *A semi-empirical assessment of plunge pool scour : Two-dimensional application of Annandale's erodibility index method on four dams in British Columbia, Canada* (Masters Thesis). Colorado School of Mines, USA.

Safari, M., Doulati Ardejani, F., Maghsoudy, S., Butscher, C., & Taherdangkoo, R. (2025). Estimating Hydraulic Conductivity in Fractured Rocks Using Factorial Design and Borehole Imaging. *Geotechnical and Geological Engineering*, *43*(2), 116. https://doi.org/10.1007/s10706-025-03082-6

Saiang, D., Idris, M. A., & Nordlund, E. (2022). *Block Erosion of Unlined Rock Spillway Canals* (Rapport No. BeFo Report 230). Stockholm, Sweden: Stiftelsen Bergteknisk Forskning Rock Engineering Research Foundation. Repéré à https://www.befoonline.org/UserFiles/Archive/5198/BeFo_Report_230_web.pdf

Salmasi, F., Razi, S., & Abraham, J. (2023). Hydraulics of flow in gabion stepped spillways an experimental study. *Journal of Hydraulic Structures*, *9*(2). https://doi.org/10.22055/jhs.2023.40421.1257

Sawadogo, O. (2010). *Scour of unlined dam spillways*. Masters Thesis. Stellenbosch : University of Stellenbosch. (Accepted: 2010-11-23T11:02:27Z). Repéré à https://scholar.sun.ac.za:443/handle/10019.1/5331

Schleiss, A. J., Erpicum, S., & Matos, J. (2023). Advances in Spillway Hydraulics : From Theory to Practice. *Water*, *15*(12), 2161. https://doi.org/10.3390/w15122161

Simoẽs, G. F., Vargas, E. do A., & de Lima, R. T. (1997). Numerical modelling of erosion phenomena in fractured rock masses downstream of spillways. Dans *Applications of Computational Mechanics in Geotechnical Engineering* (pp. 71-83). Balkema, Rotterdam: CRC Press.

St»hle, L., & Wold, S. (1989). Analysis of variance (ANOVA). *Chemometrics and Intelligent Laboratory Systems*, *6*(4), 259-272. https://doi.org/10.1016/0169-7439(89)80095-4

Stofleth, J., Shields, D., Downs, G., Stegman, T., & Bowles, C. (2023). An assessment of changes to physical habitat resulting from the 2017 Oroville Dam spillway incident : An application of a 2D

sediment transport model to characterize potential effects. Dans *12th Sedimentation Conference and 7th Hydrologic Modeling Conference*. St. Louis, Missouri, USA. Repéré à https://www.sedhyd.org/2023Program/1/164.pdf

Teng, P., Hellström, J. G. I., Johansson, F., & Nilsson, C.-O. (2023a). Modelling of Erosion in Rock Spillway Channels. Communication présentée au Canadian Dam Association (CDA) 2023 Annual Conference & Trade Show, Winnipeg, Manitoba, Canada, October 22-25, 2023, Canadian Dam Association (CDA). Repéré à https://urn.kb.se/resolve?urn=urn:nbn:se:ltu:diva-102359

Teng, P., Johansson, F., & Hellström, J. G. I. (2023b). Modelling erosion of a single rock block using a coupled CFD-DEM approach. *Journal of Rock Mechanics and Geotechnical Engineering*, *15*(9), 2375-2387. https://doi.org/10.1016/j.jrmge.2023.06.001

Thistlethwaite, J., Minano, A., Blake, J. A., Henstra, D., & Scott, D. (2018). Application of re/insurance models to estimate increases in flood risk due to climate change. *Geoenvironmental Disasters*, *5*(1), 8. https://doi.org/10.1186/s40677-018-0101-9

Umumararungu, M. G. (2016). *Physical modelling investigation of rock scour extent due to a plunging jet for typicalhigh head dams*. M.S. Thesis. Faculty of Engineering, Stellenbosch University, Stellenbosch, South Africa. Repéré à https://scholar.sun.ac.za/handle/10019.1/98521

Van Schalkwyk, A., Jordaan, J., & Dooge, N. (1994a). *Die erodeerbaarheid van verskillende rotsformasies onder varierende vloeitoestande (No. WNK Verslag No. 302/1/95). Verslag aan die waternavorsingskommissie deur die Departement of Geologie, Universiteit van Pretoria, South Africa*. Universiteit van Pretoria, South Africa.

Van Schalkwyk, A., Jordaan, J., & Dooge, N. (1994b). Erosion of rock in unlined spillways. *Proceeding of International Commission on Large Dams, Paris*, *71*(37), 555-571.

Velloso, R. Q., & Vargas Jr, E. A. (2011). Experimental and numerical studies of erosion processes downstream of spillways in large dams. (pp. 26-29). Communication présentée au 45th US Rock Mechanics/Geomechanics Symposium.

Wahl, T. L., Frizell, K. W., & Falvey, H. T. (2019). Uplift Pressures below Spillway Chute Slabs at Unvented Open Offset Joints. *Journal of Hydraulic Engineering*, *145*(11), 04019039. https://doi.org/10.1061/(ASCE)HY.1943-7900.0001637

Wahl, T. L., & Heiner, B. J. (2024a). Discharge through Open Offset Joints and Cracks in Spillway Chutes. *Journal of Hydraulic Engineering*, *150*(5), 04024032. https://doi.org/10.1061/JHEND8.HYENG-13898

Wahl, T. L., & Heiner, B. J. (2024b). Laboratory Measurements of Hydraulic Jacking Uplift Pressure at Offset Joints and Cracks. *Journal of Hydraulic Engineering*, *150*(4), 04024016. https://doi.org/10.1061/JHEND8.HYENG-13871

Wang, D., Leonardi, C. R., & Aminossadati, S. M. (2018). Improved coupling of time integration and hydrodynamic interaction in particle suspensions using the lattice Boltzmann and discrete element methods. *Computers & Mathematics with Applications*, *75*(7), 2593-2606. https://doi.org/10.1016/j.camwa.2018.01.002

Wang, L., Xu, L., Feng, S., Meng, M. Q.-H., & Wang, K. (2013). Multi-Gaussian fitting for pulse waveform using Weighted Least Squares and multi-criteria decision making method. *Computers in Biology and Medicine*, *43*(11), 1661-1672. https://doi.org/10.1016/j.compbiomed.2013.08.004

Whipple, K. X., Hancock, G. S., & Anderson, R. S. (2000). River incision into bedrock : Mechanics and relative efficacy of plucking, abrasion, and cavitation. *GSA Bulletin*, *112*(3), 490-503. https://doi.org/10.1130/0016-7606(2000)112%253C490:RIIBMA%253E2.0.CO;2

Whittaker, J. G., & Schleiss, A. (1984). *Scour Related to Energy Dissipators for High Head Structures*. Mitteilungen der Versuchsanstalt fur Wasserbau, Hydrologie und Glaziologie ETH, Zurich. Repéré à https://ethz.ch/content/dam/ethz/special-interest/baug/vaw/vaw-dam/documents/das-institut/mitteilungen/1980-1989/073.pdf

Wibowo, J. L., & Lin, J. S. (2009). Stability Analysis of Spillways : Toward a Computational Approach. *Powerpoint presentation taken from the internet*.

Wisse, M.-H. (2022). *Déterminer les effets des paramètres géométriques du massif rocheux sur l'érosion à l'aide d'un modèle réduit d'évacuateur de crues*. Université du Québec à Chicoutimi.

Wisse, M.-H., Koulibaly, A. S., Saeidi, A., & Quirion, M. (2023). Small-Scale Physical Model for Studying the Effect of Rock Mass Parameters in the Hydraulic Erosion Process of Unlined Spillways. Dans *World Environmental and Water Resources Congress 2023* (pp. 89-98). Henderson, Nevada: American Society of Civil Engineers. https://doi.org/10.1061/9780784484852.009

Wisse, M.-H., Saeidi, A., & Quirion, M. (2022). Relative Importance of Rock Mass Geometrical Parameters on Erosion in a Dam Spillway Tailrace using a Small-Scale Physical Model 2022. Dans *GeoCalgary*. Calgary, AB, Canada. Repéré à https://geocalgary2022.ca/wp-content/uploads/papers/106.pdf

Wisse, M.-H., Saeidi, A., Quirion, M., & Nilsson, C.-O. (2023). Effects of joint opening and block protrusion on the hydraulic parameters affecting rock block erosion in unlined spillways using a reduced-scale model. *Acta Geotechnica*. https://doi.org/10.1007/s11440-023-02085-y

Wisse, M.-H., Saeidi, A., Quirion, M., & Nilsson, C.-O. (2024). Effects of joint opening and block protrusion on the hydraulic parameters affecting rock block erosion in unlined spillways using a reduced-scale model. *Acta Geotechnica*, *19*(4), 1965-1979. https://doi.org/10.1007/s11440-023-02085-y

Yu, S., Li, Y., Hao, J., Wang, Y., Lv, Z., & Jia, S. (2025). Insights into the Eping Dam, China 2021 Spillway Incident. *Journal of Performance of Constructed Facilities*, *39*(2), 04024060. https://doi.org/10.1061/JPCFEV.CFENG-4426

Yusuf, F., & Micovic, Z. (2020). Prototype-Scale Investigation of Spillway Cavitation Damage and Numerical Modeling of Mitigation Options. *Journal of Hydraulic Engineering*, *146*(2), 04019057. https://doi.org/10.1061/(ASCE)HY.1943-7900.0001671

Zanial, W. N. C. W., Zawawi, M. H., Sidek, L. M., Abas, M. A., Dullah, H., Hassan, N. H., … Rahman, A. H. A. (2023). A Review : Cavitation on Dam Spillway. Dans L. Mohd Sidek, G. H. A. Salih, A. N. Ahmed, I. Escuder-Bueno, & H. Basri (Éds), *Proceedings of the 2nd International Conference on Dam Safety Management and Engineering* (pp. 837-845). Singapore: Springer Nature Singapore. https://doi.org/10.1007/978-981-99-3708-0_58

Zhang, L., & Zhang, J. (2025). Predicting erosion of cohesive sediment by submerged impinging jets through coupling CFD-DEM-VOF method. *Journal of Hydraulic Research*, *63*(5), 594-606. https://doi.org/10.1080/00221686.2025.2556437

Zhang, X., Wang, C., Chen, X., Dong, J., Hu, M., & Liu, S. (2024a). Insights into the cause of the Oroville dam spillway failure, 2017, California. *Environmental Science and Pollution Research*, *31*(14), 21356-21369. https://doi.org/10.1007/s11356-024-32462-3

Zhang, X., Wang, C., Chen, X., Dong, J., Hu, M., & Liu, S. (2024b). Insights into the cause of the Oroville dam spillway failure, 2017, California. *Environmental Science and Pollution Research*. https://doi.org/10.1007/s11356-024-32462-3

ANNEXE A

SCALING RELATIONSHIPS AND FROUDE SIMILARITY CONSIDERATIONS

Scaling relationships

As explained in section 3.3, the design of the reduced-scale model at UQAC is made following Froude similarity criteria, which is a standard criterion for modeling the open-channel flows that are governed by gravity forces. This is achieved by maintaining the constant Froude number (defined as the square root of ratio of inertia force to the gravity force) in both prototype (Fr_{Pr}) and reduced-scale model (Fr_{RM}) as shown in Eq. A1. The dimensional scale adopted for the reduced-scale model is 1:40 which represents that the length scale ratio (λ_L) defined as ratio of length dimension in prototype (L_{Pr}) to that in reduced-scale model (L_{RM}) is 40 as shown in Eq. A2. Applying Eq. A2 in Eq. A1 results in velocity scale ratio (λ_v) as shown in Eq. A3. As the velocity is defined as ratio of displacement (length) to time, the time scale ratio (λ_T) can be determined as shown in Eq. A4. Similarly, as the discharge is defined as the product of flow velocity and the flow cross-sectional area (length x length), the discharge scale ratio can be determined as shown in Eq. A5. The dynamic pressure measured around the model blocks is represented as velocity head (H). Thus, the pressure head scale ratio (λ_H) is equal to length scale ratio (λ_L) as shown in Eq. A6.

$$Fr_{Pr} = \frac{v_{Pr}}{\sqrt{g\ L_{Pr}}} = Fr_{RM} = \frac{v_{RM}}{\sqrt{g\ L_{RM}}} \qquad \text{Eq. A 1}$$

$$\lambda_L = \frac{L_{Pr}}{L_{RM}} = 40 \qquad \text{Eq. A 2}$$

$$\lambda_v = \frac{v_{Pr}}{v_{RM}} = \sqrt{\lambda_L} = \sqrt{40} = 6.325 \qquad \text{Eq. A 3}$$

$$\lambda_T = \frac{T_{Pr}}{T_{RM}} = \frac{\lambda_L}{\lambda_v} = \sqrt{40} = 6.325 \qquad \text{Eq. A 4}$$

$$\lambda_Q = \frac{Q_{Pr}}{Q_{RM}} = \lambda_v \lambda_L^2 = {\lambda_L}^{\frac{5}{2}} = 40^{\frac{5}{2}} = 10{,}119.19 \qquad \text{Eq. A 5}$$

$$\lambda_H = \frac{H_{Pr}}{H_{RM}} = \lambda_L = 40 \qquad \text{Eq. A 6}$$

Where,

λ_L = Length scale ratio (prototype/model)

λ_v = Velocity scale ratio

λ_T = Time scale ratio

λ_Q = Discharge scale ratio

λ_H = Dynamic pressure head or velocity head scale ratio

L = Characteristic length (subscript $_{Pr}$ indicates prototype and subscript $_{RM}$ indicates reduced-scale model) (m)

Q = Characteristic discharge or flow rate (subscript $_{Pr}$ indicates prototype and subscript $_{RM}$ indicates reduced-scale model) (m^3/s)

T = Characteristic time (subscript $_{Pr}$ indicates prototype and subscript $_{RM}$ indicates reduced-scale model) (s)

v = Flow velocity (subscript $_{Pr}$ indicates prototype and subscript $_{RM}$ indicates reduced-scale model) (m/s)

Reynold's number limitation

Although by achieving Froude similarity, the gravity-driven flow behavior is correctly simulated, achieving similar Reynold's number (defined as the ratio of inertia force to viscous force) in reduced-scale models is not possible. The Reynold's numbers in reduced-scale models (Re_{RM}) are lower than those in the prototypes (Re_{Pr}), which indicates that small-scale turbulence and its related pressure fluctuation details cannot be exactly reproduced (Bollaert & Schleiss, 2003a, 2003b; George, 2015). However, the flow conditions in the reduced-scale model used in UQAC remained largely in the turbulent setting as observed by the Reynold's number (Re_{RM} = 73.05 x 10^6 > 2000) (Koulibaly et al., 2023; Wisse, 2022).

Linking pressures from reduced-scale model to prototype

The scale effects are reduced and the comparison across discharges and configurations are initially achieved by expressing the pressure data in a non-dimensional setting as explained in section 3.4. This enables the scaling of pressure data to prototype velocity heads as shown in Eq. A7. As explained in the discussion section, development of a coupled CFD-DEM numerical model is currently under progress which will allow the verification of scale effects in the future.

$$H_{Pr} = C_A \, H_{RM} \qquad \text{Eq. A 7}$$

ANNEXE B

ANALYSIS OF VARIANCE (ANOVA) RESULTS

The correlation between the f_d values and the study parameters, i.e., *JO*, *Conf.*, *BP* and *Q* is determined by performing single factor analysis of variance (*ANOVA*) (Kaufmann & Schering, 2007; St»hle & Wold, 1989). To achieve this, the f_d values are grouped together considering the variation of each parameter individually. Table B1 shows the results of *ANOVA* with significance level of 0.05 for different study parameters (*JO*, *Conf.*, *BP* and *Q*). The sum of squares and degrees of freedom values for each study parameter were 106.9546 and 107 respectively. The dependent (study) parameter with F-value greater than F-Crit has significant effect on the independent parameter, f_d.

Table B1 Single factor *ANOVA* for study parameters

Parameter	**Levels**	**Source of Variation**	**Sum of squares**	**Degrees of freedom**	**Mean squares**	**F-Value**	**P-value**	**F-Crit**
JO	3, 10, 20 mm	Between Groups	18.6392	2	9.3196	11.0803	0.000043	3.0829
		Within Groups	88.3153	105	0.8411			
Conf.	0, 1, 2, 3, 4	Between Groups	6.3747	4	1.5937	1.6320	0.1718	2.4599
		Within Groups	100.5799	103	0.9765			
BP	0, 6, 13, 20 mm	Between Groups	4.4941	3	1.4980	1.5205	0.2136	2.6920
		Within Groups	102.4605	104	0.9852			
Q	*Q1-Q4*	Between Groups	1.6485	3	0.5495	0.5427	0.6542	2.6920
		Within Groups	105.3061	104	1.0126			

ANNEXE C

COMPARISON OF NORMALIZATION RESULTS USING DIFFERENT JO BASELINES

The normalization process explained in section 3.5.6 uses *JO 03 MVR* equation to normalize the *MVR* equations as shown in Figure 3.26. This process is repeated using *JO 10* and *JO 20* as alternate baselines and the results of normalization using other *JO*s to calculate *MVR-JO* and *AR-JO* are shown in Figure C1 - C2. These results show that, for *MVR-JO*, the slopes of the trendlines remain nearly identical across different baselines. Although the slopes of the trendlines for *AR-JO* vary slightly more than those of *MVR-JO*, the changes are not very significant. These findings demonstrate that the normalization trend retains the same monotonic behavior and regression quality regardless of the *JO* baseline.

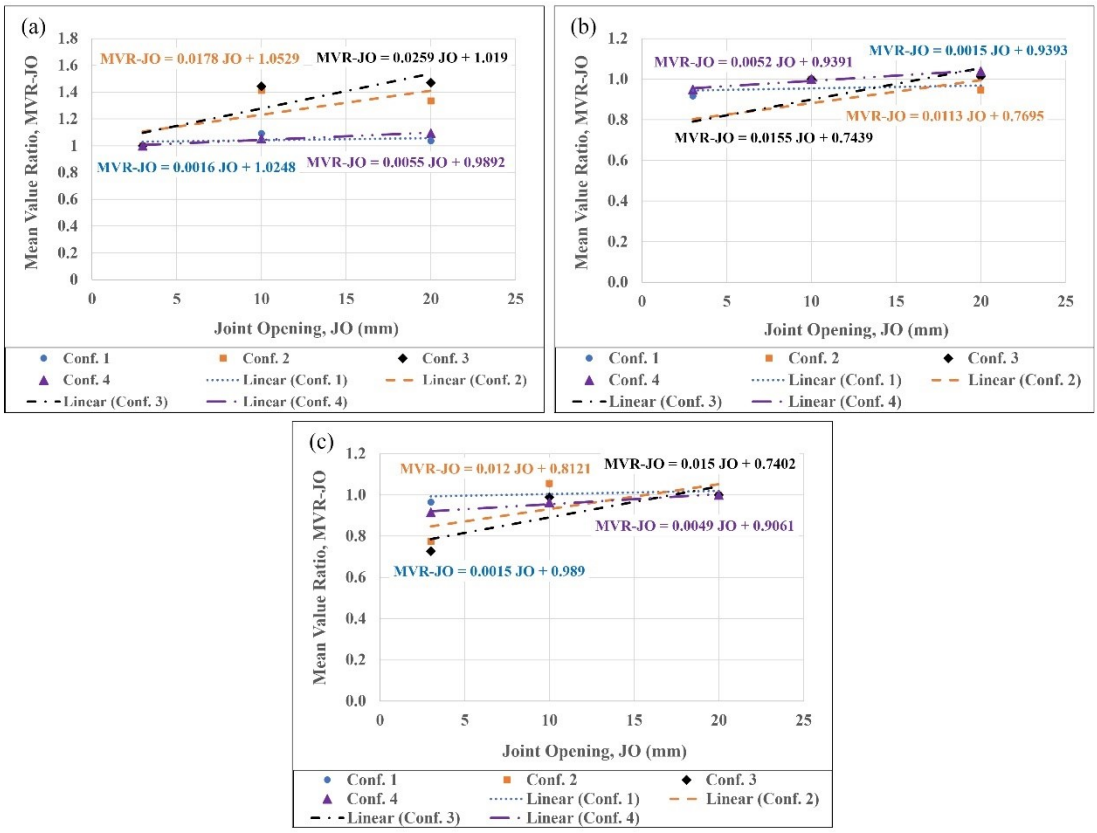

Figure C1 Normalization results for *MVR-JO* under different *JO* baselines: (a) *JO 03*; (b) *JO 10*; (c) *JO 20*

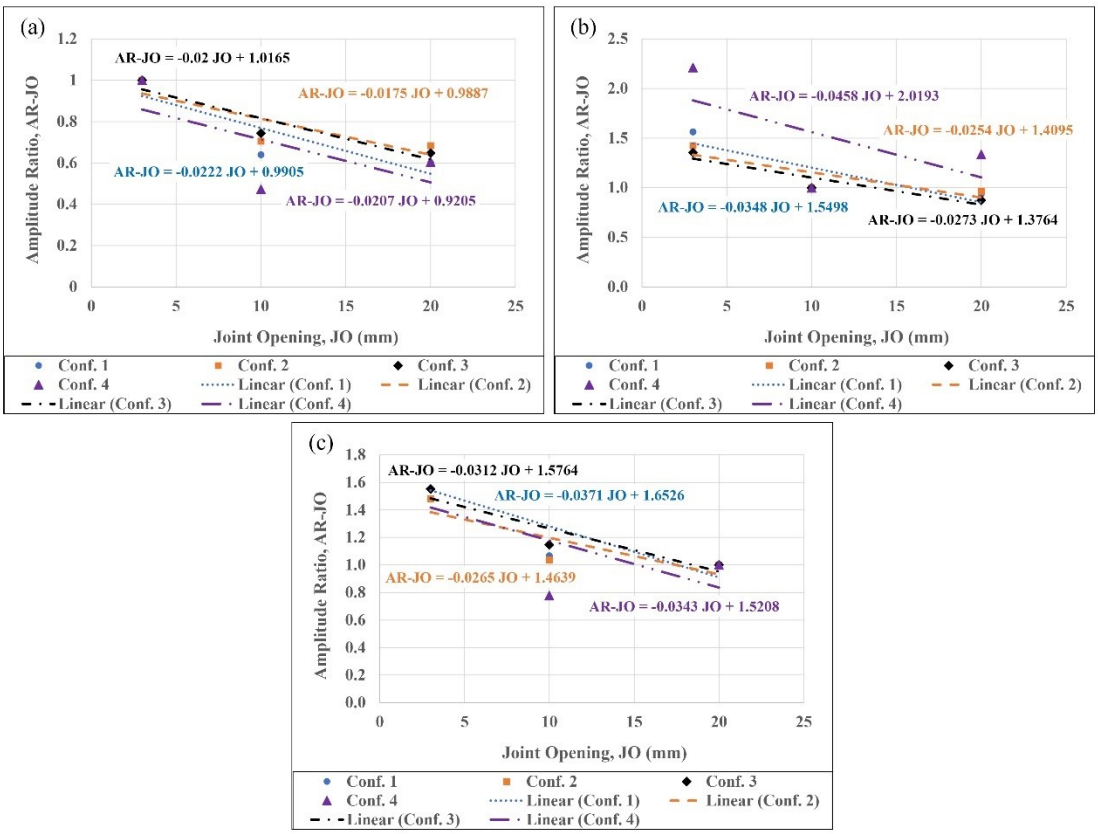

Figure C2 Normalization results for *AR-JO* under different *JO* baselines: (a) *JO 03*; (b) *JO 10*; (c) *JO 20*

ANNEXE D

DETAILED METHODOLOGICAL STEPS IN CHAPTER 5

Non-dimensional pressures and coefficient of uplift

The C_{up}' values are calculated as the difference between the normalized dynamic pressures, C_{px}' (x represents the pressure inlet position), at the top and bottom of the block. Determination of C_{px}' and C_{up}' values is explained in Eq. D1 – D2 respectively.

$$C_{px}^{'} = H_{d,x}/H_{d,Ch} \quad \text{Eq. D1}$$

$$C_{up}^{'} = C_{pB}^{'} - C_{pA}^{'} \quad \text{Eq. D2}$$

Where $H_{d,x}$ represents dynamic head measured at the inlet position 'x', $H_{d,Ch}$ represents mean channel velocity head at the instrumented block level in m, and C_{pA}' and C_{pB}' represent normalized dynamic pressures at the top and bottom of the block, respectively.

Different test conditions used in the model tests

3 joint openings, *JO* (3, 10 and 20 mm); 5 different protrusion configurations, *Conf.* (the configurations are shown in Figures 5.6-5.7): numbered 0, 1, 2, 3 and 4 (1 no protrusion condition (*Conf.* 0), 2 positive (*Conf.* 1 and 4) and 2 negative protrusion (*Conf.* 2 and 3) conditions[1]); 2 protrusion heights, *BP* in each *Conf.* (except for no protrusion condition); and 3 joint orientations, *JOr* (-45°, 0° and +45° with the flow direction). The test arrangements have been subjected to a range of flowrates, Q, from the lowest to highest possible values in the physical model: 180 l/s, 240 l/s, 315 l/s, and 340 l/s.

Determination of uncertainty of extreme values

The procedure to determine the uncertainty of extreme values is depicted in Figure D1. The data is collected at a data collection frequency of 100 Hz for 60 s duration resulting in 6000 data points. The fluctuating dynamic head data shown in Figure D1(a) is initially analyzed to obtain the mean, μ and the standard deviation, σ. Then an arbitrary line ($\mu - p*\sigma$ for minimum values on top and $\mu + p*\sigma$ for maximum values at the bottom) is chosen to identify the extreme values as presented in Figure D1(b). The number of extreme values (below the $\mu - p*\sigma$ line for top and above the $\mu + p*\sigma$ line for bottom, where p is a constant = 2) is determined as presented in Figure D1(c) and is verified if it is about 3% (i.e., about 3% of 6000 data ~ 170 - 180 no.s). When this condition is not satisfied, arbitrary value, p, is varied, and this process is repeated until this requirement is achieved.

[1] The positive protrusion condition presents that the first row of block is arranged in a low level compared to the row with instrumented block, whereas the negative protrusion condition presents that the first row of block is arranged in a high level compared to the row with instrumented block.

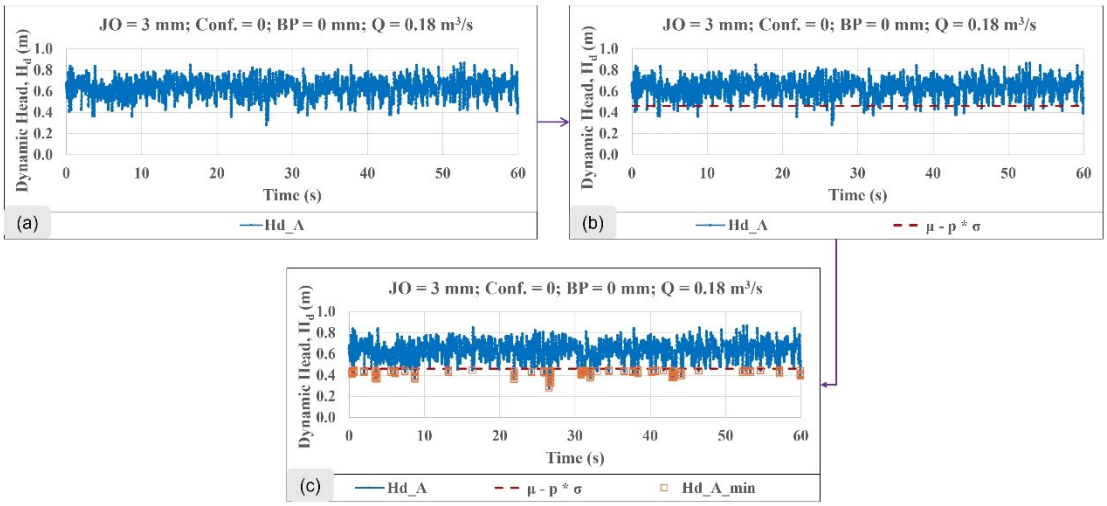

Figure D1 Description of the process for the determination of extreme values along with their uncertainty: (a) Temporal variation of the fluctuating dynamic head; (b) Determination of an arbitrary line separating the extreme 3% data; and (c) Determination of the extreme values

ANNEXE E

PRESENTATION OF HYDRAULIC FORCES ACTING ON THE BLOCK IN CHAPTER 5

Forces on the blocks oriented against the flow (-45°)

Table E1 Forces acting on the block and eccentricity about point *C* in the stability analysis against overturning

Symbol	Description	Force	Eccentricity about *C*
F_{AB}	Hydraulic Force on the top surface of the block (kN/m)	$\gamma_w * \frac{C_{pAc}^{'} + C_{pAd}^{'}}{2} * H_{d,Ch} * S_1$	$\frac{S_1}{3} * \frac{C_{pAc}^{'} + 2C_{pAd}^{'}}{C_{pAc}^{'} + C_{pAd}^{'}}$
F_{BC}	Hydraulic Force on the upstream surface of the block (kN/m)	$\gamma_w * C_{pB}^{'} * H_{d,Ch} * (S_2 - a)$	$\frac{S_2 - a}{2}$
F_{CD}	Hydraulic Force on the bottom surface of the block (kN/m)	$\gamma_w * C_{pB}^{'} * H_{d,Ch} * S_1$	$\frac{S_1}{2}$
F_{AD}	Hydraulic Force on the downstream surface of the block (kN/m)	$\gamma_w * C_{pB}^{'} * H_{d,Ch} * S_2$	$\frac{S_2}{2}$
W_o'	Submerged weight of the block (kN/m)	$\gamma_r^{'} * S_1 * S_2$	-
W_X'	Weight component in the X-direction (kN/m)	$\gamma_r^{'} * S_1 * S_2 * \sin\psi_2$	$\frac{S_2}{2}$
W_Y'	Weight component in the Y-direction (kN/m)	$\gamma_r^{'} * S_1 * S_2 * \cos\psi_2$	$\frac{S_1}{2}$

Forces on the blocks in the uplift analysis

Table E2 Forces acting on the block in the stability analysis against block uplift

Symbol	Description	Force
F_{AB}*	Hydraulic Force on the top surface of the block (kN/m)	$\gamma_w * C_{pA}^{'} * H_{d,Ch} * S_1$
F_{BC}	Hydraulic Force on the upstream surface of the block (kN/m)	$\gamma_w * C_{pB}^{'} * H_{d,Ch} * S_2$
F_{CD}	Hydraulic Force on the bottom surface of the block (kN/m)	$\gamma_w * C_{pB}^{'} * H_{d,Ch} * S_1$
F_{AD}	Hydraulic Force on the downstream surface of the block (kN/m)	$\gamma_w * C_{pB}^{'} * H_{d,Ch} * S_2$
W_o'	Submerged weight of the block (kN/m)	$\gamma_r^{'} * S_1 * S_2$
W_X'	Weight component in the X-direction (kN/m)	$\gamma_r^{'} * S_1 * S_2 * \cos\psi_2$
W_Y'	Weight component in the Y-direction (kN/m)	$\gamma_r^{'} * S_1 * S_2 * \sin\psi_2$

* $C_{pA}^{'} = \frac{C_{pAc}^{'} + C_{pAd}^{'}}{2}$ for +45° condition

ANNEXE F

BLOCK STABILITY ANANLYSIS USING REALISTIC BLOCK UNIT WEIGHT

The block stability analysis considering the same geomechanical conditions, i.e., *JO = 3 mm*; same block dimensions; same hydraulic pressure coefficients from laboratory testing; same *JOr* (-45^o, 0^o and +45^o); same *Conf.*s and same *BP* is carried out using a realistic block unit weight of 27 kN/m^3 (γ_r' = *17.19 kN/m^3*). Use of same pressure coefficients is appropriate as the pressure within the joints and on the top of the block does not depend on the block unit weight. The results of the block stability analysis for -45^o, +45^o and 0^o blocks (*Conf. 2* and *Conf. 3*) are presented in Tables F1-F3. The value of total resisting force in +45^o and 0^o blocks used in Tables F2 and F3 respectively are calculated as 5.44 kN and 5.56 kN respectively.

Table F1 $F_{s,O}$ analysis in the blocks oriented against the flow (-45º) under model testing conditions

Discharge, Q (m^3/s)	**Minimum $F_{s,O}$**			**Mean $F_{s,O}$**			**Maximum $F_{s,O}$**		
	ΣM_{Mo} (Eq. 5.6)	**ΣM_R (Eq. 5.7)**	**$F_{s,O}$ (Eq. 5.8)**	**ΣM_{Mo} (Eq. 5.6)**	**ΣM_R (Eq. 5.7)**	**$F_{s,O}$ (Eq. 5.8)**	**ΣM_{Mo} (Eq. 5.6)**	**ΣM_R (Eq. 5.7)**	**$F_{s,O}$ (Eq. 5.8)**
0.18	0.115	0.261	2.26	0.142	0.260	1.84	0.197	0.268	1.36
0.24	0.145	0.269	1.86	0.178	0.268	1.51	0.247	0.278	1.12
0.315	0.182	0.279	1.53	0.223	0.278	1.24	0.310	0.290	0.93
0.34	0.194	0.282	1.45	0.238	0.281	1.18	0.331	0.294	0.89

Table F2 $F_{s,Up}$ analysis in the blocks oriented towards the flow (+45°) under model testing conditions

Discharge, Q (m^3/s)	**Using Mean C_{up}'**		**Using Maximum C_{up}'**	
	ΣF_{up} (Eq. 5.9)	**$F_{s,Up}$ (Eq. 5.11)**	**ΣF_{up} (Eq. 5.9)**	**$F_{s,Up}$ (Eq. 5.11)**
0.18	0.52	10.52	2.46	2.21
0.24	0.65	8.38	3.09	1.76
0.315	0.81	6.68	3.88	1.40
0.34	0.87	6.26	4.14	1.31

Table F3 $F_{s,Up}$ analysis for selected cases in the blocks oriented perpendicular to the flow (0°) under model testing conditions

Discharge, Q (m^3/s)	**Using Mean C_{up}' for *Conf. 2; BP 20 mm***		**Using Maximum C_{up}' for *Conf. 2; BP 13 mm***		**Using Maximum C_{up}' for *Conf. 2; BP 20 mm***		**Using Mean C_{up}' for *Conf. 3; BP 13 mm***		**Using Maximum C_{up}' for *Conf. 3; BP 13 mm***	
	ΣF_{up} (Eq. 5.9)	**$F_{s,Up}$ (Eq. 5.11)**	**ΣF_{up} (Eq. 5.9)**	**$F_{s,Up}$ (Eq. 5.11)**	**ΣF_{up} (Eq. 5.9)**	**$F_{s,Up}$ (Eq. 5.11)**	**ΣF_{up} (Eq. 5.9)**	**$F_{s,Up}$ (Eq. 5.11)**	**ΣF_{up} (Eq. 5.9)**	**$F_{s,Up}$ (Eq. 5.11)**
0.18	0.08	72.49	1.01	5.52	1.06	5.24	0.18	31.26	0.96	5.77
0.24	0.10	57.73	1.26	4.40	1.33	4.17	0.22	24.89	1.21	4.60
0.315	0.12	46.02	1.59	3.50	1.67	3.33	0.28	19.84	1.52	3.67
0.34	0.13	43.11	1.69	3.28	1.78	3.12	0.30	18.59	1.62	3.43

ANNEXE G

PUBLICATIONS DES CONFÉRENCES

ARMA 23– 0469

Effect of Joint Opening and Block Protrusion on the Hydraulic Pressure around Rock Blocks in Unlined Dam Spillways

Karnati, V.R.[1*], Saeidi, A.[2] and Rouleau, A.[3]
Département des sciences appliquées, Université du Québec à Chicoutimi, Chicoutimi, Québec, Canada
Quirion, M.[4]
Hydro-Québec, Unité expertise en géologie, Montréal, Québec, Canada
* Author to whom correspondence should be addressed. Email: vineethkarnati@gmail.com

This paper was prepared for presentation at the 57th US Rock Mechanics/Geomechanics Symposium held in Atlanta, Georgia, USA, 25-28 June 2023. This paper was selected for presentation at the symposium by an ARMA Technical Program Committee based on a technical and critical review of the paper by a minimum of two technical reviewers.

ABSTRACT: Rock mass erosion has been a serious safety concern in recent years especially in the case of dam spillways. Rock block removal by uplift depends on the weight of the block, shearing resistance developed along the sliding faces and hydraulic forces around the block. The effects of several geomechanical and hydraulic parameters on the hydraulic pressures around a block are being studied using a pilot plant scale laboratory spillway model. This study focusses on the effect of joint opening (JO) and block protrusion (JP) on the hydraulic pressures inside the joint and on the top of the block. The blocks are placed in 5 different configurations for testing with three different opening values between the blocks (3, 10 and 20mm) and different block protrusion heights. The test results show that the pressure on the top of the block has dominating effect in the uplift of the block as the pressure on the bottom of the block remained almost constant with different JO and JP conditions. Tests results revealed that block protrusion plays a very important role in the uplift of a block.

1. INTRODUCTION

During the flood season, the excessive water stored in the reservoirs shall be released downstream through spillways considering the safety of the dams. These spillways can be broadly classified into two types: parallel flow spillways and plunging jet spillways. In both cases, the flowing water with huge hydraulic energy could cause significant erosion of the rock mass, which may incur unnecessary expenses in repairs and public safety risks (Annandale, 2012; Pells, 2016). In recent years, the damage from the hydraulic erosion has become an important concern in frequently operating spillways. Rock mass erosion is a complex phenomenon that depends on both hydraulic and geomechanical parameters. Rock mass erosion occurs when the resistive capacity of the rock mass is exceeded by the erosive capacity of flowing water (Annandale, 2012; Boumaiza, 2019; Pells, 2016). The erosive capacity is dependent on the flow conditions and the common parameters used to represent the erosive capacity are unit stream power dissipation (Annandale, 2006; Pells, 2016), flow velocity and shear stress (Bollaert, 2010, 2016). The resistive capacity represents the ability of rock mass to withstand the hydraulic forces from the flowing water which is dependent on several geomechanical parameters like joint shear strength, joint opening, joint protrusion, joint orientation, block volume, etc. Boumaiza et al. (2019, 2021) studied the existing rock mass

geomechanical indices that represents the rock mass resistive capacity against hydraulic erosion and concluded that they considered improper weightage to some parameters or completely ignore some other relevant parameters like joint opening, 3D rock block volume, while considering unimportant parameter like the unconfined compressive strength of intact rock specimens. A comprehensive description of the erosion prediction models developed in the past few decades is provided by Jalili Kashtiban et al. (2021) most of which are based on empirical relationships. The underlying mechanisms behind the erosion has not been studied to the full extent (Saiang et al., 2022).

The major mechanisms behind the erosion phenomenon are found to be abrasion, fracturing of intact rock and plucking (Bollaert, 2016; Jalili Kashtiban et al., 2021; Saiang et al., 2022). Among these mechanisms, abrasion affects the rock mass in a long-run and is dependent on flow velocity, discharge, hardness of the rock mass and its grain size composition. Intact rock mass fracturing occurs when the closed-end joints are subjected to turbulent pressures of the flowing water thereby propagating the joints. The fracturing depends on the hydraulic pressure intensity, tensile strength of intact rock and toughness of fracture, and it can occur instantaneously or over time under fatigue (Bollaert & Schleiss, 2002). Plucking or removal of individual rock blocks is often observed in many erosion cases of spillways and bedrock channels with sub-meter rock blocks (Joint spacing less than 1 m) with continuous joints that isolate the blocks (K.-W. Li et al., 2016; Pan et al., 2014), making it the most important mechanism of the hydraulic erosion. Under the action of fluctuating pressures around the block, rock block plucking occurs when the uplifting forces exceed the pressures overlying the rock, weight of the block and shear forces on the sides of the block (Annandale, 2006; George, 2015; K.-W. Li et al., 2016). The pressures around the block are dependent on several joint conditions such as joint opening, rock surface protrusion, rock block volume, etc.

Several laboratory model and numerical model studies have been carried out to study this erosion process in last few decades (Dasgupta et al., 2011; Simoẽs et al., 1997; Velloso et al., 2011). However, most of these studies are attributed to single block studies. Coleman et al. (2003) studied the block protrusion and block surface length and concluded that a nominal value of block protrusion could affect its stability significantly and this parameters should be considered for the assessment of rock mass erosion using the methods based on stream power dissipation. Frizell (2007) studied the uplift pressures generated due to the presence of a small amount of different types of offsets using a simple laboratory model. Dubinski (2009) studied the physical process of block quarrying in a jointed rock mass by physical modelling and proposed that the huge amount of erosion could be possible after the removal of a few key blocks which requires huge expense of hydraulic power. He also mentioned that the joint spacing and its associated block size are also key parameters governing the erosion efficacy. George et al. (2015) carried out model scale studies on a single tetrahedral block and concluded that the erodibility process is governed by the orientation of the block to the flow direction, flow velocity and the degree of turbulence. George and Sitar (2016) studied the effect of orientation and found that the mode of uplifting of a tetrahedral block is varied with the block mold orientations. George and Sitar (2016a) observed from the spectral analysis of pressure and displacement data that the block displacements could occur at lower to higher end of frequency spectrum depending on the kinematic resistance of the block. Umumararungu (2016) studied different hydraulic parameters affecting the scour depth of a plunge pool using a 1:40 scaled down laboratory model. Liu et al. (1998) studied the pressure fluctuations at the bottom of a plunge pool and identified that the pressure fluctuation at the bottom of plunge pool follows a gaussian distribution. Li and liu (2010) studied the propagation of scour hole in plunge pools through numerical simulation with discrete fracture networks (DFN). The current article presents a study of the effect of the joint opening and the protrusion of blocks on the pressures around the block using a pilot plant scale laboratory spillway model.

2. SPILLWAY MODEL DESCRIPTION

A laboratory spillway model, scaled down from Hydro-Québec's Romaine IV spillway, has been developed at Université du Québec à Chicoutimi (UQAC), Québec, Canada to study the effects of several geomechanical and hydraulic parameters on the rock mass erosion process in parallel flow spillways. The design details of this spillway model shown in Fig. 1 are presented in Koulibaly et al. (2021, 2022). In the spillway model,

concrete blocks are used to represent the isolated rock blocks which are placed perpendicular to the spillway surface. A metal support casing containing 9 concrete blocks as shown in Fig. 1, each of size 15 cm x 15 cm x 30 m, is placed near the end of the spillway channel. The central block is instrumented to measure the pressure distribution around the block. A carbon rod that floats on water, connected to LVDT, is placed close to the concrete blocks allowing measurement of the height of water near the blocks. The discharge in the channel is varied as a function of the height of water in the overhead tank upstream of the channel.

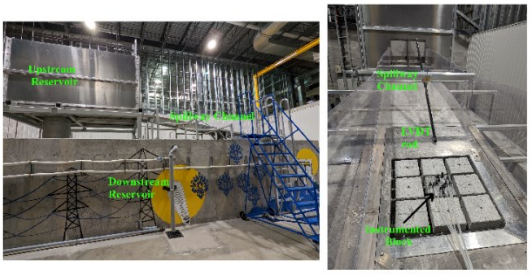

Fig. 1. Laboratory spillway model with 15X15X30 cm blocks at the end of spillway channel.

The instrumented block shown in Fig. 2 was equipped with 11 internal copper tubes allowing pressure measurement. These copper tubes are equipped with elbows at each end to facilitate the water flow. One end of these tubes acts as water entry and the other end acts as water outlet which is connected to the one of the 6 pressure transducers, equipped adjacent to the spillway channel, with the help of plastic tubes. The pressure sensors used are of the measuring range 0-70.31 mH_2O (0-100 psi). The top and bottom faces of the block are called A and B respectively. The vertical faces (upstream and downstream) opposing the flow are called C and D respectively. The vertical faces to the left and right side of the flow direction (along the flow) are called faces E and F respectively. The pressure on face A is measured by water entry A on the top of the block. Along each vertical side of the block, two water entries are used with elbows, one facing upwards (indexed 1) and the other facing downwards (indexed 2). For example, on face C, the water entry with elbow facing upwards is called 'C1' and the one with elbow faced downwards is called 'C2'. On the bottom face, two water entries were used with elbows facing faces C & D and are termed as 'Bc' & 'Bd' respectively.

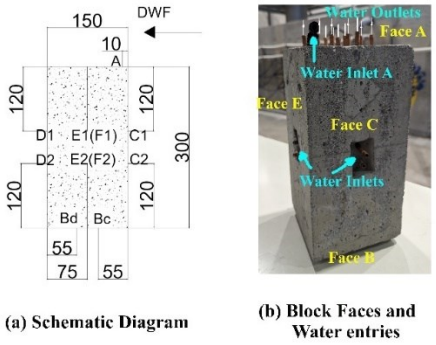

Fig. 2. Instrumented block used to measure the hydraulic pressures around the block.

3. TESTING METHODOLOGY

This study aims at the determination of the effect of joint opening and the block protrusion on the hydraulic pressures around the block. Three different joint openings (JO), 03 mm, 10 mm and 20 mm, were selected to represent the open, wide and very wide apertures respectively (ISRM, 1978). To represent different field protrusion conditions, five different block configurations were selected as shown in Table. 1. In each configuration, two different block protrusion heights (JP) as mentioned in Table. 1 were tested in the model. A constant opening of 7 mm is provided at the bottom of blocks in all the test cases to allow for the water flow and pressure measurement at the bottom of the instrumented block. The measurements of JO and JP are maintained to an accuracy of 0.5 mm. In the stability analysis of the block against uplift, the pressures on the top and bottom of the block are significant whereas the pressures on the vertical faces affect the shearing resistance against the uplift. Hence, this article focusses on the effect of joint opening and protrusion on the pressures at these locations, though the pressures are measured at all these locations. The pressure data is recorded for a period of 60 s of operation at a constant flow rate of Q=0.18 m^3/s (180 L/s) in all the cases. This discharge corresponds to a mean static head of about 50 mm in the channel at the section of the instrumented block. The testing plan adopted is as shown in Fig. 3.

Table. 1. Block configuration parameters and protrusion heights

Setup	Configuration #	Block protrusion value, JP (mm)	Protrusion in 1st row (mm)	Protrusion in 2nd row (mm)	Protrusion in 3rd row (mm)
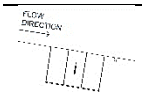	0	JP0=00	00	00	00
	1*	JP1=06 JP2=13	00 00	06 13	12 26
	2*	JP1=13 JP2=20	13 20	0 0	13 20
	3*	JP1=06 JP2=13	13 26	06 13	0 0
	4*	JP1=13 JP2=20	00 00	13 20	00 00

*Two tests each with different protrusion heights (JP1 and JP2)

The pressure transducers are calibrated to give the pressure values in head of water. The transducers are adjusted to a data collection frequency of 10,000 Hz which is then averaged to get a final data collection frequency of 100Hz so as to reduce the quantum of data to work with. The measured pressure head is the sum of the datum head (corresponding to the position of water entry from the line of measurement), static water head and the velocity head due to the flow of water. The hydraulic pressures (Static and dynamic pressure heads) acting at different locations on the block are determined by deducing the datum head from the recorded values. Further, it should be noted that for the case of JO 03 mm, the pressure measurements could be made only at the top and bottom of the block since the elbows couldn't be positioned at vertical faces with openings less than 10 mm.

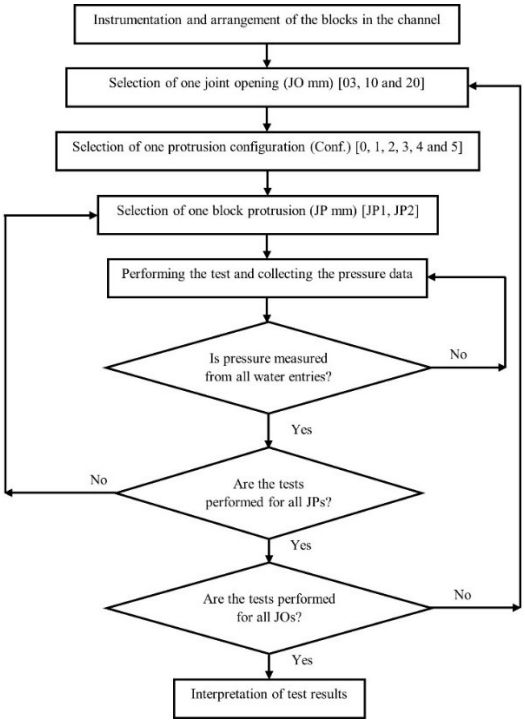

Fig. 3. Testing plan used in the study.

4. RESULTS AND DISCUSSIONS

The results obtained from the model tests are corrected for the position (datum head) and the variation of pressure as a function of time for 60 s is presented in this section. The variability of these hydraulic pressures at top and bottom of the instrumented block are presented in Fig. 4, 5 and 6 for the JO values of 03 mm, 10 mm, and 20 mm respectively. As the flow in parallel flow spillways is usually rapidly varied, huge fluctuations in the hydraulic pressures is expected on the top of the block. However, the pressures under the block are less affected by these fluctuations, particularly with blocks of much larger height (30 cm) than the flow thickness. Besides the fluctuations in flow inside the joint could be relatively less than those in the channel. Another significant observation is that the pressures at the bottom of the block measured in both 'Bc' and 'Bd' are close to each other and is close to the static pressure at that level. The fluctuating pressures often create a situation that the pressure on the top of block is so low that the resultant vertical force becomes upwards and allows the block to move upwards. Thus, the pressure on the top of the block has domination over the uplift of the block. To study the effect of joint opening and the block protrusion, the variation in the hydraulic pressures on the top and

bottom is presented in terms of the variation in the respective mean values.

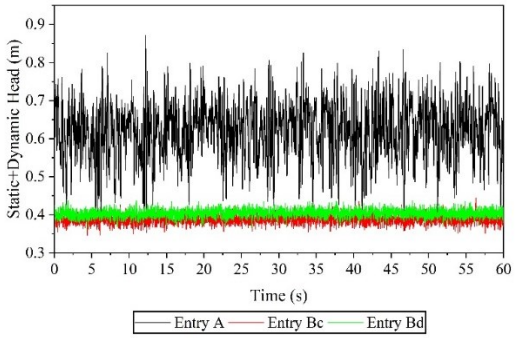

Fig. 4. Hydraulic pressures on the top and bottom of instrumented block for JO 03 mm.

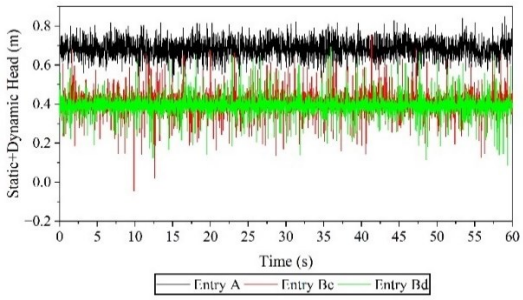

Fig. 5. Hydraulic pressures on the top and bottom of instrumented block for JO 10 mm.

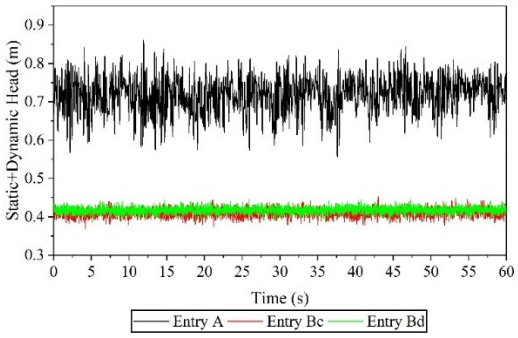

Fig. 6. Hydraulic pressures on the top and bottom of instrumented block for JO 20 mm.

4.1 Effect of Joint Opening (JO)

The variation of the mean value of the hydraulic pressures as a function of joint opening for configuration 0 is presented in Fig. 7. From Fig. 4, 5, 6 and 7 it is evident that the pressure on the top is increasing along with the joint opening. Also, the joint opening has very little effect on the pressures at the bottom of the block. The effect of JO in different configurations on the mean values of the hydraulic pressures at top of the block (entry A) is presented in Fig. 8. Fig. 8 shows that for most of the protrusion conditions, the similar variation as that of no protrusion condition is observed. Three cases are found different; (i) Configuration 1 with JP=13 mm, (ii) Configuration 2 with JP=20 mm and (iii) Configuration 3 with JP=13 mm, where significant block protrusion disrupts the flow.

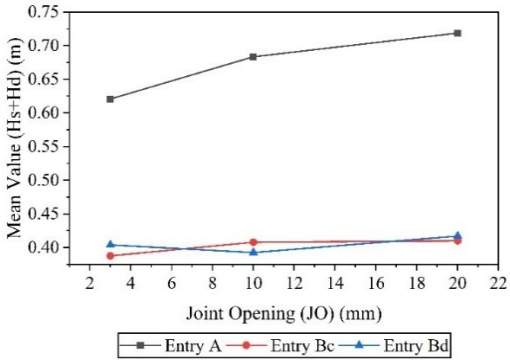

Fig. 7. Variation of mean values of hydraulic pressures on the top and bottom of the block with the joint opening.

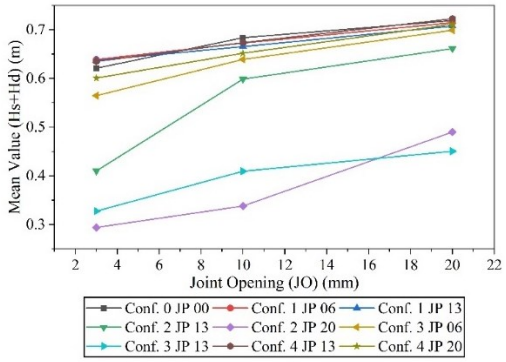

Fig. 8. Variation of mean values of hydraulic pressures on the top of block with the joint opening for different protrusion conditions.

4.2 Effect of Block Protrusion Height (JP)

To study the effect of the block protrusion, the variation of mean value of the pressures at top and bottom of the block as a function of block protrusion height is presented in Fig. 9, 10, 11 and 12 respectively for configurations 1, 2, 3 and 4. Configuration 0 in which the top of blocks coincides with the spillway surface is considered as “0” protrusion height for all these Fig. Fig. 9-12 show that the pressure on the top of the block is reduced, whereas that on the bottom of the

blocks is increased with increasing protrusion height, and the amount of reduction is dependent on the type of configuration. This reduction could be attributed to the reduction in the velocity of the flow and the development of a small hydraulic jump at the protruded surface as shown in Fig. 13. The formation of this jump could result in the reduced flow velocity at the top of the instrumented block.

In configuration 1, where the blocks are arranged in an ascending stepped protrusion pattern, the fluctuations of the blocks (Block vibrations) are observed in the trailing row of the blocks. In configuration 2, the leading and trailing rows are protruded, and this situation diminishes the pressure on the top. The pressure on the bottom of the block is observed to be increasing, and at 20 mm protrusion the pressure at the top is much lower than the pressure at the bottom of the block, which could be a favourable scenario for the block uplift to occur. At the current flow rate, the block uplift was not observed. However, with increasing flow rate, the pressure build-up could be critical enough to initiate the block vibrations and complete removal. In configuration 3, where blocks are arranged in descending stepped protrusion pattern, a noticeable observation is that both the pressures at the top and bottom are diminished as compared to no protrusion condition. This condition couldn't potentially cause uplift of the block positioned in the middle row, but little fluctuations in the leading row blocks are noticed. In configuration 4, no much noticeable differences are observed in the pressure at the top of block, however at higher protrusion values a little reduction in pressure is observed. The pressures at the bottom of the block are showing a small increase with the protrusion value, that could be considered as the effect of the development of stagnation pressure at the protruded portion of the block.

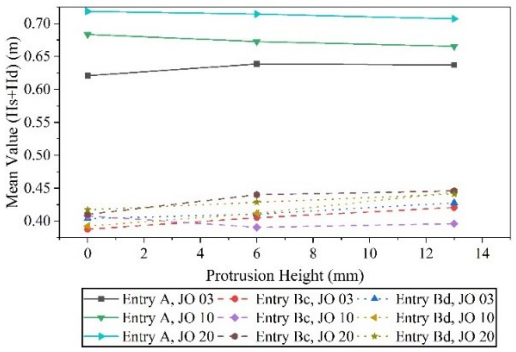

Fig. 9. Variation of mean values of hydraulic pressures on the top and bottom of block with the protrusion height for configuration 1.

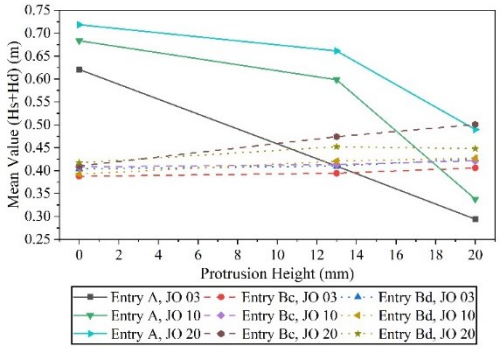

Fig. 10. Variation of mean values of hydraulic pressures on the top and bottom of block with the protrusion height for configuration 2.

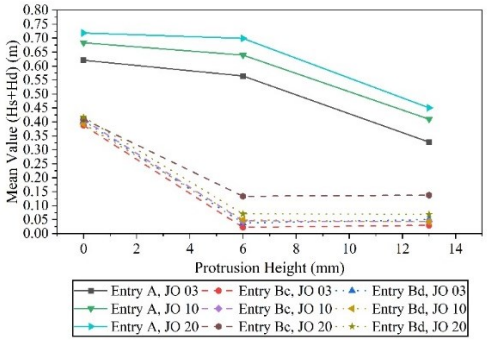

Fig. 11. Variation of mean values of hydraulic pressures on the top and bottom of block with the protrusion height for configuration 3.

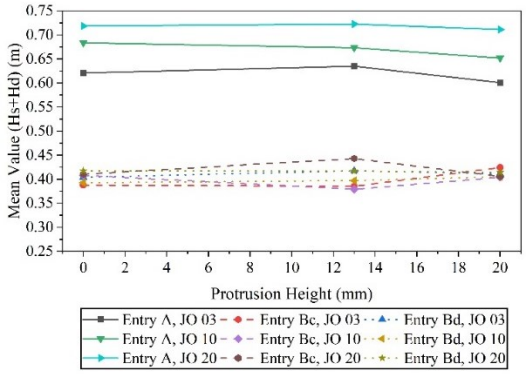

Fig. 12. Variation of mean values of hydraulic pressures on the top and bottom of block with the protrusion height for configuration 4.

Fig. 13. Development of hydraulic jump at protruded surface for configuration 3.

4.3 Effect of Block Protrusion Configuration

To study the effect of the block protrusion configuration (Conf.), a comparison in mean values of hydraulic pressures at top and bottom is made by choosing a common protrusion height of 13 mm for different configurations along with configuration 0 with 0 mm protrusion height. The variation of the mean values as a function of protrusion configuration is presented in Fig. 14.

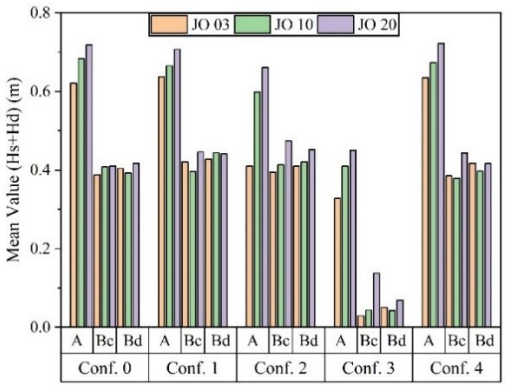

Fig. 14. Variation of mean values of hydraulic pressures on the top and bottom of block with the protrusion configuration (JP = 13 mm).

It could be understood from Fig. 14 that for a given protrusion height (13 mm), the pressure on the top of the blocks is reduced moderately and that on the bottom of the block is slightly increased for configurations 1 and 2, whereas for configuration 4, the pressure value remains almost constant as that of no protrusion configuration (Conf. 0). The development of a hydraulic jump at the first row of blocks explains the huge reductions in the pressures at top and bottom of the block. The first row remains similar in the case of the conf. 2 and 3, but the reduced pressures are observed only in conf. 2 but not in conf. 3, that could be explained from the development of stagnation pressures at the trailing row of blocks (3rd row of blocks).

5. CONCLUSIONS

The major rock mass erosion mechanism, plucking/uplift, depends on the hydraulic pressures which is dependent on several hydraulic and geomechanical conditions. A laboratory scale spillway model constructed at UQAC allows for studying the effect of these parameters on the pressures around the block. In this study, several tests are conducted to study the effect of joint opening and block protrusion on the pressures around the block. Three different JO (03, 10 and 20 mm) values, with blocks arranged in 5 protrusion configurations are tested under a constant flow rate of 0.18 m^3/s (180 L/s). It is observed that the pressure on the top of the block has more impact on the uplift process than those at the bottom of the block. With increasing JO values, the pressure at the top of the block is found to increase in almost all cases, whereas the pressure at the bottom of the block remains almost constant. Block protrusion height is observed to be having a predominant effect on the pressures but depending on the type of configuration. In the presence of a protrusion, the pressure on the top is always found to be reduced and the pressure at the bottom is found to be increased except for conf. 3. Conf. 2 is found to be most critical for uplift, as the pressure at the top diminished close to the pressure value at the bottom of the block; however, uplift is not observed while testing under the given flow rate. Further testing with varied flow rates will allow us to check the occurrence of uplift of blocks in the critical configurations and the uplift mechanism can be studied for all the above-mentioned cases.

ACKNOWLEDGEMENTS

The authors would like to acknowledge the Natural Sciences and Engineering Research Council of Canada (NSERC) and Hydro-Québec, and Uniper (CRDPJ 537350 - 18) for funding the research.

REFERENCES

Annandale, G. W. (2006). *Scour technology: Mechanics and engineering practice*. McGraw Hill Professional.

Annandale, G. W. (2012). *Current state-of-the-art Rock Scouring Technology*. 1–12. https://doi.org/10.1061/40911(230)2

Bollaert, E. (2010). *The comprehensive scour model: Theory and feedback from practice*. 7–10.

Bollaert, E. (2016, September 12). *Simplified Comprehensive Scour Model compared to Erodibility Index Method*. ICSE 2016 (8th International Conference on Scour and Erosion), Oxford, UK. https://eprints.hrwallingford.com/1028/

Bollaert, E., & Schleiss, A. (2002). *Transient water pressures in joints and formation of rock scour due to high-velocity jet impact* (No. 1661–1179). EPFL-LCH.

Boumaiza, L. (2019). *Rock mass parameters governing the hydraulic erodibility of rock in unlined spillways* [Doctoral dissertation, Université du Québec à Chicoutimi]. https://constellation.uqac.ca/id/eprint/5755/1/Boumaiza_uqac_0862D_10682.pdf

Boumaiza, L., Saeidi, A., & Quirion, M. (2019). A method to determine relevant geomechanical parameters for evaluating the hydraulic erodibility of rock. *Journal of Rock Mechanics and Geotechnical Engineering*, *11*(5), 1004–1018. https://doi.org/10.1016/j.jrmge.2019.04.002

Boumaiza, L., Saeidi, A., & Quirion, M. (2021). A method to determine the relative importance of geological parameters that control the hydraulic erodibility of rock. *Quarterly Journal of Engineering Geology and Hydrogeology*, *54*(4), qjegh2020-154. https://doi.org/10.1144/qjegh2020-154

Coleman, S. E., Melville, B. W., & Gore, L. (2003). Fluvial Entrainment of Protruding Fractured Rock. *Journal of Hydraulic Engineering*, *129*(11), 872–884. https://doi.org/10.1061/(ASCE)0733-9429(2003)129:11(872)

Dasgupta, B., Basu, D., Das, K., & Green, R. (2011). *Development of computational methodology to assess erosion damage in dam spillways*. 11–15.

Dubinski, I. M. (2009). Physical modeling of jointed bedrock erosion by block quarrying [Ph.D., Colorado State University]. In *ProQuest Dissertations and Theses* (304861260). ProQuest Dissertations & Theses Global. https://sbiproxy.uqac.ca/login?url=https://www.proquest.com/dissertations-theses/physical-modeling-jointed-bedrock-erosion-block/docview/304861260/se-2?accountid=14722

Frizell, W. (2007). *Uplift and Crack Flow Resulting from High Velocity Discharges over Open Offset Joints—Laboratory Studies* (Report 12-2007). U.S. Dept. of the Interior, Bureau of Reclamation. https://www.usbr.gov/damsafety/TechDev/DSOTechDev/DSO-07-07.pdf

George, M. F. (2015). *3D Block Erodibility: Dynamics of Rock-Water Interaction in Rock Scour* [UC Berkeley]. https://escholarship.org/uc/item/61q7798m

George, M. F., & Sitar, N. (2016a). *3D Block Erodibility: Dynamics of Rock-Water Interaction in Rock Scour.* https://doi.org/10.13140/RG.2.2.29909.52965

George, M. F., & Sitar, N. (2016b, June 26). *Mechanics of 3D Rock Block Erodibility*. 50th U.S. Rock Mechanics/Geomechanics Symposium. https://onepetro.org/ARMAUSRMS/proceedings-pdf/ARMA16/All-ARMA16/ARMA-2016-848/1329162/arma-2016-848.pdf

George, M. F., Sitar, N., & Sklar, L. (2015). *Experimental Evaluation of Rock Erosion in Spillway Channels*. ARMA-2015-700. https://escholarship.org/uc/item/82s7c2f9

ISRM. (1978). International society for rock mechanics commission on standardization of laboratory and field tests. *International Journal of Rock Mechanics and Mining Sciences & Geomechanics Abstracts*, *15*(6), 319–368. https://doi.org/10.1016/0148-9062(78)91472-9

Jalili Kashtiban, Y., Saeidi, A., Farinas, M.-I., & Quirion, M. (2021). A Review on Existing Methods to Assess Hydraulic Erodibility Downstream of Dam Spillways. *Water*, *13*(22), Article 22. https://doi.org/10.3390/w13223205

Koulibaly, A. S. (2021). *Conception d'un modèle de laboratoire d'un évacuateur de crue pour étudier l'érosion des masses rocheuses* [Masters, Université du Québec à Chicoutimi]. https://constellation.uqac.ca/8100/1/Koulibaly_uqac_0862N_10875.pdf

Koulibaly, A. S., Saeidi, A., Rouleau, A., & Quirion, M. (2022). A Reduced-Scale Physical Model of a Spillway to Evaluate the Hydraulic Erodibility of a Fractured Rock Mass. *Rock Mechanics and Rock Engineering*. https://doi.org/10.1007/s00603-022-03101-5

Li, A., & Liu, P. (2010). Mechanism of rock-bed scour due to impinging jet. *Journal of Hydraulic Research*, *48*(1), 14–22. https://doi.org/10.1080/00221680903565879

Li, K.-W., Pan, Y.-W., & Liao, J.-J. (2016). A comprehensive mechanics-based model to describe bedrock river erosion by plucking in a jointed rock mass. *Environmental Earth Sciences*, *75*(6), 1–17.

Liu, P., Dong, J., & Yu, C. (1998). Fluctuating uplift on rock blocks at the bottom of a scour pool by overfall jets. *Science in China Series E: Technological Sciences*, *41*(2), 130–139. https://doi.org/10.1007/BF02919675

Pan, Y.-W., Li, K.-W., & Liao, J.-J. (2014). Mechanics and response of a surface rock block subjected to pressure fluctuations: A plucking model and its application. *Engineering Geology*, *171*, 1–10. https://doi.org/10.1016/j.enggeo.2013.12.008

Pells, S. E. (2016). *Erosion of Rock in Spillways* [Ph.D. Thesis]. University of South Wales.

Saiang, D., Idris, M. A., & Nordlund, E. (2022). *Block Erosion of Unlined Rock Spillway Canals* (BeFo Report 230). Stiftelsen Bergteknisk Forskning Rock Engineering Research Foundation. https://www.befoonline.org/UserFiles/Archive/5198/BeFo_Report_230_web.pdf

Simoẽs, G. F., Vargas, E. do A., & de Lima, R. T. (1997). Numerical modelling of erosion phenomena in fractured rock masses downstream of spillways. In *Applications of Computational Mechanics in Geotechnical Engineering* (pp. 71–83). CRC Press.

Umumararungu, M. G. (2016). *Physical modelling investigation of rock scour extent due to a plunging jet for typicalhigh head dams* [M.S. Thesis, Faculty of Engineering, Stellenbosch University]. https://scholar.sun.ac.za/handle/10019.1/98521

Velloso, R. Q., Vargas, E. A., Marques, M., Mello Franco, J. A., Canellas, A. V., Simoes, G., & Gusmao, L. (2011). *Experimental and numerical studies of erosion processes downstream of spillways in large dams.* 26–29. https://onepetro.org/ARMAUSRMS/proceedings-abstract/ARMA11/All-ARMA11/ARMA-11-299/120299

ARMA 24–0753

Effect of Joint Orientation on Rock Mass Erosion based on Experimental Results using a Pilot Plant Spillway Model

Karnati, V.R.[1*], Saeidi, A.[2] and Rouleau, A.[3]

Département des sciences appliquées, Université du Québec à Chicoutimi, Chicoutimi, Québec, Canada

Quirion, M.[4]

Hydro-Québec Production Unité Expertise en Barrages intégrée - Géologie, 75 Boulevard René-Lévesque Ouest, Montréal, Québec, Canada

* Author to whom correspondence should be addressed. Email: vineethkarnati@gmail.com

ABSTRACT: Hydraulic rock mass erosion is termed as the gradual removal of intact rock blocks due to excessive erosive forces of flowing water. Understanding the mechanism of this erosion process requires to study the hydraulic pressures on rock block surfaces, especially at the top and bottom of intact blocks. These intricate hydraulic conditions depend on several hydraulic and geomechanical factors. In the current study, the effect of joint orientation on the hydraulic pressures is studied using the pilot plant scale spillway model constructed at Université du Québec à Chicoutimi, Québec, Canada. Two metal boxes were used to vary the orientation of the joints to -45°, 0° and 45° inclinations with respect to the direction of water flow. The 9 blocks are arranged in 3 rows with 3 blocks in each row; the central block is instrumented to measure the hydraulic pressures. The static and dynamic head (H_s + H_d) at the top of block is much higher than that at the bottom of block for 0° orientation arrangement. However, in the case of inclined joints, the pressure at the top of block is found to be almost equal to that at the bottom of block.

1. INTRODUCTION

Hydraulic rock mass erosion is considered critical in the design of hydraulic structures in recent years especially in the case of unlined dam spillways. The stability and safe operation of hydraulic structures is compromised with the higher erosion rates of rock (Gardner, 2023) under flood conditions. Historic erosion cases like the Oroville Dam, California (Koskinas et al., 2019; Wahl et al., 2019), Mokolo Dam in South Africa and Copeton Dam in Australia (Pells, 2016), Ricobayo Dam in Spain (Annandale, 2006) and Spaulding Dam in California (George, 2015) are a few examples of disasters that occurred either under normal operating discharges or flows below the design flow rates. These historical examples illustrate the limitations in existing hydraulic erosion hazard assessment including the mechanism and rate of erosion. The widely used erodibility index method (Annandale, 2006, 2012) is prominent in erosion prediction, given its simplicity. However, due to its empirical nature, it cannot provide the details of the failure modes and mechanisms. Additionally, the resistive capacity of the rock mass given by this method does not incorporate all the hydraulic and geomechanical parameters affecting the erosion process. Other recent empirical methods developed by Pells (2016) also suffer from the similar limitations. The rock mass resistive capacity is governed by the material parameters and the joint characteristics such as joint spacing, joint orientation, shape and volume of the block, joint filling, block protrusion and toughness of the block (Annandale, 2012; Boumaiza et al., 2019; Pells, 2016). Cameron et al. (1986, 1990) have presented various geological aspects of the rock

mass that affect the erosion process and highlighted the headward migration of knickpoint with the erosion towards the spillway crest. Pitsiou (1990) have explained the importance of various parameters of the rock mass discontinuities on the hydraulic erosion process and the importance of a classification of the geological data into different categories based on the spillway type. The hydraulic erosive power depends especially on the velocity of the flow, the stream power dissipation and the bed shear stress (Coleman et al., 2003; Dubinski, 2009). The complex interaction of the flowing water with the spillway bed rock determines the erosion process resulting in a complex erosion mechanism.

Several physical model studies tried to understand the effect of the individual hydraulic and geomechanical parameters on the erosion process, where most of the studies include testing of a single block. Coleman et al. (2003), from their physical model studies pointed out the importance of incorporating block protrusion in the erodibility assessments involving the use of stream power dissipation. A nominal protrusion value can significantly affect the hydraulic pressures around the block and hence the uplift pressures generated on the block (Coleman et al., 2003; Frizell, 2007; Wahl et al., 2019). The physical model tests of Dubinski (2009) explored the possibility of block quarrying under varied flow conditions and concluded that most of the erosive hydraulic power will be expended by the removal of some key blocks that shall trigger further erosion. His studies focused on the effect of joint opening and the associated model block size. George and Sitar (2016) studied several failure modes of a tetrahedral block oriented in several directions and subjected to flows with varying degrees of turbulence intensities and varying flow velocities.

The mechanisms of the hydraulic rock mass erosion process are well explained by the Comprehensive Scour Model (CSM) proposed by Bollaert (Bollaert, 2004, 2010, 2016) based on physical model tests. Plucking is found to be the most important mechanism especially in the site conditions with sub-meter blocks (size less than a meter) (Li et al., 2016; Pan et al., 2014). Umumararungu (2016) applied CSM approach and studied the effects of the shape and size of the blocks in the erosion process using a 1:40 scale physical model and proposed quantitative methods to determine the scour hole dimensions in plunging jet spillways. Simoẽs et al. (1997) presents an example of hydromechanical coupling to determine the possibility of uplift of a single block using finite element modelling. Liu et al. (1998) studied the pressure fluctuations as a function of block size and the tail water depth using a model of scale 1:100. Several case specific numerical models have been developed to predict the erosion depth under the plunge pool (Dasgupta et al., 2011; A. Li & Liu, 2010; Moren & Sjoberg, 2007). Application of these methods to parallel flow spillway requires modification of these methods to adapt for the changes in the flow conditions. This study focuses on studying the impact of the changes in joint orientation on the hydraulic pressures around the rock blocks based on the pilot-plant scale spillway model tests.

2. PILOT-PLANT SPILLWAY MODEL

Fig. 1 presents the pilot-plant spillway model constructed at Université du Québec à Chicoutimi (UQAC), Canada that permits studying the effect of various hydraulic and geomechanical aspects involved in the hydraulic rock mass erosion process. The comprehensive specifications and technical design details of the spillway model scaled down at the ratio of 1:40 from Romaine IV Hydro-Québec spillway can be found in (Koulibaly, 2021; Koulibaly et al., 2023). This model, with a inclination of about 9^{o}, is equipped with metal containers at the end of the spillway channel that supports concrete blocks mimicking isolated rock blocks with continuous joints. Nine concrete blocks each measuring 15 cm x 15 cm x 30 cm are arranged in a 3 x 3 matrix, as depicted in Fig. 1 (b), out of which the central block is instrumented with internal copper tubes to measure the pressure distribution around it. The discharge within the channel is regulated by adjusting the operating frequency of the submersible pump that pumps water from downstream reservoir to the upstream reservoir above the channel generating a manometric head.

The specially designed instrumented block presented in Fig. 2 is equipped with 11 internal copper tubes that allow the flow of water within them. These tubes incorporate elbows at both ends to serve as hydraulic inlets and outlets. The top and bottom faces of the block are termed as A and B, respectively. The lateral faces upstream and downstream of the block are termed C and D, respectively, and the other lateral faces are termed E and F. The inlet elbow on the top of the block is oriented in the direction opposite to the flow so that it allows for the measurement of total

pressure including the dynamic pressure. Two inlets are used in each lateral joint with elbows placed towards the top and bottom surfaces of the block index as 1 and 2, respectively. For example, the elbows on face C are termed as C1 and C2, where C1 is facing top and C2 is facing bottom. The elbows at the bottom of the block are placed towards the upstream and downstream of the channel, termed as Bc and Bd, respectively. The hydraulic outlets of all the inlets are situated on the top of the block which are connected to pressure transducers of suitable capacity with the help of tight connecting tubes.

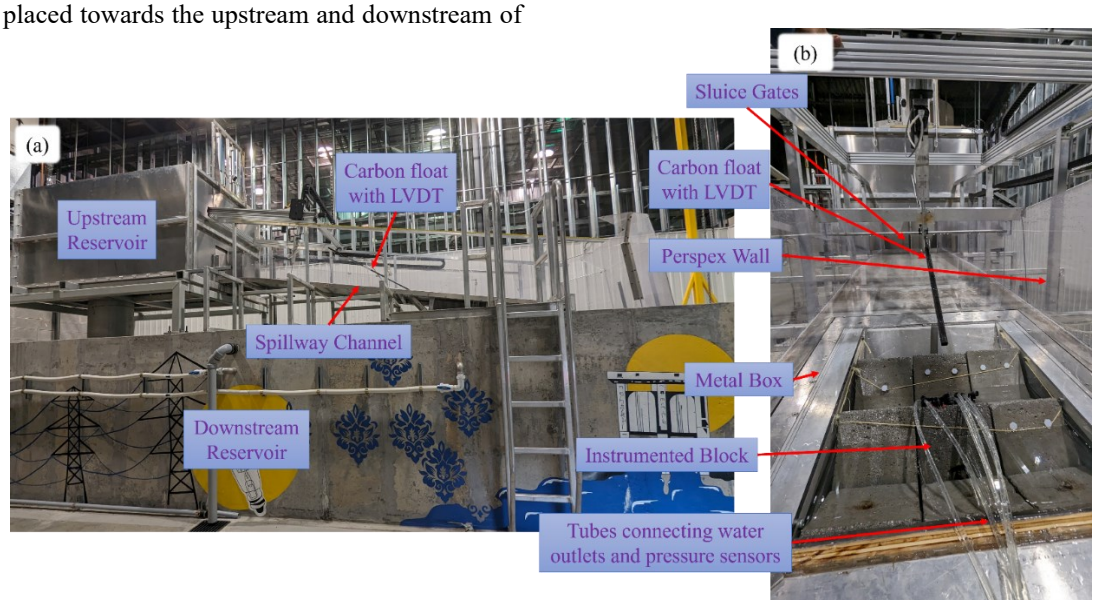

Fig. 1. Pilot-plant spillway model: (a) side view of the model and (b) channel view from the downstream

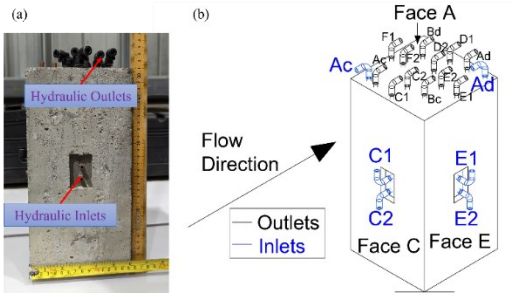

Fig. 2. Specifications of the instrumented block: (a) model concrete block exhibiting hydraulic inlets and outlets of internal copper tubes and (b) Isometric view presenting the hydraulic inlets and outlets.

3. SPILLWAY MODEL TESTING PLAN

The aim of this study is to investigate the effect of joint orientation on the hydraulic pressures around the block. In order to achieve this, a preliminary selection of three joint orientations of one of the orthogonal joint sets: – 45º, 0º and + 45º, respectively with the flow direction is made as presented in Fig. 3. These orientations represent the extreme conditions of the inclined blocks for the chosen block aspect ratio that the height of the block is more than the width or length of the block. A constant joint opening of 10 mm is provided all around the blocks in all orientations to present the continuous joints around the block, which is achieved by using Teflon bolts as spacers. To capture the fluctuations in the pressures, several data collection frequencies are tested and concluded that 100 Hz data collection frequency captures the pressure fluctuations with reasonable accuracy. The 0º inclination involves the blocks arranged in the metal box with their height dimensions placed perpendicular to the flow direction as shown in Fig. 3(b). For arrangement of blocks in – 45º inclination, a different metal box is used with necessary triangular wedge supports at their bottom as shown in Fig. 3(a). To arrive at + 45º inclination, the box is rotated about 180º in the spillway model. An important observation to be made in the arrangements of – 45º and + 45º is that the top surface is not parallel to the flow direction and hence for obtaining the pressure distribution along the surface the pressure needs to be measured at least at two locations. Hence the testing in these orientations (– 45º and + 45º) is repeated twice by rotating the instrumented block by 180º in its position to allow the measurement in two locations. The pressure results on the top of the block with the hydraulic inlet close to the faces C and D are termed as "Ac" and "Ad", respectively.

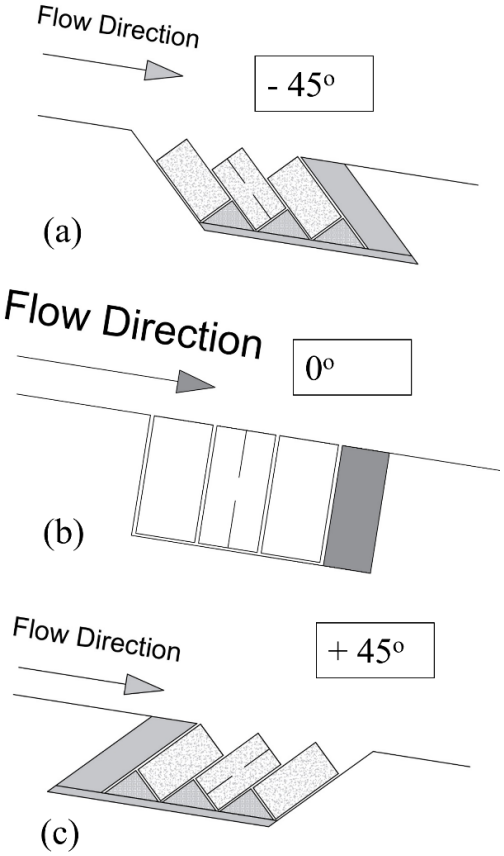

Fig. 3. Block arrangements in various test conditions: (a) – 45º inclination, (b) 0º inclination and (c) + 45º inclination.

Once the blocks are arranged in position, they are subjected to the flow with various flow rates ranging from 0.18 m^3/s to 0.4 m^3/s; however, only the results of the tests with flow rate 0.18 m^3/s are presented in this article. The total head data obtained from each hydraulic inlet is corrected for the datum head which is equal to the vertical difference between the respective hydraulic inlets as presented in Fig. 4 (water entry, A in 0º inclination) and the sensor level obtained from the AutoCAD detailing. The test results of the static + dynamic heads at each position along the instrumented block are presented in the following sections.

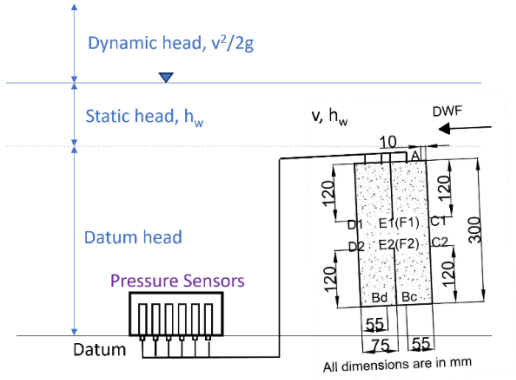

Fig. 4. Presentation of different pressure heads recorded.

4. MODEL TEST RESULTS

4.1 Pressure head fluctuations on the top of the instrumented block

The corrected pressure head fluctuations for the top of the block in various test configurations are presented in Fig. 5. The results indicate that the pressure on the top of the block is reduced when the blocks are inclined which is the result of stagnation pressures developed at the height of the inversed triangular space on the top of the blocks serving as a block protrusion. These pressure head distributions exhibit a normal distribution and hence a presentation of variation of mean value and standard deviation of these pressure results as a function of block inclination would give a better picture as compared to a temporal variation.

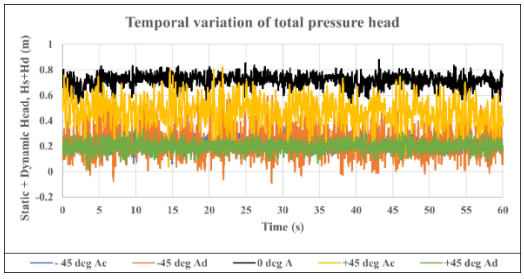

Fig. 5. Temporal variation of static + dynamic head for different block inclinations on the top of the block, i.e., face A.

The variation of mean head and standard deviation of the pressure head data on the top of the block are presented in Figure 6 in which the error bars present the standard deviation. The results of inlet A for 0° inclination are used for both the curves in Fig. 6 since, in this inclination, the variation along the surface is found negligible during the preliminary tests and testing is carried out only at Ac. The lengths of error bars of Ac and Ad are approximately interchanged for the inclinations – 45° and + 45° which indicates the higher standard deviation of the pressure results close to the spillway surface (Ad in – 45° and Ac in + 45° orientations) and lower values away from it. The length of error bars for 0° inclination is slightly higher than those of inlets away from the spillway surface and very less than those of inlets near the spillway surface. The lesser standard deviation in 0° inclination could be attributed to the no protrusion of blocks in this arrangement which do not arise the higher pressure fluctuations.

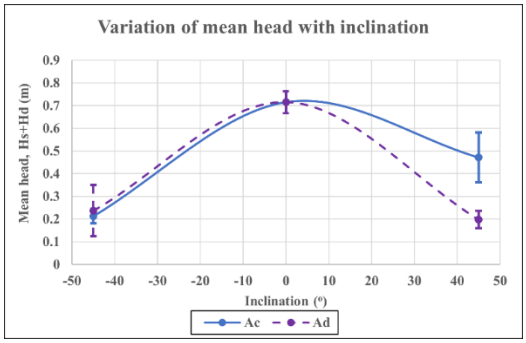

Fig. 6. Variation of mean and standard deviation of pressure head on the top of the block, i.e. face A.

4.2 Pressure head fluctuations on the bottom of the instrumented block

The corrected pressure head fluctuations for the bottom of the block in various test configurations are presented in Fig. 7. The variation of the mean values and standard deviation of the pressure head data at the bottom of the block as a function of block inclinations is presented in Fig. 8. Fig.s 7 and 8 show that the pressures at the bottom of the block are higher in – 45° inclination than those at 0° inclination which are in turn higher than those at + 45° inclination. This is related to the easy flow entrainment into the joints in – 45° block arrangement as compared to the other arrangements. Importantly, the fluctuations observed in the inclined block conditions are huge compared to those at 0° block arrangement.

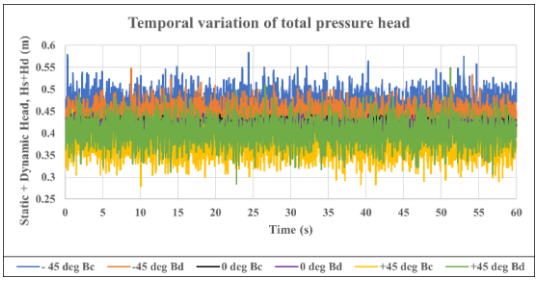

Fig. 7. Temporal variation of static + dynamic head for different block inclinations on the bottom of the block, i.e., face B.

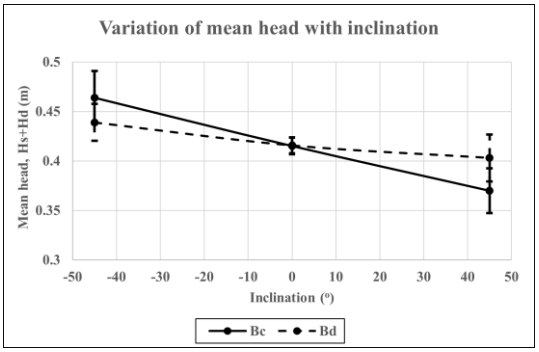

Fig. 8. Variation of mean and standard deviation of pressure head on the bottom of the block, i.e. face B.

4.3 Pressure head fluctuations on the lateral faces of the instrumented block

The mean and standard deviation of the pressure head fluctuations on the opposite lateral faces of the block are presented in Fig.s 9 and 10. The hydraulic inlets D1 in the case of – 45° inclination and C1 in the case of + 45° inclination are completely exposed to the flowing water and not within the joint but at a knickpoint; whereas the inlets D2 in the case of – 45° inclination and C2 in the case of + 45° inclination are facing in the direction of flow which could not result in lesser dynamic heads due to the generation of eddies at these inlets. However, the standard deviation of all the pressure fluctuations in the cases of inclined arrangements are found to be approximately similar. These pressures on the faces C and D in the case of 0° inclination are approximately similar with very few pressure fluctuations as that of the bottom of the block.

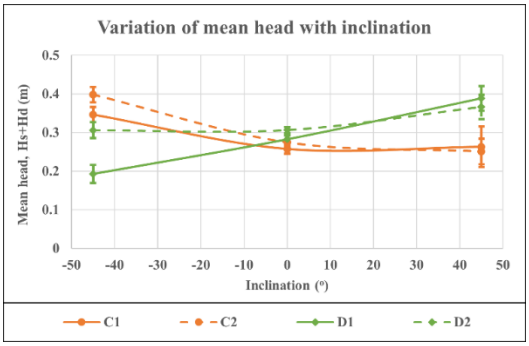

Fig. 9. Variation of mean and standard deviation of pressure head on the lateral sides of the block, i.e. faces C and D.

The hydraulic inlets on both the faces E and F are completely within the joints and hence the pressure results are approximately similar. However, small differences in the mean values are observed which arise due to the difference in the vertical position of the hydraulic inlets (E1 & E2 and F1 & F2) resulting in smaller pressure differences. However, the standard deviation values for the inclined block conditions are similar indicating similar pressure fluctuations.

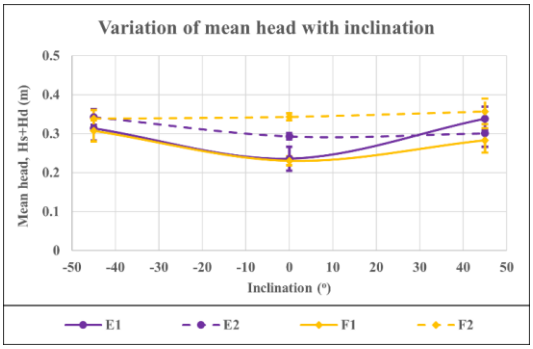

Fig. 10. Variation of mean and standard deviation of pressure head on the lateral sides of the block, i.e. faces E and F.

5. CONCLUSIONS

The hydraulic rock mass erosion process in the parallel flow spillways is dominated by the fluctuating hydraulic pressures and the amount of shear stress transferred by the flowing water to the rock mass. These hydraulic forces are in turn dependent on several hydraulic and geomechanical conditions of the spillway site. In this study, the effect of joint orientation is studied using a pilot-plant scale spillway model tests by varying the orientation of one of the orthogonal joint sets as – 45°, 0° and + 45° with the flow direction. The preliminary test results presented indicated that the pressures on the top of the block

and within the joints are severely affected with the inclination of the blocks. The reason for this behavior could be attributed to the development of stagnation pressures at the protruded surface formed from the inclined blocks at the top and further flow separations at the knickpoints. The fluctuations in the pressures at the top of the block and within the joints are found to be increasing in the inclined conditions as compared to the 0° inclination. The reduction of pressures at the top of the block and augmentation of pressures within the joints for the inclined test conditions present with the higher possibility of block uplift. The + 45° inclination is found to be more critical for block uplift to occur as explained with the Edoa factor of the eGSI method (Pells, 2016) and the J_s parameter of Kirsten index (Kirsten, 1982). The experimental tests made with pilot-plant model serve as a valuable source of validation of numerical models that shall estimate the pressure values around the blocks in real spillway scenarios. Further tests in the near future on various inclinations and the numerical modelling will yield the exact effect of joint orientation on the erosion process.

ACKNOWLEDGEMENTS

The authors acknowledge the Natural Sciences and Engineering Research Council of Canada and Hydro-Québec (NSERC, Hydro-Québec [CRDPJ 537350 – 18] and NSERC [RGPIN-2019-06693]. The authors also acknowledge the *Fonds de Recherche du Québec Nature et technologies* for granting the *programme de bourses d'excellence pour étudiants étrangers (PBEEE)* scholarship (Grant No.: 2023-2024 - 1I - 334721) for this research. The authors are highly indebted to the R2Eau research group at the *Université du Québec à Chicoutimi* for their valuable suggestions during our research.

REFERENCES

1. Annandale, G. W. (2006). *Scour technology: Mechanics and engineering practice*. McGraw Hill Professional.
2. Annandale, G. W. (2012). *Current state-of-the-art Rock Scouring Technology*. 1–12. https://doi.org/10.1061/40911(230)2
3. Bollaert, E. (2004). A comprehensive model to evaluate scour formation in plunge pools. *International Journal on Hydropower & Dams*, *11*(1), 94–101.
4. Bollaert, E. (2010). The comprehensive scour model: Theory and feedback from practice. *Proceedings of the 5th International Conference on Scour and Erosion*, 7–10.
5. Bollaert, E. (2016, September 12). *Simplified Comprehensive Scour Model compared to Erodibility Index Method*. ICSE 2016 (8th International Conference on Scour and Erosion), Oxford, UK. https://eprints.hrwallingford.com/1028/
6. Boumaiza, L., Saeidi, A., & Quirion, M. (2019). A method to determine relevant geomechanical parameters for evaluating the hydraulic erodibility of rock. *Journal of Rock Mechanics and Geotechnical Engineering*, *11*(5), 1004–1018. https://doi.org/10.1016/j.jrmge.2019.04.002
7. Cameron, C. P., Cato, K. D., McAneny, C. C., & May, J. H. (1986). *GEOTECHNICAL ASPECTS OF ROCK EROSION IN EMERGENCY SPILLWAY CHANNELS* (Report 1). Department of the Armt Waterways Experiment Station, Corps of Engineers. https://apps.dtic.mil/sti/pdfs/ADA173163.pdf
8. Cameron, C. P., Patrick, D. M., May, J. H., Palmerton, J. B., McAneny, C. C., Hatheway, A. W., Bartholomew, C. O., Mathewson, C. C., & Cato, K. D. (1990). Geotechnical aspects of rock erosion in emergency spillway channels. Report 5, Summary of results, conclusions, and recommendations. In *This Digital Resource was created from scans of the Print Resource.* (Report 5). Geotechnical Laboratory (U.S.) Engineer Research and Development Center (U.S.). http://hdl.handle.net/11681/4458
9. Coleman, S. E., Melville, B. W., & Gore, L. (2003). Fluvial Entrainment of Protruding Fractured Rock. *Journal of Hydraulic Engineering*, *129*(11), 872–884. https://doi.org/10.1061/(ASCE)0733-9429(2003)129:11(872)
10. Dasgupta, B., Basu, D., Das, K., & Green, R. (2011, April). Development of computational methodology to assess erosion damage in dam spillways. *31st Annual United States Society on Dam Conference*.
11. Dubinski, I. M. (2009). Physical modeling of jointed bedrock erosion by block quarrying [Ph.D. Thesis, Colorado State

University]. In *ProQuest Dissertations and Theses* (304861260). ProQuest Dissertations & Theses Global. https://sbiproxy.uqac.ca/login?url=https://www.proquest.com/dissertations-theses/physical-modeling-jointed-bedrock-erosion-block/docview/304861260/se-2?accountid=14722

12. Frizell, W. (2007). *Uplift and Crack Flow Resulting from High Velocity Discharges over Open Offset Joints—Laboratory Studies* (Report 12-2007). U.S. Dept. of the Interior, Bureau of Reclamation. https://www.usbr.gov/damsafety/TechDev/DSOTechDev/DSO-07-07.pdf
13. Gardner, M. (2023). Toward a Complete Kinematic Description of Hydraulic Plucking of Fractured Rock. *Journal of Hydraulic Engineering*, *149*(7), 04023015. https://doi.org/10.1061/JHEND8.HYENG-13193
14. George, M. F. (2015). *3D Block Erodibility: Dynamics of Rock-Water Interaction in Rock Scour* [Ph.D. Thesis, University of California, Berkeley]. https://escholarship.org/uc/item/61q7798m
15. George, M. F., & Sitar, N. (2016, June). Mechanics of 3D Rock Block Erodibility. *50th U.S. Rock Mechanics/Geomechanics Symposium*. https://onepetro.org/ARMAUSRMS/proceedings-pdf/ARMA16/All-ARMA16/ARMA-2016-848/1329162/arma-2016-848.pdf
16. Kirsten, H. A. D. (1982). A classification system for excavating in natural materials. *Civil Engineering = Siviele Ingenieurswese*, *1982*(7), 293–308. https://doi.org/10.10520/AJA10212019_15379
17. Koskinas, A., Tegos, A., Tsira, P., Dimitriadis, P., Iliopoulou, T., Papanicolaou, P., Koutsoyiannis, D., & Williamson, T. (2019). Insights into the Oroville Dam 2017 Spillway Incident. *Geosciences*, *9*(1), 37. https://doi.org/10.3390/geosciences9010037
18. Koulibaly, A. S. (2021). *Conception d'un modèle de laboratoire d'un évacuateur de crue pour étudier l'érosion des masses rocheuses* [Masters, Université du Québec à Chicoutimi]. https://constellation.uqac.ca/8100/1/Koulibaly_uqac_0862N_10875.pdf
19. Koulibaly, A. S., Saeidi, A., Rouleau, A., & Quirion, M. (2023). A Reduced-Scale Physical Model of a Spillway to Evaluate the Hydraulic Erodibility of a Fractured Rock Mass. *Rock Mechanics and Rock Engineering*, *56*, 933–951. https://doi.org/10.1007/s00603-022-03101-5
20. Li, A., & Liu, P. (2010). Mechanism of rock-bed scour due to impinging jet. *Journal of Hydraulic Research*, *48*(1), 14–22. https://doi.org/10.1080/00221680903565879
21. Li, K.-W., Pan, Y.-W., & Liao, J.-J. (2016). A comprehensive mechanics-based model to describe bedrock river erosion by plucking in a jointed rock mass. *Environmental Earth Sciences*, *75*(6), 1–17.
22. Liu, P., Dong, J., & Yu, C. (1998). Fluctuating uplift on rock blocks at the bottom of a scour pool by overfall jets. *Science in China Series E: Technological Sciences*, *41*(2), 130–139. https://doi.org/10.1007/BF02919675
23. Moren, L., & Sjoberg, J. (2007, July). Rock Erosion In Spillway Channels-A Case Study of the Ligga Spillway. *11th ISRM Congress*.
24. Pan, Y.-W., Li, K.-W., & Liao, J.-J. (2014). Mechanics and response of a surface rock block subjected to pressure fluctuations: A plucking model and its application. *Engineering Geology*, *171*, 1–10. https://doi.org/10.1016/j.enggeo.2013.12.008
25. Pells, S. E. (2016). *Erosion of Rock in Spillways* [Ph.D. Thesis]. University of South Wales.
26. Pitsiou, S. (1990). *The effect of discontinuities on the erodibility of rock in unlined spillways of dams* [M.S. Thesis, University of Pretoria]. https://repository.up.ac.za/handle/2263/37300
27. Simoẽs, G. F., Vargas, E. do A., & de Lima, R. T. (1997). Numerical modelling of erosion phenomena in fractured rock masses downstream of spillways. In *Applications of Computational Mechanics in Geotechnical Engineering* (pp. 71–83). CRC Press.
28. Umumararungu, M. G. (2016). *Physical modelling investigation of rock scour extent due to a plunging jet for typicalhigh head dams* [M.S. Thesis, Faculty of Engineering,

Stellenbosch University]. https://scholar.sun.ac.za/handle/10019.1/98521

29. Wahl, T. L., Frizell, K. W., & Falvey, H. T. (2019). Uplift Pressures below Spillway Chute Slabs at Unvented Open Offset Joints. *Journal of Hydraulic Engineering*, *145*(11), 04019039. https://doi.org/10.1061/(ASCE)HY.1943-7900.0001637

Hydraulic Pressure Distribution on Inclined Rock Blocks using an Experimental Spillway Model

Vineeth Reddy Karnati, Ali Saeidi & Alain Rouleau
Département des sciences appliquées, Université du Québec à Chicoutimi, Chicoutimi, QC G7H 2B1, Canada
Marco Quirion
Hydro-Québec, Expertise intégrée – Géologie, Direction Sécurité des barrages et infrastructures, 75 Boul. René-Lévesque Ouest, Montréal, QC H2Z 1A4, Canada

ABSTRACT
The hydraulic rock mass erosion involves a complex hydrogeological process influenced by several factors such as flow parameters, rock-mass parameters, and environmental conditions, that requires an accurate understanding of the fluctuating hydraulic pressure around the rock blocks under several hydraulic and geomechanical conditions. In this study, the effect of joint orientation on the hydraulic pressure fluctuations around modeled blocks is studied using reduced-scale spillway model tests. The blocks are arranged in a 3x3 matrix at different joint orientations of -45º, 0º, and +45º to the spillway surface. The value of dynamic pressure at the top of the blocks for inclined blocks is observed to be much lower compared to the blocks with 0º inclination. However, the pressure at the bottom is found to be less affected compared to that at the top of the instrumented block.

RÉSUMÉ
L'érosion hydraulique des masses rocheuses implique un processus hydrogéologique complexe influencé par plusieurs facteurs tels que les paramètres hydrauliques, ceux de la masse rocheuse et les conditions environnementales, qui nécessitent une bonne compréhension de la pression hydraulique fluctuante autour des blocs rocheux dans plusieurs conditions hydrauliques et géomécaniques. Dans cet article, l'effet de l'orientation des joints sur les fluctuations de la pression hydraulique autour des blocs modélisés est étudié à l'aide d'essais sur un modèle d'évacuateur de crues à échelle réduite. Les blocs sont disposés dans une matrice 3x3 selon différentes orientations des joints de -45º, 0º et +45º par rapport à la surface de l'évacuateur de crue. La valeur de la pression dynamique en haut des blocs pour les blocs inclinés s'avère bien inférieure à celle des blocs avec une inclinaison de 0°. Cependant, la pression en bas s'avère moins affectée par rapport à celle en haut du bloc instrumenté.

1. INTRODUCTION

Hydraulic structures have been experiencing severe safety concerns in terms of hydraulic rock mass erosion in recent years. Increase in the erosion rate under flood conditions pose significant threat to their stability and their safe operation (Gardner 2023). Several historical disasters as observed in the case of Ricobayo Dam spillway in Spain (Annandale 2006), Spaulding Dam spillway in California, USA (George 2015), Mokolo Dam spillway in South Africa and Copeton Dam spillway in Australia (Pells 2016) and recently Oroville Dam spillway in California, USA (Koskinas et al. 2019, Zhang et al. 2024) urge the researchers to explore further into the mechanisms of this hydraulic rock mass erosion process. These historic erosion cases are observed under both normal and flood operating conditions which signify that the erosion process depends on several complex factors other than the flow conditions. In most cases the erodibility of rock mass is assessed using empirical methods that relate the resistive capacity of rock mass with the hydraulic erosive power under different flow conditions. Several existing dam spillways in the world are designed based on the widely used Annandale's method (Annandale et al. 1995, Annandale 2012) due to the simplicity in its application. However, wide differences have been noted between the predicted values based on this method and the actual erosion values observed in the field. The reason behind this behaviour is attributed to the empirical nature of this method which uses the Kirsten index (Kirsten 1982) to represent the resistive capacity of the rock mass against the hydraulic erosive forces. This index was originally developed for assessing the excavatability of geomaterials which was later modified to study the hydraulic erodibility of the rock mass (Boumaiza 2019). Thus, this method cannot provide different failure mechanisms under the hydraulic forces. Additionally, the Kirsten index

do not incorporate all the important geomechanical parameters that affect the erosion process (Boumaiza et al. 2019, Kashtiban et al. 2021).

Recently, Pells (2016) proposed two different semi-empirical approaches based on more than 100 spillway erosion case studies to assess the resistive capacity of rock mass. The first approach is to use the Erosion Geological Strength Index (eGSI) (Pells et al. 2015) which is modified from the Geological Strength Index (GSI) developed by Marinos and Hoek (2000). The eGSI approach involves the determination of GSI value for a given site condition based on the look up chart provided by Marinos and Hoek (2000) to which an additional term, erosion discontinuity orientation adjustment (E_{doa}) factor is added to include the effect of joint orientation and the relative block size formed by different joint sets. The second approach involves the use of Rock Mass Erodibility Index (RMEI) which is calculated as the product of Likelihood factors (LF) and the relative importance factor (RF) for different parameters, the details of which can be found in Pells (2016). The erosion assessment using the RMEI approach proposed by Pells is modified by Douglas et al. (2018). These semi-empirical approaches proposed by Pells (2016) also suffer from similar limitations as that of Annandale's approach. The differences are attributed to the variation in the assessment of the geomechanical parameters by different field engineers (Boumaiza et al. 2019, Kashtiban et al. 2021).

The significant problem with the semi-empirical approaches is that they do not explain the mechanisms of the erosion process. The mechanisms of this erosion process are better understood from the Comprehensive Scour Model (CSM) presented by Bollaert (2004, 2010, 2016) which is based on the physical plunge pool model tests. These mechanisms include dynamic impulsion (plucking) and quasi-static impulsion which are dependent on the hydraulic pressure distribution around an intact rock block with continuous joints. These processes have been found to be more prominent in the rock blocks of size less than a meter (Pan et al. 2014, Li et al. 2016). The quantification of the erosion process to determine the scour hole dimensions in plunging jet spillways is made by Umumararungu (2016) using a 1 :40 scaled down physical model and studied the effect of the shape and size of the blocks. This CSM approach requires modifications to be applied for a parallel flow type spillway. Various geological aspects of the rock mass that affect the erosion process is presented by Cameron et al. (1986, 1990). They have highlighted the headward migration of the knickpoint towards the spillway crest as the erosion progresses. The importance of several rock mass parameters and their classification into different categories based on the spillway type is explained by Pitsiou (1990). Liu et al. (1998) carried out the physical plunge pool model tests at a scale of 1:100 to study the pressure fluctuations as a function of rock block size and tail water depth. The hydraulic erosive power is determined by several parameters like flow velocity, stream power dissipation and bed shear stress (Coleman et al. 2003, Dubinski 2009). The hydraulic pressure distribution around the rock block is dependent on several geomechanical parameters such as joint spacing, joint orientation, joint aperture & filling, block shape, volume, block protrusion and toughness of the block (Annandale 2012, Pells et al. 2015, Boumaiza et al. 2019).

Several physical model tests are used to understand the effect of the individual hydraulic and geomechanical parameters on the erosion process; however, most of these studies are carried out on a single model block. The importance of implying the block protrusion in erosion assessment is pointed out by Coleman et al. (2003). A nominal value of block protrusion can affect significantly the hydraulic pressures and thus the uplift pressures generated on the block (Frizell 2007, Wahl et al. 2019). The possibility of block quarrying under different flow conditions is explored by Dubinski (2009) through physical model testing. His studies that focused on the effect of joint opening and associated size of model block concluded that significant amount of erosive energy is expended for the removal of a few key blocks triggering further erosion. The effect of orientation and several failure modes of a tetrahedral block under flow conditions of varied turbulence intensities and flow velocities are studied using the physical model testing carried out by George (George 2012, 2015, George et al. 2015, George and Sitar 2016). The model studies cannot reflect the turbulent intensities generated by the actual dam spillways due to the reduced-scale modelling (Bollaert 2002); however, they provide a better source of data to validate the numerical simulations applied to real field scenarios. Simoẽs et al. (1997) presented a methodology to carry-out hydromechanical coupling of the complex hydro-geomechanical process to model the uplift of a single block using finite element modelling (FEM). Recently several case specific numerical models have been developed to assess the erosion depth under the plunge pools (Moren and Sjoberg 2007, Li and Liu 2010, Dasgupta et al. 2011). Application of these methods to the parallel flow spillway conditions demands their modification to adapt for different flow conditions. Gardner (2023) developed a coupled hydrogeomechanical model to predict the erosion depth in the parallel flow spillways using the experimental data of George (2015). The aim of this article is to study the effect of joint

orientation on the variation of hydraulic pressures around an intact rock block using a pilot plant scale spillway model scaled at 1:40, the results of which will be useful in the validation of the coupled numerical model under development.

2. REDUCED-SCALE SPILLWAY MODEL

A reduced-scale spillway model scaled of one of Hydro-Québec dams, Romaine IV, spillway at a ratio of 1:40 using the Froude similitude criterion (Koulibaly 2021, Koulibaly et al. 2023) is constructed at Université du Québec à Chicoutimi (UQAC), Canada. The physical model presented in Figure 1 permits studying the effect of several important parameters involved in the hydraulic rock mass erosion process. The model consists of a spillway channel inclined at about 9° with the horizontal with vertical walls made of Perspex glass. The end of the channel is equipped with openings that support metal containers as presented in Figure 1(a). These metal containers support 9 concrete blocks, each measuring 15 cm x 15 cm x 30 cm arranged in a 3x3 matrix, as depicted in Figure 1(b). The metal containers are modified to allow for the blocks to be arranged in different inclinations. Out of the 9 concrete blocks, the central block is instrumented using internally connected copper rods that allow the measuring of pressure distribution around it. The blocks are positioned with a specified joint opening between them, using Teflon bolts, simulating continuous joints around the intact rock blocks. The water from the downstream reservoir is pumped into the upstream reservoir using a submersible pump, the water is then allowed into the spillway channel by opening the sluice gates at the bottom of the upstream reservoir. The water flowing in the channel carries both potential and kinetic energy which shall be transferred to the simulated rock blocks and finally reaches the downstream reservoir. The physical model is equipped with a carbon float and an ultrasound sensor that measure the water level in the channel close to the instrumented block that provides the static head above the channel level.

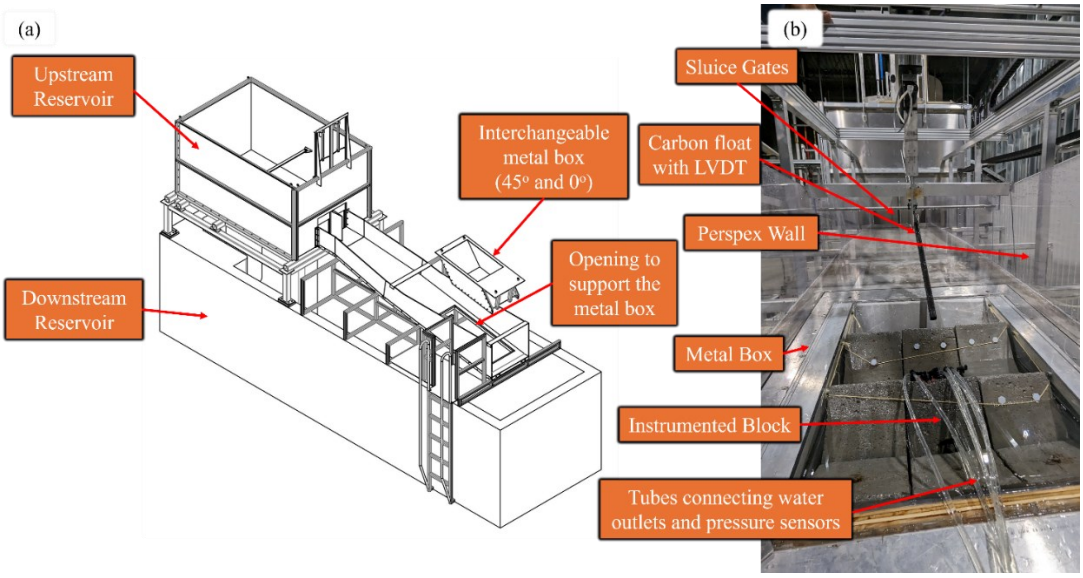

Figure 1. Reduced-scale spillway model: (a) Schematic of the model (modified from (Koulibaly et al. 2023)); (b) Channel view from downstream of the model

By varying the operating frequency and sluice gate opening, the manometric head between the upstream and downstream reservoir is varied which is related to the discharge in the channel (provided by the operator). The details regarding the instrumented block are depicted in Figure 2. This block is equipped with 12 internal copper tubes to measure hydraulic pressure at a minimum of two points on each face of the block. The inlets of the copper tubes are connected with elbows to simulate the conditions of miniature pitot tubes that allow the measurement of both static and dynamic head of the flow within the joints (Wisse et al. 2023).

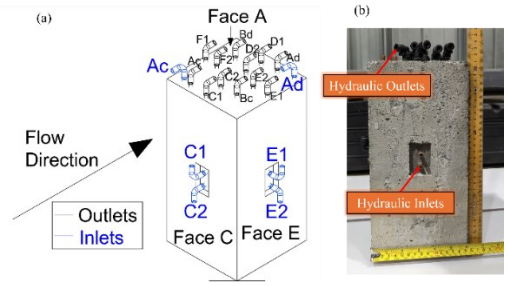

Figure 2. Description of instrumented block: (a) Isometric view and (b) model concrete block pointing out the inlets and outlets of the copper tubes

The top and bottom faces of the instrumented block are called faces A and B respectively, whereas the lateral faces upstream and downstream of the flow are called faces C and D respectively. The other lateral faces parallel to the flow are called E and F. Each of the two elbows on the top and bottom faces are pointed towards the faces C and D and are respectively called Ac & Ad on the top and Bc & Bd on the bottom. On the lateral faces of the block, the elbows are pointed towards the top and bottom as depicted in Figure 2(a) and are respectively indexed 1 and 2 on each face. All the outlets of the copper tubes are situated on the top of the block which are connected to the pressure transducers of suitable capacity, positioned outside of the channel, by means of air-tight connecting tubes (Figure 1(b)).

3. TESTING METHODOLOGY

The objective of this study is to examine the effect of the orientation of the joint sets on the hydraulic pressure distribution around the intact rock block with continuous joints. A preliminary selection of 3 orientations: - 45º, 0º, and + 45º are chosen for the physical model testing. The arrangement of the blocks is presented in Figure 3 for different inclinations. These orientations are the extreme conditions of the inclined blocks that allow the uplifting in the height dimension for the chosen block aspect ratio. In each arrangement, the metal containers are designed such that the top end of the blocks is exactly at the level of the spillway channel bottom. Triangular support blocks are used in the - 45º and + 45º inclinations as presented in Figures 3(b) and 3(c). A constant joint aperture of 3 mm is provided between the adjacent blocks and a constant aperture of 10 mm is provided at the bottom of the blocks to allow for the positioning of the elbows. The pressure fluctuations are studied under varied data collection frequencies; it is concluded that 100 Hz frequency is suitable to represent the actual distribution. Hence the pressure data is collected for 60 s period at this chosen data collection frequency. For the 0º inclination condition, the hydraulic inlets Ac and Ad presented the similar results during the preliminary trial tests and hence the data collection is made only for the Ac during the actual tests. Once the blocks are arranged in position, the flow rates ranging from 0.18 m^3/s to 0.34 m^3/s are used to study the pressure distribution around the blocks. However, the test results of only 0.18 m^3/s are presented in this paper.

The positioning of elbows in the lateral joints requires a minimum joint opening of 10 mm. As the available joint opening is only 3 mm under current testing conditions, the elbows are not provided in the lateral faces and the pressure measurement is made only on the top and bottom of the block. The total head data obtained from each point of measurement is corrected for datum and static heads to obtain the dynamic head. The test results of the dynamic head at top and bottom of the block are presented in the following sections.

4. MODEL TEST RESULTS

The hydraulic pressure data measured from the physical model testing is corrected for datum and static heads to obtain the dynamic head at top and bottom of the block.

4.1 Hydraulic Pressure Fluctuations on the Top and Bottom of the Block

The dynamic head fluctuations on the top and bottom of the block in various inclination conditions along with respective 100 period moving averages are presented in Figures 4 and 5 respectively. Figure 4 depicts that the dynamic head on the top is decreasing for the inclined conditions with the highest values at 0º inclination. The reason for this reduction is attributed to the occurrence of flow separation at the protruded part of the triangular portion of inclined block as observed from Figures 3(b) and 3(c). It is also noted that the pressure on the top close to the spillway surface is having more fluctuations in inclined testing conditions. Figure 5 depicts that there is no huge difference on the pressures at the bottom of the block (within the joint) with change in inclination. However, there is an increase in the pressure fluctuations with inclination.

4.2 Variation of Mean and Standard Deviation of the Dynamic Head and the Top and Bottom of the Block

The temporal variations presented in Figures 4 and 5 for each hydraulic inlet at different orientations are found to be following a normal distribution and hence the presentation of each fluctuation as mean and standard deviation for different inclinations is considered optimal. Each dynamic head variation is analysed to obtain the mean dynamic head and the standard deviation of the pressure data. The variations of the mean dynamic head with inclination for the top and bottom of the block are presented in Figure 6 where the error bars indicate the standard deviation of each pressure data. Figure 6 depicts that the pressure on the top of the block is more affected by the inclination of the joint than those at the bottom of the block and little higher standard deviation values are noticed for the hydraulic inlets Ad and Bd as compared to those of the inlets Ac and Bc respectively.

4.3 Analysis of Possibility of Block Uplift

The critical condition of the occurrence of block uplift is the case when a lower pressure on the top occurs at the same time as a higher pressure on the bottom of the block. To analyze the possibility of block uplift, the variation of mean values with error bars pointing the minimum and maximum values obtained in the pressure measurement as a function of the block inclination is presented in Figure 7. Figure 7 depicts that there is no possibility of block uplift at 0º inclination as the pressure on the top of the block is always higher than that at the bottom of the block, whereas under - 45º and + 45º inclination conditions, the pressure on the top is falling below the pressure on the bottom of the block resulting in uplift pressures at various instants. Also, it is observed that in inclined testing conditions, the dynamic pressure on the top of the blocks is found to be negative indicating the possibility of the development of cavitation.

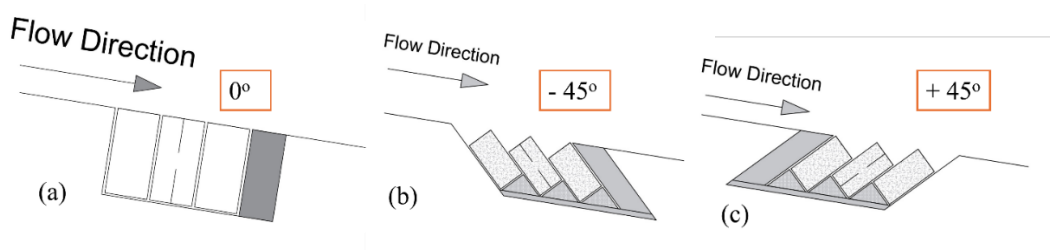

Figure 3. Schematic of the block arrangement in various inclinations tested: (a) 0º, (b) - 45º, and (c) + 45º

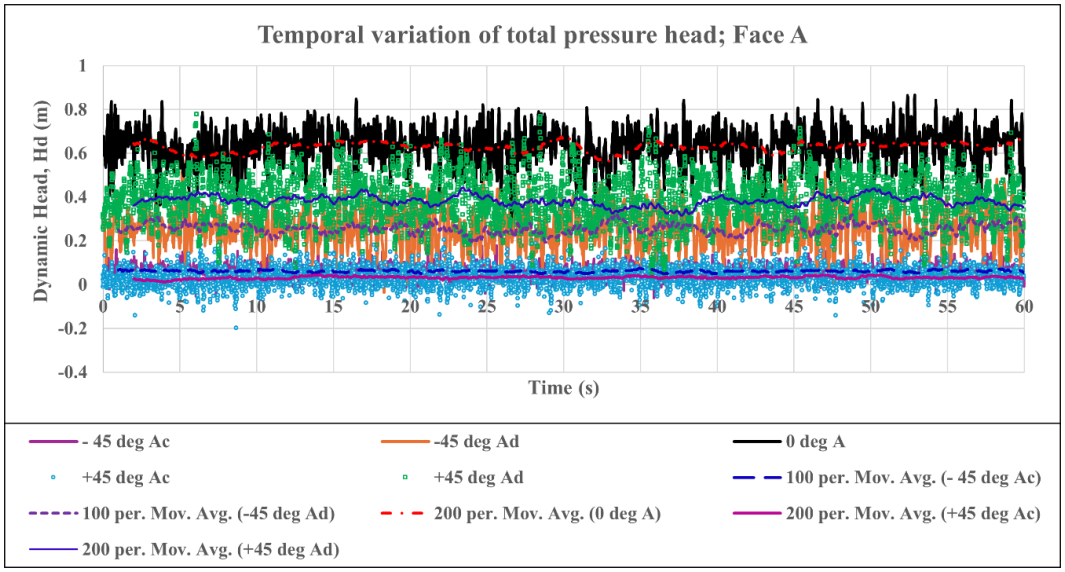

Figure 4. Temporal variation of dynamic head fluctuations at the top of the block, i.e., face A for various inclinations

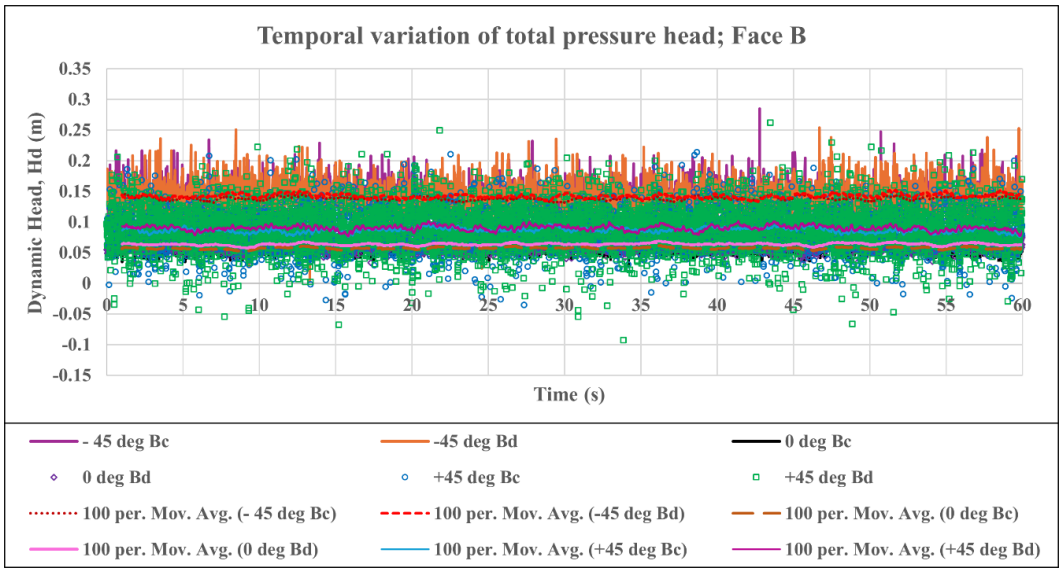

Figure 5. Temporal variation of dynamic head fluctuations at the bottom of the block, i.e., face B for various inclinations

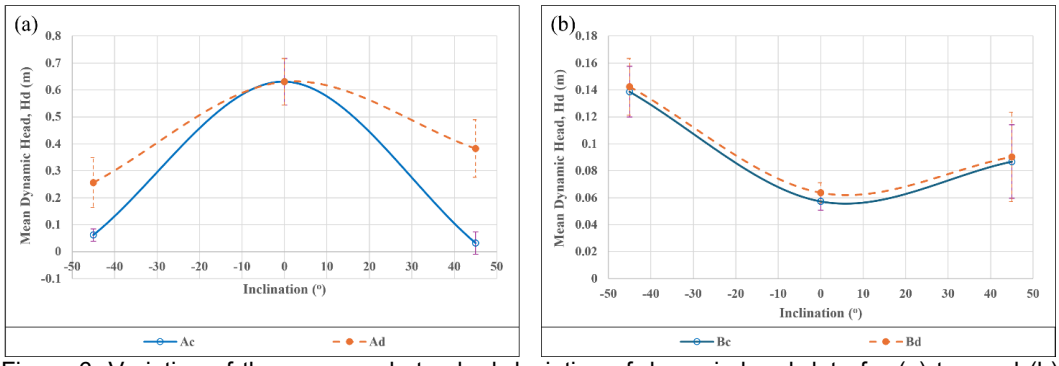

Figure 6. Variation of the mean and standard deviation of dynamic head data for (a) top and (b) bottom of the block

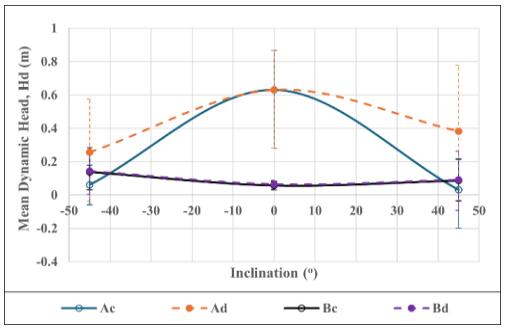

Figure 7. Variation mean, minimum and maximum values of the dynamic head on the top and bottom of the block as a function of joint orientation.

5. CONCLUSION

The mechanisms behind the hydraulic rock mass erosion process are well explained by the determination of hydraulic pressure distribution around the block which in turn depends on various hydraulic and geomechanical parameters. In this study, the preliminary test results of the physical reduced-scale model test results are presented which study the effect of joint orientation on the pressure distribution on the top and bottom of the blocks. The variation of dynamic head results indicates that the dynamic head on the top of the block is significantly affected with the joint orientation as compared to those on the bottom of the block. Development of negative dynamic head is observed in several instants on the top of the block which presents the possibility of development of cavitation pressures. The reason for this behaviour is attributed to the flow

separation occurring at the triangular wedges (knickpoints) formed on the top of the blocks under inclined testing conditions. With further tests in the near future with different flow rates and numerical modelling results, the effect of joint orientation on the erosion process will be more fully evaluated.

REFERENCES

Annandale, G.W. 2006. Scour technology: mechanics and engineering practice. McGraw Hill Professional.

Annandale, G.W. 2012. Current state-of-the-art Rock Scouring Technology. : 1–12. American Society of Civil Engineers. doi:10.1061/40911(230)2.

Annandale, G.W., Wittler, R.J., and Mefford, B.W. 1995. Spillway and foundation erosion: Predicting erosion threshold. American Society of Civil Engineers, New York, NY (United States).

Bollaert, E. 2002. Transient water pressures in joints and formation of rock scour due to high-velocity jet impact. Ph.D. Thesis, École Polytechnique Fédérale de Lausanne - Laboratory of Hydraulic Constructions (EPFL-LCH), Lausanne, Switzerland.

Bollaert, E. 2004. A comprehensive model to evaluate scour formation in plunge pools. International Journal on Hydropower & Dams, **11**(1): 94–101.

Bollaert, E. 2010. The comprehensive scour model: Theory and feedback from practice. *In* Proceedings of the 5th International Conference on Scour and Erosion. San Francisco, California, USA. pp. 7–10.

Bollaert, E. 2016. Simplified Comprehensive Scour Model compared to Erodibility Index Method. Oxford, UK.

Boumaiza, L. 2019. Rock mass parameters governing the hydraulic erodibility of rock in unlined spillways. Doctoral dissertation, Université du Québec à Chicoutimi, Chicoutimi.

Boumaiza, L., Saeidi, A., and Quirion, M. 2019. A method to determine relevant geomechanical parameters for evaluating the hydraulic erodibility of rock. Journal of Rock Mechanics and Geotechnical Engineering, **11**(5): 1004–1018. doi:10.1016/j.jrmge.2019.04.002.

Cameron, C.P., Cato, K.D., McAneny, C.C., and May, J.H. 1986. GEOTECHNICAL ASPECTS OF ROCK EROSION IN EMERGENCY SPILLWAY CHANNELS. Report, Department of the Armt Waterways Experiment Station, Corps of Engineers.

Cameron, C.P., Patrick, D.M., May, J.H., Palmerton, J.B., McAneny, C.C., Hatheway, A.W., Bartholomew, C.O., Mathewson, C.C., and Cato, K.D. 1990. Geotechnical aspects of rock erosion in emergency spillway channels. Report 5, Summary of results, conclusions, and recommendations. *In* This Digital Resource was created from scans of the Print Resource. Report, Geotechnical Laboratory (U.S.) Engineer Research and Development Center (U.S.).

Coleman, S.E., Melville, B.W., and Gore, L. 2003. Fluvial Entrainment of Protruding Fractured Rock. Journal of Hydraulic Engineering, **129**(11): 872–884. doi:10.1061/(ASCE)0733-9429(2003)129:11(872).

Dasgupta, B., Basu, D., Das, K., and Green, R. 2011. Development of computational methodology to assess erosion damage in dam spillways. *In* 31st Annual United States Society on Dam Conference. San Diego, California.

Douglas, K., Pells, S., Fell, R., and Peirson, W. 2018. The influence of geological conditions on erosion of unlined spillways in rock. Quarterly Journal of Engineering Geology and Hydrogeology, **51**(2): 219–228. doi:10.1144/qjegh2017-087.

Dubinski, I.M. 2009. Physical modeling of jointed bedrock erosion by block quarrying. Ph.D. Thesis, Colorado State University, United States -- Colorado.

Frizell, W. 2007. Uplift and Crack Flow Resulting from High Velocity Discharges over Open Offset Joints—Laboratory Studies. U.S. Dept. of the Interior, Bureau of Reclamation, Denver, CO, USA.

Gardner, M. 2023. Toward a Complete Kinematic Description of Hydraulic Plucking of Fractured Rock. Journal of Hydraulic Engineering, **149**(7): 04023015. doi:10.1061/JHEND8.HYENG-13193.

George, M.F. 2012. Block theory application to scour assessment of unlined rock spillways. Masters Thesis, University of California, Berkeley, California, USA.

George, M.F. 2015. 3D Block Erodibility: Dynamics of Rock-Water Interaction in Rock Scour. Ph.D. Thesis, University of California, Berkeley, Berkeley, USA.

George, M.F., and Sitar, N. 2016. Mechanics of 3D Rock Block Erodibility. *In* 50th U.S. Rock Mechanics/Geomechanics Symposium. OnePetro, Houston, Texas.

George, M.F., Sitar, N., and Sklar, L. 2015. Experimental Evaluation of Rock Erosion in Spillway Channels. *In* 49th U.S. Rock Mechanics/Geomechanics Symposium. San Francisco, California, USA.

Kashtiban, Y.J., Saeidi, A., Farinas, M.-I., and Quirion, M. 2021. A Review on Existing Methods to Assess Hydraulic Erodibility Downstream of Dam Spillways. Water, **13**(22): 3205. Multidisciplinary Digital

Publishing Institute. doi:10.3390/w13223205.
Kirsten, H.A.D. 1982. A classification system for excavating in natural materials. Civil Engineering = Siviele Ingenieurswese, **1982**(7): 293–308. South African Institution Of Civil Engineering (SAICE). doi:10.10520/AJA10212019_15379.
Koskinas, A., Tegos, A., Tsira, P., Dimitriadis, P., Iliopoulou, T., Papanicolaou, P., Koutsoyiannis, D., and Williamson, T. 2019. Insights into the Oroville Dam 2017 Spillway Incident. Geosciences, **9**(1): 37. doi:10.3390/geosciences9010037.
Koulibaly, A.S. 2021. Conception d'un modèle de laboratoire d'un évacuateur de crue pour étudier l'érosion des masses rocheuses. Masters, Université du Québec à Chicoutimi, Québec, Canada.
Koulibaly, A.S., Saeidi, A., Rouleau, A., and Quirion, M. 2023. A Reduced-Scale Physical Model of a Spillway to Evaluate the Hydraulic Erodibility of a Fractured Rock Mass. Rock Mechanics and Rock Engineering, **56**: 933–951. doi:10.1007/s00603-022-03101-5.
Li, A., and Liu, P. 2010. Mechanism of rock-bed scour due to impinging jet. Journal of Hydraulic Research, **48**(1): 14–22. Taylor & Francis. doi:10.1080/00221680903565879.
Li, K.-W., Pan, Y.-W., and Liao, J.-J. 2016. A comprehensive mechanics-based model to describe bedrock river erosion by plucking in a jointed rock mass. Environmental Earth Sciences, **75**(6): 1–17. Springer.
Liu, P., Dong, J., and Yu, C. 1998. Fluctuating uplift on rock blocks at the bottom of a scour pool by overfall jets. Science in China Series E: Technological Sciences, **41**(2): 130–139. doi:10.1007/BF02919675.
Marinos, P., and Hoek, E. 2000. GSI: a geologically friendly tool for rock mass strength estimation. Melbourne, Australia. pp. 1422–1446.
Moren, L., and Sjoberg, J. 2007. Rock Erosion In Spillway Channels-A Case Study of the Ligga Spillway. *In* 11th ISRM congress. OnePetro, Lisbon, Portugal.
Pan, Y.-W., Li, K.-W., and Liao, J.-J. 2014. Mechanics and response of a surface rock block subjected to pressure fluctuations: A plucking model and its application. Engineering Geology, **171**: 1–10. doi:10.1016/j.enggeo.2013.12.008.
Pells, S.E. 2016. Erosion of Rock in Spillways. Ph.D. Thesis, University of South Wales, Australia.
Pells, S.E., Pells, P.J., Peirson, W.L., Douglas, K., and Fell, R. 2015. Erosion of unlined spillways in rock–does a "scour threshold" exist? Proceeding of Australian National Committee on Large Dams, Brisbane, Queensland, Australia, **1**(9).
Pitsiou, S. 1990. The effect of discontinuities on the erodibility of rock in unlined spillways of dams. M.S. Thesis, University of Pretoria.
Simoẽs, G.F., Vargas, E. do A., and de Lima, R.T. 1997. Numerical modelling of erosion phenomena in fractured rock masses downstream of spillways. *In* Applications of Computational Mechanics in Geotechnical Engineering. CRC Press, Balkema, Rotterdam. pp. 71–83.
Umumararungu, M.G. 2016. Physical modelling investigation of rock scour extent due to a plunging jet for typicalhigh head dams. M.S. Thesis, Faculty of Engineering, Stellenbosch University, Stellenbosch, South Africa.
Wahl, T.L., Frizell, K.W., and Falvey, H.T. 2019. Uplift Pressures below Spillway Chute Slabs at Unvented Open Offset Joints. Journal of Hydraulic Engineering, **145**(11): 04019039. doi:10.1061/(ASCE)HY.1943-7900.0001637.
Wisse, M.-H., Saeidi, A., Quirion, M., and Nilsson, C.-O. 2023. Effects of joint opening and block protrusion on the hydraulic parameters affecting rock block erosion in unlined spillways using a reduced-scale model. Acta Geotechnica,. doi:10.1007/s11440-023-02085-y.
Zhang, X., Wang, C., Chen, X., Dong, J., Hu, M., and Liu, S. 2024. Insights into the cause of the Oroville dam spillway failure, 2017, California. Environmental Science and Pollution Research,. doi:10.1007/s11356-024-32462-3.

Effect of joint orientation on the non-dimensional uplift pressure coefficient based on spillway model tests

Vineeth Reddy Karnati[1[0000-0002-7543-2065]], Ali Saeidi[1[0000-0001-6954-5453]], Alain Rouleau[1[0000-0001-5174-8156]] and Marco Quirion[2[0000-0003-2568-6339]]

[1] Université du Québec à Chicoutimi, Chicoutimi QC G7H 4M9, Canada
vrkarnati@etu.uqac.ca
[2] Hydro-Québec, Montréal QC H2Z 1A4, Canada

Presented at 2024 ISRM International Symposium: ARMS13 - 13th Asian Rock Mechanics Symposium "Advances in Rock Mechanics - Infrastructure Development"

Abstract. The unlined dam spillways are subjected to significant safety risk from the hydraulic rock mass erosion. The current rock mass erosion assessment methods rely on semi-empirical approaches; however, discrepancies have been observed between the measured and actual erosion depths. Semi-analytical methods based on the comprehensive scour model (CSM) provides a promising solution which requires adaptation for the parallel flow spillways. This study focuses on investigating the effect of joint orientation on the non-dimensional dynamic uplift pressure coefficient for parallel flow spillways using reduced-scale dam spillway model tests. The experimental setup consists of arrangement of nine blocks in a 3x3 matrix in different orientations within a metal box, i.e. -45º, 0º and +45º to the spillway surface, where the central block is instrumented. The hydraulic pressures around the instrumented block are measured under different flow rates and the dynamic uplift pressure coefficients are obtained which are related to the joint orientation. The findings provide valuable insights into mitigating hydraulic erosion risks in dam spillways by understanding block stability under the action of destabilizing hydraulic forces and resistive forces.

Keywords: Hydraulic Rock Mass Erosion, Reduced-Scale Model, Uplift Pressure Coefficient, Joint Orientation, Block Stability.

1. Introduction

In recent years, the hydraulic rock mass erosion has become a major concern in the field of hydropower management. During the flood scenarios, the flowing water with huge hydraulic energy entails the gradual dislodgement and ejection of entire rock mass blocks [1, 2]. Thus, this erosion process is a complex phenomenon depending on both hydraulic and geomechanical parameters [3–5]. The effects of this erosion ranges from losses of human life and property, to the safety concerns of the whole hydraulic structure as observed

in the recent catastrophic Oroville dam spillway erosion in California, USA [6, 7]. To ensure the safe operation of dams, it is vital to understand the mechanisms of this erosion process in order to prevent excessive damage and their related consequences. Dam spillways are majorly of two categories: plunging jet (chute) spillways and the parallel flow spillways. The existing erosion assessment methods are broadly categorized into semi-empirical methods suitable for parallel flow spillways [1, 2] and semi-analytical method (Comprehensive Scour Model) developed for plunging jet spillways [8, 9], out of which the semi-empirical method developed by Annandale [10] is broadly used. Several deviations have been noticed between the semi-empirical predictions and the actual erosion results [4, 5], given the semi-empirical nature and the uncertainties associated with the field observation of the rock mass parameters. The semi-analytical approach represents fairly well the mechanisms behind the erosion process; however, these methods do not study the effect of various geomechanical parameters on the erosion process.

Among various mechanisms of the rock mass erosion, plucking has been recognized as the major mechanism in rock masses with open joints, and it is more pronounced with blocks of size less than 1m [11–13]. This plucking process depends on the uplift forces generated by the pressure differences between the top and bottom surfaces of a block. When the uplift pressure exceeds the resistive shearing forces and the submerged weight of the block, the block is ejected from its position [2, 12, 14]. The hydraulic pressure distribution around the block depends not only on the spillway hydraulics but also on the geomechanical parameters of the rock mass. Boumaiza et al. [5] studied the most relevant geomechanical parameters that affect the hydraulic rock mass erosion process and Boumaiza et al. [15] presented the relative importance of these relevant parameters. In this study, the variation of these hydraulic pressures as a function of the joint orientation, one of these most important geomechanical parameters, is studied. The semi-empirical rock mass indices developed by Kirsten [16] and Pells [2] also incorporate the joint orientation in their methods. Several physical models tried to study the effect of joint orientation, for instance, the experiments conducted by Reinius [17] focused on the hydraulic pressures under different joint orientations and the experiments conducted by George [18, 19] focused on the orientation of a tetrahedral block. The most common block shape is prismoidal in the site conditions. Although the results presented by Reinius [17] are for the prismoidal blocks, they are placed very close to the spillway opening and the measurement of the dynamic pressure within the joints is doubtful in his studies. Thus, there is a need to study the dynamic pressure distribution around the blocks accurately to understand the effect of the joint orientation on the erosion process.

2. Pilot Plant Reduced-scale Spillway Model

A reduced-scale spillway model is constructed at Université du Québec à Chicoutimi, Canada representing the case of Romaine IV dam of Hydro-Québec at a scale of 1:40 following the Froude similitude criterion. The design of the physical model (Fig. 1) is based

on the comprehensive specification described in [20]. Near the downstream end of the spillway channel an opening at base supports an interchangeable metal box that allows the blocks to be oriented in 45^{o} and vertical orientations with respect to the flow direction. As the erosion mechanism is purely based on the stability of the blocks under the applied forces, this process is modelled for the blocks with continuous joints. The erosion process is purely independent of the strength of the intact rock material itself [3] and it is easy to control the quality of the concrete instead of natural rock. The metal box supports 9 concrete blocks, each of size 15cm x 15cm x 30xm, arranged with a specified joint opening using Teflon bolts as spacers that mimic the intact rock blocks with continuous joints. The test set up on the pilot plant model is presented in Fig. 2. The blocks are arranged in a 3 x 3 matrix out of which the central block is instrumented to record the hydraulic pressure distribution around the block as presented in Fig. 3. The top and bottom faces of the block as designated as A and B respectively. The instrumented block is provided with 12 internally connected copper tubes that shall have two inlets on each block face and all the outlets on the top of the block. Elbows are provided at each water inlet inspiring from the theory of pitot tube to measure the actual dynamic head along each face [21]. The elbows on the top and bottom of the block are designated as “Ac” and “Bc” respectively when they are close to the upstream side of the block and “Ad” and “Bd” respectively when they are close to the downstream side of the block. Since the focus of this paper is on the pressure distribution on the top and bottom of the block, the connections located on the lateral sides of the block are ignored in the following description. The pressure outlets are connected to the pressure sensors by means of tightly connected plastic tubes which are placed next to the spillway channel.

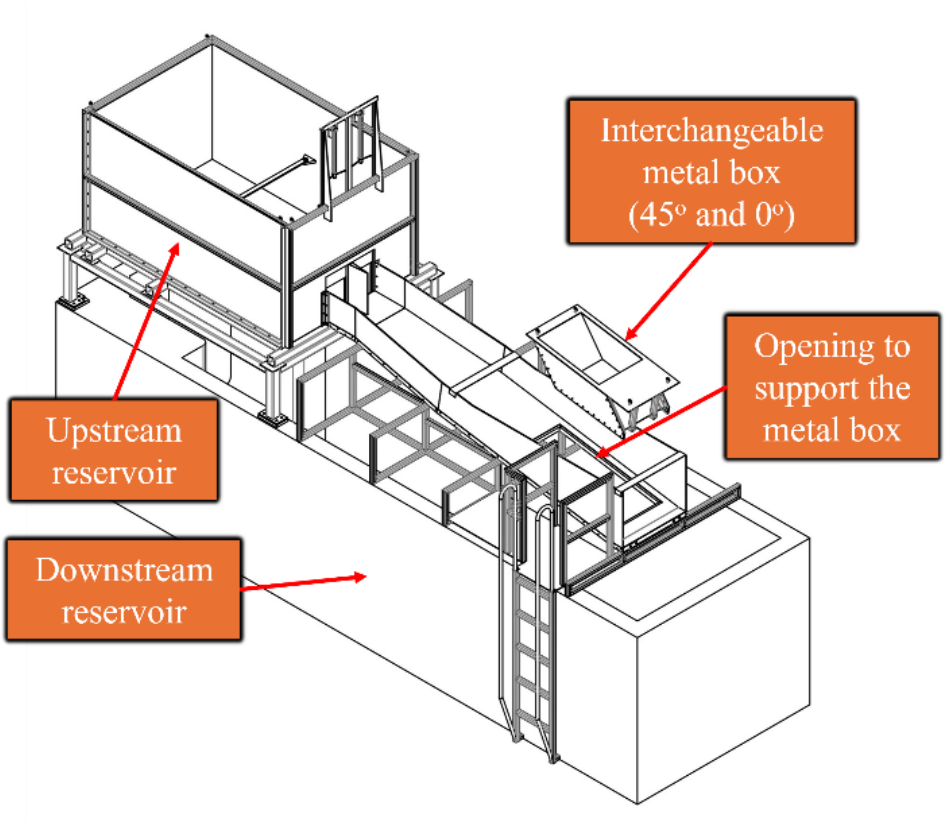

Fig. 1. Design of the physical model (modified from [20]).

3. Testing Methodology

In the current study the effect of joint orientation is studied by a preliminary selection of three joint orientations is made: -45°, 0° and +45° orientations, of the height dimension of the prismatic block with the flow direction inspired from the [20], where the -45° and +45° represents the surface inclination of the blocks with the spillway surface i.e., rotated in anti-clockwise and clockwise directions compared to the blocks placed at 0°. These orientations exhibit the extreme scenarios in which the height of the block exceeds either the width or the length of the block for the selected block aspect ratio. The blocks are placed at 03mm aperture between the blocks and a constant opening of 10 mm below the blocks to allow the positioning of elbows below the block by means of Teflon bolts. In each orientation, measures are taken to avoid the block movement from its position to obtain the accurate pressure measurement. Once the blocks are positioned in each orientation, the blocks are

subjected to two different flow rates, 0.18m^3/s, and 0.34m^3/s, the minimum and the maximum possible discharge for the current model setup. The hydraulic pressure is recorded at a data collection frequency of 100Hz for a period of 60s to an accuracy of 0.0001m. The measured head includes the datum, static and dynamic heads. The flow height in the channel above the blocks is measured by means of a carbon float connected to LVDT and an ultrasound pressure sensor mounted above the instrumented block. The datum head (the difference between the sensor level and the pressure inlet) and the static head (height of water surface from the pressure inlet) are removed from the total head during the tests to yield the dynamic head fluctuations at the top and bottom of the block. The dynamic head of the flow in the channel above the instrumented block, v, is recorded during the tests. Thus, a non-dimensional pressure coefficient, C_p' is defined as shown in Eq. (1). Inspiring from the Reinius [17] studies, a non-dimension uplift coefficient, C_{up}' is calculated as shown in Eq. (2), where $C_{p,Top}'$ and $C_{p,Bottom}'$ are the non-dimensional pressure coefficients at the top and bottom of the block respectively. The C_{up}' can be used to calculate the uplift pressure experienced by the block as shown in Eq. (3), where γ_w is the unit weight of water and A_{face} is the area of the top or bottom face. The C_{up}' value is calculated for the critical condition where the maximum pressure acts on the bottom of the block and minimum pressure acts on the top of the block. Finally, the C_{up}' value is presented as a function of joint orientation.

$$C_p' = \frac{Dynamic\ head\ at\ the\ pressure\ inlet}{\frac{v^2}{2g}} \quad (1)$$

$$C_{up}' = C_{p,Bottom}' - C_{p,Top}' \quad (2)$$

$$Uplift\ Force = C_{up}' * \gamma_w * \frac{v^2}{2g} * A_{face} \quad (3)$$

4. Results and Discussion

The temporal variation of corrected dynamic head fluctuations as mentioned in the methodology is analysed to obtain the mean dynamic head along with minimum and maximum values. The results of the dynamic head fluctuations for various tests are presented as a variation of mean dynamic head with joint orientation with the minimum and maximum values shown as error bars in Fig. 4. The variation of the pressure results shows that the mean dynamic head on the top of the blocks is highest and on the bottom of the blocks is lowest in the case of 0^o orientation where the block height is perpendicular to the flow direction. Also, the dynamic head recorded within the joints at both inlets, i.e. at Bc and Bd is found to be same in all the orientations, however, the mean dynamic head at Ac and Ad are not always constant in inclined conditions.

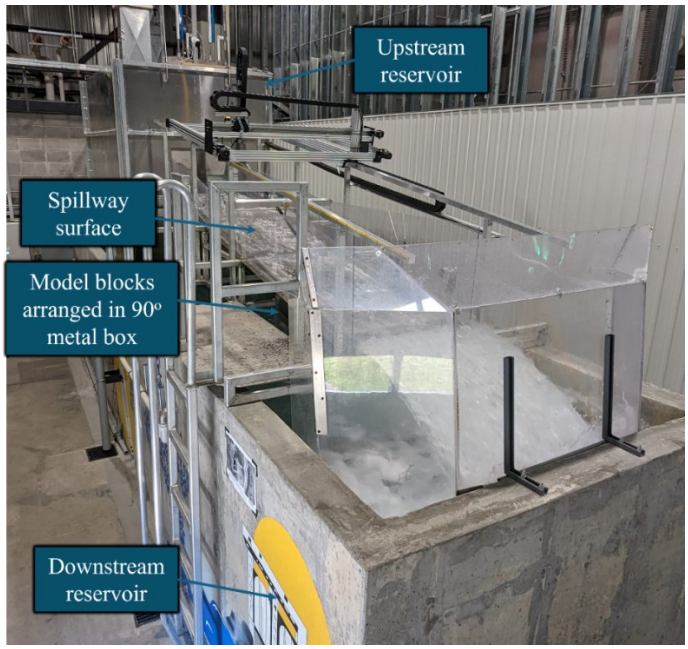

Fig. 2. Test set-up of the physical model.

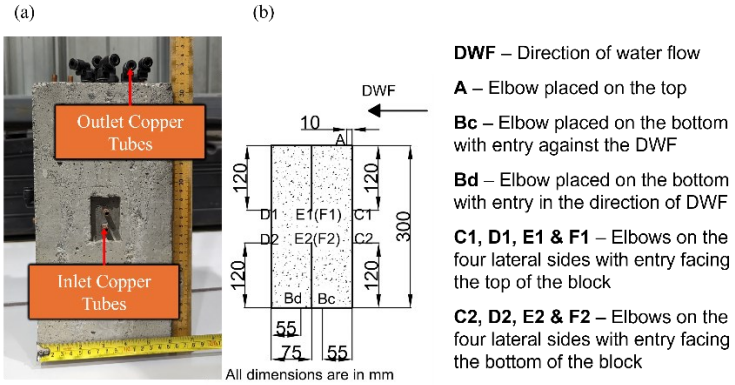

Fig. 3 Description of instrumented block; (a) model block showing inlets and outlets of internally connected tubes and (b) Schematic diagram of the block.

This is due to the flow separations and the eddies formed at the protrusion created by the inclined block portion on the top surface. Also, with the block inclination (both -45° and

+45°), the pressure on the top of the block is found to be decreasing. The error bars present the assessment of occurrence of uplift, i.e., when the negative error bars of the top of the block are below the positive error bars of the bottom of the block, the situation indicates uplift condition. Thus, the uplift condition shall be observed at the inclined block conditions; however, since the block is restricted from any movements, the realistic recording of block uplift is not available.

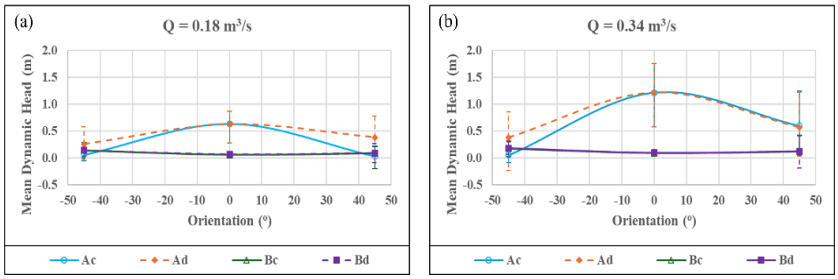

Fig. 4. Variation of dynamic head fluctuations with joint orientation for flow rates: (a) Q = 0.18m^3/s and (b) Q = 0.34m^3/s.

The non-dimensional coefficient of uplift, Cup' is calculated for the test conditions as presented in Eq. (1) and (2) and the variation of Cup' as a function of joint orientation is presented in Fig. 5. In the calculation of Cup', the pressure on the top of the block is considered zero when the minimum pressure on the top is found to be negative to be conservative. These values shall be useful in the block uplift analysis under the action of uplift forces, shearing resistance and the submerged weight of the block. Fig. 5 presents the possibility of uplift in the inclined block conditions and no uplift condition is observed when the blocks are vertical, and the top surface is matching exactly the spillway surface. Thus, the inclination of blocks is introducing a roughness on the spillway surface resulting in the flow separation and eddies formation which in turn creates reduced pressure conditions on the surface of spillway resulting in uplift occurrence. These surface irregularities also result in the development of cavitation pressures which shall further disintegrate the blocks easing the uplift occurrence; however, the reduced-scale models are not capable of generating huge cavitation pressures as those in the case of real spillways. Also, the -45o orientation is considered unfavourable and is highly susceptible to overturning rather than uplifting as pointed out by George and Sitar [22] that the block tries to rotate to align itself in most favourable orientation before leaving its position. The confirmation of these possibilities shall be possible with the further tests to be performed. The variation of Cup' with joint orientation shall be studied effectively with the tests that shall be performed in the future and the numerical modelling validated using the experimental results.

5. Conclusions

The hydraulic rock mass erosion is governed by the fluctuating hydraulic pressures around the block which are further dependent on several hydraulic and geomechanical parameters. In this study, the effect of joint orientation on these pressures is studied using pilot plant spillway model tests using three different orientations and two flow rates. The preliminary test results presented indicate the possibility of occurrence of block uplift with inclined joint conditions. The non-dimensional uplift coefficient is found to be positive for the inclined conditions and negative for no inclination. The experimental tests made with the physical spillway model serve as a valuable source of validation to the numerical model and further tests on the other inclinations shall yield a better physical understanding of the effect of joint orientation on the block uplift process.

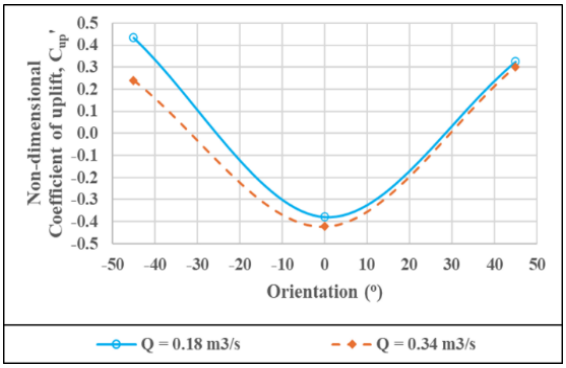

Fig. 5. Variation of non-dimensional coefficient of uplift with joint orientation.

References

1. Annandale, G.W.: Current state-of-the-art Rock Scouring Technology. 1–12 (2012). https://doi.org/10.1061/40911(230)2
2. Pells, S.E.: Erosion of Rock in Spillways, (2016)
3. Pells, P.J., Bieniawski, Z.T., Hencher, S.R., Pells, S.E.: Rock quality designation (RQD): time to rest in peace. Can. Geotech. J. 54, 825–834 (2017). https://doi.org/10.1139/cgj-2016-0012
4. Kashtiban, Y.J., Saeidi, A., Farinas, M.-I., Quirion, M.: A Review on Existing Methods to Assess Hydraulic Erodibility Downstream of Dam Spillways. Water. 13, 3205 (2021). https://doi.org/10.3390/w13223205
5. Boumaiza, L., Saeidi, A., Quirion, M.: A method to determine relevant geomechanical parameters for evaluating the hydraulic erodibility of rock. Journal of Rock Mechanics

and Geotechnical Engineering. 11, 1004–1018 (2019). https://doi.org/10.1016/j.jrmge.2019.04.002
6. Zhang, X., Wang, C., Chen, X., Dong, J., Hu, M., Liu, S.: Insights into the cause of the Oroville dam spillway failure, 2017, California. Environ Sci Pollut Res. (2024). https://doi.org/10.1007/s11356-024-32462-3
7. Koskinas, A., Tegos, A., Tsira, P., Dimitriadis, P., Iliopoulou, T., Papanicolaou, P., Koutsoyiannis, D., Williamson, T.: Insights into the Oroville Dam 2017 Spillway Incident. Geosciences. 9, 37 (2019). https://doi.org/10.3390/geosciences9010037
8. Bollaert, E.: Simplified Comprehensive Scour Model compared to Erodibility Index Method. Presented at the ICSE 2016 (8th International Conference on Scour and Erosion) , Oxford, UK September 12 (2016)
9. Bollaert, E.: Transient water pressures in joints and formation of rock scour due to high-velocity jet impact, https://infoscience.epfl.ch/record/116162/files/Comm_LCH_13.pdf, (2002)
10. Annandale, G.W.: Scour technology: mechanics and engineering practice. McGraw Hill Professional (2006)
11. Gardner, M.: Toward a Complete Kinematic Description of Hydraulic Plucking of Fractured Rock. J. Hydraul. Eng. 149, 04023015 (2023). https://doi.org/10.1061/JHEND8.HYENG-13193
12. Pan, Y.-W., Li, K.-W., Liao, J.-J.: Mechanics and response of a surface rock block subjected to pressure fluctuations: A plucking model and its application. Engineering Geology. 171, 1–10 (2014). https://doi.org/10.1016/j.enggeo.2013.12.008
13. Li, K.-W., Pan, Y.-W., Liao, J.-J.: A comprehensive mechanics-based model to describe bedrock river erosion by plucking in a jointed rock mass. Environmental Earth Sciences. 75, 1–17 (2016)
14. Annandale, G.: Erosion of rock by hydraulic forces. Presented at the Vail Rocks 1999, The 37th US Symposium on Rock Mechanics (USRMS) (1999)
15. Boumaiza, L., Saeidi, A., Quirion, M.: A method to determine the relative importance of geological parameters that control the hydraulic erodibility of rock. Quarterly Journal of Engineering Geology and Hydrogeology. 54, qjegh2020-154 (2021). https://doi.org/10.1144/qjegh2020-154
16. Kirsten, H.A.D.: A classification system for excavating in natural materials. Civil Engineering = Siviele Ingenieurswese. 1982, 293–308 (1982). https://doi.org/10.10520/AJA10212019_15379
17. Reinius, E.: Rock erosion. International Water Power and Dam Construction. 38, 43–48 (1986)

18. George, M.F.: Block theory application to scour assessment of unlined rock spillways, https://damfailures.org/wp-content/uploads/2021/08/MichaelGeorge_Thesis.pdf, (2012)
19. George, M.F.: 3D Block Erodibility: Dynamics of Rock-Water Interaction in Rock Scour, https://escholarship.org/uc/item/61q7798m, (2015)
20. Koulibaly, A.S., Saeidi, A., Rouleau, A., Quirion, M.: A Reduced-Scale Physical Model of a Spillway to Evaluate the Hydraulic Erodibility of a Fractured Rock Mass. Rock Mech Rock Eng. 56, 933–951 (2023). https://doi.org/10.1007/s00603-022-03101-5
21. Wisse, M.-H., Saeidi, A., Quirion, M., Nilsson, C.-O.: Effects of joint opening and block protrusion on the hydraulic parameters affecting rock block erosion in unlined spillways using a reduced-scale model. Acta Geotech. (2023). https://doi.org/10.1007/s11440-023-02085-y
22. George, M.F., Sitar, N.: Mechanics of 3D Rock Block Erodibility. In: 50th U.S. Rock Mechanics/Geomechanics Symposium. OnePetro, Houston, Texas (2016)

International Society for Rock Mechanics and Rock Engineering
Norwegian Group for Rock Mechanics

ISRM International Symposium
Eurock 2025 – Expanding the Underground Space
Trondheim, Norway, 16-20 June
ISBN 978-82-8208-079-8

Impact of Joint Orientation on Rock Mass Erosion: Insights from Model Testing

V.R. Karnati, A. Saeidi & A. Rouleau
Université du Québec à Chicoutimi, Saguenay, Québec, Canada
vrkarnati@etu.uqac.ca (email of corresponding author)

M. Quirion
Expertise intégrée-Géologie, Hydro-Québec, Montréal, Québec, Canada

Abstract

Rock mass erosion is a critical factor posing threat to the long-term stability of hydraulic structures, especially in unlined spillways. The erosion extent is determined by the hydraulic pressure generated around rock blocks by the flow during flood events. The hydraulic pressure is significantly affected by various on site hydraulic and geomechanical conditions. Among important parameters, joint orientation demonstrates a significant effect on the hydraulic pressure. Determination of hydraulic pressure at a spillway site, especially within the channel and within the joints, is complicated and physical model testing becomes a reliable approach to study the impact of individual parameters on the fluctuating hydraulic pressure. In this study, physical model tests are carried out on nine model blocks arranged in 3x3 configuration. Three different block orientations are tested at a constant joint opening of 10 mm and the hydraulic pressure is analyzed at different locations around the central block. The results are used to analyze the possibilities of block instability under the action of hydraulic pressure, the weight of the block and the joint shear resistance. The resulting non-dimensional coefficient of uplift was observed around 0.2, indicating a potential for block uplift. The results of stability analysis indicate that the blocks oriented against the flow exhibit a tendency to topple and tend to realign with the flow. In contrast the blocks aligned with the flow readily demonstrated a higher potential for block uplift. The blocks oriented perpendicular to the flow without any block protrusion at the surface show more stable behavior. The results provide key insights into the impact of joint orientation on the rock mass erosion.

Keywords

Rock mass erosion, Pilot-plant physical spillway model, Block Instability, Joint orientation, Non-dimensional coefficient of uplift

ISRM

NBG

1. Introduction

Hydraulic rock mass erosion is found to be more prominent in the unlined dam spillways threatening the safety and sustainability of the whole hydraulic structure. The flood water with huge hydraulic energy flowing over unlined spillways, interacts with the discontinuities in the rock mass resulting in noticeable quantities of rock mass erosion. The complex interaction between the hydraulic power transferred to the rock mass and the resistance offered by the rock-mass, which depends on various geomechanical properties, renders the comprehension of the erosion process difficult (Pells et al. 2017; Boumaiza et al. 2019; Kashtiban et al. 2021). Historic examples of spillway erosion cases, as observed from Oroville dam spillway (Zhang et al. 2024), Ricobayo dam spillway (Pells 2016; Liu and Kieffer 2021) and Copeton dam spillway (Pells et al. 2016, 2024), presents the devastating losses experienced. Existing rock mass erosion assessment methods can be broadly classified into two categories: semi-empirical and semi-analytical (Kashtiban et al. 2021).

Literature presents different erosion mechanisms, namely, plucking/uplift (instantaneous and time-dependent), abrasion, fracturing (brittle and fatigue) (Kashtiban et al. 2021), out of which block uplift is determined to be the most common mechanism in rock mass erosion, especially with blocks of size less than 1 m (Pan et al. 2014; Wahl et al. 2019). This uplift mechanism is highly dependent on the hydraulic pressure distribution on the top of the block and within the joints. Different flow characteristics such as flow rate, degree of aeration of the water, flow turbulence and formation of hydraulic jump (Wilkinson et al. 2018; Kote and Nangare 2019) and different geomechanical characteristics such as joint opening, joint orientation, protrusion of blocks, joint shear properties, block size and spillway surface characteristics (Bollaert 2002; Pells 2016; Boumaiza et al. 2019) determine the hydraulic pressure distribution around an intact rock block which may result in the possibility of block dislodgement. The hydraulic pressure is often found to be highly fluctuating and the determination of these fluctuating pressures at actual spillway sites would be highly challenging due to its associated cost and complexity. In this scenario, physical reduced-scale models can be useful tools to estimate these pressures. Physical models allow studying the effect of individual hydraulic and geomechanical parameters. Many researchers developed various reduced-scale models, however, most models are using a single large block (George 2012, 2015) or a group of very small blocks (Sawadogo 2010). The joint orientation is one of the important parameters influencing the erodibility process as it determines the dislodgement of a block kinematically under the combination of destabilizing and resisting forces. Reinius (1986) studied the effects of block protrusion and joint orientation on the hydraulic pressures and presented non-dimensional uplift coefficient (C_{up}') values for different conditions. These values are used for the development of the Quasi-Static Impulsion (QSI) method of Comprehensive Scour Model (CSM) by Bollaert (2012). The measurements from Reinius (1986) are based on piezometric measurements and the fluctuations in the hydraulic pressure are taken into account in the development of C_{up}' values for different arrangements.

In our previous article (Karnati et al. 2024), we have presented the impact of joint orientation on the hydraulic pressure distribution around the block using physical model tests under different flow rates. The current article focuses on obtaining the C_{up}' values based on the fluctuating pressures and analysing the stability of the blocks under the action of hydraulic forces in different block orientations. The paper initially presents a description of reduced-scale model, then describes the methodology employed to obtain the hydraulic pressures and C_{up}' values, and finally determines the stability of the blocks inclined with the flow direction.

2. Reduced-scale physical spillway model

The reduced-scale physical model presented in Fig. 1 is constructed at Université du Québec à Chicoutimi, Canada which represents a scaled down version of Romaine IV Hydro-Québec dam spillway at a level of 1:40 following the Froude similarity criterion (Koulibaly et al. 2023). This model allows for studying the individual effect of several important parameters mentioned in the previous

section. The functional details of this model are presented in Wisse et al. (2023). The flowrate in the channel is controlled by the operating frequency of the submersible pump and the opening of the sluice gate (Fig. 1). This system allows for the measurement of the flow height and the flow velocity in 3-dimensions of the flow. The downstream end of the channel is provided with an opening to support metal boxes containing the model blocks (Fig. 1(b)). Nine prismoid concrete blocks, each of size 15 x 15 x 30 cm are used to represent a network of rock-mass with intact blocks having connected joints. Lightweight concrete is used for the preparation of concrete blocks to facilitate the placement of the blocks in the metal box. A constant aperture of 10 mm is provided between the blocks at all levels using Teflon bolts. The dimensions of the metal boxes are such that the top of the blocks always coincides with the spillway surface unless blocks are provided with a protrusion. The central instrumented block consists of 12 internal connected copper rods. The outlets of all the copper rods are provided on the top of the block which are connected to calibrated sensors. The water inlet level is supported with elbows that are placed facing the flow of water acting as a minute pitot tube allowing the accurate measurement of dynamic head (Wisse et al. 2023b). The details of the instrumented block are presented in Karnati et al. (2023, 2024). Each face of the instrumented block is provided with two water inlets. The different faces of the block and corresponding water inlets are termed as mentioned in Table 1.

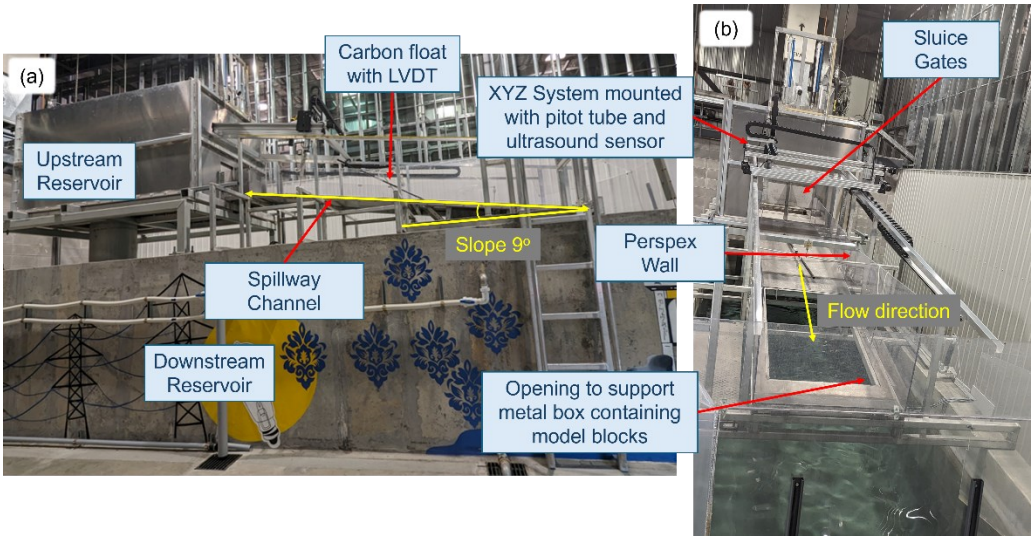

Fig. 1 Reduced-scale physical spillway model: (a) Different elements of the physical model; (b) View of the channel surface from model downstream (modified from Karnati et al. (2024)).

Table 1 Different face of the instrumented block and corresponding water inlets

Face	Description	Water inlet	Description
A	Top face of the block	*Ac*	Water inlet close to the face *C*
		Ad	Water inlet close to the face *D*
B	Bottom face of the block	*Bc*	Water inlet close to the face *C*
		Bd	Water inlet close to the face *D*
C	Upstream face of the block	*C1*	Water inlet close to the face *A*
		C2	Water inlet close to the face *B*
D	Downstream face of the block	*D1*	Water inlet close to the face *A*
		D2	Water inlet close to the face *B*
E	Face of the block towards the right side of the flow	*E1*	Water inlet close to the face *A*
		E2	Water inlet close to the face *B*
F	Face of the block towards the left side of the flow	*F1*	Water inlet close to the face *A*
		F2	Water inlet close to the face *B*

3. Methodology

The primary objective of this study is to determine the impact of joint opening on the hydraulic pressure and the corresponding C_{up}' values using the physical model tests. Based on the model block aspect ratio (r=1:2), preliminary critical orientations, i.e., -45°, 0° and +45° are chosen for this purpose, where -45° represents the blocks aligned against the flow direction, 0° represents the block with height dimension placed perpendicular to the flow direction and +45° represents the blocks aligned towards the flow direction. The block alignment under different orientations selected is presented in Fig. 2. Triangular wedge blocks are used to support the blocks under inclined conditions. The block set-up representing the fractured rock-mass is subjected to different flowrates ranging from 0.18 to 0.34 m^3/s, however, only the results of 0.34 m^3/s are presented in this article. A data collection frequency of 100 Hz is used for the collection of pressure data.

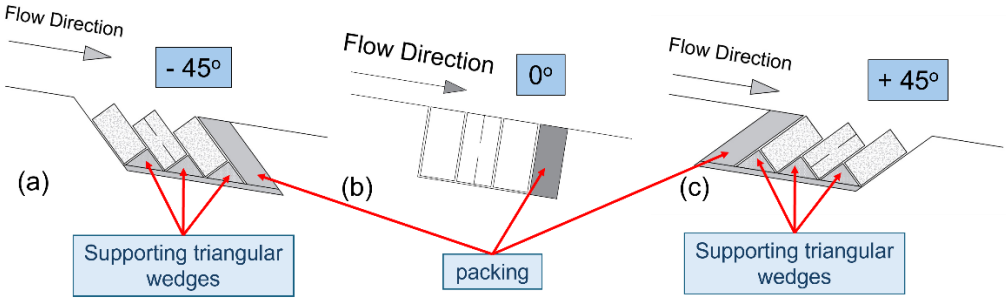

Fig. 2 Schematic of alignment of blocks in different orientations selected: (a) -45°; (b) 0°; (c) +45°.

3.1 Determination of C_{up}'

The hydraulic pressure measured as the head of water at different locations of the block, presented in Table 1, is corrected for static and datum pressure heads to obtain the dynamic pressure head. The dynamic head representing mean flow velocity in the channel at selected flowrate (0.34 m^3/s) at the instrumented block level is calculated to be 1.25 m. Uplift pressure head acting on the instrumented block, can be calculated as the difference between the dynamic heads at the bottom and the top of the block (Eq. 1). Bollaert (2002) defined the C_{up}' as the ratio of the uplift head to the mean velocity head of the flow in the channel at critical conditions (Eq. 2). The hydraulic force acting on each face is

calculated as the product of unit weight of water, γ_w, dynamic head and the length along which the pressure is acting. Thus C_{up}' calculations allow the determination of the uplift force acting on a block.

$$h_{up} = h_B - h_A \tag{1}$$

$$C'_{up} = \frac{h_{up}}{h_{ch}} \tag{2}$$

Where h_{up} Uplift pressure head acting on the block in m
h_B Dynamic pressure head at the bottom of the block in m
h_A Dynamic pressure head at the top of the block in m
C_{up}' Non-dimensional coefficient of uplift
h_{ch} Mean flow velocity in the channel at the instrumented block level in m

3.2 Stability analysis of blocks

The pressure results are also used to analyse the stability of the blocks against the dislodgement from its initial position. The blocks presented a tendency to topple and align towards the flow when they are arranged in -45° alignment, whereas they presented a tendency to uplift when arranged in +45° alignment during the trail analysis. To determine the pressures at arrangements designed, the blocks are restrained against any displacements. However, the observed instabilities are analysed under model test conditions using the obtained pressure results. For the blocks in -45° alignment, the toppling and resisting moments are calculated about the downstream bottom corner and the factor of safety against toppling, $F_{s,\ topple}$ is calculated as the ratio of sum of resisting moments to sum of toppling moments. For the blocks in +45° alignment, the uplift force is determined for critical condition (Eq. 1) and the factor of safety against uplift, $F_{s,\ up}$ is calculated as the ratio of the uplift force generated to the sum of resisting forces (generated by weight of the block and shear resistance along the sides). The calculations are presented in Tables 3 and 4 respectively. The blocks aligned in 0° alignment did not show any signs of instability during the preliminary tests.

4. Results and discussion

4.1 Hydraulic pressure distribution

The pressures at inlets *Ac* and *Ad* are found to be similar in the case of 0° alignment during the trial tests and hence the dynamic head is measured only at Ac under this alignment and the results obtained at *Ac* are used for *Ad* as well. The dynamic pressure head results obtained from the model tests are presented in Fig. 3 for the top of the block for the three block orientations selected. In addition to the pressure fluctuations, 50 period moving average is also presented to identify the trend in the fluctuations. Fig. 3 shows that the pressure on the top of the block is high for 0° alignment, and this pressure is decreasing with the inclined alignments. However, the fluctuations in dynamic head are increasing under inclined alignments for the inlet close to the spillway surface and are decreasing for the inlet away from the spillway surface. The variation of pressure results for different water inlets is presented in Fig. 4 as variation of mean values with error bars pointing out to the maximum and minimum values of the fluctuating pressures. Fig. 4(a) presents a possibility of block uplift under the critical condition where the dynamic head on the top of the block is minimum and that on the bottom is maximum. Fig. 4(b) shows that the dynamic head within the joints (Faces *B* to *F*; see Table 1) is remaining constant with change in block alignment, however, the fluctuations are increasing under inclined alignments.

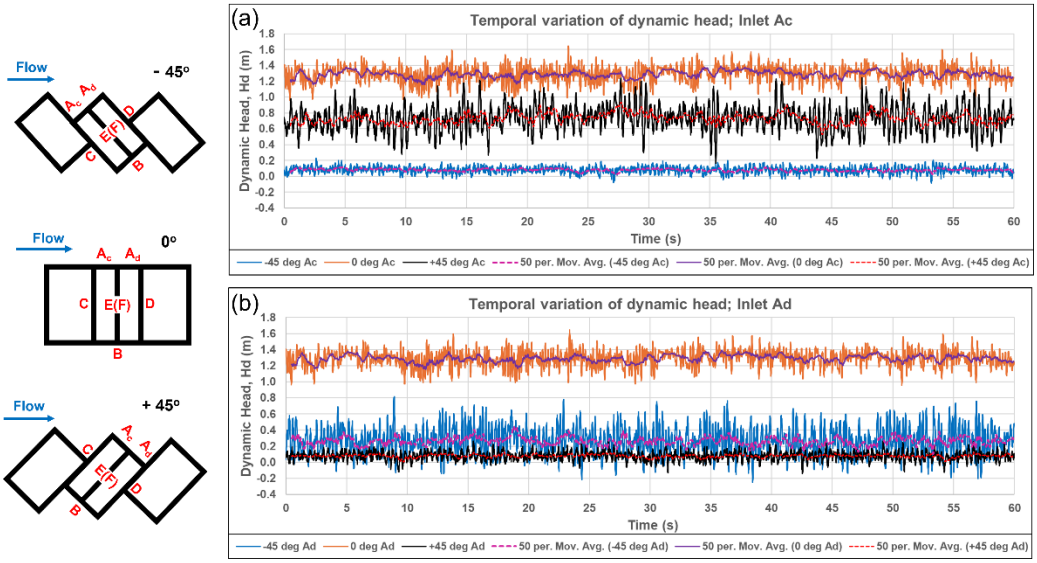

Fig. 3 Temporal variation of dynamic head on the top of the block for different joint orientations: (a) Water inlet Ac; (b) Water inlet Ad.

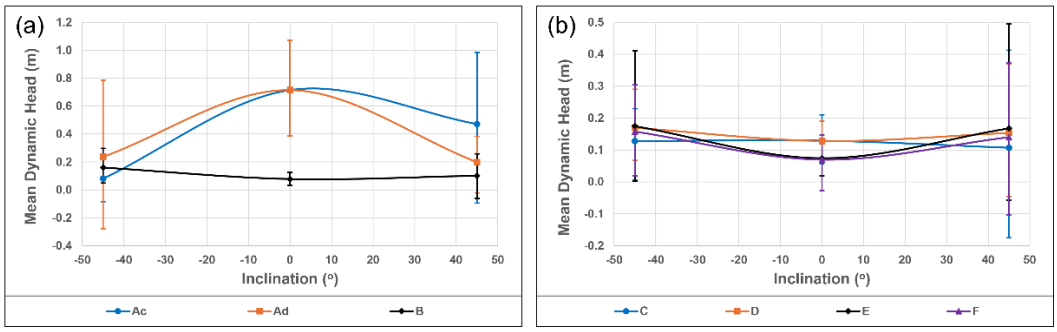

Fig. 4 Variation of dynamic head with joint orientation at different joint inlets: (a) Top and bottom of the block; (b) Lateral sides of the block. (Table 1explains different faces of the block)

4.2 Non-dimensional coefficient of uplift

A linear variation of the pressure head is considered on the top of the block under inclined alignment conditions. The minimum dynamic pressure on the top of the block is considered zero when it is found to be negative due to the cavitation condition. The value of uplift head and C_{up}' are calculated as per Eq. 1 and 2 respectively for all the alignment conditions and are presented in Table 2.

Table 2 Uplift head and non-dimensional coefficient of uplift for different orientations

Orientation	**-45º**	**0º**	**+45º**
h_A (Minimum value)	0.0000	0.9582	0.0127
h_B (Maximum value)	0.2975	0.1239	0.2585
h_{up}	0.2975	-0.8343	0.2458
C_{up}'	0.24	-0.67	0.20

The negative C_{up}' value for 0º alignment shows that there is no possibility of block uplift under this condition as observed during the preliminary tests. However, the positive C_{up}' values under -45º and +45º alignments indicate the possibility of block instability by uplift.

4.3 Stability analysis

4.3.1 Blocks aligned against the flow

The C_{up}' value shown the possibility of uplift, however, during the trial tests, the blocks tend to topple and align towards the flow direction. Hence the instability arising in this alignment could be a combination of sliding and toppling. The pressures around the instrumented block are considered as presented in Fig. 5. In this alignment, due to the protruded surface developed at the top of the blocks near the triangular edges, a hydraulic jump is being developed creating a negative pressure zone on the leeside of the blocks. This zone is termed as "Exposure zone, *a*" whose length is taken equal to the length of the block exposed to the flow in the channel, i.e. 16 cm in the model testing scenario. The pressure in this zone is considered zero under critical conditions. The pressures within the joint are found to be similar and hence it is considered uniform within a joint as presented in Fig. 5. The stability against overturning is calculated considering the values presented in Fig. 5, where the head values are obtained from the model testing. The calculation equations and the factor of safety of the block against toppling about point *C* is calculated as presented in Table 3.

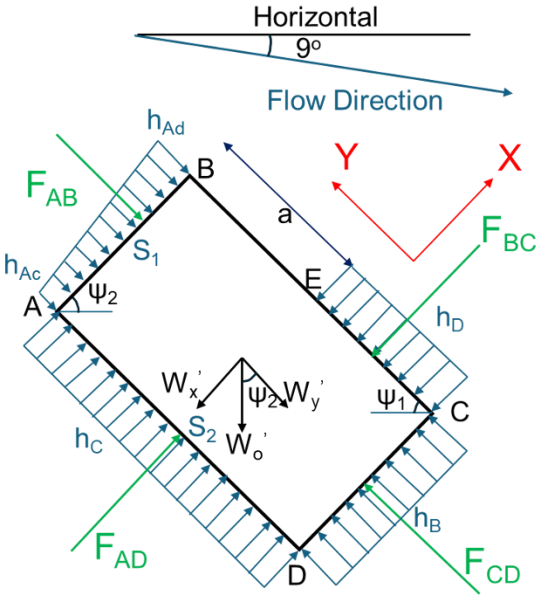

Values used in the stability calculations:

1. Unit weight of water, γ_w = 9.81 kN/m^3
2. Unit weight of the blocks used in model tests, γ_r = 13.5 kN/m^3
3. Dip of the top surface of the block, ψ_2 = 45º – 9º = 36º
4. Width of the block, S_1 = 15 cm
5. Height of the block, S_2 = 30 cm
6. Exposure length, a = 16 cm
7. h_{Ac} = 0 (min value is found to be negative and hence considered 0)
8. h_{Ad} = 0 (min value is found to be negative and hence considered 0)
9. h_B = 0.298 m
10. h_C = 0.230 m
11. h_D = 0.290 m
12. Submerged unit weight of the block per unit length, $W_o' = (\gamma_r - \gamma_w) * S_1 * S_2$

Fig. 5 Pressure distribution around the blocks aligned against the direction of flow (Considering unit length along the lateral direction).

The calculations are made for the case of laboratory scenario, where light weight concrete blocks are used to represent intact blocks. Under this scenario, the blocks are unstable and tend to topple as

observed from the trial tests. However, in reality the unit weight of rock blocks is about 27 kN/m^3. The blocks are found to be stable against toppling under this scenario as observed from the calculations in second row of

made with realistic unit weight of rock blocks (27 kN/m^3).

Table 3 Calculations involved in the stability analysis for the -45° blocks – Toppling about downstream corner point C

Toppling moments, M_o (kN-m/m)		**Resisting moments, M_R (kN-m/m)**				ΣM_o (kN-m/m)	ΣM_R (kN-m/m)	$F_{s,topple} = \frac{\Sigma M_o}{\Sigma M_R}$
$F_{CD} * \frac{S_1}{2}$	$F_{AD} * \frac{S_2}{2}$	$F_{AB} * eccentricity$	$F_{BC} * \frac{S_2 - a}{2}$	$W'_y * \frac{S_1}{2}$	$W'_x * \frac{S_2}{2}$			
0.033	0.102	0	0.028	0.010	0.015	0.134	0.053	0.39
0.033	0.102	0	0.028	0.047	0.068	0.134	0.143	1.06*

* This factor of safety is related to the calculations made using realistic unit weight of rock blocks.

4.3.2 Blocks aligned towards the flow

As observed in the trial tests, the blocks arranged in this alignment are uplifting. Thus, the instability calculations are made for sliding along the surface *BC*. The pressures are assumed constant along a surface under critical condition, i.e., minimum pressure on the top of the block and maximum pressure within the joints. The pressures within the joint are found to be similar and hence it is considered uniform within a joint as presented in Fig. 6. The stability against sliding is calculated considering the values presented in Fig. 6, where the head values are obtained from the model testing. The factor of safety of the block against sliding along surface *BC* is calculated as presented in Table 4.

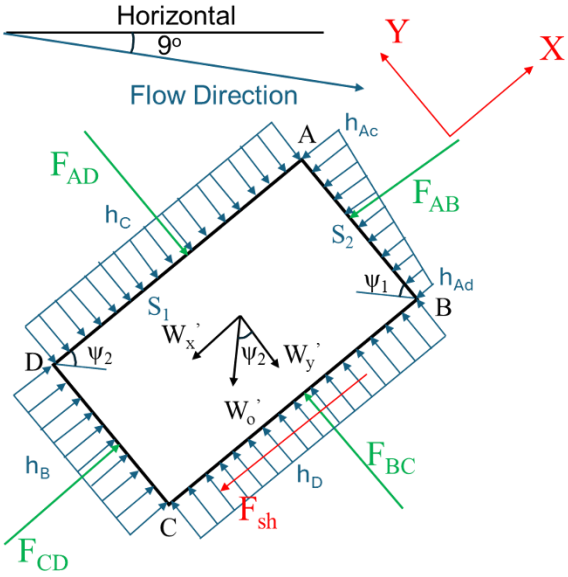

Values used in the stability calculations:

1. Unit weight of water, γ_w = 9.81 kN/m^3
2. Unit weight of the blocks used in model tests, γ_r = 13.5 kN/m^3
3. Dip of the top surface of the block, ψ_1 = 45° + 9° = 54°
4. Width of the block, S_2 = 15 cm
5. Height of the block, S_1 = 30 cm
6. C_{up}' = 0.20
7. Mean flow velocity (head) in the channel, h_{ch} = 1.25 m
8. h_{Ac} = 0 (min value is found to be negative and hence considered 0)
9. h_{Ad} = 0 (min value is found to be negative and hence considered 0)
10. h_C = 0. 412 m
11. h_D = 0.370 m
12. Angle of shearing resistance, ϕ = 30°
13. Uplift force, $F_u = C_{up}' * h_{ch} * \gamma_w * S_2$

Fig. 6 Pressure distribution around the blocks aligned towards the direction of flow (Considering unit length along the lateral direction).

Table 4 Calculations involved in the stability analysis for the +45° blocks – Sliding along surface BC

Uplift force ΣF_u	**Forces on lateral sides**			**Resisting forces,** F_R		ΣF_R	$F_{s,up} = \frac{\Sigma F_u}{\Sigma F_R}$
	F_{AD}	W_y'	F_{BC}	W_x'	F_{sh}		
0.368	1.213	0.134	1.090	0.098	0.149	0.246	0.67
0.368	1.213	0.626	1.090	0.455	0.433	0.887	2.41*

* This factor of safety is related to the calculations made using realistic unit weight of rock blocks.

The calculations are made for the case of laboratory scenario, where light weight concrete blocks are used to represent intact blocks. Under this scenario, the blocks are unstable and tend to slide as observed from the trial tests. However, in reality the unit weight of rock blocks is about 27 kN/m^3. The blocks are found to be stable against sliding under this scenario as observed from the calculations in second row of Table 4 made with realistic unit weight of rock blocks (27 kN/m^3).

5. Conclusion

In this study, the hydraulic pressure distribution around an intact model block is determined using physical model tests with different block orientation arrangements. The variation of dynamic head indicated that the pressure fluctuations are increasing under the inclined block arrangements which are necessarily creating unstable situations. The non-dimensional coefficient of uplift values show that the blocks arranged in 0° alignment are stable against uplift, and blocks arranged in -45° and +45° alignments are under critical conditions. The primary instabilities observed in -45° and +45° alignments are determined to be toppling and sliding respectively. The stability analysis carried out using the laboratory scenario confirms the instability as observed from the factor of safety less than 1. However, the blocks are found to be stable when the calculations are made under realistic rock block unit weight. Further tests with different inclined conditions, varied block sizes and numerical modelling will help us develop a relationship between the critical pressure heads with the joint orientation which further improves the understanding of the rock mass erosion mechanism.

References

Bollaert E (2012) Wall jet rock scour in plunge pools: A quasi-3D prediction model. Hydropower and Dams 20:

Bollaert E (2002) Transient water pressures in joints and formation of rock scour due to high-velocity jet impact. Ph.D. Thesis, École Polytechnique Fédérale de Lausanne - Laboratory of Hydraulic Constructions (EPFL-LCH)

Boumaiza L, Saeidi A, Quirion M (2019) A method to determine relevant geomechanical parameters for evaluating the hydraulic erodibility of rock. Journal of Rock Mechanics and Geotechnical Engineering 11:1004–1018. https://doi.org/10.1016/j.jrmge.2019.04.002

George MF (2012) Block theory application to scour assessment of unlined rock spillways. Masters Thesis, University of California, Berkeley

George MF (2015) 3D Block Erodibility: Dynamics of Rock-Water Interaction in Rock Scour. Ph.D. Thesis, University of California, Berkeley

Karnati VR, Saeidi A, Rouleau A, Quirion M (2024) Effect of Joint Orientation on Rock Mass Erosion Based on Experimental Results Using a Pilot Plant Spillway Model. In: 58th U.S. Rock Mechanics/Geomechanics Symposium. ARMA, Golden, Colorado, USA, p ARMA-2024-0753

Karnati VR, Saeidi A, Rouleau A, Quirion M (2023) Effect of Joint Opening and Block Protrusion on the Hydraulic Pressure Around Rock Blocks in Unlined Dam Spillways

Kashtiban YJ, Saeidi A, Farinas M-I, Quirion M (2021) A Review on Existing Methods to Assess Hydraulic Erodibility Downstream of Dam Spillways. Water 13:3205. https://doi.org/10.3390/w13223205

Kote AS, Nangare PB (2019) Hydraulic Model Investigation on Stepped Spillway's Plain and Slotted Roller Bucket. Eng Technol Appl Sci Res 9:4419–4422. https://doi.org/10.48084/etasr.2837

Koulibaly AS, Saeidi A, Rouleau A, Quirion M (2023) A Reduced-Scale Physical Model of a Spillway to Evaluate the Hydraulic Erodibility of a Fractured Rock Mass. Rock Mech Rock Eng 56:933–951. https://doi.org/10.1007/s00603-022-03101-5

Liu Q, Kieffer DS (2021) LiDAR Based Three-Dimensional Rock Structure Model for Evaluating Spillway Scour at Ricobayo Dam, Zamora, Spain

Pan Y-W, Li K-W, Liao J-J (2014) Mechanics and response of a surface rock block subjected to pressure fluctuations: A plucking model and its application. Engineering Geology 171:1–10. https://doi.org/10.1016/j.enggeo.2013.12.008

Pells P, Pells S, van Schalkwyk M (2016) A TALE OF TWO SPILLWAYS. In: International Symposium on "Appropriate technology to ensure proper Development, Operation and Maintenance of Dams in Developing Countries." Johannesburg, South Africa, pp 279–288

Pells PJ, Bieniawski ZT, Hencher SR, Pells SE (2017) Rock quality designation (RQD): time to rest in peace. Can Geotech J 54:825–834. https://doi.org/10.1139/cgj-2016-0012

Pells S, Duwell A, Parmar H (2024) Copeton Dam: Performance of the Great Scour Case Study in the floods of 2022. In: ANCOLD 2023. Cairns, Australia

Pells SE (2016) Erosion of Rock in Spillways. Ph.D. Thesis, University of South Wales

Reinius E (1986) Rock erosion. International Water Power and Dam Construction 38:43–48

Sawadogo O (2010) Scour of unlined dam spillways. Masters Thesis, Stellenbosch : University of Stellenbosch

Wahl TL, Frizell KW, Falvey HT (2019) Uplift Pressures below Spillway Chute Slabs at Unvented Open Offset Joints. J Hydraul Eng 145:04019039. https://doi.org/10.1061/(ASCE)HY.1943-7900.0001637

Wilkinson C, Harbor DJ, Helgans E, Kuehner JP (2018) Plucking phenomena in nonuniform flow. Geosphere 14:2157–2170. https://doi.org/10.1130/GES01623.1

Wisse M-H, Koulibaly AS, Saeidi A, Quirion M (2023a) Small-Scale Physical Model for Studying the Effect of Rock Mass Parameters in the Hydraulic Erosion Process of Unlined Spillways. In: World Environmental and Water Resources Congress 2023. American Society of Civil Engineers, Henderson, Nevada, pp 89–98

Wisse M-H, Saeidi A, Quirion M, Nilsson C-O (2023b) Effects of joint opening and block protrusion on the hydraulic parameters affecting rock block erosion in unlined spillways using a reduced-scale model. Acta Geotech. https://doi.org/10.1007/s11440-023-02085-y

Zhang X, Wang C, Chen X, et al (2024) Insights into the cause of the Oroville dam spillway failure, 2017, California. Environ Sci Pollut Res. https://doi.org/10.1007/s11356-024-32462-3

IMPACT OF BLOCK GEOMETRY ON THE ROCK MASS EROSION: A LABORATORY-SCALE MODEL STUDY

Vineeth Reddy Karnati, Ali Saeidi & Alain Rouleau
Département des sciences appliquées, Université du Québec à Chicoutimi, Chicoutimi, QC G7H 2B1, Canada
Marco Quirion
Hydro-Québec, Expertise intégrée – Géologie, Direction Sécurité des barrages et infrastructures, 75 Boul. René-Lévesque Ouest, Montréal, QC H2Z 1A4, Canada

ABSTRACT
Rock mass erosion in spillways is a critical factor in assessing the safety and durability of hydraulic structures. Laboratory-scale physical modelling allows to study the effect of individual parameters on the erosion process. This paper studies the influence of the rock block geometry under the configuration where the modelled blocks are arranged against the flow direction. Trial tests exhibited the possibility of block rotation under the action of hydraulic forces by the flowing water. The effect of block geometry on the block rotation possibility was studied by estimating the factor of safety against rotation as a function of exposure length on the leeside (a), block volume (V), joint spacing ratio (r), and block inclination (ψ_2). Studying the hydraulic forces arresting the block movement allows us to validate the developed theory. Results from the analysis show that block stability is highly dependent on the block aspect ratio, the dip of the block surface and the exposure length. Variations in block height revealed that increased height appears to counterbalance the rotational forces. The factor of safety is found to be higher than 1 when the joint spacing ratio r is more than 1:1.

RÉSUMÉ
L'érosion du massif rocheux dans l'évacuateur de crues est un facteur crucial pour évaluer la sécurité et la durabilité des structures hydrauliques. La modélisation physique à l'échelle du laboratoire permet d'étudier l'impact des paramètres individuels sur ce processus. Cet article analyse l'influence de la géométrie des blocs lorsqu'ils sont disposés dans le sens contraire au flux. Des essais ont montré que les blocs peuvent pivoter sous l'effet des forces hydrauliques. L'effet de la géométrie des blocs sur la rotation a été étudié en déterminant le facteur de sécurité contre la rotation en fonction de la longueur d'exposition sur le côté protégé du courant (a), du volume du bloc (V), du rapport d'espacement des joints (r), et de l'inclinaison des blocs (ψ_2). L'étude des forces hydrauliques opposées au mouvement du bloc permet de valider la théorie développée. Les résultats montrent que la stabilité du bloc dépend fortement du rapport d'aspect du bloc, de l'inclinaison de la surface et de la longueur d'exposition. Les variations de hauteur du bloc révèlent qu'une hauteur accrue contrebalance les forces de rotation. Le facteur de sécurité est supérieur à 1 lorsque le ratio d'espacement des joints r est supérieur à 1:1.

1. INTRODUCTION

Many occurrences of rock scour with removal of rock material under the action of hydraulic forces, have been observed in dam spillways in the past few decades. The continuous interaction of water, with huge hydraulic energy in the flood season, with rock mass may result in huge scour quantities. Historic erosion examples include Copeton dam spillway (Pells 2016, Pells et al. 2024), Ricobayo dam spillway (Liu and Kieffer 2021), Mokolo dam spillway (Pells 2016) and recently Oroville dam spillway (Koskinas et al. 2019, Zhang et al. 2024). They present devastating destruction due to spillway erosion. The scour assessment is generally made using the semi-empirical methods (Annandale 2012, Pells 2016) due to their simplicity; however, several differences are observed between the predicted and actual scour depths (Jalili Kashtiban et al. 2021). The reason for these differences is due to the empirical nature of these methods and the complexity involved in calculating the scour resistance offered by the rock mass. The development of a new assessment method requires a proper understanding of the scour mechanisms. Different erosion mechanisms have been observed in nature, such as block removal by uplift, fracturing (brittle and fatigue), abrasion, undercutting, etc. (Carling et al. 2017, Wilkinson et al. 2018, Krzaczek et al. 2020, Ferrill and Ferrill 2021). It appears that block uplift or plucking is predominant, especially in a fully-fractured rock mass. This uplift mechanism is highly dependent on the hydraulic pressure distribution around the blocks. The pressure distribution is in turn affected by various

geometrical, hydraulic and geomechanical parameters.

Flood events can remove even huge rock blocks. Depending on the flow conditions and the pressure distribution, various modes of block removal are possible. For instance, lifting or sliding or toppling of blocks downstream when the downstream faces are exposed to the fluid flow (Whipple et al. 2000, Snyder et al. 2003, Dubinski and Wohl 2013). When the upstream faces are exposed in such a way that it prevents the lifting, the uplifting forces combine with the fluid force resulting in block toppling (Wende 1999). The obstructions downstream of the exposed block defines the ease of the block movement (Wende 1999, Carling et al. 2002). The scour threshold by block removal is dependent on various factors such as block size, orientation, friction against the adjacent blocks, rather than strength of the rock block itself (Whipple et al. 2000, Pells et al. 2017). The resistance to block displacement is dependent on various parameters such as dip of the bedding plane, the geometry and the condition of the joints (Annandale 1995, Wende 1999, Dubinski and Wohl 2013).

Determination of the effect of several parameters on the block stability and thus the scour threshold is made possible by physical model testing. Over years, several physical models have been developed by various researchers, however, most models have used either single large block (George 2015) or a group of very small blocks (Sawadogo 2010, Wilkinson et al. 2018). In our previous study (Karnati et al. 2024), we have presented the effect of joint orientation on the hydraulic pressure distribution using physical model tests on the reduced-scale model developed at Université du Québec à Chicoutimi (UQAC) (Koulibaly et al. 2023, Wisse et al. 2023). During the trail physical testing on the blocks oriented against the flow, the block toppling is noticed as presented by Wende (1999). In this paper, a methodology is first developed to analyze the stability of the blocks, oriented against the flow, against toppling. In the next step, the effect of block geometry on the block stability against toppling is determined.

2. METHODOLOGY

The primary objective of this study is to develop an analysis to determine the stability against toppling of the blocks oriented against the flow. To attain this objective, the results of the physical model tests with blocks positioned against the flow at 45^{o} to the flow direction are utilized. Figure 1 presents the channel view from the downstream of the blocks positioned in the model. The details of the model, model blocks and the instrumented block are provided in our previous studies (Karnati et al. 2023, 2024, Wisse et al. 2024). The model tests are performed for various flowrates, Q (0.18, 0.24, 0.315 and 0.34 m^3/s) and various joint openings, JO (3, 10 and 20 mm); however, the results of the Q = 0.315 m^3/s at JO 20 mm are only presented in this paper.

2.1 Block Stability Analysis

The hydraulic pressure distribution around the blocks measured from the model tests is used to analyze the block stability. As the hydraulic pressure at each block face follows a stochastic distribution, analyzing the stability against toppling becomes very complex. The critical condition arises when the pressure on the bottom of the block is maximum whereas the pressure on the top is minimum. A uniform pressure distribution is assumed on each face within the joint and a linear distribution is assumed on the top of the block. The position of the water entries where the pressure measurement is made, and the assumed pressure distribution is presented in Figure 2. Different faces of the block and the corresponding water entries are termed as presented in Table 1. Various terms of Figure 2(c) are presented in Table 2. In Figure 2(c), the dynamic pressure is measured to be negative due to the formation of eddies arising a negative pressure zone. Hence the pressure along the exposure length '*a*' is assumed to be zero.

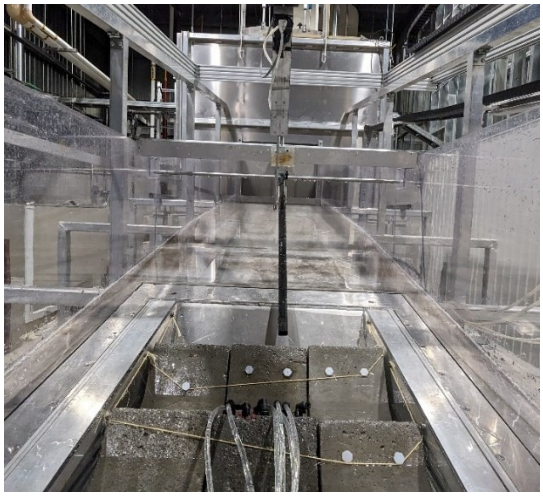

Figure 1. Channel view from downstream with blocks positioned against the flow direction at 45^{o} to the flow

As observed during the trial tests, the block tends to topple. Hence the stability against the toppling about point 'R' (Figure 2(c)) is analyzed as the factor of safety, F_s calculated as the ratio of resisting and mobilizing moments. Under the action of the hydraulic forces, the mobilizing and resisting moments about point 'R' against toppling could be calculated as presented in equations 1-6.

Mobilizing moments, M_O (in kN-m/m):

Due to force F_{RS}: $\gamma_w * h_B * S_1 * \frac{S_1}{2}$ [1]

Due to force F_{PS}: $\gamma_w * h_C * S_2 * \frac{S_2}{2}$ [2]

Resisting moments, M_R (in kN-m/m):

Due to force F_{PQ}: $\gamma_w * \frac{h_{Ac}+h_{Ad}}{2} * S_1 * \frac{h_{Ad}+2h_{Ac}}{h_{Ac}+h_{Ad}} * \frac{S_1}{3}$ [3]

Due to force F_{QR}: $\gamma_w * h_D * (S_2 - a) * \frac{S_2-a}{2}$ [4]

Due to force W_x': $W_x' * \frac{S_2}{2}$ [5]

Due to force W_y': $W_y' * \frac{S_1}{2}$ [6]

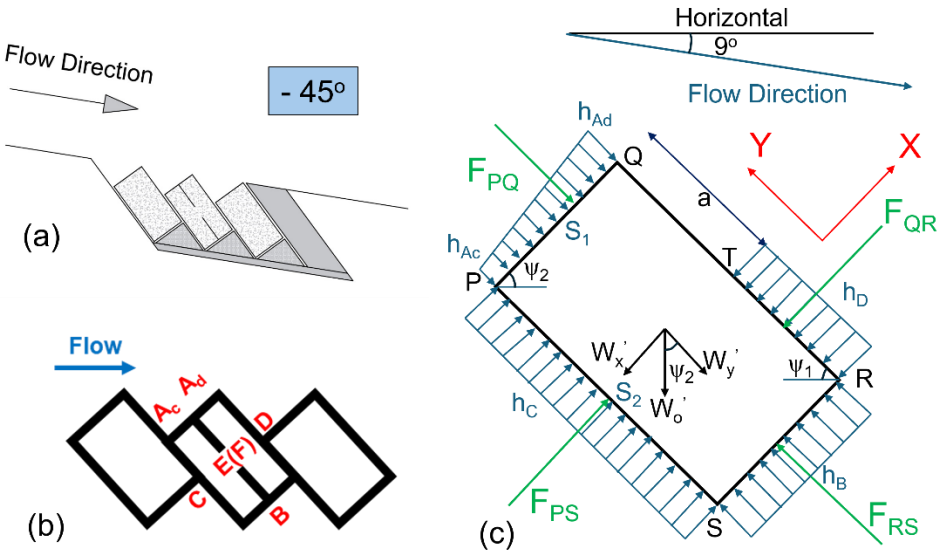

Figure 2. Positioning of blocks and assumed pressure distribution: (a) Arrangement of blocks at 45° inclination; (b) Positioning of various hydraulic inlets; and (c) Assumed pressure distribution around the blocks

Table 1. Different faces of the instrumented block and corresponding water inlets

Face	Description	Water inlet	Description
A	Top face of the block	*Ac*	Water inlet close to the face *C*
		Ad	Water inlet close to the face *D*
B	Bottom face of the block	*Bc*	Water inlet close to the face *C*
		Bd	Water inlet close to the face *D*
C	Upstream face of the block	*C1*	Water inlet close to the face *A*
		C2	Water inlet close to the face *B*
D	Downstream face of the block	*D1*	Water inlet close to the face *A*
		D2	Water inlet close to the face *B*
E	Face of the block towards the right side of the flow	*E1*	Water inlet close to the face *A*
		E2	Water inlet close to the face *B*
F	Face of the block towards the left side of the flow	*F1*	Water inlet close to the face *A*
		F2	Water inlet close to the face *B*

Table 2. Different terms used in the block stability analysis

Term	Description	Actual value in the model tests
h	Dynamic pressure head[1]	-
F	Hydraulic force on each block face[2]	-
S_1	Joint spacing along the width of the block	0.15 m
S_2	Joint spacing along the height of the block	0.30 m
a	Exposure length along the leeside of the block	0.17 m
Ψ_1	Dip of the joint faces	54°
Ψ_2	forming the blocks	36°
γ_w	Unit weight of water	9.81 kN/m^3
γ_r	Unit weight of the block	13.5 kN/m^3
r	Joint spacing ratio, $\frac{S_1}{S_2}$	0.5
V	Block volume, $S_1 * S_2$	0.045 m^3/m
W_o'	Submerged weight of the block per unit width, $\gamma_r' * S_1 * S_2$	(13.5-9.81)*0.15*0.30 = 0.166 kN/m
W_x'	X - Component of W_o', $W_o' \sin \Psi_2$	0.0976 kN/m
W_y'	Y - Component of W_o', $W_o' \cos \Psi_2$	0.1343 kN/m

[1]Subscript indicates the water entry
[2]Subscript indicates the face on which force acts

3. SENSITIVITY ANALYSIS

The equations 1-6 present the importance of various parameters involved in the block stability such as '*a*', '*r*', '*V*' and 'ψ_2'. To study the sensitivity of these parameters, one parameter is varied while keeping the other parameters constant. Due to the limited availability of the test data, one assumption made is that the pressure remains constant around the block with the variation of the parameters '*a*', '*r*' and '*V*'. This assumption is valid as the inclination of the block remains constant. For the sensitivity analysis with respect to inclination, the variation of the hydraulic pressure with inclination is used to obtain the dynamic head at various faces of the block at different inclinations. As mentioned earlier, due to the uneven surface arising from the block inclination, several zones of negative dynamic head are observed during the model tests. To be conservative, negative dynamic heads representing cavitation conditions are ignored and pressure is taken zero in that condition. The dynamic head data and hence the respective moments about '*R*' due to hydraulic forces on various faces of the block from the model test under the test condition (Q = 0.315 m^3/s and JO = 20 mm) are presented in Table 3. For the purpose of sensitivity analysis, a realistic unit weight of the rock blocks which is about 27 kN/m^3 is considered (modifies only the submerged unit weight and its components). The factor of safety, F_s value in Table 3 indicates that the block is unstable and can topple about point '*R*'.

Table 3. Model test data and corresponding moments about point '*R*'

Parameter	Value
h_{Ac}	-0.076 m
h_{Ad}	-0.202 m
h_B	0.378 m
h_C	0.262 m
h_D	0.437 m
Moment due to F_{PQ}	0.0 kN-m/m
Moment due to F_{RS}	0.042 kN-m/m
Moment due to F_{PS}	0.116 kN-m/m
Moment due to F_{QR}	0.036 kN-m/m
Moment due to W_x'	0.068 kN-m/m
Moment due to W_y'	0.047 kN-m/m
ΣM_o	0.157 kN-m/m
ΣM_R	0.151 kN-m/m
F_s	0.960

3.1 Sensitivity of parameter '*a*'

The exposure length, '*a*' is physically dependent on the arrangement of blocks in a rock mass and the surface irregularities arose by blasting patterns. This parameter is varied as a percentage of the spacing 'S_2'. The factor of safety against varying exposure length (as a ratio 'a/S_2') is presented in Figure 3. Figure 3

shows that as the block exposure length increases, the F_s decreases reaching 1 when a/S_2 is about 50%. When '*a*' value is 0%, it represents a physical condition where the block is completely surrounded by other rock blocks, where the value 100%, it represents the block is completely free to displace without any resistance from the leading blocks. For the sensitivity analysis of other parameters, the parameter '*a*' is considered zero to ensure a stable initial condition (F_s > 1).

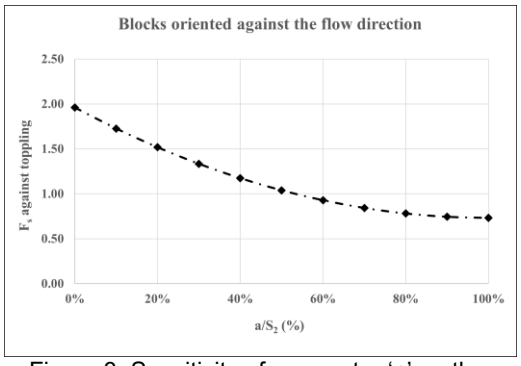

Figure 3. Sensitivity of parameter '*a*' on the block stability with r = 0.5, V = 0.045 m^3/m and ψ_2 = 36°

3.2 Sensitivity of parameter '*r*'

The aspect ratio of the block, i.e., *r* represents the shape of the block. 'r' values less than 1 represents deep blocks, values more than 1 represent wide flat blocks and value of 1 represents a square block in a 2D domain. The *r* value is varied as 4/1, 3/1, 2/1, 1.5/1, 1/1, 1/1.5, 1/2, 1/3 and 1/4. Keeping the volume of the blocks as constant as that used in model testing, the values of S_1 and S_2 are varied as $\sqrt{r * V}$ and $\sqrt{r/V}$ respectively. The factor of safety against varying aspect ratio is presented in Figure 4. Figure 4 presents that as r values increases, the stability against toppling is high for the deep columnar blocks. This Figure also presents that the flat blocks could be overturned which is valid as the little block uplift could create the pressure conditions such that the block topples rather than uplift due to the combination of thrust and lift forces.

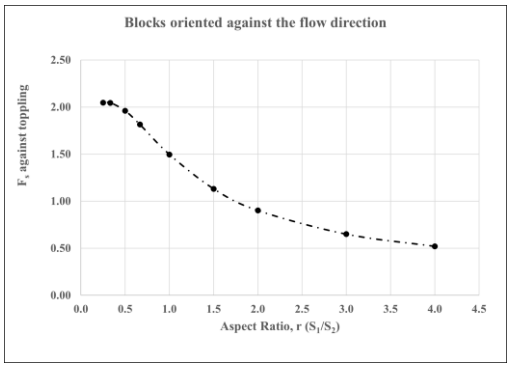

Figure 4. Sensitivity of parameter '*r*' on the block stability with a = 0, V = 0.045 m^3/m and ψ_2 = 36°

3.3 Sensitivity of parameter '*V*'

The volume of the block per unit width is calculated as the product of the two spacings presented in Figure 2(c). Keeping a constant *r* of 0.5, assuming various values of S_1 i.e., 0.05, 0.1,…., 0.55 is made such that the corresponding height of the block becomes more than 1m (until which the block removal is more pronouncing) and corresponding S_2 values are calculated for r = 0.5. The factor of safety against varying block volume per unit width is presented in Figure 5. According to Figure 5, the increase in the block volume enhances the block stability as it increases the resisting forces due to the increased block weight.

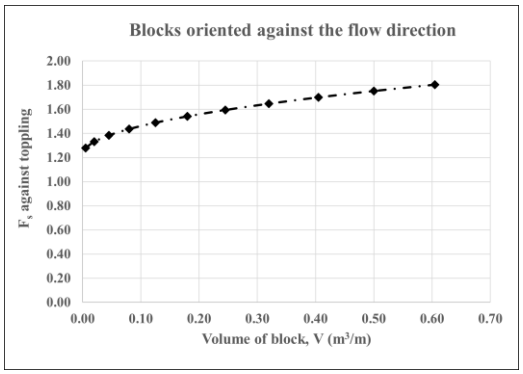

Figure 5. Sensitivity of parameter '*V*' on the block stability with a = 0, r = 1/2 and ψ_2 = 36°

3.4 Sensitivity of parameter 'ψ_2'

The determination of sensitivity of dip of block surface against flow requires the model testing at various inclinations. However, due to limitations in testing capacity, only a single inclination condition is tested. However, tests are also carried out at other inclinations, i.e., 0° and 45° towards the flow direction. The variation

of the pressure obtained for different water entries (A and B) is presented in Figure 6. Reinius (1986) in his experimental studies presented that the variation of joint orientation results in different hydraulic pressure distribution. Thus, studying the sensitivity of parameter 'ψ_2' requires further model testing and/or numerical modeling which is considered under the future scope of this study.

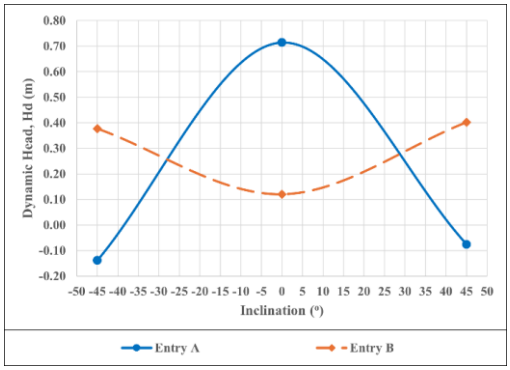

Figure 6. Variation of dynamic head on top (*A*) and bottom (*B*) of the block with block inclination with the flow direction

4. CONCLUSIONS

This paper developed a methodology to study the possibility of block instability by toppling using the pressure distribution around a model rock block obtained from physical model tests. The blocks are found to be unstable and to topple under the model test condition when they are oriented against the flow, which is confirmed with the factor of safety 'F_s' less than 1.0. A sensitivity analysis was performed on the important parameters affecting the block stability, i.e., exposure length '*a*', aspect ratio '*r*' and volume of the block '*V*'. Effect of each parameter on the factor of safety 'F_s', keeping the other parameters constant, was studied. Among the parameters studied, the aspect ratio was found to be the most important factors with significant effect on the block stability. Blocks with aspect ratio less than 1.75:1 were found to be stable. The length of exposure surface on the leeside of the block significantly reduced the block stability when it was more than 50% of the block height. The effect of dip of the block requires further model testing with varied block inclination which falls under the future scope of this study.

REFERENCES

Annandale, G.W. 1995. Erodibility. Journal of Hydraulic Research, 33(4): 471–494. Taylor & Francis. doi:10.1080/00221689509498656.

Annandale, G.W. 2012. Current state-of-the-art Rock Scouring Technology, 1–12. American Society of Civil Engineers. doi:10.1061/40911(230)2.

Carling, P.A., Hoffmann, M., and Blatter, A.S. 2002. Initial Motion of Boulders in Bedrock Channels. *In* Water Science and Application. *Edited by* P.K. House, R.H. Webb, V.R. Baker, and D.R. Levish. American Geophysical Union, Washington, D. C. pp. 147–160.

Carling, P.A., Perillo, M., Best, J., and Garcia, M.H. 2017. The bubble bursts for cavitation in natural rivers: laboratory experiments reveal minor role in bedrock erosion. Earth Surface Processes and Landforms, 42(9): 1308–1316. doi:10.1002/esp.4101.

Dubinski, I.M., and Wohl, E. 2013. Relationships between block quarrying, bed shear stress, and stream power: A physical model of block quarrying of a jointed bedrock channel. Geomorphology, 180–181: 66–81. doi:10.1016/j.geomorph.2012.09.007.

Ferrill, N.S.L., and Ferrill, D.A. 2021. Influence of mechanical layering and natural fractures on undercutting and rapid headward erosion (recession) at Canyon Lake spillway, Texas, U.S.A. Engineering Geology, 280: 105897. doi:10.1016/j.enggeo.2020.105897.

George, M.F. 2015. 3D Block Erodibility: Dynamics of Rock-Water Interaction in Rock Scour. Ph.D. Thesis, University of California, Berkeley, Berkeley, USA.

Jalili Kashtiban, Y., Saeidi, A., Farinas, M.-I., and Quirion, M. 2021. A Review on Existing Methods to Assess Hydraulic Erodibility Downstream of Dam Spillways. Water, 13(22): 3205. Multidisciplinary Digital Publishing Institute. doi:10.3390/w13223205.

Karnati, V.R., Saeidi, A., Rouleau, A., and Quirion, M. 2023. Effect of Joint Opening and Block Protrusion on the Hydraulic Pressure Around Rock Blocks in Unlined Dam Spillways.

Karnati, V.R., Saeidi, A., Rouleau, A., and Quirion, M. 2024. Effect of Joint Orientation on Rock Mass Erosion Based on Experimental Results Using a Pilot Plant Spillway Model. *In* 58th U.S. Rock Mechanics/Geomechanics Symposium. ARMA, Golden, Colorado, USA. p. ARMA-2024-0753.

Koskinas, A., Tegos, A., Tsira, P., Dimitriadis, P., Iliopoulou, T., Papanicolaou, P.,

Koutsoyiannis, D., and Williamson, T. 2019. Insights into the Oroville Dam 2017 Spillway Incident. Geosciences, 9(1): 37. doi:10.3390/geosciences9010037.

Koulibaly, A.S., Saeidi, A., Rouleau, A., and Quirion, M. 2023. A Reduced-Scale Physical Model of a Spillway to Evaluate the Hydraulic Erodibility of a Fractured Rock Mass. Rock Mechanics and Rock Engineering, 56: 933–951. doi:10.1007/s00603-022-03101-5.

Krzaczek, M., Nitka, M., Kozicki, J., and Tejchman, J. 2020. Simulations of hydro-fracking in rock mass at meso-scale using fully coupled DEM/CFD approach. Acta Geotechnica, 15(2): 297–324. doi:10.1007/s11440-019-00799-6.

Liu, Q., and Kieffer, D.S. 2021. LiDAR Based Three-Dimensional Rock Structure Model for Evaluating Spillway Scour at Ricobayo Dam, Zamora, Spain.

Pells, P.J., Bieniawski, Z.T., Hencher, S.R., and Pells, S.E. 2017. Rock quality designation (RQD): time to rest in peace. Canadian Geotechnical Journal, 54(6): 825–834. doi:10.1139/cgj-2016-0012.

Pells, S., Duwell, A., and Parmar, H. 2024. Copeton Dam: Performance of the Great Scour Case Study in the floods of 2022. *In* ANCOLD 2023. Cairns, Australia.

Pells, S.E. 2016. Erosion of Rock in Spillways. Ph.D. Thesis, University of South Wales, Australia.

Reinius, E. 1986. Rock erosion. International Water Power and Dam Construction, 38(6): 43–48.

Sawadogo, O. 2010. Scour of unlined dam spillways. Masters Thesis, Stellenbosch : University of Stellenbosch.

Snyder, N.P., Whipple, K.X., Tucker, G.E., and Merritts, D.J. 2003. Importance of a stochastic distribution of floods and erosion thresholds in the bedrock river incision problem. Journal of Geophysical Research: Solid Earth, 108(B2): 2001JB001655. doi:10.1029/2001JB001655.

Wende, R. 1999. Boulder bedforms in jointed-bedrock channels. *In* Varieties of Fluvial Form: International Association of Geomorphologists Publication. *Edited by* A.J. Miller and A. Gupta. pp. 189–216.

Whipple, K.X., Hancock, G.S., and Anderson, R.S. 2000. River incision into bedrock: Mechanics and relative efficacy of plucking, abrasion, and cavitation. GSA Bulletin, 112(3): 490–503. doi:10.1130/0016-7606(2000)112<490:RIIBMA>2.0.CO;2.

Wilkinson, C., Harbor, D.J., Helgans, E., and Kuehner, J.P. 2018. Plucking phenomena in nonuniform flow. Geosphere, 14(5): 2157–2170. doi:10.1130/GES01623.1.

Wisse, M.-H., Koulibaly, A.S., Saeidi, A., and Quirion, M. 2023. Small-Scale Physical Model for Studying the Effect of Rock Mass Parameters in the Hydraulic Erosion Process of Unlined Spillways. *In* World Environmental and Water Resources Congress 2023. American Society of Civil Engineers, Henderson, Nevada. pp. 89–98.

Wisse, M.-H., Saeidi, A., Quirion, M., and Nilsson, C.-O. 2024. Effects of joint opening and block protrusion on the hydraulic parameters affecting rock block erosion in unlined spillways using a reduced-scale model. Acta Geotechnica, 19(4): 1965–1979. doi:10.1007/s11440-023-02085-y.

Zhang, X., Wang, C., Chen, X., Dong, J., Hu, M., and Liu, S. 2024. Insights into the cause of the Oroville dam spillway failure, 2017, California. Environmental Science and Pollution Research, 31(14): 21356–21369. doi:10.1007/s11356-024-32462-3.